Extremum-seeking control for data-based performance optimization of high-tech systems

Extremum-Seeking Control for Data-Based Performance Optimization of High-Tech Systems

Leroy Hazeleger

Extremum-Seeking Control for Data-Based Performance Optimization of High-Tech Systems

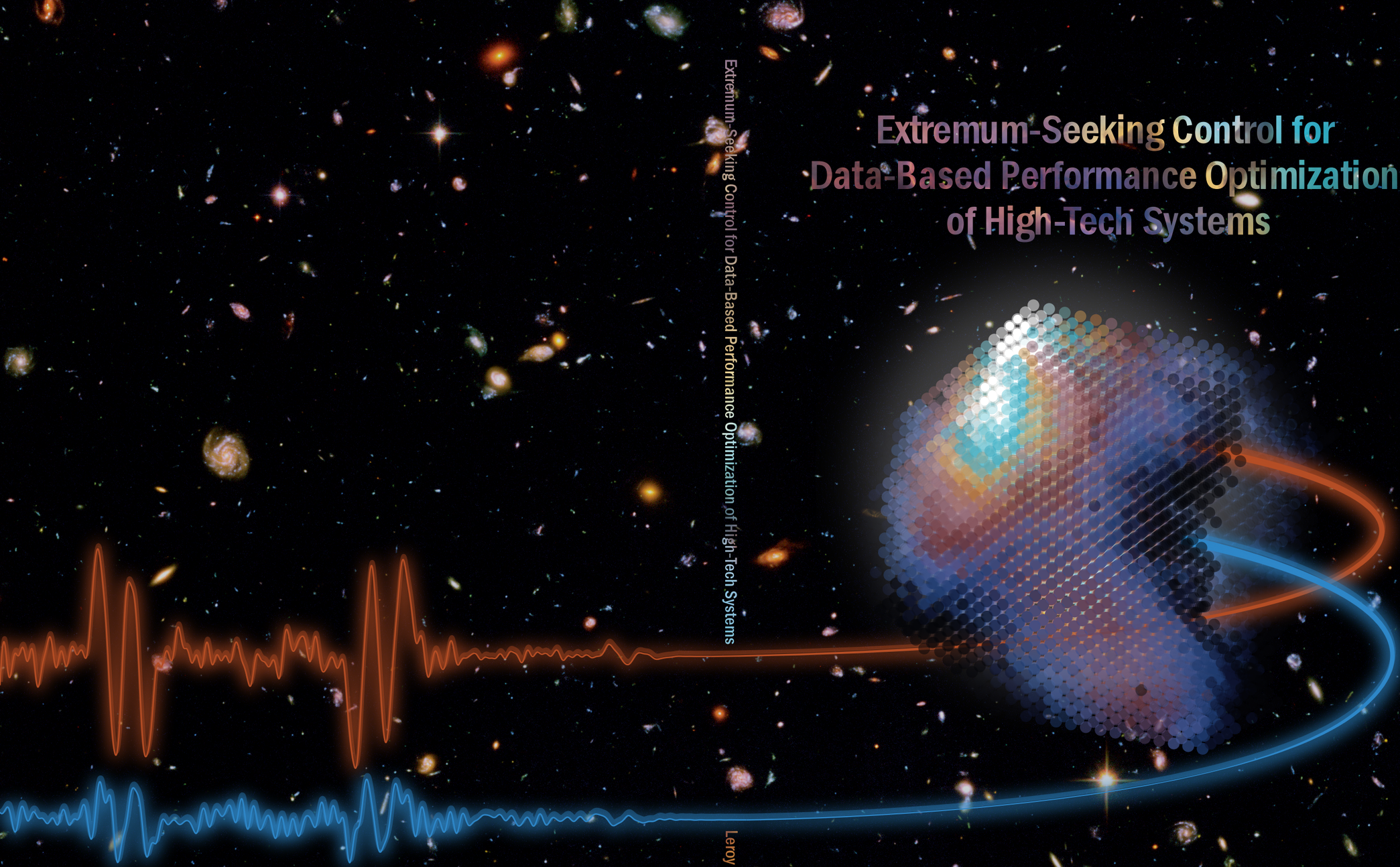

Leroy Hazeleger

Uitnodiging

tot het bijwonen van de openbare verdediging van mijn proefschrift

Extremum-Seeking Control for Data-Based Performance Optimization of High-Tech Systems

De verdediging vindt plaats op donderdag 15 oktober 2020 om 11:00 uur in Lecture Room 4 in gebouw Auditorium van de Technische Universiteit Eindhoven

Leroy Hazeleger
hazeleger.leroy@gmail.com

Extremum-Seeking Control for Data-Based Performance Optimization of High-Tech Systems

Leroy Hazeleger

The research reported in this thesis is part of the research programme of the Dutch Institute of Systems and Control (DISC). The author has successfully completed the educational program of the Graduate School DISC.

The work described in this thesis was carried out at the Eindhoven University of Technology and is part of the research programme "CHAMeleon" with project number 13896, which is (partly) financed by the Netherlands Organisation for Scientific Research (NWO).

A catalogue record is available from the Eindhoven University of Technology Library.
ISBN: 978-90-386-5082-1

Reproduction: Ipskamp Printing, Enschede, the Netherlands

FSC keurmerk hier

Cover background image: NASA, ESA, and S. Beckwith (STScI) and the HUDF Team.
Cover design: L. Hazeleger.

Extremum-Seeking Control for Data-Based Performance Optimization of High-Tech Systems

PROEFSCHRIFT

ter verkrijging van de graad van doctor aan de
Technische Universiteit Eindhoven, op gezag van de
rector magnificus prof.dr.ir. F.P.T. Baaijens, voor een
commissie aangewezen door het College voor
Promoties, in het openbaar te verdedigen
op donderdag 15 oktober 2020 om 11:00 uur

door

Leroy Hazeleger

geboren te Nieuwegein

Dit proefschrift is goedgekeurd door de promotoren en de samenstelling van de promotiecommissie is als volgt:

voorzitter:	prof.dr. L.P.H. de Goey
1e promotor:	prof.dr.ir. N. van de Wouw
2e promotor:	prof.dr. H. Nijmeijer
leden:	prof.dr.ir. W.P.M.H. Heemels
	prof.dr. D. Nešić (University of Melbourne)
	prof.dr. A. Pavlov (Norwegian University of Science and Technology)
	prof.dr.ir. J.W. van Wingerden (Technische Universiteit Delft)
	dr.ir. A.G. de Jager

Het onderzoek dat in dit proefschrift wordt beschreven is uitgevoerd in overeenstemming met de TU/e Gedragscode Wetenschapsbeoefening.

Preface

Mechatronic system designs for high-tech applications in many areas of technology often rely on high-cost solutions to achieve highly predictable and understandable system dynamics on the basis of accurate system models. These models have enabled skillful control engineers in the high-tech industry to use conventional and well-understood control solutions to meet stringent performance requirements in terms of machine accuracy, operating speed, stability, and reliability. However, major economic, social and technological trends push performance, cost, and reliability requirements for current and future high-tech systems to unparalleled levels, and will progressively challenge purely model-based approaches to automatic control and system optimization. In particular, the increasing complexity in terms of uncertainty, non-stationary nature of system dynamic properties and disturbances, and mode-of-use dependent performance specifications, constitute real challenges in achieving *optimal* performance in current and future high-tech systems using model-based approaches.

To account for changing, uncertain, or unknown dynamics and disturbance characteristics, and enable the satisfaction of accuracy and robustness demands in high-tech systems, this dissertation focusses on supplementing model-based control engineering by a data-based, model-free, automated optimization technique named *extremum-seeking control*. Attributable to its model-free nature, extremum-seeking control is especially valuable in cases where the dynamical behavior of the system at hand can not be represented by an accurate or comprehensible model, or cases where the disturbances are unknown, changing, or mode-of-use dependent. Namely, this technique enables the possibility of achieving optimal system performance despite the lack of an (accurate) system model.

This dissertation presents newly developed extremum-seeking control methods that enable data-based automated performance optimization for a richer class of optimization problems. The theoretical developments in this work are inspired by a large variety of industrially relevant optimization problems, and are experimentally demonstrated on industrial applications to illustrate the value it may provide in supporting control engineers to get the most out of their high-tech systems.

Contents

Chapter 1

Introduction

1.1 Automatic control in the high-tech systems industry

Automatic control of dynamic processes is a key enabling methodology in a substantial variety of technological innovations in many branches of our society, and has proven indispensable in realizing the social welfare and economic prosperity that we benefit today. This becomes particularly evident from the broad range of high-tech industrial applications in which control plays a pivotal role, ranging from photolithography systems in the semi-conductor industry to instruments for research and analysis in biology, and life and material sciences such as electron microscope systems, pick-and-place machinery in the manufacturing industry to industrial (three-dimensional) printing and copying systems, robotics to medical imaging systems, and so on. Namely, these high-tech systems rely heavily on advanced control solutions, enabling exceptional machine precision and high operating speeds, while guaranteeing reliability, stability, and efficiency in machine usage. The importance of and dependence on automatic control in the high-tech systems industry is expected to only increase in the future (Lamnabhi-Lagarrigue et al., 2017).

Mechatronic system designs for high-tech applications in these areas of technology often rely on high-cost mechatronic solutions for system components such as sensing equipment, bearings, actuators, transmissions, computational hardware, communication technology, among others. These high-cost design choices are usually made in favor of achieving highly predictable and understandable system dynamics on the basis of accurate (mathematical) system models. These models have enabled the use of conventional and well-understood control solutions to meet stringent performance requirements in terms of machine accuracy, operating speed, stability, and reliability. In particular, achieving top-level system performance by means of these control solutions in the high-tech industry is still largely realized by skillful control engineers on the basis of accurate system models and expert knowledge. A benefit of such a model-based approach is the fact that knowledge and experience of these control engineers on system dynamics, disturbance characteristics, and performance specifications for the particular

(a) ASML's NXE:3300 lithography system[1]

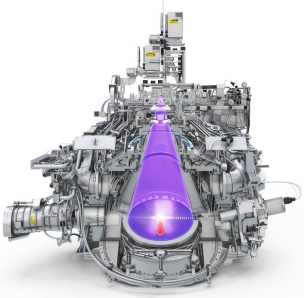

(b) EUV light source system within ASML's lithography system[2]

Figure 1.1: Artist impression of next-generation extreme ultraviolet (EUV) lithography system by company ASML.

application at hand can be exploited.

However, major economic, social and technological trends push performance, cost, and reliability requirements for current and future high-tech systems to unparalleled levels. For example, the ever-increasing demand for more functionality in, e.g., consumer electronics, and ongoing developments in, e.g., artificial intelligence (AI) and automotive technology such as autonomous driving and interacting cars, dictates the manufacturing of more powerful, smaller, cheaper, and energy-efficient microchips. To achieve the imaging resolution and accurate overlay[1] required to manufacture these microchips, and achieve the desired machine productivity for high-volume and reliable manufacturing, increasingly complex lithography systems such as extreme ultraviolet (EUV) lithography are devised and constructed, see, e.g., Fig 1.1 and Wagner and Harned (2010). Another example can be found in electron microscope technology, which is required to provide ever-increasing magnification with extreme sample positioning accuracy, e.g., for the purpose of fault and failure analysis in the nanometer structures of ever-smaller integrated circuit designs, and to support research in life sciences and biology. Currently, resolution advances in state-of-the-art cryogenic electron microscope systems enable the analysis of, e.g., protein structures, molecular structures, and viruses at near atomic-resolution, see, e.g., Fig 1.2 and Egelman (2016).

The inevitable and increasing complexity in terms of uncertainty and non-

[1]The image is acquired from Heertjes et al. (2016).

[2]The image is acquired from https://www.asml.com/en/investors/financial-calendar/past-events-and-presentations, June 24th 2019 UBS Investor Forum presentation.

[3]Measure for the alignment of a lithographic pattern relative to a successive lithographic pattern on a wafer.

(a) Thermo Fisher's cryogenic transmission electron microscope Krios G4 Cryo-TEM[1]

(b) Images using Cryo-TEM. 3D visualization of a Golgi apparatus from a green alga with 2 nm resolution (left, Bykov et al. (2017)), 3D reconstruction of the GABA receptor membrane protein with .275 nm resolution (right,Masiulis et al. (2019)).

Figure 1.2: Cryogenic transmission electron microscope (Cryo-TEM) by company Thermo Fisher.

stationary nature of system dynamic properties and disturbances, and mode-of-use dependent performance specifications in current high-tech systems and future engineering developments, will progressively challenge purely model-based approaches to automatic control and optimization. For example, the availability of accurate, but simple system models for accurate system performance predictions relies on physical insight and first-principle relations, which may be too challenging with the increasingly complex technologies being developed. For instance, accurate modelling of the working principle of Laser-Produced Plasma (LPP) source systems for EUV light generation in next-generation lithography systems, see, e.g., Fig. 1.1(b), may lead to far too complex models for control (if possible at all). Namely, modelling of complex plasma physics phenomena and droplet-laser interactions is required to study the generation of EUV light, while modelling of and motion control design for the laser beam delivery system within such an EUV light source is required for accurate positioning of driving lasers to realize optimal EUV light generation. Another example arises in the use of nonlinear motion control methods to improve performance of motion systems in terms of improved disturbance rejection capabilities over the use of well-known linear motion control methods. For example, methods such as

[1]The image is acquired from https://www.thermofisher.com/nl/en/home/electron-microscopy/products/transmission-electron-microscopes/krios-g4-cryo-tem.html.

nonlinear PID control (Zheng et al., 2005; Heertjes et al., 2009), variable-gain control (van de Wouw et al., 2008; Pavlov et al., 2013), reset control (Clegg, 1958; Aangenent et al., 2010; Beker et al., 2004; van Loon et al., 2017), split-path nonlinear integral control (van Loon et al., 2016; Foster et al., 1966) hybrid control (Heertjes et al., 2019; Deenen et al., 2017) among others, can ensure superior performance compared to that achievable by linear control strategies suffering from fundamental limitations like Bode's sensitivity integral (Freudenberg et al., 2000; Seron et al., 1997). However, due to the lack of the superposition principle in nonlinear motion control and the presence of (unknown and external) disturbances, the relation between tunable parameters and performance measures such as positioning and reference tracking accuracy are non-trivial, thereby making model-based performance optimization challenging and less intuitive for control engineers.

Undoubtedly, system modelling will continue to serve as a basis for (performance-optimal) control design. However, the increasing complexity, uncertainty, and non-stationary nature of system dynamic properties and disturbances, and mode-of-use dependent performance specifications, constitute real challenges in achieving *optimal* performance in current and future high-tech systems using merely model-based approaches. In those cases, the state-of-practice control engineering intuition may fail in achieving optimal performance. To account for changing, uncertain, or unknown dynamics and disturbance characteristics, and enable the satisfaction of accuracy and robustness demands, a lot can be gained by combining or supporting model-based control engineering in future complex high-tech systems with *data-based*, *automated* and *adaptive* performance optimization techniques.

1.2 Extremum-seeking control for data-based optimization

In this dissertation, data-based automated performance optimization of high-tech systems is addressed by an adaptive control technique known as *extremum-seeking control*. Extremum-seeking control is a data-driven and model-free method for optimizing system performance in real-time, by continuously or iteratively adapting system parameters (Krstić and Wang, 2000; Teel and Popović, 2001; Nešić et al., 2010; Tan et al., 2006).

Fig. 1.3 depicts a schematic representation of an extremum-seeking control scheme, which typically consists of 1) a stable or stabilized *system* to-be-optimized, for which we can tune or adapt certain input parameters and measure performance relevant outputs, 2) a user-defined *cost function* to quantify the system performance on the basis of measurable outputs (and inputs), and 3) an *extremum-seeking controller* that utilizes the measured system performance to adapt the system inputs to their performance-optimal values. The majority of extremum-seeking control techniques in the literature assume that, for constant input parameters to the stable system, the (transient) dynamic behavior is

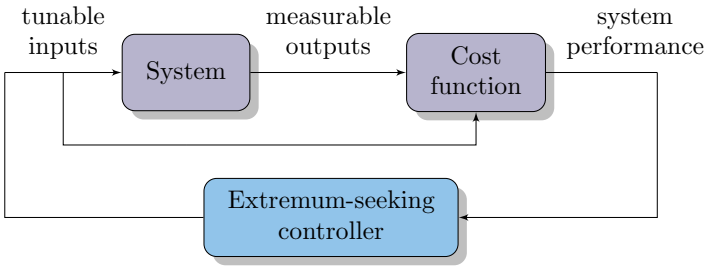

Figure 1.3: A schematic representation of an extremum-seeking control scheme.

sufficiently fast and all outputs of the system converge to constant steady-state outputs, so-called equilibria solutions. In particular, the general requirement in the extremum-seeking control literature is the existence of a *time-invariant, parameter-to-steady-state performance map*, the extremum of which corresponds to the optimal steady-state (equilibrium) plant performance (Krstić and Wang, 2000; Teel and Popović, 2001; Tan et al., 2006; Nešić et al., 2010; Guay and Dochain, 2015). On the basis of an appropriate exploration of the system to-be optimized, and without any (mathematical) models of the system or knowledge about the performance map, extremum-seeking control is able to utilize the measurements of the system performance and steer the tunable system inputs to that extremum.

Due to its model-free nature, extremum-seeking control is especially valuable in cases where the dynamic behavior of the system at hand can not be represented by an accurate or comprehensible model, or cases where the disturbances are unknown, changing, or mode-of-use dependent. As a result, extremum-seeking control and its practical application has been studied in many different engineering domains, such as, e.g., internal combustion engines (Popović et al., 2006; Killingsworth et al., 2009; van der Weijst et al., 2019; Mohammadi et al., 2014), continuous variable transmissions (CVTs) (van der Meulen et al., 2012; van der Meulen et al., 2014), anti-lock braking (ABS) systems (Drakunov et al., 1995; Zhang and Ordónez, 2007; Dinçmen et al., 2014), nuclear fusion (Centioli et al., 2005; Carnevale et al., 2009; Bolder et al., 2012; Lanctot et al., 2016), light source systems for (EUV) lithography, (Ren et al., 2012), wind turbines (Creaby et al., 2009; Johnson and Fritsch, 2012; Ghaffari et al., 2014; Xiao et al., 2019), process and reaction systems (Wang et al., 1999; Guay et al., 2004; Bastin et al., 2009; Dewasme et al., 2011), and high-precision motion systems (Haring et al., 2013; Hunnekens et al., 2015). More examples of application domains of extremum-seeking control are provided in the survey by Tan et al. (2010) and references therein.

1.2.1 Extremum-seeking control frameworks

Throughout the literature, two main extremum-seeking approaches to exploration and optimization of general nonlinear systems can be identified. Namely, so-called *continuous-time* approaches (see Fig. 1.4), and *discrete* or *sampling-based* approaches (see Fig. 1.5). In continuous-time extremum-seeking control approaches, optimization and exploration are performed continuously and simultaneously, while in sampling-based approaches, exploration is done through sequential step-wise input variations and periodically-sampled output measurements, and in which the optimization step is performed after the exploration sequence is completed. Here, both approaches are briefly discussed.

Continuous-time extremum-seeking control

The working principle of the classical continuous-time extremum-seeking control approach is schematically depicted in Fig. 1.4, see, e.g., Krstić and Wang (2000) and Nešić et al. (2010). The scheme consists of the to-be-optimized dynamical system and a user-defined cost function, a gradient estimator, and an optimizer. For the dynamical system with cost function, it is assumed that there exists a (unknown) static input-output relation between the (constant) system inputs and the steady-state performance, denoted by F. Typically, the requirements for the existence of such a static input-output relation have been formalized in terms of (globally) asymptotic or exponential stability properties for dynamical systems that admit equilibria solutions in steady-state for constant system inputs, see, e.g., Krstić and Wang (2000), Tan et al. (2006), Nešić et al. (2010). In particular, the static input-output relation between the system inputs and the steady-state performance of a dynamical system is characterized by these equilibria solutions, which are dependent on the constant system inputs. Exploration of the input-output performance map F is usually done by perturbing the system inputs with sinusoidal perturbation signals, so-called sinusoidal dither signals (see the system input u depicted by (—) in Fig. 1.4). On the basis of the correlation between this continuous excitation and the continuously measured outputs, the gradient estimator provides continuously an approximate gradient of the input-output mapping, and hence the means to locate an extremum. Various gradient estimators are proposed in the literature. In, e.g., Krstić and Wang (2000) and Tan et al. (2006), band-pass filters are used to extract gradient information on the input-output map F from the measured outputs. In Haring et al. (2013), a moving average filter for gradient estimation is proposed. In, e.g., Haring (2016) and Moase and Manzie (2012), observers are employed to provide a gradient estimate. Then, on the basis of the gradient estimation, a gradient-based optimizer is typically employed to steer the tunable system input towards its minimizer in real-time.

An important aspect in (continuous-time) extremum-seeking control is the *time-scale separation* between the various elements in the extremum-seeking con-

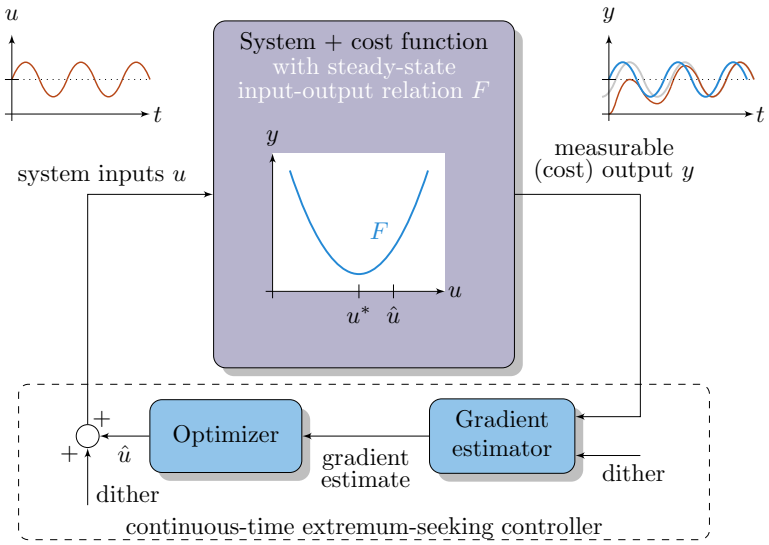

Figure 1.4: A schematic representation of the continuous-time extremum-seeking control framework. The outputs depicted by (—), (—), and (—), denote the static output $F(u)$, the steady-state system output $\bar{y}(t)$, and the system output $y(t)$, respectively.

trol scheme, which explains the typical trade-off between accuracy and convergence speed in extremum-seeking control. Namely, the measured system output y, depicted by (—) in Fig. 1.4, as used by the gradient estimator, differs from the steady-state performance F, depicted by (—) in Fig. 1.4, since the output measurement y also contain transient behavior of the system dynamics and the dynamical effect of the supplied perturbations in the system inputs. Typically, the supplied perturbations are designed to be small and slow enough. A small perturbation amplitude allows for a more accurate gradient estimate of F around the nominal input parameter $\hat{u}$. In the presence of system dynamics, a slow perturbation signal can lead to a measured output y, which suffers less from transients and phase delay, leading to a better approximation of the steady-state performance map F around $\hat{u}$. However, in general, for a properly working extremum-seeking control scheme, it is required that the dynamical system operates on the fastest time-scale, the periodic perturbation operates on a medium time-scale, and the gradient estimator with optimizer operates on the slowest time-scale (Krstić and Wang, 2000). As a result, slow periodic perturbation signals for improved accuracy of extremum-seeking schemes typically comes at the expense of a deterioration of convergence speed.

The required time-scale separation typically limits the convergence speed of extremum-seeking schemes. Nevertheless, the idea of time-scale separation between the adaptation mechanism and the system dynamics is important to be able to reach the unknown extremum in this dynamic context. Moreover, the time-scale separation has also been exploited in the analysis of stability of many closed-loop extremum-seeking schemes, see, e.g., Krstić and Wang (2000), Tan et al. (2006), Dürr et al. (2017), Nešić et al. (2010), Haring et al. (2013), Nešić (2009). Specifically, in Tan et al. (2006), Haring et al. (2013), and Nešić (2009), it is shown that *semi-global practical asymptotic stability* of the closed-loop extremum-seeking scheme is achievable under appropriate conditions. In particular, it is shown, under appropriate assumptions, that for an arbitrarily large set of initial conditions for the dynamical system and the extremum-seeking controller, there exist settings for the extremum-seeking controller so that all solutions of the closed-loop extremum-seeking scheme converge to an arbitrarily small neighborhood of the extremum (see Tan et al. (2006, Definition 1) for a more rigorous definition of semi-global practical asymptotic stability). Reducing the extremum-seeking controller parameters such as the perturbation amplitude, perturbation frequency, and optimizer gain, typically increases the domain of attraction and reduces the size of the neighborhood of convergence. However, the improved convergence accuracy by reduction of these parameters often comes at the expense of a reduced convergence speed of the closed-loop extremum-seeking schemes.

Extensions to the classical continuous-time extremum-seeking control framework have been provided in the literature to, e.g., improve convergence speed and accuracy of the closed-loop extremum-seeking scheme. In Krstić (2000), dynamic compensators are added to the extremum-seeking scheme to improve convergence speed. In Tan et al. (2008), the use of different non-sinusoidal periodic perturbations in an extremum-seeking context is studied to enable faster convergence to the extremum. Dither signals with a time-varying amplitude are studied that can lead to asymptotic convergence to the extremum (Stanković and Stipanović, 2010; Moura and Chang, 2013; Haring and Johansen, 2018) as opposed to often practical asymptotic convergence to the extremum. Using time-varying dither amplitudes can even lead to the ability to find the global extremum amongst multiple local extrema (Tan et al., 2008; Nešić, 2009). Even dither-free or self-driving approaches have emerged, which can lead to faster and asymptotic convergence to the extremum as well, but without the disadvantage of externally supplied excitations (Frait and Eckman, 1962; Carnevale et al., 2009; Hunnekens et al., 2014; Castanos and Kunusch, 2015; Haring, 2016). For systems with a so-called (Wiener-)Hammerstein structure, that is, a series connection of (linear dynamics followed by) a static nonlinearity and linear dynamics, and under the assumption that prior knowledge about the system's relative order is available, arbitrarily fast convergence of the extremum-seeking scheme is achievable under high-frequency perturbation (Atta and Guay., 2017;

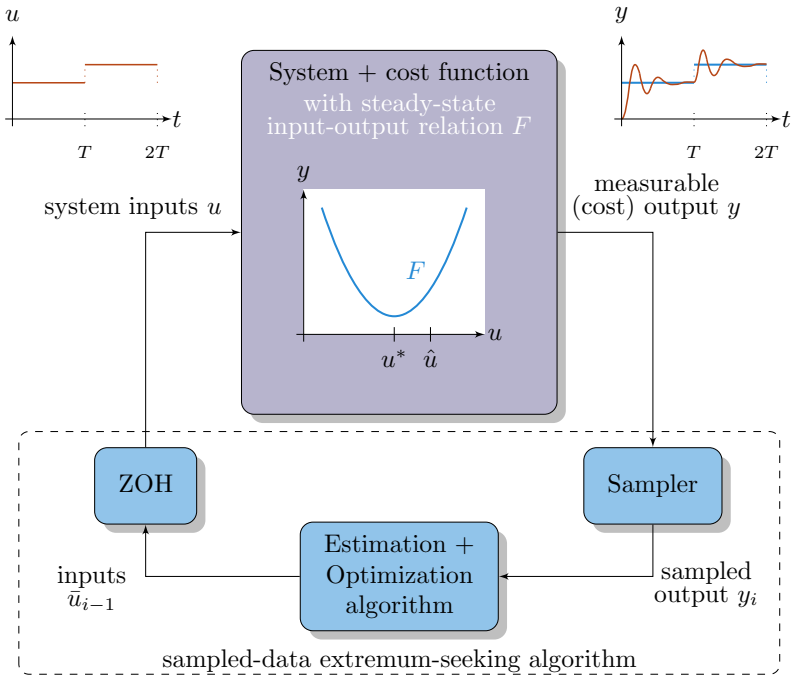

Figure 1.5: A schematic representation of the sampled-data extremum-seeking control framework. The outputs depicted by (—), and (—) denote the static output $F(u)$, and the system output $y(t)$, respectively.

Moase and Manzie, 2012; Moase and Manzie, 2012).

Sampled-data extremum-seeking control

The working principle of the sampled-data extremum-seeking control approach is schematically depicted in Fig. 1.5, see, e.g., Teel and Popović (2001), Kvaternik and Pavel (2011) and Khong et al. (2013b). The sampled-data scheme consists of the interconnection of the to-be-optimized dynamical system and a user-defined cost function, a T-periodic sampler, a zero-order-hold, and some (discrete-time) optimization algorithm. Similar to the continuous-time setting, it is assumed that there exists a (unknown) static input-output relation between the system inputs and the steady-state performance, denoted by F. Also, the requirements for the existence of such a static input-output relation have been formalized in terms of (globally) asymptotic or exponential stability properties for dynamical systems that admit equilibria solutions in steady-state for constant system inputs, see, e.g., Teel and Popović (2001), Kvaternik and Pavel (2011), Khong

et al. (2013b). In this sampled-data context, exploration of the input-output performance map F is done by supplying a sequence of n step-like inputs to the system (see the system input u depicted by (—) in Fig. 1.5), and, for each step input and after a user-defined waiting time $T > 0$, the output measurement y, depicted by (—) in Fig. 1.5, is sampled and stored. The waiting time T is selected sufficiently long and the step-size is typically selected small, such that the transient behavior of the system dynamics has sufficiently decayed and the output measurements indeed reflect the steady-state performance of the system. The tuning guidelines for the waiting time and step size are the sampled-data equivalent of the tuning guidelines for the perturbation frequency and amplitude of the dither signals in the continuous-time extremum-seeking context. On the basis of a suitable discrete-time optimization algorithm, dedicated step-like inputs, and the T-periodically sampled outputs, an update of the input after nT seconds can be realized using the optimization algorithm that will bring the nominal input closer to the extremum. For example, a gradient-descent optimization algorithm can be employed, the gradient of which can be estimated by using finite difference computations, and for which the elements of the finite difference computation can be obtained by supplying $n = 2$ distinct inputs and sampling the respective system outputs, see, e.g., Teel and Popović (2001), Khong et al. (2013).

Different from the continuous-time approach in, e.g., Krstić and Wang (2000), which comes with certain smoothness requirements on the dynamics of the system, assumptions of convexity on the steady-state performance map, and for which the extremum-seeking controller is typically gradient-based, the periodic sampled-data framework in Teel and Popović (2001) allows for the use of a wide class of smooth and nonsmooth optimization algorithms for achieving optimization of a larger class of nonlinear, possibly infinite-dimensional, dynamical systems. Namely, the sampled-data extremum-seeking framework in Teel and Popović (2001) requires less stringent assumptions on the system dynamics and convergence properties of the extremum-seeking algorithms. Additionally, the sampled-data framework in Khong et al. (2013b), which provides an extension of the work in Teel and Popović (2001), also encompasses sampling-based (global) optimization methods capable of non-convex optimization, enabling extremum seeking for an even wider class of (global) optimization problems, see, e.g., Khong et al. (2013a). Namely, their framework relies on the notion of attractivity as opposed to asymptotic stability of the extremum-seeking algorithms, allowing sampling-based, global optimization algorithms such as the so-called DIRECT and Shubert algorithms (see Jones et al. (1993) and Shubert (1972), respectively) for non-convex optimization problems.

1.2.2 Challenges for optimization of high-tech systems

Both the continuous-time and sampled-data extremum-seeking control frameworks have proven successful in many engineering domains. Moreover, many extensions and adaptations to, and analysis tools for, the classical continuous-time and sampled-data extremum-seeking control methods in Krstić and Wang (2000) and Teel and Popović (2001), respectively, are provided throughout the literature. However, for data-based performance optimization in the context of high-tech systems, the state-of-practice extremum-seeking control methods face three major challenges which we discuss here.

Optimization of time-varying steady-state behavior in high-tech systems

In the first place, extremum-seeking control methods are tailored primarily towards the steady-state performance optimization of systems that admit *equilibria solutions* (Krstić and Wang, 2000; Tan et al., 2006; Nešić et al., 2010), or *periodic* system responses with a *known* period time (Haring et al., 2013; Wang and Krstić, 2000; Guay et al., 2007). Performance of high-tech systems, however, is generally related to *generically time-varying steady-state behavior*, and the dynamical behavior of these high-tech systems is heavily dependent on (time-varying) disturbances, reference trajectories, and the operating condition at hand. In particular, time-varying system behavior emerges, for example, in reference tracking or disturbance attenuation problems, which are encountered, for example, in industrial motion systems, such as, pick-and-place systems (van Loon et al., 2016), electron microscopes, and wafer scanning systems (Heertjes and Nijmeijer, 2012; Heertjes et al., 2009). To enable extremum-seeking control for data-based performance optimization of time-varying steady-state behavior in high-tech systems, it is essential to consider generically time-varying disturbances and the resulting to-be-optimized system performance in terms of generically time-varying state responses an integral part of the extremum-seeking control problem formulation.

Sampled-data extremum-seeking and constrained optimization

In the second place, extremum-seeking control methods are generally focussed on finding tunable system parameters that optimize steady-state system performance. However, many complex high-tech systems also have to deal with constraints on operating conditions, originating from *constraints on measurable variables*, while the relation between the constraints and the system inputs is unknown. Indeed, constraints on measurable variables are typically unknown in terms of their relationship with the tunable parameters. These constraints may conflict with the otherwise performance-optimal operational condition of these (high-tech) systems, and should be taken into account in the extremum-seeking optimization procedure. Extremum-seeking approaches for constrained

optimization problems with unknown but measurable constraint functions are studied in, e.g., Srinivasan et al. (2008), Guay et al. (2015), Dürr et al. (2013), van der Weijst et al. (2019), Ramos et al. (2017) and Liao et al. (2019), however, solely in the continuous-time extremum-seeking setting. The sampled-data extremum-seeking setting, however, is compelling, given the larger class of nonlinear, possibly infinite-dimensional, systems it addresses, and the potential of including diverse types of optimization algorithms (Teel and Popović, 2001; Khong et al., 2013b). This would allow the use of extremum-seeking control for a richer class of optimization problems, relevant in the scope of the performance optimization of high-tech systems.

Transient performance optimization in high-tech systems

In the third place, extremum-seeking control is aimed at finding *constant* input parameters that optimize the steady-state behavior of dynamical systems, while *transient behavior* in many high-tech systems may impair the achievable performance. Data-driven, transient performance optimization techniques such as, e.g., iterative learning control (ILC) (Moore et al., 1993; Longman, 2000; Steinbuch and van de Molengraft, 2000; Bristow et al., 2006), and repetitive control (RC) (Wang et al., 2009; Hara et al., 1988), are able to improve (transient) performance of industrial systems that perform time-varying, repetitive tasks or are subject to time-varying, repetitive disturbances. However, classical ILC and RC require (accurate) model knowledge to achieve and guarantee fast convergence, while extremum-seeking control is able to deal with unknown, uncertain, time-varying and general nonlinear systems. Extremum-seeking control in the context of iterative learning control and optimizing transient behavior has been studied in, e.g., Killingsworth and Krstic (2006), Ren et al. (2012), Frihauf et al. (2013), Khong et al. (2016), Benosman (2016). Killingsworth and Krstic (2006) and Benosman (2016) iteratively tune PID controllers having constant gains, and in Ren et al. (2012) and Khong et al. (2016) a time-varying, step-like system input signal is tuned. However, system performance may benefit from a more generic, time-varying, system input obtained through extremum-seeking control to shape the transient behavior of general nonlinear systems.

1.3 Objectives and contributions of the dissertation

This dissertation presents novel extremum-seeking control methods that enable data-based performance optimization for a richer class of optimization problems, such as i) the data-based optimization of generic time-varying system behavior, ii) data-based, constrained optimization on the basis of measurable to-be-optimized objective function and constraint functions, and iii) data-based, transient performance optimization for repetitive system operations on fixed-time intervals. The developments in this dissertation in data-based optimization

through extremum-seeking control are inspired by a large variety of industrially-relevant optimization problems, and are experimentally demonstrated to illustrate their value in supporting model-based control engineering.

First, the main objectives of this dissertation are highlighted. Second, the contributions of this dissertation are outlined.

1.3.1 Objectives

In view of the challenges described in Section 1.2, we can formulate four main objectives of this dissertation. The first objective can be formalized as follows:

Objective 1. *Develop an extremum-seeking control method for the data-based optimization of time-varying steady-state responses of general nonlinear systems, which is applicable for the optimization of time-varying behavior in industrial high-tech systems.*

The second objective can be formalized as follows:

Objective 2. *Develop a sampled-data extremum-seeking control framework for data-based constrained optimization of nonlinear dynamical systems, in which information on system performance and constraints on system inputs is solely obtainable through output measurements.*

The third objective can be formalized as follows:

Objective 3. *Develop a sampled-data extremum-seeking control method for optimization of transient system behavior, inspired by and applicable to optimization of time-varying, repetitive tasks in high-tech positioning systems.*

The fourth objective can be formalized as follows:

Objective 4. *Implementation and validation of the developed extremum-seeking control methods in industrially-relevant case studies.*

The main contributions of this dissertation are outlined in the next section.

1.3.2 Contributions

The five main contributions of this dissertation are directly related to the four objectives mentioned above.

Contribution 1. The first main contribution, addressing **Objective 1** and presented in Chapter 2, is the development of a novel *extremum-seeking control approach for optimization of generically time-varying steady-state behavior of nonlinear dynamical systems.* In particular, an extension of the class of extremum-seeking problems from those involving equilibria solutions or periodic

time-varying steady-state responses, to those involving systems exhibiting generically time-varying steady-state responses is provided. Generically time-varying disturbances and the resulting to-be-optimized performance, characterized in terms of generically time-varying steady-state system responses, are considered an integral part in the extremum-seeking control problem formulation. The convergent systems property is exploited, being the time-varying analogue of the global exponential stability property for systems with equilibria solutions as commonly exploited in the extremum-seeking control literature, and is essential in this generic, time-varying extremum-seeking context. A series connection of a user-defined static cost function and user-defined generic filter structure, the so-called dynamic cost function, is introduced to facilitate the use of extremum seeking control in this more generic, time-varying context. Semi-global practical asymptotic stability of the closed-loop extremum-seeking control scheme is proven in the presence of bounded and time-varying external disturbances.

Contribution 2. The second contribution, addressing **Objective 1** and presented in Chapter 3, is a novel extension of the observer-based extremum-seeking control strategy for optimization of generically time-varying steady-state behavior of nonlinear dynamical systems, exploited in Chapter 2. The extended approach exploits knowledge about the user-defined dynamic cost function in the observer-based extremum-seeking control strategy employed in Chapter 2 to cope with the additional time-scale introduced by the dynamic cost function, and facilitates enhanced convergence speed of the resulting extremum-seeking control scheme. Moreover, a stability analysis for this extended approach is performed.

Contribution 3. The third contribution, addressing **Objective 2** and presented in Chapter 4, is the development of a *sampled-data extremum-seeking control framework for constrained optimization of nonlinear dynamical systems.* In particular, an extension of the classical sampled-data extremum-seeking framework is provided that encompasses 1) a class of dynamical systems in which both the to-be-optimized objective function and the constraint functions are available through measurement only, and 2) a class of smooth and nonsmooth optimization algorithms to facilitate extremum-seeking in the presence of unknown but measurable constraints, inspired by the use of barrier function methods. Under the assumption that the initialization of the system inputs yield operating conditions that do not violate the constraints, it is proven that 1) the resulting closed-loop dynamics is stable, 2) steady-state constraint satisfaction of the inputs is guaranteed for all iterations of the optimization process, and 3) constrained optimization is achieved.

Contribution 4. The fourth contribution, addressing **Objective 3** and presented in Chapter 5, is the development of an *iterative learning control strategy based on extremum-seeking control for high-accuracy repetitive setpoint control of frictional motion systems.* First, a novel proportional-integral-derivative-based

controller with a time-varying integrator gain design is proposed that facilitates improved time-domain behavior in terms of overshoot and setpoint accuracy for repetitive motion in frictional motion systems. Second, on the basis of a suitable basis function parametrization, the optimal time-varying integrator gain design is obtained through an automatic iterative controller tuning procedure based on a sampled-data extremum-seeking algorithm, ensuring optimal setpoint positioning accuracy despite unknown friction characteristics and unknown disturbances.

Contribution 5. The fifth contribution, addressing **Objective 4**, is the implementation and (experimental) validation of the Contributions 1 to 4 in industrially-relevant case studies. The working principle of the developed extremum-seeking method for optimization of time-varying steady-state system behavior in Chapter 2, and described in Contribution 1, is illustrated in simulation by means of the real-time performance optimal tuning of a nonlinear control strategy for a motion control application. The effectiveness of the extremum-seeking control methods for optimization of time-varying steady-state system behavior in Chapters 2 and 3, and described in Contributions 1 and 2, respectively, are both evidenced experimentally in Chapter 3 by application to an industrial motion stage set-up which represents the short-stroke motion of a wafer stage system commonly found within lithography systems. The working principle of the proposed sampled-data extremum-seeking framework for constrained optimization in Chapter 4, and described in Contribution 3, is illustrated by means of a representative industrial case study of constrained optimization of extreme ultraviolet light generation in a laser produced plasma source system within a state-of-the-art lithography system. The effectiveness of the proposed approach for transient performance optimization in Chapter 5, and described in Contribution 4, is evidenced experimentally by application to an industrial nano-positioning motion stage set-up of a high-end electron microscope.

1.4 Outline of the dissertation

This dissertation consists of three parts; Part I, entitled *Continuous-time extremum-seeking control*, consists of Chapters 2 and 3, part II, entitled *Sampled-data extremum-seeking control*, consists of Chapters 4 and 5, and part III, entitled *Closing*, consists of Chapter 6. All chapters, except Chapter 6, are based on research papers, and are therefore self contained and can be read independently.

Part I: Continuous-time extremum-seeking control

Chapters 2 and **3** present novel continuous-time extremum-seeking control methods for the optimization of time-varying steady-state responses of general nonlinear systems. In **Chapter 2**, the effectiveness of the approach is illustrated

by the real-time performance optimal tuning of a nonlinear control strategy for a motion control application.

In **Chapter 3**, an extension of the continuous-time extremum-seeking control method from Chapter 2 is presented, which enables enhanced convergence speed of the extremum-seeking scheme compared to the one in Chapter 2. In **Chapter 3**, the methods presented in Chapters 2 and 3 are experimentally demonstrated for the performance-optimal tuning of a variable-gain control strategy employed on a high-accuracy industrial motion stage set-up.

Part II: Sampled-data extremum-seeking control

Chapter 4 presents a sampled-data extremum-seeking control framework for constrained optimization of nonlinear dynamical systems. The working principle of the proposed framework is illustrated by means of an industrial case study of the constrained optimization of extreme ultraviolet light generation in a laser-produced plasma source within a state-of-the-art lithography system.

Chapter 5 presents a novel proportional-integral-derivative (PID) based feedback controller with a time-varying integrator gain design to enable superior setpoint performance for frictional motion systems in a repetitive motion setting. A sampled-data extremum-seeking control architecture is employed to ensure optimal setpoint positioning accuracy and enable transient performance optimization. The method is evidenced experimentally by application to an industrial nano-positioning motion stage set-up of a high-end electron microscope.

Part III: Closing

Chapter 6 presents conclusions and recommendations for future research.

1.5 Dissertation as part of research programme CHAMeleon

The research presented in this dissertation has been performed within the research programme *CHAMeleon: Hybrid solutions for cost-aware high-performance motion control*. This project is (partly) financed by the Netherlands Organisation for Scientific Research (NWO) under project number 13896.

The objective envisioned in this research programme is to develop novel control techniques that are able to cope with the tradeoffs between, on the one hand, system cost and performance, and on the other hand, system performance and adaptability to changing operating conditions. Moreover, the research programme envisions these novel control techniques to have practical value in the high-tech systems industry. The research programme consists of two main topics. Topic I focusses on the development of novel control strategies that i) are able to deal with nonlinear effects in high-tech (motion) systems such as, e.g., friction, originating from the use of cost-aware hardware components, and ii)

venture beyond the state-of-practice, often linear, control strategies, to overcome fundamental limitations in linear motion control by means of hybrid and nonlinear control solutions. Topic II involves the development of data-driven performance optimization techniques to ensure optimal performance in diverse, uncertain, and changing conditions of machine usage.

The research reported in this dissertation has been mainly devoted to Topic II. Chapters 2 and 3 present novel data-driven performance optimization techniques to cope with generic time-varying system behavior, and enable optimal performance in complex high-tech systems. Chapter 4 presents a novel framework in which data-driven, constrained performance optimization for generic dynamical systems is achievable, ensuring optimal and safe operating conditions of machine usage. Additionally, in Chapter 5 a novel control architecture has been proposed to enable high-accuracy repetitive positioning of frictional motion systems, which benefits from similar optimization techniques as developed in Chapter 4, but at the same time contributes to Topic I.

All contributions in this dissertation are inspired by case studies from the high-tech systems industry amongst others, and (experimental) validation of the developments in this dissertation are done in collaboration with the industrial partners ASML and Thermo Fisher of the research programme.

Part I

Continuous-Time Extremum-Seeking Control

Chapter 2

Extremum-seeking control for optimization of time-varying steady-state responses of nonlinear systems

Abstract - *Extremum-seeking control is a useful tool for the steady-state performance optimization of plants for which limited knowledge about its dynamical behavior and disturbance situation is known. The case when the steady-state plant responses correspond to equilibrium solutions received a lot of attention. However, in many industrial applications plant performance is characterized by time-varying steady-state behavior, generally induced by complex disturbances and reference trajectories. In those cases, no static parameter-to-steady-state performance map can be defined, which limits state-of-practice extremum-seeking control approaches in achieving optimal system performance. In this chapter, an extremum-seeking control method is proposed for optimization of generically time-varying steady-state behavior of nonlinear dynamical systems. Generically time-varying disturbances and the resulting to-be-optimized performance, characterized in terms of generically time-varying steady-state system responses, are considered an integral part in the extremum-seeking control problem formulation. The proposed extremum-seeking control method utilizes a so-called dynamic cost function to cope with time-varying steady-state responses of general nonlinear systems, and enables securing performance-optimal operating conditions. Semi-global practical asymptotic stability of the closed-loop extremum-seeking control scheme is proven in the presence of bounded and time-varying external disturbances. Moreover, the working principle of the extremum-seeking control method is illustrated by means of the real-time performance-optimal tuning of a nonlinear control strategy for a motion control application.*

The content of this chapter is based on: L. Hazeleger, M. Haring, N. van de Wouw, Extremum-seeking control for optimization of time-varying steady-state responses of nonlinear systems. Automatica (2020) 109068, https://doi.org/10.1016/j.automatica.2020.109068.

2.1 Introduction

In most of the work on extremum-seeking control (ESC), the general requirement for optimizing performance of a stable or stabilized plant is the existence of a (unknown) time-invariant parameter-to-steady-state performance map, i.e., a *static* input-output relation between tunable plant parameters and the steady-state plant performance, the extremum of which corresponds to the optimal steady-state (equilibrium) plant performance, see, e.g., Krstić and Wang (2000), Teel and Popović (2001), Tan et al. (2006), Nešić et al. (2010), Dürr et al. (2017), and Guay and Dochain (2015). In those references, the requirements for the existence of such a static input-output relation have been formalized in terms of stability properties for dynamical systems that admit *equilibria* solutions in steady-state. Even in the presence of (high-frequency) measurement noise, see, e.g., Zhang and Ordónez (2009), Stanković and Stipanović (2010), Fu and Özgüner (2011), Tan et al. (2010), Haring and Johansen (2018), and Haring (2016), extremum-seeking in the equilibrium setting to a neighborhood of the optimum can be achieved, the size of which is often dependent on the noise level. However, in many (industrial) applications plant performance is generally related to *generic, time-varying* steady-state plant behavior. In those cases, no static parameter-to-steady-state performance map can be defined, limiting state-of-practice extremum-seeking control approaches in achieving optimal system performance. Time-varying plant behavior emerges, for example, in reference tracking or disturbance attenuation problems, which are encountered, for example, in industrial motion systems, such as, pick-and-place systems (van Loon et al., 2016), electron microscopes, and wafer scanning systems (Heertjes and Nijmeijer, 2012; Heertjes et al., 2009). In those examples, optimal steady-state plant performance and the corresponding optimal tuning of plant parameters are heavily dependent on the (time-varying) disturbance situation and reference trajectory at hand. Therefore, it is essential to consider generically time-varying disturbances and the resulting to-be-optimized plant performance in terms of generically time-varying steady-state responses an integral part of the ESC problem formulation for performance optimization of time-varying steady-state plant behavior.

In Wang and Krstić (2000), Guay et al. (2007), and Haring et al. (2013), ESC approaches have been proposed to deal with time-varying, *periodic* steady-state plant behavior. Key in the proposed approaches is the design of a cost function that defines a constant performance measure in terms of the periodic steady-state plant response. In Wang and Krstić (2000), a so-called detector is proposed that is able to capture the amplitude of sinusoidal-like limit cycle responses, and has been exploited in, e.g., resonant mode-matching of vibrating gyroscopes (Antonello et al., 2009), sawtooth period control in tokamaks (Bolder et al., 2012), instability control of gas turbine combustors (Banaszuk et al., 2004), and suppression of subsonic cavity flow resonances (Kim et al.,

2009). In Guay et al. (2007), a class of differentially flat periodic nonlinear systems is considered. By exploiting flatness and explicit plant knowledge, a period of the periodic steady-state plant output and the corresponding steady-state plant performance are computed. In Höffner et al. (2007), a similar approach is pursued for a class of periodic Hamiltonian systems. In Haring et al. (2013), general nonlinear plants with arbitrary periodic steady-state responses with known period time are considered. A cost functional based on an $\mathcal{L}^p$-norm, evaluated over the *known* periodic time interval, is employed that links periodic steady-state responses to a time-invariant performance measure. In Hunnekens et al. (2015), this method was experimentally demonstrated for the adaptive design of variable-gain controllers for a motion control application. In many (industrial) applications, however, the steady-state response characterizing system performance is generically time-varying, and periodicity of the steady-state response is not evident due to the fact that responses can be induced by complex time-varying (non-periodic) disturbances and reference signals. In such generic cases, a static parameter-to-steady-state performance map may not be readily defined as in the periodic cases in Hunnekens et al. (2015), Wang and Krstić (2000), and Haring et al. (2013).

In this chapter, an extremum-seeking control method is proposed to optimize generic time-varying steady-state behavior of general nonlinear systems. The method utilizes a so-called *dynamic cost function* to cope with the time-varying system behavior, and allows for the characterization of a time-invariant parameter-to-steady-state performance map. The ESC problem formulation presented in this chapter generalizes the work in Haring and Johansen (2018) in the sense that, in this work, generically time-varying disturbances and resulting to-be-optimized performance characterized in terms of generically time-varying steady-state responses are considered an integral part of the ESC problem formulation. In general, we extend the class of problems from those involving dynamical systems admitting equilibria solutions, as mostly considered in ESC literature, or periodically time-varying steady-state responses in Wang and Krstić (2000), Guay et al. (2007), and Haring et al. (2013), to those involving systems exhibiting generically time-varying steady-state responses. We prove semi-global practical asymptotic stability of the closed-loop extremum-seeking control scheme that includes general nonlinear systems subject to bounded and time-varying external disturbances. The region to which the ESC scheme converges can be made arbitrarily small, even in the presence of generically time-varying, bounded disturbances. Moreover, the working principle of the extremum-seeking control method is illustrated by means of the real-time performance-optimal tuning of a nonlinear control strategy for a motion control application within an industrial wafer scanner exhibiting time-varying steady-state responses.

Other works, which have studied extremum-seeking control in the presence of time-varying system behavior, are, e.g., Scheinker and Krstić (2014), Scheinker and Scheinker (2016) and Scheinker and Krstić (2013). In these references,

extremum-seeking controllers are utilized directly as feedback controller, able to, on the one hand, control unstable and time-varying input-affine systems, and on the other hand, optimize steady-state equilibria in the presence of noise. We care to emphasize that, in this chapter, we consider the problem of optimizing time-varying steady-state responses of stable or stabilized plants, which is a different problem from the one considered in Scheinker and Krstić (2014), Scheinker and Scheinker (2016) and Scheinker and Krstić (2013). Moreover, we remark that the methods in Scheinker and Krstić (2014), Scheinker and Scheinker (2016) and Scheinker and Krstić (2013) typically rely on high dither frequencies relative to the time-varying system dynamics, while the ESC method proposed in this chapter can employ small dither frequencies relative to the time-varying system dynamics, even in the presence of high-frequency disturbances. Additionally, in the case of extremum-seeking control for already stable or stabilized systems, the class of systems considered in this chapter is more general.

ESC for slowly time-varying performance maps is considered in, e.g., Grushkovskaya et al. (2017), Sahneh et al. (2012), Cao et al. (2017), Fu and Özgüner (2011), and Rušiti et al. (2019). Herein, optimal plant performance is obtained by tracking optimal, slowly time-varying, plant parameters. We remark that this problem setting is different from the one considered in this chapter. Namely, we consider the problem of optimizing *static* performance maps in the spirit of Hunnekens et al. (2015), Wang and Krstić (2000), and Haring et al. (2013), although more general in terms of the time-varying nature of the disturbances. We propose an ESC method that seeks *constant* plant parameter settings that optimize steady-state plant performance in terms of time-varying steady-state system responses.

The main contributions of this chapter can be summarized as follows. The first contribution is the proposition of an ESC approach for the optimization of *general, time-varying* steady-state responses of general nonlinear systems. A so-called dynamic cost function in terms of generically time-varying output responses is utilized, allowing for the characterization of a time-invariant parameter-to-steady-state performance map. The second contribution is a semi-global practical stability analysis of the closed-loop ESC scheme that includes general nonlinear systems that are subject to bounded and time-varying external disturbances. The region to which the ESC scheme converges can be made arbitrarily small, even in the presence of generically time-varying, bounded disturbances. The third contribution is a demonstration of the ESC approach by means of a case study of the performance-optimal tuning of a nonlinear control strategy for a motion control application.

The chapter is organized as follows. Section 2.2 presents the problem formulation. Section 2.3 gives the extremum-seeking controller. In Section 2.4, the semi-global practical asymptotic stability result is stated and proven. In Section 2.5, an industrial case study is provided. Section 2.6 closes with conclusions.

2.2 Extremum-seeking control problem formulation for optimization of time-varying steady-state system responses

Consider the following generic description of a multiple-input-multiple-output nonlinear system:

$$\Sigma_p : \begin{cases} \dot{\mathbf{x}}(t) = \mathbf{f}(\mathbf{x}(t), \mathbf{u}(t), \mathbf{w}(t)) \\ \mathbf{e}(t) = \mathbf{g}(\mathbf{x}(t), \mathbf{u}(t), \mathbf{w}(t)), \end{cases} \tag{2.1}$$

where $\mathbf{x} \in \mathbb{R}^{n_\mathbf{x}}$ denotes the state of the system, $\mathbf{u} \in \mathbb{R}^{n_\mathbf{u}}$ denotes the input of the system, $\mathbf{e} \in \mathbb{R}^{n_\mathbf{e}}$ denotes the output of the system, $\mathbf{w} \in \mathbb{R}^{n_\mathbf{w}}$ are disturbances, and $t \in \mathbb{R}$ is time. In the context of ESC, Σ_p represents the system to be optimized, where the input $\mathbf{u}$ can be regarded as a vector of tunable system parameters, the output $\mathbf{e}$ can be regarded as a vector of measured performance variables, and $\mathbf{w}$ are piecewise continuous (time-varying) disturbances, defined and bounded on $t \in \mathbb{R}$. We denote this class of disturbances by $\overline{\mathbb{PC}}_\mathbf{w}$, and define the following set of disturbances:

$$\mathcal{W} := \{\mathbf{w} \in \overline{\mathbb{PC}}_\mathbf{w} : \|\mathbf{w}(t)\| \leq \rho_\mathbf{w} \ \forall \ t \in \mathbb{R}\} \tag{2.2}$$

with $\rho_\mathbf{w} \in \mathbb{R}_{>0}$.

Remark 2.1. *In this chapter, we consider the time-varying disturbances* $\mathbf{w}(t)$ *to be of an external nature. In particular, we consider the external disturbances to be independent of the tunable system inputs* $\mathbf{u}$*. A problem setting in which disturbances are dependent on (variations of) the system inputs, for example, disturbances caused complex interactions between various subcomponents within a complex system which may vary with the tunable system parameters* $\mathbf{u}$*, are not considered in this chapter. On the other hand, the effect of the external disturbances* $\mathbf{w}(t)$ *on the measurable performance variable* $\mathbf{e}$ *may depend on the system inputs* $\mathbf{u}$*.*

Although the functions $\mathbf{f}$ and $\mathbf{g}$ in (2.1) are considered unknown, we adopt the following assumption.

Assumption 2.2. *The functions* $\mathbf{f} : \mathbb{R}^{n_\mathbf{x}} \times \mathbb{R}^{n_\mathbf{u}} \times \mathbb{R}^{n_\mathbf{w}} \to \mathbb{R}^{n_\mathbf{x}}$ *and* $\mathbf{g} : \mathbb{R}^{n_\mathbf{x}} \times \mathbb{R}^{n_\mathbf{u}} \times \mathbb{R}^{n_\mathbf{w}} \to \mathbb{R}^{n_\mathbf{e}}$ *are twice continuously differentiable in* $\mathbf{x}$ *and* $\mathbf{u}$ *and continuous in* $\mathbf{w}$*. Moreover, given any disturbance* $\mathbf{w} \in \mathcal{W}$*, there exist constants* $L_\mathbf{fx}$*,* $L_\mathbf{fu}$*,* $L_\mathbf{gx}$*,* $L_\mathbf{gu} \in \mathbb{R}_{>0}$ *such that*

$$\begin{aligned} \left\| \frac{\partial \mathbf{f}}{\partial \mathbf{x}}(\mathbf{x}, \mathbf{u}, \mathbf{w}) \right\| &\leq L_\mathbf{fx}, \qquad \left\| \frac{\partial \mathbf{f}}{\partial \mathbf{u}}(\mathbf{x}, \mathbf{u}, \mathbf{w}) \right\| \leq L_\mathbf{fu}, \\ \left\| \frac{\partial \mathbf{g}}{\partial \mathbf{x}}(\mathbf{x}, \mathbf{u}, \mathbf{w}) \right\| &\leq L_\mathbf{gx}, \qquad \left\| \frac{\partial \mathbf{g}}{\partial \mathbf{u}}(\mathbf{x}, \mathbf{u}, \mathbf{w}) \right\| \leq L_\mathbf{gu}, \end{aligned} \tag{2.3}$$

for all $\mathbf{x} \in \mathbb{R}^{n_\mathbf{x}}$*, and all* $\mathbf{u} \in \mathbb{R}^{n_\mathbf{u}}$*.*

To define the class of systems considered in the ESC problem setting, we first give a definition of so-called convergent systems which we have adopted from Pavlov et al. (2006). Thereto, consider a system of the form

$$\dot{\mathbf{x}} = \mathbf{F}(\mathbf{x}, t), \tag{2.4}$$

where $\mathbf{x} \in \mathbb{R}^{n_\mathbf{x}}$, $t \in \mathbb{R}$, and $\mathbf{F}(\mathbf{x}, t)$ locally Lipschitz in $\mathbf{x}$ and piecewise continuous in t.

Definition 2.3. *(Pavlov et al., 2006, Section 2.2.1, Definition 2.14). System* (2.4) *is said to be*

- *convergent in a set $\mathcal{X} \subset \mathbb{R}^{n_\mathbf{x}}$ if there exists a solution $\bar{\mathbf{x}}(t)$, called the steady-state solution, satisfying the following conditions:*

  i) $\bar{\mathbf{x}}(t)$ is defined and bounded for all $t \in \mathbb{R}$,
  ii) $\bar{\mathbf{x}}(t)$ is asymptotically stable in $\mathcal{X}$.

- *uniformly convergent in $\mathcal{X}$ if it is convergent in $\mathcal{X}$ and $\bar{\mathbf{x}}(t)$ is uniformly asymptotically stable in $\mathcal{X}$.*
- *exponentially convergent in $\mathcal{X}$ if it is convergent in $\mathcal{X}$ and $\bar{\mathbf{x}}(t)$ is exponentially stable in $\mathcal{X}$.*
- *uniformly exponentially convergent in $\mathcal{X}$ if it is convergent in $\mathcal{X}$ and $\bar{\mathbf{x}}(t)$ is uniformly exponentially stable in $\mathcal{X}$.*

If system (2.4) *is (uniformly, exponentially) convergent in $\mathcal{X} = \mathbb{R}^{n_\mathbf{x}}$, then it is called globally (uniformly, exponentially) convergent.*

From Definition 2.3 we have that, if the system is globally, uniformly convergent, then there exists a $\mathcal{KL}$-function $\beta(r, s)$ such that the solution $\mathbf{x}(t)$ of system (2.6) satisfies

$$\|\mathbf{x}(t) - \bar{\mathbf{x}}(t)\| \leq \beta(\|\mathbf{x}(t_0) - \bar{\mathbf{x}}(t_0)\|, t - t_0). \tag{2.5}$$

The time-dependency of the right-hand side of the system in (2.4) can usually be attributed to some input, for example, a disturbance or a control input. The next definition defines the convergence property for systems with inputs. Thereto, consider a system of the form

$$\dot{\mathbf{x}} = \mathbf{F}(\mathbf{x}, \mathbf{v}(t)), \tag{2.6}$$

with state $\mathbf{x} \in \mathbb{R}^{n_\mathbf{x}}$, input $\mathbf{v} \in \mathbb{R}^{n_\mathbf{v}}$, and $\mathbf{F}(\mathbf{x}, \mathbf{v})$ locally Lipschitz in $\mathbf{x}$ and continuous in $\mathbf{v}$.

Definition 2.4. *(Pavlov et al., 2006, Section 2.2.2, Definition 2.16). System* (2.6) *is said to be (uniformly, exponentially) convergent in $\mathcal{X} \subset \mathbb{R}^{n_\mathbf{x}}$ for a class of inputs $\mathcal{V} \subset \overline{\mathbb{PC}}_\mathbf{v}$ if it is (uniformly, exponentially) convergent in $\mathcal{X}$ for every input $\mathbf{v}(\cdot) \in \mathcal{V}$. In order to emphasize the dependency of the steady-state solution on the input $\mathbf{v}(t)$, it is denoted by $\bar{\mathbf{x}}_\mathbf{v}(t)$.*

The following definition is useful for studying the convergence property of interconnected systems.

Definition 2.5. *(Pavlov et al., 2006, Section 2.2.2, Definition 2.18). System* (2.6) *is said to be (exponentially) input-to-state convergent if it is globally uniformly (exponentially) convergent for the class of inputs* $\overline{\mathbb{PC}}_{\mathbf{v}}$*, and for every input* $\mathbf{v}(\cdot) \in \overline{\mathbb{PC}}_{\mathbf{v}}$ *system* (2.6) *is input-to-state stable (ISS) with respect to the steady-state solution* $\bar{\mathbf{x}}_{\mathbf{v}}(t)$*, i.e., given an input* $\mathbf{v}(\cdot) \in \overline{\mathbb{PC}}_{\mathbf{v}}$ *there exist a* $\mathcal{KL}$*-function* $\beta(r,s)$ *and a* $\mathcal{K}_\infty$*-function* $\gamma(r)$ *such that the solution* $\mathbf{x}(t)$ *of system* (2.6) *corresponding to some perturbed input* $\hat{\mathbf{v}}(t) := \mathbf{v}(t) + \Delta\mathbf{v}(t)$ *satisfies*

$$\|\mathbf{x}(t) - \bar{\mathbf{x}}_{\mathbf{v}}(t)\| \leq \beta(\|\mathbf{x}(t_0) - \bar{\mathbf{x}}_{\mathbf{v}}(t_0)\|, t - t_0) + \gamma\left(\sup_{t_0 \leq \tau \leq t} \|\Delta\mathbf{v}(\tau)\|\right). \tag{2.7}$$

In general, the functions $\beta(r,s)$ *and* $\gamma(r)$ *may depend on the particular input* $\mathbf{v}(\cdot)$*.*

We adopt the following assumption on the system in (2.1).

Assumption 2.6. *The nonlinear system* Σ_p *in* (2.1) *is globally uniformly exponentially convergent for a class of disturbances* $\mathbf{w}(\cdot) \in \mathcal{W}$*, and for all constant inputs* $\mathbf{u} \in \mathbb{R}^{n_\mathbf{u}}$*, uniformly in* $\mathbf{u}$*. In addition, given a disturbance* $\mathbf{w} \in \mathcal{W}$ *the globally exponentially stable (GES) steady-state solution, which we denote by* $\bar{\mathbf{x}}_{\mathbf{w}}(t, \mathbf{u})$*, is twice continuously differentiable in* $\mathbf{u}$ *and satisfies*

$$\left\| \frac{\partial \bar{\mathbf{x}}_{\mathbf{w}}}{\partial \mathbf{u}}(t, \mathbf{u}) \right\| \leq L_{\mathbf{xu}}, \tag{2.8}$$

for all $t \in \mathbb{R}$*, all* $\mathbf{u} \in \mathbb{R}^{n_\mathbf{u}}$*, and some constant* $L_{\mathbf{xu}} \in \mathbb{R}_{>0}$*.*

Remark 2.7. *Assumption 2.6 is the time-varying analogue of the common assumption in the extremum-seeking control literature on the system exhibiting globally exponentially stable equilibria (Krstić and Wang, 2000; Tan et al., 2006, 2010). This assumption is not considered restrictive, as it is exactly this property that extends the needed stability property from the equilibria setting to the time-varying steady-state setting considered in this work. A similar assumption is imposed on the nonlinear plant in the periodic steady-state setting in Haring et al. (2013). Moreover, in many (nonlinear) control problems, for example reference tracking, synchronization, observer design and output regulation problems, the convergent system property that all solutions of a closed-loop system converges to the same steady-state solution and thus "forget" their initial condition plays an important role (Pavlov et al., 2006; Pavlov and van de Wouw, 2016). In addition, the exponential property is immediate for asymptotically stable linear time-invariant systems with inputs.*

Remark 2.8. *A different notation for the steady-state solution can be* $\bar{\mathbf{x}}_{\mathbf{w},\mathbf{u}}(t)$*, which agrees with Definition 2.4 and* $\mathbf{v}^\top := [\mathbf{u}^\top, \mathbf{w}^\top]$*. Here, we opt for the notation* $\bar{\mathbf{x}}_{\mathbf{w}}(t, \mathbf{u})$*, on the one hand, to emphasize the dependency on time-varying disturbances* $\mathbf{w}(t)$*, and on the other hand, to be able to explicitly distinguish between the dependency on either constant inputs* $\mathbf{u}$ *or time-varying inputs* $\mathbf{u}(t)$*. This will prove instrumental in the scope of the stability analysis of the extremum-seeking control scheme proposed later.*

Given Assumption 2.6, for constant inputs $\mathbf{u} \in \mathbb{R}^{n_\mathbf{u}}$ and a given disturbance $\mathbf{w} \in \mathcal{W}$, there exists a unique, time-varying steady-state output of the system Σ_p in (2.1), denoted by $\bar{\mathbf{e}}_\mathbf{w}(t, \mathbf{u})$, which is given by

$$\bar{\mathbf{e}}_\mathbf{w}(t, \mathbf{u}) = \mathbf{g}(\bar{\mathbf{x}}_\mathbf{w}(t, \mathbf{u}), \mathbf{u}, \mathbf{w}(t)). \tag{2.9}$$

We aim to find constant inputs $\mathbf{u}$ that optimize the steady-state performance of the system in (2.1). Common practice in the ESC literature is to define a cost function in terms of the system responses and inputs that quantifies the performance of interest for the system under study. For example, consider performance measures of the following form and adopted from Haring et al. (2013):

$$\begin{aligned} L_p(t, \mathbf{e}(t)) &:= \frac{1}{T} \int_{t-T}^{t} \|\mathbf{e}(\tau)\|^p d\tau, \\ L_\infty(t, \mathbf{e}(t)) &:= \max_{\tau \in [t-T, t]} \|\mathbf{e}(\tau)\|, \end{aligned} \tag{2.10}$$

with $p \in [1, \infty)$ and $t \in \mathbb{R}$, where $T \in \mathbb{R}_{>0}$ is a known performance relevant time-interval. In cases where, for constant inputs $\mathbf{u}$, the steady-state plant outputs $\bar{\mathbf{e}}_\mathbf{w}$ in (2.9) are *constant* for all time or *periodic* with *known* period time T, the steady-state output of the cost functions in (2.10) is constant for all time as well. Having a constant steady-state output of the cost function for constant inputs $\mathbf{u}$ is one of the basic requirements in the extremum-seeking control literature that study the data-based optimization of stable (nonlinear) systems by means of extremum-seeking control (Krstić and Wang, 2000; Tan et al., 2006; Haring et al., 2013). However, in many (industrial) applications this requirement is not met, as the steady-state plant outputs $\bar{\mathbf{e}}_\mathbf{w}$ that characterize system performance are generically *time-varying* in nature (also for constant $\mathbf{u}$). In addition, periodicity of the steady-state plant outputs $\bar{\mathbf{e}}_\mathbf{w}$ is not evident due to the fact that system responses can be induced by complex time-varying, possibly non-periodic disturbances and reference trajectories. In those cases, often the neighborhood to which the ESC scheme converges can not be made arbitrarily small, thereby limiting the achievable performance benefits.

To deal with the time-varying nature of the system responses, consider the series connection of the system Σ_p as in (2.1), a cost function Z of the form

$$y(t) = Z(\mathbf{e}(t), \mathbf{u}(t)), \tag{2.11}$$

where $y \in \mathbb{R}$, and additionally a user-defined filter, denoted by Σ_f, of the general form:

$$\Sigma_f : \begin{cases} \dot{\mathbf{z}}(t) = \alpha_{\mathbf{z}} \mathbf{h}(\mathbf{z}(t), y(t)) \\ l(t) = k(\mathbf{z}(t)), \end{cases} \tag{2.12}$$

where $\alpha_{\mathbf{z}} \in \mathbb{R}_{>0}$ is a tuning parameter, $\mathbf{z} \in \mathbb{R}^{n_{\mathbf{z}}}$ is the state of the filter, $y \in \mathbb{R}$ is the input of the filter defined by (2.11), and $l \in \mathbb{R}$ is the output of the filter. We call the series connection of the cost function Z and the filter Σ_f the *dynamic cost function*. The function $Z : \mathbb{R}^{n_{\mathbf{e}}} \times \mathbb{R}^{n_{\mathbf{u}}} \to \mathbb{R}$ is designed to be twice continuously differentiable with respect to both arguments. Moreover, we choose Z in such a way that there exist constants $L_{Z\mathbf{e}}$, $L_{Z\mathbf{u}} \in \mathbb{R}_{>0}$ such that

$$\left\| \frac{\partial^2 Z}{\partial \mathbf{e} \partial \mathbf{e}^\top}(\mathbf{e}, \mathbf{u}) \right\| \leq L_{Z\mathbf{e}}, \quad \left\| \frac{\partial^2 Z}{\partial \mathbf{e} \partial \mathbf{u}^\top}(\mathbf{e}, \mathbf{u}) \right\| \leq L_{Z\mathbf{u}}, \tag{2.13}$$

for all $\mathbf{e} \in \mathbb{R}^{n_{\mathbf{e}}}$, and all $\mathbf{u} \in \mathbb{R}^{n_{\mathbf{u}}}$. Given a disturbance $\mathbf{w} \in \mathcal{W}$, for all constant inputs $\mathbf{u} \in \mathbb{R}^{n_{\mathbf{u}}}$, the steady-state output of Z is denoted by $\bar{y}_{\mathbf{w}}(t, \mathbf{u})$ and reads

$$\bar{y}_{\mathbf{w}}(t, \mathbf{u}) = Z(\mathbf{g}(\bar{\mathbf{x}}_{\mathbf{w}}(t, \mathbf{u}), \mathbf{u}, \mathbf{w}(t)), \mathbf{u}). \tag{2.14}$$

The functions $\mathbf{h} : \mathbb{R}^{n_{\mathbf{z}}} \times \mathbb{R} \to \mathbb{R}^{n_{\mathbf{z}}}$ and $k : \mathbb{R}^{n_{\mathbf{z}}} \to \mathbb{R}$ in (2.12) are designed to be twice continuously differentiable with respect to all arguments. Moreover, we design Σ_f in such a way that there exist constants $L_{\mathbf{hz}}$, $L_{\mathbf{h}y}$, $L_k \in \mathbb{R}_{>0}$ such that

$$\left\| \frac{\partial \mathbf{h}}{\partial \mathbf{z}}(\mathbf{z}, y) \right\| \leq L_{\mathbf{hz}}, \left\| \frac{\partial \mathbf{h}}{\partial y}(\mathbf{z}, y) \right\| \leq L_{\mathbf{h}y}, \left\| \frac{dk}{d\mathbf{z}}(\mathbf{z}) \right\| \leq L_k, \tag{2.15}$$

for all $\mathbf{z} \in \mathbb{R}^{n_{\mathbf{z}}}$, and all $y \in \mathbb{R}$. In addition, we design the dynamic cost function to satisfy the following property.

Property 2.9. *The dynamic cost function consisting of the cascade of Z and Σ_f, given by* (2.11) *and* (2.12)*, respectively, is exponentially input-to-state convergent (see Definition 2.5) for all constant inputs $\mathbf{u} \in \mathbb{R}^{n_{\mathbf{u}}}$ and all $\alpha_{\mathbf{z}} \in \mathbb{R}_{>0}$, uniformly in $\mathbf{u}$.*

Intuitively, the filter Σ_f is introduced to act as an averaging operator on $y(t)$, utilized to quantify performance of the system similar to the use of exponentially weighting filters (Wang and Krstić, 2000; Antonello et al., 2009). By tuning $\alpha_{\mathbf{z}}$ small the solution $\mathbf{z}(t)$ will vary "slowly" in time, i.e., the output of the filter $l(t)$ will be quasi-constant and determined predominantly by the average of $y(t)$. By properly designing cost function Z and tuning $\alpha_{\mathbf{z}}$ in (2.12) small, the output of the dynamic cost function $l(t)$ is quasi-constant and reflects the performance of the system, while being characterized by the time-varying system response $\mathbf{e}(t)$. By subsequently minimizing $l(t)$ using ESC, we optimize the time-varying system response $\mathbf{e}(t)$.

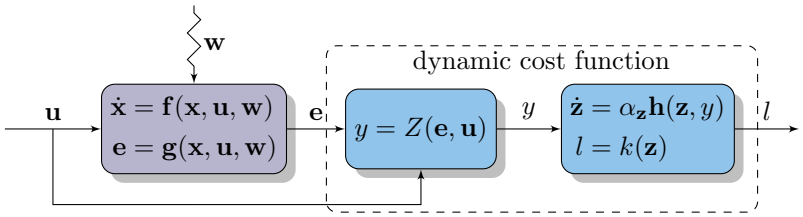

Figure 2.1: The extended plant Σ, i.e., series connection of the nonlinear system Σ_p, the user-defined cost function Z, and the to-be-designed filter Σ_f.

Remark 2.10. *In the scope of the proposed approach, a sufficiently slow filter Σ_f is able to approximate the time-average of $y(t)$ in real-time. This reveals the fact that the proposed approach introduces an additional time-scale to the extremum-seeking loop. That is, the filter Σ_f must operate on a slower time-scale than the slowest one in $y(t)$, but fast enough for gradient estimation in ESC. Depending on the disturbance situation, this may lead to an increased convergence time*[1] *of the ESC strategy. However, the introduction of the dynamic cost function, and the associated time scale, is essential to enable dealing with generic time-varying steady-state responses. Note that, also in cases where time-varying disturbances contain both low- and high-frequency behavior, our approach can still be used to achieve extremum seeking.*

The series connection of the nonlinear system Σ_p in (2.1) and the dynamic cost function is referred to as the extended plant Σ and is schematically depicted in Fig. 2.1. The dynamics of the extended plant is given by

$$\Sigma : \begin{cases} \dot{\mathbf{x}}(t) = \mathbf{f}(\mathbf{x}(t), \mathbf{u}(t), \mathbf{w}(t)) \\ \dot{\mathbf{z}}(t) = \alpha_{\mathbf{z}}\mathbf{h}(\mathbf{z}(t), Z(\mathbf{g}(\mathbf{x}(t), \mathbf{u}(t), \mathbf{w}(t)), \mathbf{u}(t))) \\ l(t) = k(\mathbf{z}(t)). \end{cases} \tag{2.16}$$

The following lemma deals with the series connection of a globally exponentially convergent system as in Definition 2.4 and an exponentially input-to-state convergent system as in Definition 2.5 and will prove instrumental in the scope of the stability analysis of the ESC scheme proposed later.

Lemma 2.11. *Consider the cascaded system*

$$\begin{cases} \dot{\mathbf{x}} = \mathbf{F}(\mathbf{x}, \mathbf{v}), \\ \dot{\mathbf{z}} = \mathbf{G}(\mathbf{z}, \mathbf{x}), \end{cases} \tag{2.17}$$

[1] In Chapter 3, a modified extremum-seeking controller design is proposed that incorporates knowledge about the user-defined dynamic cost function, enhancing convergence speed of the resulting extremum-seeking control scheme, especially in cases where the time-scale of the dynamic cost function is slow due to a relatively small value of $\alpha_{\mathbf{z}}$ being used.

with $\mathbf{x} \in \mathbb{R}^{n_\mathbf{x}}$, $\mathbf{z} \in \mathbb{R}^{n_\mathbf{z}}$, $\mathbf{v} \in \mathbb{R}^{n_\mathbf{v}}$, *and* $\mathbf{F}$ *and* $\mathbf{G}$ *locally Lipschitz in their first argument and continuous in their second argument. Consider inputs* $\mathbf{v} \in \mathcal{V} \subset \overline{\mathbb{PC}}_\mathbf{v}$. *Suppose the* $\mathbf{x}$*-subsystem is globally uniformly exponentially convergent, and the* $\mathbf{z}$*-subsystem with* $\mathbf{x}$ *as input is exponentially input-to-state convergent. Then, the cascaded system in* (2.17) *is globally uniformly exponentially convergent.*

Proof. *The proof of Lemma 2.11 can be found in Appendix 2.B* □

Given Assumption 2.6 and Property 2.9, it follows from Lemma 2.11 that the extended plant Σ in (2.16) is globally uniformly exponentially convergent for all constant inputs $\mathbf{u} \in \mathbb{R}^{n_\mathbf{u}}$, uniformly in $\mathbf{u}$. There exists a unique steady-state solution of Σ_f, induced by the extended plant, which is defined and bounded on $t \in \mathbb{R}$ and GES. We denote this steady-state solution by $\bar{\mathbf{z}}_\mathbf{w}(t, \mathbf{u}, \alpha_\mathbf{z})$ to emphasize the dependency the time-varying disturbance $\mathbf{w}(t)$, constant inputs $\mathbf{u}$, and the tunable parameter $\alpha_\mathbf{z}$, and satisfies

$$\dot{\bar{\mathbf{z}}}_\mathbf{w}(t, \mathbf{u}, \alpha_\mathbf{z}) = \alpha_\mathbf{z} \mathbf{h}(\bar{\mathbf{z}}_\mathbf{w}(t, \mathbf{u}, \alpha_\mathbf{z}), \bar{y}_\mathbf{w}(t, \mathbf{u})). \tag{2.18}$$

For the steady-state solution of the extended plant Σ, we adopt the following assumption.

Assumption 2.12. *Given a disturbance* $\mathbf{w}(t) \in \mathcal{W}$, *there exists a twice continuously differentiable function* $\mathbf{q}_\mathbf{w} : \mathbb{R}^{n_\mathbf{u}} \to \mathbb{R}^{n_\mathbf{z}}$, *referred to as the constant performance cost, such that*

$$\mathbf{q}_\mathbf{w}(\mathbf{u}) = \lim_{\alpha_\mathbf{z} \to 0} \bar{\mathbf{z}}_\mathbf{w}(t, \mathbf{u}, \alpha_\mathbf{z}), \tag{2.19}$$

for all $t \in \mathbb{R}$, *and all* $\mathbf{u} \in \mathbb{R}^{n_\mathbf{u}}$. *Moreover, there exist constants* $\delta_{\mathbf{z}1}, \delta_{\mathbf{z}2} \in \mathbb{R}_{\geq 0}$, *related to the disturbance* $\mathbf{w}(t)$ *and the extended plant* Σ, *such that the difference between the steady-state solution* $\bar{\mathbf{z}}_\mathbf{w}(t, \mathbf{u}, \alpha_\mathbf{z})$ *and the function* $\mathbf{q}_\mathbf{w}(\mathbf{u})$ *satisfies*

$$\|\bar{\mathbf{z}}_\mathbf{w}(t, \mathbf{u}, \alpha_\mathbf{z}) - \mathbf{q}_\mathbf{w}(\mathbf{u})\| \leq \alpha_\mathbf{z} \left(\delta_{\mathbf{z}1} + \delta_{\mathbf{z}2} \|\mathbf{u} - \mathbf{u}^*_\mathbf{w}\|^2\right), \tag{2.20}$$

for all $t \in \mathbb{R}$, *all* $\mathbf{u} \in \mathbb{R}^{n_\mathbf{u}}$, *and all* $0 < \alpha_\mathbf{z} \leq \epsilon_\mathbf{z}$ *for some constant* $\epsilon_\mathbf{z} \in \mathbb{R}_{>0}$, *where* $\mathbf{u}^*_\mathbf{w}$ *denotes the optimal vector of tunable system parameters. In addition,* $\bar{y}_\mathbf{w}(t, \mathbf{u})$ *and* $\bar{\mathbf{z}}_\mathbf{w}(t, \mathbf{u}, \alpha_\mathbf{z})$ *are twice continuously differentiable in* $\mathbf{u}$. *There exist constants* $L_{y1}, L_{y2}, L_\mathbf{q}, L_{\mathbf{z}1}, L_{\mathbf{z}2} \in \mathbb{R}_{>0}$ *such that*

$$\left\| \frac{\partial \bar{y}_\mathbf{w}(t, \mathbf{u})}{\partial \mathbf{u}} \right\| \leq L_{y1} + L_{y2} \|\mathbf{u} - \mathbf{u}^*_\mathbf{w}\|, \tag{2.21}$$

$$\left\| \frac{d\mathbf{q}_\mathbf{w}}{d\mathbf{u}}(\mathbf{u}) \right\| \leq L_\mathbf{q} \left\|\mathbf{u} - \mathbf{u}^*_\mathbf{w}\right\|, \tag{2.22}$$

and

$$\left\| \frac{\partial \bar{\mathbf{z}}_\mathbf{w}}{\partial \mathbf{u}}(t, \mathbf{u}, \alpha_\mathbf{z}) - \frac{d\mathbf{q}_\mathbf{w}}{d\mathbf{u}}(\mathbf{u}) \right\| \leq \alpha_\mathbf{z} \left(L_{\mathbf{z}1} + L_{\mathbf{z}2} \left\|\mathbf{u} - \mathbf{u}^*_\mathbf{w}\right\|\right), \tag{2.23}$$

for all $t \in \mathbb{R}$, *all* $\mathbf{u} \in \mathbb{R}^{n_\mathbf{u}}$, *all* $0 < \alpha_\mathbf{z} \leq \epsilon_\mathbf{z}$.

Remark 2.13. *Let us give an example of the working principles of the dynamic cost function, and provide intuition about Assumption 2.12. Consider, e.g., the time-varying steady-state output* $\bar{e}_{\mathbf{w}}$ *of* (2.1) *to be* $\bar{e}_{\mathbf{w}}(t,u) = (u - u^*_{\mathbf{w}})\sin(t)$ *for which we want to minimize the amplitude, similar to the work in Wang and Krstić (2000). Here, we employ the following dynamic cost function, with cost function* $Z : y(t) = e(t)^2$, *and filter* Σ_f *given by a first-order low-pass filter* $\dot{z}(t) = \alpha_{\mathbf{z}}(y(t) - z(t))$, $l(t) = z(t)$ *with* $\alpha_{\mathbf{z}} \in \mathbb{R}_{>0}$ *the cut-off frequency. The steady-state solution* $\bar{z}_{\mathbf{w}}(t,u,\alpha_{\mathbf{z}})$ *can be derived analytically. Namely, the general solution reads*

$$z(t) = e^{-\alpha_{\mathbf{z}}t}z(0) + \alpha_{\mathbf{z}}\frac{(u-u^*_{\mathbf{w}})^2}{2}\int_0^t e^{-\alpha_{\mathbf{z}}(t-\tau)}(1-\cos(2\tau))d\tau,$$

where we have used that $2\sin^2(t) := 1-\cos(2t)$. *By calculating the integral term we obtain the following expression:*

$$\begin{aligned} z(t) = e^{-\alpha_{\mathbf{z}}t}\left(z(0) - \frac{(u-u^*_{\mathbf{w}})^2}{2}\left(1-\frac{\alpha_{\mathbf{z}}^2}{\alpha_{\mathbf{z}}^2+4}\right)\right) \\ + \frac{(u-u^*_{\mathbf{w}})^2}{2}\left(1-\alpha_{\mathbf{z}}\frac{\alpha_{\mathbf{z}}\cos(2t)+2\sin(2t)}{\alpha_{\mathbf{z}}^2+4}\right). \end{aligned}$$

For the limit $t \to \infty$ *and* $\alpha_{\mathbf{z}} > 0$, *the first term of the solution vanishes. The steady-state solution* $\bar{z}_{\mathbf{w}}(t,u,\alpha_{\mathbf{z}})$ *reads*

$$\bar{z}_{\mathbf{w}}(t,u,\alpha_{\mathbf{z}}) = \frac{(u-u^*_{\mathbf{w}})^2}{2}\left(1-\alpha_{\mathbf{z}}\frac{\alpha_{\mathbf{z}}\cos(2t)+2\sin(2t)}{\alpha_{\mathbf{z}}^2+4}\right).$$

From (2.19) *in Assumption 2.12, we obtain the constant performance cost as*

$$q_{\mathbf{w}}(u) = \lim_{\alpha_{\mathbf{z}}\to 0}\bar{z}_{\mathbf{w}}(t,u,\alpha_{\mathbf{z}}) = \frac{(u-u^*_{\mathbf{w}})^2}{2}.$$

The function $q_{\mathbf{w}}(u)$ *is twice continuously differentiable. Moreover, it follows that the difference between* $\bar{z}_{\mathbf{w}}(t,u,\alpha_{\mathbf{z}})$ *and* $q_{\mathbf{w}}$ *can be bounded as follows*

$$|\bar{z}_{\mathbf{w}}(t,u,\alpha_{\mathbf{z}}) - q_{\mathbf{w}}(u)| \leq \frac{1}{2}\alpha_{\mathbf{z}}|u-u^*_{\mathbf{w}}|^2.$$

Clearly, the inequality in (2.20) *in Assumption 2.12 is satisfied with* $\delta_{\mathbf{z}1} = 0$ *and* $\delta_{\mathbf{z}2} = \frac{1}{2}$. *Basically, inequality* (2.20) *tells us that the bound on the difference between the time-varying steady-state solution and the constant performance cost of the extended plant* Σ *is tunable by* $\alpha_{\mathbf{z}}$, *and by tuning* $\alpha_{\mathbf{z}}$ *small, the steady-state solution of the extended plant* $z_{\mathbf{w}}(t,u,\alpha_{\mathbf{z}})$ *can be made arbitrarily close to the constant performance cost* $q_{\mathbf{w}}(u)$, *see Fig. 2.2. In cases of constant or no*

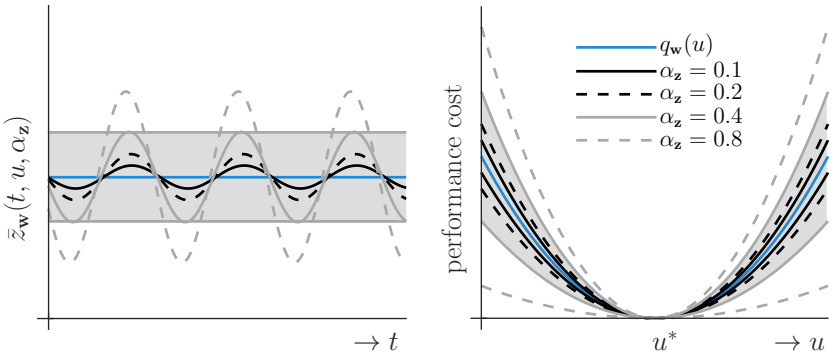

Figure 2.2: A visualization of the steady-state solution $z_{\mathbf{w}}(t, u, \alpha_{\mathbf{z}})$ with a particular value of u (left) and the performance cost $q_{\mathbf{w}}(u)$ (right) for different values of $\alpha_{\mathbf{z}}$ for the example given in Remark 2.13. By tuning $\alpha_{\mathbf{z}}$ small, $z_{\mathbf{w}}(t, u, \alpha_{\mathbf{z}})$ can be made arbitrarily close to $q_{\mathbf{w}}(u)$. The gray shaded area in the right figure corresponds to the area in which $z_{\mathbf{w}}(t, u, \alpha_{\mathbf{z}})$ lies when $\alpha_{\mathbf{z}} = 0.4$.

disturbances $\mathbf{w}$ *and, as a result, constant steady-state responses, this difference will be zero (i.e.,* $\delta_{\mathbf{z}1} = \delta_{\mathbf{z}2} = 0$ *in* (2.20)*) for any value of the tuning parameter* $\alpha_{\mathbf{z}}$*, as the steady-state solution will be independent of time. In case of time-varying disturbances* $\mathbf{w}(t)$ *(i.e.,* $\delta_{\mathbf{z}1}, \delta_{\mathbf{z}2} > 0$*) the tuning parameter* $\alpha_{\mathbf{z}}$ *should be tuned small in order to ensure a sufficiently close approximation of the constant performance cost* $\mathbf{q}_{\mathbf{w}}(u)$*.*

Remark 2.14. *The choice for the functions* $\mathbf{h}(\mathbf{z}, y)$ *and* $k(\mathbf{z})$ *in* (2.12) *depends on the specific optimization problem considered and the nature of the time-varying disturbances* $\mathbf{w}(t)$*. In cases where the steady-state output of the cost function* Z*, denoted by* $\bar{y}_{\mathbf{w}}(t, \mathbf{u})$*, are generally time-varying, a good choice for the filter* Σ_f *would be a (first- or second-order) low-pass filter with a sufficiently small cut-off frequency to suppress the (high-frequency) variations present in* $\bar{y}_{\mathbf{w}}(t, \mathbf{u})$*. If, for example, a-priori knowledge is available about the specific nature of the external disturbances and the effect on the steady-state output of the cost function* $\bar{y}_{\mathbf{w}}(t, \mathbf{u})$ *in the frequency domain, notch filters can be introduced in addition to the low-pass filter to suppress specific frequencies in* $\bar{y}_{\mathbf{w}}(t, \mathbf{u})$*. Suppressing a specific known frequency in the measured output of the cost function* Z *can be helpful in improving the convergence rate of the extremum-seeking scheme proposed later, as it may allow for a higher cut-off frequency for the low-pass filter.*

Hence, by Assumption 2.12, under steady-state conditions of the system Σ_p, the cost function Z, the filter Σ_f, the limit $\alpha_{\mathbf{z}} \to 0$, and for constant inputs $\mathbf{u}$, we have that the static parameter-to-steady-state performance map of the

system can be characterized by

$$F_{\mathbf{w}}(\mathbf{u}) := k(\mathbf{q}_{\mathbf{w}}(\mathbf{u})), \quad \forall\ \mathbf{u} \in \mathbb{R}^{n_{\mathbf{u}}}. \tag{2.24}$$

We refer to the map $F_{\mathbf{w}}$ as the objective function. To optimize the steady-state system output $\bar{\mathbf{e}}_{\mathbf{w}}$, we aim to find the system parameter values for which the objective function in (2.24) is minimal. We further assume that, given a disturbance $\mathbf{w}(t) \in \mathcal{W}$, the dynamic cost function is designed such that there exists a unique minimum of the objective function $F_{\mathbf{w}}$, where the minimum of the map $F_{\mathbf{w}}$ corresponds to the optimal system performance.

Assumption 2.15. *Given a disturbance $\mathbf{w}(t) \in \mathcal{W}$, the objective function $F_{\mathbf{w}} : \mathbb{R}^{n_{\mathbf{u}}} \to \mathbb{R}$ in (2.24) is twice continuously differentiable and exhibits a unique minimum in $\mathbb{R}^{n_{\mathbf{u}}}$. Let the corresponding optimal input $\mathbf{u}^*_{\mathbf{w}}$ be defined as*

$$\mathbf{u}^*_{\mathbf{w}} = \underset{\mathbf{u}\in\mathbb{R}^{n_{\mathbf{u}}}}{\arg\min}\, F_{\mathbf{w}}(\mathbf{u}). \tag{2.25}$$

There exist constants $L_{F1}, L_{F2} \in \mathbb{R}_{>0}$ such that

$$\frac{dF_{\mathbf{w}}}{d\mathbf{u}}(\mathbf{u})(\mathbf{u} - \mathbf{u}^*_{\mathbf{w}}) \geq L_{F1}\|\mathbf{u} - \mathbf{u}^*_{\mathbf{w}}\|^2, \tag{2.26}$$

and

$$\left\| \frac{d^2F_{\mathbf{w}}}{d\mathbf{u}d\mathbf{u}^\top}(\mathbf{u}) \right\| \leq L_{F2}, \tag{2.27}$$

for all $\mathbf{u} \in \mathbb{R}^{n_{\mathbf{u}}}$.

Information of the objective function can only be obtained through measured outputs l of the extended plant in (2.16). The measured output differs from the objective function $F_{\mathbf{w}}$ in (2.24) in two ways: i) due to the dynamics of the system in (2.1) and the filter in (2.12) not being in steady-state, i.e., $\bar{\mathbf{x}}_{\mathbf{w}}(t, \mathbf{u})$ and $\bar{\mathbf{z}}_{\mathbf{w}}(t, \mathbf{u}, \alpha_{\mathbf{z}})$, respectively, and ii) due to the presence of time-varying disturbances $\mathbf{w}(t)$ and the design parameter $\alpha_{\mathbf{z}}$ which, in the presence of time-varying disturbances $\mathbf{w}(t)$, is typically designed to be small, but still non-zero and positive. This causes $\bar{\mathbf{z}}_{\mathbf{w}}(t, \mathbf{u}, \alpha_{\mathbf{z}})$ to differ from $\mathbf{q}_{\mathbf{w}}(\mathbf{u})$ (Assumption 2.12). Nevertheless, we aim to steer the inputs $\mathbf{u}$ to their performance optimizing values $\mathbf{u}^*_{\mathbf{w}}$ by using the measured extended plant output $l(t)$ as feedback to an extremum-seeking controller that is introduced in the next section.

2.3 Extremum-seeking controller design

The extremum-seeking controller design that we exploit here is based on the one in (Haring, 2016, Chapter 2). In contrast with classical ESC approaches as in Krstić and Wang (2000) and Tan et al. (2006), where an estimate of the gradient of the objective function is obtained solely by correlating the measured

system performance with a user-supplied dither signal, this extremum-seeking controller exploits both the user-supplied dither signal and the nominal system parameter. This leads to a more accurate gradient estimate, and may lead to a faster convergence (Haring and Johansen, 2018; Gelbert et al., 2012; Guay and Dochain, 2015).

In Section 2.3.1, a dither signal design is presented, in Section 2.3.2, a model of the input-to-output behavior of the extended plant is presented to be used as a basis for gradient estimation, and in Section 2.3.3, a least-squares observer to estimate the state of that model (and therewith the gradient) and a normalized optimizer to steer the system parameters $\mathbf{u}$ to the minimizer $\mathbf{u}_{\mathbf{w}}^*$ are presented.

2.3.1 Dither signal

In order to estimate the gradient of the objective function and use this estimated gradient to drive $\mathbf{u}$ towards $\mathbf{u}_{\mathbf{w}}^*$ by an optimizer, we supply the following dither signal:

$$\mathbf{u}(t) = \hat{\mathbf{u}}(t) + \alpha_{\boldsymbol{\omega}}\boldsymbol{\omega}(t), \tag{2.28}$$

where $\alpha_{\boldsymbol{\omega}}\boldsymbol{\omega}$ is a vector of perturbation signals with amplitude $\alpha_{\boldsymbol{\omega}} \in \mathbb{R}_{>0}$, and $\hat{\mathbf{u}}$ is referred to as the nominal system parameter to be generated by the extremum-seeking controller. The vector $\boldsymbol{\omega}$ is defined by $\boldsymbol{\omega}(t) = [\omega_1(t), \omega_2(t), ..., \omega_{n_{\mathbf{u}}}(t)]^\top$, with

$$\omega_i(t) = \begin{cases} \sin\left(\dfrac{i+1}{2}\eta_{\boldsymbol{\omega}} t\right), & \text{if } i \text{ is odd,} \\ \cos\left(\dfrac{i}{2}\eta_{\boldsymbol{\omega}} t\right), & \text{if } i \text{ is even,} \end{cases} \tag{2.29}$$

for $i = \{1, 2, ..., n_{\mathbf{u}}\}$, where $\eta_{\boldsymbol{\omega}} \in \mathbb{R}_{>0}$ is a tuning parameter.

2.3.2 Model of input-output behavior of the extended plant

To obtain an estimate of the gradient of the objective function, we model the input-to-output behavior of the extended plant in (2.16), that is, from the nominal system parameter input $\hat{\mathbf{u}}$ to the measured output of the extended plant l, in a general form. Let the state vector of the model be given by

$$\mathbf{m}(t) = \begin{bmatrix} F_{\mathbf{w}}(\hat{\mathbf{u}}(t)) \\ \alpha_{\boldsymbol{\omega}} \dfrac{dF_{\mathbf{w}}}{d\mathbf{u}^\top}(\hat{\mathbf{u}}(t)) \end{bmatrix}. \tag{2.30}$$

The measured output of the extended plant l in (2.16) can be written as

$$l(t) = k(\mathbf{z}(t)) - k(\bar{\mathbf{z}}_{\mathbf{w}}(t, \mathbf{u}(t), \alpha_{\mathbf{z}})) + F_{\mathbf{w}}(\mathbf{u}(t)) + d(t), \tag{2.31}$$

with the signal $d(t)$ defined as

$$d(t) := k(\bar{\mathbf{z}}_{\mathbf{w}}(t, \mathbf{u}(t), \alpha_{\mathbf{z}})) - k(\mathbf{q}_{\mathbf{w}}(\mathbf{u}(t))). \tag{2.32}$$

Using Taylor's Theorem and (2.28), the objective function $F_{\mathbf{w}}$ can be written as

$$\begin{aligned} F_{\mathbf{w}}(\mathbf{u}(t)) &= F_{\mathbf{w}}(\hat{\mathbf{u}}(t) + \alpha_{\boldsymbol{\omega}}\boldsymbol{\omega}(t)) \\ &= F_{\mathbf{w}}(\hat{\mathbf{u}}(t)) + \alpha_{\boldsymbol{\omega}} \frac{dF_{\mathbf{w}}}{d\mathbf{u}}(\hat{\mathbf{u}}(t))\boldsymbol{\omega}(t) + \frac{1}{2}\alpha_{\boldsymbol{\omega}}^2 \boldsymbol{\omega}^\top(t)\mathbf{H}(t, \hat{\mathbf{u}}(t))\boldsymbol{\omega}(t), \end{aligned} \tag{2.33}$$

where $\mathbf{H}(t, \hat{\mathbf{u}}(t))$ reads

$$\mathbf{H}(t, \hat{\mathbf{u}}(t)) = 2 \int_0^1 (1-\sigma) \frac{d^2 F_{\mathbf{w}}}{d\mathbf{u} d\mathbf{u}^\top}(\hat{\mathbf{u}}(t) + \sigma\alpha_{\boldsymbol{\omega}}\boldsymbol{\omega}(t)) d\sigma. \tag{2.34}$$

The dynamics of the state vector in (2.30) is then governed by

$$\begin{aligned} \dot{\mathbf{m}}(t) &= \mathbf{A}(t)\mathbf{m}(t) + \alpha_{\boldsymbol{\omega}}^2 \mathbf{B}\mathbf{s}(t) \\ l(t) &= \mathbf{C}(t)\mathbf{m}(t) + \alpha_{\boldsymbol{\omega}}^2 v(t) + r(t) + d(t), \end{aligned} \tag{2.35}$$

with the matrices $\mathbf{A}$, $\mathbf{B}$ and $\mathbf{C}$ defined as

$$\begin{aligned} \mathbf{A}(t) &= \frac{1}{\alpha_{\boldsymbol{\omega}}} \begin{bmatrix} 0 & \dot{\hat{\mathbf{u}}}^\top(t) \\ \mathbf{0}^{n_{\mathbf{u}} \times 1} & \mathbf{0}^{n_{\mathbf{u}} \times n_{\mathbf{u}}} \end{bmatrix}, \ \mathbf{B} = \begin{bmatrix} \mathbf{0}^{1 \times n_{\mathbf{u}}} \\ \mathbf{I}^{n_{\mathbf{u}} \times n_{\mathbf{u}}} \end{bmatrix}, \\ \mathbf{C}(t) &= \begin{bmatrix} 1 & \boldsymbol{\omega}^\top(t) \end{bmatrix}, \end{aligned} \tag{2.36}$$

and the signals $\mathbf{s}$, v, and r defined as

$$\begin{aligned} \mathbf{s}(t) &:= \frac{d^2 F_{\mathbf{w}}}{d\mathbf{u} d\mathbf{u}^\top}(\hat{\mathbf{u}}(t)) \frac{\dot{\hat{\mathbf{u}}}(t)}{\alpha_{\boldsymbol{\omega}}}, \\ v(t) &:= \frac{1}{2}\boldsymbol{\omega}^\top(t)\mathbf{H}(t, \hat{\mathbf{u}}(t))\boldsymbol{\omega}(t), \\ r(t) &:= k(\mathbf{z}(t)) - k(\bar{\mathbf{z}}_{\mathbf{w}}(t, \mathbf{u}(t), \alpha_{\mathbf{z}})). \end{aligned} \tag{2.37}$$

The signals $\mathbf{s}$, v, r, and d can be interpreted as unknown disturbances to the model in (2.35). The influences of $\mathbf{s}$, v, r, and d on the state and output of the model in (2.35) are small if i) $\hat{\mathbf{u}}$ is slowly time varying, if ii) $\alpha_{\boldsymbol{\omega}}$ is small, if iii) the states $\mathbf{x}$ of the system in (2.1) and the states $\mathbf{z}$ of the filter in (2.12) are close to their steady-state values, respectively $\bar{\mathbf{x}}_{\mathbf{w}}$ and $\bar{\mathbf{z}}_{\mathbf{w}}$, and if iv) $\alpha_{\mathbf{z}}$ is small.

The state $\mathbf{m}$ in (2.30) contains the gradient of the objective function, scaled by the perturbation amplitude $\alpha_{\boldsymbol{\omega}}$. Hence, an estimate of the gradient of the objective function can be obtained from an estimate of the state $\mathbf{m}$.

2.3.3 Extremum-seeking controller

The extremum-seeking controller is composed of a dither signal as in (2.28), a least-squares observer to estimate the state $\mathbf{m}$ of the model in (2.35), and an

optimizer that uses the estimate of the state $\mathbf{m}$ of the observer, denoted by $\hat{\mathbf{m}}$, to steer the nominal system inputs $\hat{\mathbf{u}}$ to their performance-optimal values $\mathbf{u}^*_{\mathbf{w}}$.

The least-squares observer, denoted by Σ_o, is given by

$$\Sigma_o : \begin{cases} \dot{\hat{\mathbf{m}}} = \left(\mathbf{A} - \eta_{\mathbf{m}}\sigma_r \mathbf{Q}\mathbf{D}^\top \mathbf{D}\right)\hat{\mathbf{m}} + \alpha_{\boldsymbol{\omega}}^2 \mathbf{B}\hat{\mathbf{s}} \\ \qquad\quad + \eta_{\mathbf{m}}\mathbf{Q}\mathbf{C}^\top(l - \mathbf{C}\hat{\mathbf{m}} - \alpha_{\boldsymbol{\omega}}^2 \hat{v}) \\ \dot{\mathbf{Q}} = \eta_{\mathbf{m}}\mathbf{Q} + \mathbf{A}\mathbf{Q} + \mathbf{Q}\mathbf{A}^\top \\ \qquad\quad - \eta_{\mathbf{m}}\mathbf{Q}(\mathbf{C}^\top\mathbf{C} + \sigma_r \mathbf{D}^\top\mathbf{D})\mathbf{Q}, \end{cases} \tag{2.38}$$

with initial conditions $\hat{\mathbf{m}}(0) = \hat{\mathbf{m}}_0 \in \mathbb{R}^{n_{\mathbf{u}}+1}$ and $\mathbf{Q}(0) = \mathbf{Q}_0 \in \mathbb{R}^{n_{\mathbf{u}}+1 \times n_{\mathbf{u}}+1}$, where $\mathbf{Q}_0$ is a symmetric and positive definite matrix, $\mathbf{D} = [\mathbf{0}^{n_{\mathbf{u}}\times 1} \quad \mathbf{I}^{n_{\mathbf{u}}\times n_{\mathbf{u}}}]$, $\eta_{\mathbf{m}} \in \mathbb{R}_{>0}$ and $\sigma_r \in \mathbb{R}_{\geq 0}$ are tuning parameters related to the observer, referred to as a forgetting factor and a regularization constant, respectively, and signals $\hat{\mathbf{s}}$ and $\hat{v}$ being approximations of signals $\mathbf{s}$ and v in (2.37), defined as

$$\begin{aligned} \hat{\mathbf{s}}(t) &:= \hat{\mathbf{H}}(t, \hat{\mathbf{u}}(t))\frac{\dot{\hat{\mathbf{u}}}(t)}{\alpha_{\boldsymbol{\omega}}}, \\ \hat{v}(t) &:= \frac{1}{2}\boldsymbol{\omega}^\top(t)\hat{\mathbf{H}}(t, \hat{\mathbf{u}}(t))\boldsymbol{\omega}(t), \end{aligned} \tag{2.39}$$

with a user-defined function $\hat{\mathbf{H}} : \mathbb{R} \times \mathbb{R}^{n_{\mathbf{u}}} \to \mathbb{R}^{n_{\mathbf{u}}\times n_{\mathbf{u}}}$ satisfying $\|\hat{\mathbf{H}}(t, \hat{\mathbf{u}})\| \leq L_{\mathbf{H}}$, for all $t \in \mathbb{R}$, all $\hat{\mathbf{u}} \in \mathbb{R}^{n_{\mathbf{u}}}$, and with $L_{\mathbf{H}} \in \mathbb{R}_{>0}$. More details about the derivation of the least-squares observer can be found in Appendix 2.A and in Haring (2016, Chapter 2). Note that in order to arrive at the observer design in (2.38), we have considered the signals r and d in (2.35) to be zero. This is justified for steady-state conditions of the extended plant Σ, and sufficiently small $\alpha_{\mathbf{z}}$. The optimizer, denoted by Σ_r, is given by

$$\Sigma_r : \quad \dot{\hat{\mathbf{u}}}(t) = -\lambda_{\mathbf{u}} \frac{\eta_{\mathbf{u}}\mathbf{D}\hat{\mathbf{m}}(t)}{\eta_{\mathbf{u}} + \lambda_{\mathbf{u}}\|\mathbf{D}\hat{\mathbf{m}}(t)\|}, \tag{2.40}$$

with $\lambda_{\mathbf{u}}$, $\eta_{\mathbf{u}} \in \mathbb{R}_{>0}$ being tuning parameters related to the optimizer. Normalization of the adaptation gain in (2.40) is done to prevent solutions of the closed-loop ESC scheme from having a finite escape time if the state estimate $\hat{\mathbf{m}}$ is inaccurate (Haring, 2016, Chapter 2). The closed-loop system, composed of the extended plant Σ in (2.16), the observer Σ_o in (2.38), and the optimizer Σ_r in (2.40), is depicted in Fig. 2.3.

2.4 Closed-loop stability analysis

In this section, we will provide a stability result and supporting stability proof for the closed-loop system described in the previous sections and schematically depicted in Fig. 2.3. The next result states conditions on tuning parameters under which the ESC scheme guarantees that $\hat{\mathbf{u}}$ converges to an arbitrarily small set around the optimum $\mathbf{u}^*_{\mathbf{w}}$.

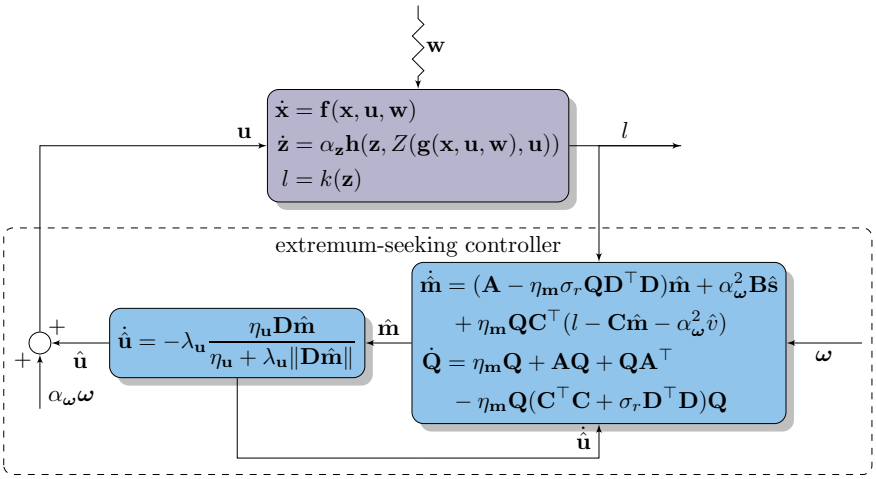

Figure 2.3: The closed-loop system composed of the extended plant Σ, the observer Σ_o, the optimizer Σ_r, and the dither signal $\alpha_{\boldsymbol{\omega}} \boldsymbol{\omega}$.

Theorem 2.16. *Consider a (time-varying) disturbance* $\mathbf{w} \in \mathcal{W}$ *and Assumptions 2.2, 2.6, 2.12, and 2.15. Moreover, consider arbitrary initial conditions* $\mathbf{x}(0) \in \mathbb{R}^{n_{\mathbf{x}}}$, $\mathbf{Q}(0) \in \mathbb{R}^{n_{\mathbf{u}}+1 \times n_{\mathbf{u}}+1}$ *symmetric and positive-definite,* $\mathbf{z}(0) \in \mathbb{R}^{n_{\mathbf{z}}}$, $\hat{\mathbf{m}}(0) \in \mathbb{R}^{n_{\mathbf{u}}+1}$, *and an arbitrary compact set* $\mathcal{U}_0 \subset \mathbb{R}^{n_{\mathbf{u}}}$ *of initial conditions for* $\hat{\mathbf{u}}(t)$. *Then, there exist sufficiently small constants* $\epsilon_0, \ldots, \epsilon_6 \in \mathbb{R}_{>0}$ *such that, for all tunable parameters* $\alpha_{\mathbf{z}}, \alpha_{\boldsymbol{\omega}}, \eta_{\mathbf{u}}, \lambda_{\mathbf{u}}, \eta_{\mathbf{m}}, \eta_{\boldsymbol{\omega}} \in \mathbb{R}_{>0}$ *and* $\sigma_r \in \mathbb{R}_{\geq 0}$ *with* $\alpha_{\boldsymbol{\omega}} \leq \epsilon_0$, $\alpha_{\mathbf{z}} \leq \alpha_{\boldsymbol{\omega}} \epsilon_1$, $\eta_{\boldsymbol{\omega}} \leq \alpha_{\mathbf{z}} \epsilon_2$, $\eta_{\mathbf{m}} \leq \eta_{\boldsymbol{\omega}} \epsilon_3$, $\alpha_{\boldsymbol{\omega}} \lambda_{\mathbf{u}} \leq \eta_{\mathbf{m}} \epsilon_4$, $\eta_{\mathbf{u}} \leq \alpha_{\boldsymbol{\omega}} \eta_{\mathbf{m}} \epsilon_5$, *and* $\sigma_r \leq \epsilon_6$, *the solutions of the closed-loop system consisting of the extended plant in* (2.16) *and the extremum-seeking controller (consisting of the dither signal in* (2.28)*, the observer* Σ_o *in* (2.38)*, and the optimizer* Σ_r *in* (2.40)*) are bounded for all* $t \geq 0$. *In addition, there exist constants* $c_1, \ldots, c_4 \in \mathbb{R}_{>0}$ *such that the solutions* $\hat{\mathbf{u}}(t)$ *with* $\hat{\mathbf{u}}(0) \in \mathcal{U}_0$ *satisfy*

$$\limsup_{t \to \infty} \|\hat{\mathbf{u}}(t) - \mathbf{u}_{\mathbf{w}}^*\| \leq \max \left\{ \alpha_{\boldsymbol{\omega}} c_1, \frac{\eta_{\boldsymbol{\omega}}}{\alpha_{\mathbf{z}}} c_2, \frac{\alpha_{\mathbf{z}} \delta_{\mathbf{z}1}}{\alpha_{\boldsymbol{\omega}}} c_3, \alpha_{\mathbf{z}} \alpha_{\boldsymbol{\omega}} \delta_{\mathbf{z}2} c_4 \right\}. \tag{2.41}$$

Remark 2.17. *Tuning guidelines. Under the conditions of Theorem 2.16 it follows that, if we are dealing with constant (or no) disturbances* $\mathbf{w}$, *i.e.,* $\delta_{\mathbf{z}1}, \delta_{\mathbf{z}2} = 0$ *(Assumption 2.12), the optimizer state* $\hat{\mathbf{u}}$ *converges to an arbitrarily small region of the performance-optimal value* $\mathbf{u}_{\mathbf{w}}^*$ *if the dither parameters* $\alpha_{\boldsymbol{\omega}}$ *and* $\eta_{\boldsymbol{\omega}}$ *are chosen sufficiently small for an arbitrary bounded* $\alpha_{\mathbf{z}}$. *Choosing* $\alpha_{\mathbf{z}}$ *large in general allows faster convergence towards the performance-optimal value* $\mathbf{u}_{\mathbf{w}}^*$. *In the case of time-varying disturbances* $\mathbf{w}(t)$, *i.e.,* $\delta_{\mathbf{z}1}, \delta_{\mathbf{z}2} > 0$, *see* (2.41)*, we subsequently tune* $\alpha_{\boldsymbol{\omega}}$ *small to make the first term in the right-hand side of* (2.41) *arbitrarily small, tune* $\alpha_{\mathbf{z}}$ *small to make the third and fourth term in the right-hand side of*

(2.41) *arbitrarily small, and finally tune* $\eta_{\boldsymbol{\omega}}$ *small to make the second term in the right-hand side of* (2.41) *arbitrarily small.*

Proof. To prove Theorem 2.16, we introduce the following coordinate transformation:

$$\begin{aligned}
\tilde{\mathbf{x}}(t) &= \mathbf{x}(t) - \bar{\mathbf{x}}_{\mathbf{w}}(t, \mathbf{u}(t)),\\
\tilde{\mathbf{z}}(t) &= \mathbf{z}(t) - \bar{\mathbf{z}}_{\mathbf{w}}(t, \mathbf{u}(t), \alpha_{\mathbf{z}}),\\
\tilde{\mathbf{u}}(t) &= \hat{\mathbf{u}}(t) - \mathbf{u}^*_{\mathbf{w}},\\
\tilde{\mathbf{m}}(t) &= \hat{\mathbf{m}}(t) - \mathbf{m}(t),\\
\tilde{\mathbf{Q}}(t) &= \mathbf{Q}^{-1}(t) - \Xi^{-1} - \eta_{\mathbf{m}}\mathbf{n}(t),
\end{aligned} \tag{2.42}$$

with

$$\mathbf{n}(t) = \int_0^t \begin{bmatrix} 0 & \boldsymbol{\omega}^\top(\tau) \\ \boldsymbol{\omega}(\tau) & \boldsymbol{\omega}(\tau)\boldsymbol{\omega}^\top(\tau) - \frac{1}{2}\mathbf{I} \end{bmatrix} d\tau, \tag{2.43}$$

and

$$\Xi = \begin{bmatrix} 1 & \mathbf{0}^{1\times n_{\mathbf{u}}} \\ \mathbf{0}^{n_{\mathbf{u}}\times 1} & \frac{2}{1+2\sigma_r}\mathbf{I}^{n_{\mathbf{u}}\times n_{\mathbf{u}}} \end{bmatrix}. \tag{2.44}$$

Define the following vector fields

$$\begin{aligned}
\tilde{\mathbf{f}}_{\mathbf{w}}(t, \tilde{\mathbf{x}}, \mathbf{u}) &:= \mathbf{f}(\tilde{\mathbf{x}} + \bar{\mathbf{x}}_{\mathbf{w}}(t, \mathbf{u}), \mathbf{u}, \mathbf{w}(t)) - \mathbf{f}(\bar{\mathbf{x}}_{\mathbf{w}}(t, \mathbf{u}), \mathbf{u}, \mathbf{w}(t)),\\
\tilde{\mathbf{h}}_{\mathbf{w}}(t, \tilde{\mathbf{z}}, \mathbf{u}, \alpha_{\mathbf{z}}) &:= \mathbf{h}(\tilde{\mathbf{z}} + \bar{\mathbf{z}}_{\mathbf{w}}(t, \mathbf{u}, \alpha_{\mathbf{z}}), \bar{y}_{\mathbf{w}}(t, \mathbf{u})) - \mathbf{h}(\bar{\mathbf{z}}_{\mathbf{w}}(t, \mathbf{u}, \alpha_{\mathbf{z}}), \bar{y}_{\mathbf{w}}(t, \mathbf{u})).
\end{aligned} \tag{2.45}$$

The analysis of the stability properties of the closed-loop system can be divided into two temporal stages, characterized by some finite time instance $t_1 \in \mathbb{R}_{>0}$, as follows:

i) for $0 \leq t < t_1$, the solutions $\tilde{\mathbf{x}}$ and $\tilde{\mathbf{Q}}$ are shown to converge to a neighborhood of the origin and remain there, while the solutions $\tilde{\mathbf{z}}$, $\tilde{\mathbf{m}}$, and $\tilde{\mathbf{u}}$ may drift, but remain bounded;

ii) for $t \geq t_1$, the solutions $\tilde{\mathbf{z}}$, $\tilde{\mathbf{m}}$, and $\tilde{\mathbf{u}}$ are shown to also converge to a neighborhood of the origin.

Firstly, bounds are derived on each of the variables in (2.42) corresponding to these two temporal stages of convergence. Secondly, we exploit the obtained bounds on the variables in (2.42) and employ the cyclic-small-gain criterion in Liu et al. (2011) to show convergence of the extremum-seeking scheme.

From the plant Σ_p in (2.1) and its steady-state solution $\bar{\mathbf{x}}_{\mathbf{w}}$, the coordinate transformation in (2.42), and the vector field defined by (2.45), it follows that the dynamics of $\tilde{\mathbf{x}}$ for *constant* inputs $\mathbf{u}$ is governed by

$$\dot{\tilde{\mathbf{x}}}(t) = \tilde{\mathbf{f}}_{\mathbf{w}}(t, \tilde{\mathbf{x}}(t), \mathbf{u}). \tag{2.46}$$

A preliminary result is presented in Lemma 2.18 on the existence of a Lyapunov function for the $\tilde{\mathbf{x}}$-dynamics for *constant* inputs $\mathbf{u}$ in (2.46).

Lemma 2.18. *Under Assumptions 2.2 and 2.6, there exists a function* $V_{\mathbf{x}} : \mathbb{R} \times \mathbb{R}^{n_{\mathbf{x}}} \times \mathbb{R}^{n_{\mathbf{u}}} \to \mathbb{R}$*, and constants* $\gamma_{\mathbf{x}1}, ..., \gamma_{\mathbf{x}5} \in \mathbb{R}_{>0}$*, such that the inequalities*

$$\gamma_{\mathbf{x}1}\|\tilde{\mathbf{x}}\|^2 \leq V_{\mathbf{x}}(t, \tilde{\mathbf{x}}, \mathbf{u}) \leq \gamma_{\mathbf{x}2}\|\tilde{\mathbf{x}}\|^2, \tag{2.47}$$

$$\frac{\partial V_{\mathbf{x}}}{\partial t}(t, \tilde{\mathbf{x}}, \mathbf{u}) + \frac{\partial V_{\mathbf{x}}}{\partial \tilde{\mathbf{x}}}(t, \tilde{\mathbf{x}}, \mathbf{u})\tilde{\mathbf{f}}_{\mathbf{w}}(t, \tilde{\mathbf{x}}, \mathbf{u}) \leq -\gamma_{\mathbf{x}3}\|\tilde{\mathbf{x}}\|^2, \tag{2.48}$$

$$\left\| \frac{\partial V_{\mathbf{x}}}{\partial \tilde{\mathbf{x}}}(t, \tilde{\mathbf{x}}, \mathbf{u}) \right\| \leq \gamma_{\mathbf{x}4}\|\tilde{\mathbf{x}}\|, \tag{2.49}$$

and

$$\left\| \frac{\partial V_{\mathbf{x}}}{\partial \mathbf{u}}(t, \tilde{\mathbf{x}}, \mathbf{u}) \right\| \leq \gamma_{\mathbf{x}5}\|\tilde{\mathbf{x}}\|, \tag{2.50}$$

are satisfied for all $t \in \mathbb{R}$*, all* $\tilde{\mathbf{x}} \in \mathbb{R}^{n_{\mathbf{x}}}$*, and all constant* $\mathbf{u} \in \mathbb{R}^{n_{\mathbf{u}}}$*.*

Proof. *See Appendix 2.C.* □

Similarly, from the system Σ_p in (2.1) and its steady-state solution $\bar{\mathbf{x}}_{\mathbf{w}}$, the coordinate transformation in (2.42), and the vector field defined by (2.45), it follows that the state equation for $\tilde{\mathbf{x}}$ for *time-varying* inputs $\mathbf{u}(t)$, generated by (2.40) and (2.28), is given by

$$\dot{\tilde{\mathbf{x}}}(t) = \tilde{\mathbf{f}}_{\mathbf{w}}(t, \tilde{\mathbf{x}}(t), \mathbf{u}(t)) - \frac{\partial \bar{\mathbf{x}}_{\mathbf{w}}}{\partial \mathbf{u}}(t, \mathbf{u}(t))\dot{\mathbf{u}}(t). \tag{2.51}$$

A bound on the solutions of the $\tilde{\mathbf{x}}$-dynamics for time-varying inputs $\mathbf{u}(t)$ in (2.51) is presented in Lemma 2.19.

Lemma 2.19. *Under Assumptions 2.2 and 2.6, for any* $\epsilon_3, \epsilon_5 \in \mathbb{R}_{>0}$*, and all tunable parameters* $\alpha_{\boldsymbol{\omega}}, \eta_{\boldsymbol{\omega}} \in \mathbb{R}_{>0}$*, there exist constants* $c_{\mathbf{x}1}$*,* $c_{\mathbf{x}2}(\epsilon_3, \epsilon_5)$*,* $\beta_{\mathbf{x}} \in \mathbb{R}_{>0}$ *such that, for all* $\eta_{\mathbf{m}} \leq \eta_{\boldsymbol{\omega}}\epsilon_3$ *and all* $\eta_{\mathbf{u}} \leq \alpha_{\boldsymbol{\omega}}\eta_{\mathbf{m}}\epsilon_5$*, the solutions* $\tilde{\mathbf{x}}$ *of system* (2.51) *satisfy*

$$\|\tilde{\mathbf{x}}(t)\| \leq \max\left\{c_{\mathbf{x}1}\|\tilde{\mathbf{x}}(0)\|e^{-\beta_{\mathbf{x}}t}, \alpha_{\boldsymbol{\omega}}\eta_{\boldsymbol{\omega}}c_{\mathbf{x}2}\right\}, \tag{2.52}$$

for all $t \geq 0$*, all* $\tilde{\mathbf{x}}(0) \in \mathbb{R}^{n_{\mathbf{x}}}$*, and all time-varying* $\mathbf{u}(t) \in \mathbb{R}^{n_{\mathbf{u}}}$*.*

Proof. *See Appendix 2.D.* □

From the observer in (2.38), the coordinate transformation in (2.42), and the model of the input-output behavior in (2.35), we obtain that the state equation for $\tilde{\mathbf{Q}}$ is given by

$$\begin{aligned}\dot{\tilde{\mathbf{Q}}}(t) = &-\eta_{\mathbf{m}}\tilde{\mathbf{Q}}(t) - \tilde{\mathbf{Q}}(t)\mathbf{A}(t) - \mathbf{A}^{\top}(t)\tilde{\mathbf{Q}}(t) - \eta_{\mathbf{m}}^2\mathbf{n}(t) \\ &- \left(\Xi^{-1} + \eta_{\mathbf{m}}\mathbf{n}(t)\right)\mathbf{A}(t) - \mathbf{A}^{\top}(t)\left(\Xi^{-1} + \eta_{\mathbf{m}}\mathbf{n}(t)\right).\end{aligned} \tag{2.53}$$

A bound on the solutions $\tilde{\mathbf{Q}}(t)$ is presented in Lemma 2.20.

Lemma 2.20. *For sufficiently small $\epsilon_3, \epsilon_5, \epsilon_6 \in \mathbb{R}_{>0}$ and all tunable parameters $\alpha_{\boldsymbol{\omega}}, \eta_{\boldsymbol{\omega}} \in \mathbb{R}_{>0}$, there exist constants $c_{\mathbf{Q}}$, $\beta_{\mathbf{Q}} \in \mathbb{R}_{>0}$ such that, for all $\eta_{\mathbf{m}} \leq \eta_{\boldsymbol{\omega}}\epsilon_3$, all $\eta_{\mathbf{u}} \leq \alpha_{\boldsymbol{\omega}}\eta_{\mathbf{m}}\epsilon_5$, and all $\sigma_r \leq \epsilon_6$, the solutions $\tilde{\mathbf{Q}}$ of system (2.53) satisfy*

$$\|\tilde{\mathbf{Q}}(t)\| \leq \max\left\{c_{\mathbf{Q}}\|\tilde{\mathbf{Q}}(0)\|e^{-\eta_{\mathbf{m}}\beta_{\mathbf{Q}}t}, \frac{1}{8}\right\}, \tag{2.54}$$

for all $t \geq 0$, all $\tilde{\mathbf{Q}}(0) \in \mathbb{R}^{n_{\mathbf{u}}+1\times n_{\mathbf{u}}+1}$ for which $\mathbf{Q}(0)$ is symmetric and positive definite, and all time-varying $\mathbf{u}(t) \in \mathbb{R}^{n_{\mathbf{u}}}$.

Proof. *See the proof of Lemma* 2.11 *in Haring (2016).* □

From Lemma 2.19 and Lemma 2.20, we conclude that there exists a finite time $t_1 \geq 0$ such that $\|\tilde{\mathbf{x}}(t)\| \leq \alpha_{\boldsymbol{\omega}}\eta_{\boldsymbol{\omega}}c_{\mathbf{x}2}$ and $\|\tilde{\mathbf{Q}}(t)\| \leq \frac{1}{8}$ for all $t \geq t_1$. These bounds on $\tilde{\mathbf{x}}(t)$ and $\tilde{\mathbf{Q}}(t)$ are utilized to obtain bounds on the solutions $\tilde{\mathbf{u}}(t)$, $\tilde{\mathbf{z}}(t)$, and $\tilde{\mathbf{m}}(t)$ in Lemmas 2.21, 2.23, and 2.24, respectively.

Firstly, consider the $\tilde{\mathbf{u}}$-dynamics. From the optimizer in (2.40) and the coordinate transformation in (2.42), it follows that the state equation for $\tilde{\mathbf{u}}$ for *time-varying* inputs $\mathbf{u}(t)$ is given by

$$\dot{\tilde{\mathbf{u}}}(t) = -\lambda_{\mathbf{u}}\frac{\eta_{\mathbf{u}}\mathbf{D}\left(\tilde{\mathbf{m}}(t)+\mathbf{m}(t)\right)}{\eta_{\mathbf{u}}+\lambda_{\mathbf{u}}\left\|\mathbf{D}\left(\tilde{\mathbf{m}}(t)+\mathbf{m}(t)\right)\right\|}. \tag{2.55}$$

A bound on the solutions $\tilde{\mathbf{u}}(t)$ in (2.55) for time-varying inputs $\mathbf{u}(t)$ is presented in Lemma 2.21.

Lemma 2.21. *Under Assumption 2.15, for any finite time $t_1 \geq 0$, and all tunable parameters $\eta_{\mathbf{u}}, \lambda_{\mathbf{u}}, \alpha_{\boldsymbol{\omega}} \in \mathbb{R}_{>0}$, the solutions $\tilde{\mathbf{u}}$ of system (2.55) are bounded for all $0 \leq t \leq t_1$, and all $\tilde{\mathbf{u}}(0) \in \mathbb{R}^{n_{\mathbf{u}}}$. In addition, there exists a constant $c_{\mathbf{u}1} \in \mathbb{R}_{>0}$ such that the solutions $\tilde{\mathbf{u}}$ of system (2.55) satisfy*

$$\sup_{t\geq t_1}\|\tilde{\mathbf{u}}(t)\| \leq \max\left\{\|\tilde{\mathbf{u}}(t_1)\|, \frac{1}{\alpha_{\boldsymbol{\omega}}}c_{\mathbf{u}1}\sup_{t\geq t_1}\|\tilde{\mathbf{m}}(t)\|\right\}, \tag{2.56}$$

and

$$\limsup_{t\to\infty}\|\tilde{\mathbf{u}}(t)\| \leq \frac{1}{\alpha_{\boldsymbol{\omega}}}c_{\mathbf{u}1}\limsup_{t\to\infty}\|\tilde{\mathbf{m}}(t)\|. \tag{2.57}$$

Proof. *See the proof of Lemma* 2.12 *in Haring (2016).* □

Secondly, consider the $\tilde{\mathbf{z}}$-dynamics. From the filter Σ_f in (2.12) and its steady-state solution $\bar{\mathbf{z}}_{\mathbf{w}}$, driven by steady-state input $\bar{y}_{\mathbf{w}}(t, \mathbf{u})$ defined by (2.14), the coordinate transformation in (2.42), and the vector field defined by (2.45), it follows that the dynamics of $\tilde{\mathbf{z}}$ for *constant* inputs $\mathbf{u}$ is governed by

$$\dot{\tilde{\mathbf{z}}}(t) = \alpha_{\mathbf{z}}\tilde{\mathbf{h}}_{\mathbf{w}}(t, \tilde{\mathbf{z}}(t), \mathbf{u}, \alpha_{\mathbf{z}}). \tag{2.58}$$

A preliminary result is presented in Lemma 2.22 on the existence of a Lyapunov function for the $\tilde{\mathbf{z}}$-dynamics for *constant* inputs $\mathbf{u}$ in (2.58).

Lemma 2.22. *Under Assumptions 2.2, 2.6, 2.12, given* (2.13), (2.15), *and Property 2.9, there exists a function* $V_{\mathbf{z}} : \mathbb{R} \times \mathbb{R}^{n_{\mathbf{z}}} \times \mathbb{R}^{n_{\mathbf{u}}} \times \mathbb{R} \to \mathbb{R}$, *and constants* $\gamma_{\mathbf{z}1}, ..., \gamma_{\mathbf{z}6} \in \mathbb{R}_{>0}$, *such that the inequalities*

$$\gamma_{\mathbf{z}1}\|\tilde{\mathbf{z}}\|^2 \leq V_{\mathbf{z}}(t, \tilde{\mathbf{z}}, \mathbf{u}, \alpha_{\mathbf{z}}) \leq \gamma_{\mathbf{z}2}\|\tilde{\mathbf{z}}\|^2, \tag{2.59}$$

$$\frac{\partial V_{\mathbf{z}}}{\partial t}(t, \tilde{\mathbf{z}}, \mathbf{u}, \alpha_{\mathbf{z}}) + \alpha_{\mathbf{z}} \frac{\partial V_{\mathbf{z}}}{\partial \tilde{\mathbf{z}}}(t, \tilde{\mathbf{z}}, \mathbf{u}, \alpha_{\mathbf{z}}) \tilde{\mathbf{h}}_{\mathbf{w}}(t, \tilde{\mathbf{z}}, \mathbf{u}, \alpha_{\mathbf{z}}) \leq -\alpha_{\mathbf{z}}\gamma_{\mathbf{z}3}\|\tilde{\mathbf{z}}\|^2, \tag{2.60}$$

$$\left\| \frac{\partial V_{\mathbf{z}}}{\partial \tilde{\mathbf{z}}}(t, \tilde{\mathbf{z}}, \mathbf{u}, \alpha_{\mathbf{z}}) \right\| \leq \gamma_{\mathbf{z}4}\|\tilde{\mathbf{z}}\|, \tag{2.61}$$

and

$$\left\| \frac{\partial V_{\mathbf{z}}}{\partial \mathbf{u}}(t, \tilde{\mathbf{z}}, \mathbf{u}, \alpha_{\mathbf{z}}) \right\| \leq \gamma_{\mathbf{z}5}\|\tilde{\mathbf{z}}\| + \gamma_{\mathbf{z}6}\|\tilde{\mathbf{z}}\|\|\mathbf{u} - \mathbf{u}^*_{\mathbf{w}}\|, \tag{2.62}$$

are satisfied for all $t \in \mathbb{R}$, *all* $\tilde{\mathbf{z}} \in \mathbb{R}^{n_{\mathbf{z}}}$, *all* $\alpha_{\mathbf{z}} \in \mathbb{R}_{>0}$, *and all constant* $\mathbf{u}, \mathbf{u}^*_{\mathbf{w}} \in \mathbb{R}^{n_{\mathbf{u}}}$.

Proof. *The proof of Lemma 2.22 follows a similar line of reasoning as Theorem* 4.14 *and Lemma* 9.8 *in Khalil (2002), and the proof of Lemma 2.18. Different from the results in Khalil (2002) and Lemma 2.18 is the inequality in* (2.62)*; this stems from the bound on* $[\partial \tilde{\mathbf{h}}_{\mathbf{w}}/\partial \mathbf{u}]$, *i.e.,* $\|\partial \tilde{\mathbf{h}}_{\mathbf{w}}/\partial \mathbf{u}\| \leq L_{\mathbf{hz}}(\epsilon_{\mathbf{z}}L_{\mathbf{z}1} + (\epsilon_{\mathbf{z}}L_{\mathbf{z}2} + L_{\mathbf{q}})\|\mathbf{u} - \mathbf{u}^*_{\mathbf{w}}\|)$, *resulting from* (2.15), *Assumption 2.12, and the coordinate transformation in* (2.42). □

From the filter Σ_f in (2.12), the coordinate transformation in (2.42), and the vector field defined by (2.45), it follows that the state equation for $\tilde{\mathbf{z}}$ for *time-varying* inputs $\mathbf{u}(t)$, and driven by (2.1), (2.40) and (2.28), is given by

$$\begin{aligned} \dot{\tilde{\mathbf{z}}}(t) = \alpha_{\mathbf{z}} \tilde{\mathbf{h}}_{\mathbf{w}}(t, \tilde{\mathbf{z}}(t), \mathbf{u}(t), \alpha_{\mathbf{z}}) - \frac{\partial \bar{\mathbf{z}}_{\mathbf{w}}}{\partial \mathbf{u}}(t, \mathbf{u}(t), \alpha_{\mathbf{z}}) \dot{\mathbf{u}}(t) \\ + \alpha_{\mathbf{z}}\big(\mathbf{h}(\mathbf{z}(t), y(t)) - \mathbf{h}(\mathbf{z}(t), \bar{y}_{\mathbf{w}}(t, \mathbf{u}(t)))\big). \end{aligned} \tag{2.63}$$

A bound on the solutions of the $\tilde{\mathbf{z}}$-dynamics for time-varying inputs $\mathbf{u}(t)$ in (2.63) is presented in Lemma 2.23.

Lemma 2.23. *Under Assumptions 2.2, 2.6, 2.12, given* (2.13), (2.15), *and Property 2.9, for any* $\epsilon_0, \ldots, \epsilon_3, \epsilon_5, \epsilon_{\mathbf{z}} \in \mathbb{R}_{>0}$, *any finite time* $t_1 \geq 0$, *and all* $\alpha_{\boldsymbol{\omega}} \leq \epsilon_0, \alpha_{\mathbf{z}} \leq \alpha_{\boldsymbol{\omega}}\epsilon_1 \leq \epsilon_{\mathbf{z}}, \eta_{\boldsymbol{\omega}} \leq \alpha_{\mathbf{z}}\epsilon_2, \eta_{\mathbf{m}} \leq \eta_{\boldsymbol{\omega}}\epsilon_3, \eta_{\mathbf{u}} \leq \alpha_{\boldsymbol{\omega}}\eta_{\mathbf{m}}\epsilon_5$, *the solutions* $\tilde{\mathbf{z}}$ *of system 2.63 are bounded for all* $0 \leq t \leq t_1$, *all* $\tilde{\mathbf{z}}(0) \in \mathbb{R}^{n_{\mathbf{z}}}$, *all* $\tilde{\mathbf{x}}(0) \in \mathbb{R}^{n_{\mathbf{x}}}$, *and all* $\tilde{\mathbf{u}}(0) \in \mathbb{R}^{n_{\mathbf{u}}}$. *In addition, there exist constants* $c_{\mathbf{z}1}, c_{\mathbf{z}2}(\epsilon_0, \epsilon_1, \epsilon_3, \epsilon_5), c_{\mathbf{z}3}(\epsilon_0, \ldots, \epsilon_3, \epsilon_5, \epsilon_{\mathbf{z}})$, *and* $c_{\mathbf{z}4}(\epsilon_0, \epsilon_1, \epsilon_3, \epsilon_5, \epsilon_{\mathbf{z}}) \in \mathbb{R}_{>0}$ *such that the solutions* $\tilde{\mathbf{z}}$ *of system 2.63 satisfy*

$$\sup_{t \geq t_1} \|\tilde{\mathbf{z}}(t)\| \leq \sup_{t \geq t_1} \max\left\{ c_{\mathbf{z}1}\|\tilde{\mathbf{z}}(t_1)\|, \frac{\alpha_{\boldsymbol{\omega}}\eta_{\boldsymbol{\omega}}}{\alpha_{\mathbf{z}}} c_{\mathbf{z}2}, \alpha^2_{\boldsymbol{\omega}} c_{\mathbf{z}3}, \frac{\alpha_{\boldsymbol{\omega}}\eta_{\boldsymbol{\omega}}}{\alpha_{\mathbf{z}}} c_{\mathbf{z}4}\|\tilde{\mathbf{u}}(t)\| \right\}, \tag{2.64}$$

and

$$\limsup_{t\to\infty} \|\tilde{\mathbf{z}}(t)\| \leq \limsup_{t\to\infty} \max\left\{ \frac{\alpha_{\boldsymbol{\omega}}\eta_{\boldsymbol{\omega}}}{\alpha_{\mathbf{z}}} c_{\mathbf{z}2}, \alpha_{\boldsymbol{\omega}}^2 c_{\mathbf{z}3}, \frac{\alpha_{\boldsymbol{\omega}}\eta_{\boldsymbol{\omega}}}{\alpha_{\mathbf{z}}} c_{\mathbf{z}4} \|\tilde{\mathbf{u}}(t)\| \right\}, \tag{2.65}$$

for all $t \geq t_1$, and all time-varying $\tilde{\mathbf{u}}(t) \in \mathbb{R}^{n_{\mathbf{u}}}$.

Proof. *See Appendix 2.E.* □

Thirdly, consider the $\tilde{\mathbf{m}}$-dynamics. From the observer in (2.38), the coordinate transformation in (2.42), the model of the input-output behavior in (2.35), and the state definition in (2.30), we obtain that the state equation for $\tilde{\mathbf{m}}$ is given by

$$\begin{aligned} \dot{\tilde{\mathbf{m}}}(t) = &\left(\mathbf{A}(t) - \eta_{\mathbf{m}}\mathbf{Q}(t)\left(\mathbf{C}^\top(t)\mathbf{C}(t) + \sigma_r \mathbf{D}^\top\mathbf{D}\right)\right)\tilde{\mathbf{m}}(t) \\ &+ \alpha_{\boldsymbol{\omega}}^2 \mathbf{B}\left(\hat{\mathbf{s}}(t) - \mathbf{s}(t)\right) - \eta_{\mathbf{m}}\sigma_r\alpha_{\boldsymbol{\omega}}\mathbf{Q}(t)\mathbf{D}^\top \frac{dF_{\mathbf{w}}}{d\mathbf{u}^\top}(\hat{\mathbf{u}}(t)) \\ &- \eta_{\mathbf{m}}\mathbf{Q}(t)\mathbf{C}^\top(t)(\alpha_{\boldsymbol{\omega}}^2\left(\hat{v}(t) - v(t)\right) - r(t) - d(t)). \end{aligned} \tag{2.66}$$

A bound on the solutions $\tilde{\mathbf{m}}(t)$ in (2.66) for time-varying inputs $\mathbf{u}(t)$ is presented in Lemma 2.24.

Lemma 2.24. *For any $\epsilon_0, \epsilon_1, \epsilon_3, \epsilon_5, \epsilon_{\mathbf{z}} \in \mathbb{R}_{>0}$, any finite time $t_1 \geq 0$, all $\alpha_{\boldsymbol{\omega}} \leq \epsilon_0, \alpha_{\mathbf{z}} \leq \alpha_{\boldsymbol{\omega}}\epsilon_1 \leq \epsilon_{\mathbf{z}}, \eta_{\boldsymbol{\omega}} \leq \alpha_{\mathbf{z}}\epsilon_2, \eta_{\mathbf{m}} \leq \eta_{\boldsymbol{\omega}}\epsilon_3, \eta_{\mathbf{u}} \leq \alpha_{\boldsymbol{\omega}}\eta_{\mathbf{m}}\epsilon_5$, all $\lambda_{\mathbf{u}}, \sigma_r \in \mathbb{R}_{>0}$ and any $\delta_{\mathbf{z}1}, \delta_{\mathbf{z}2} \in \mathbb{R}_{\geq 0}$, the solutions $\tilde{\mathbf{m}}$ of system (2.66) are bounded for all $0 \leq t \leq t_1$, all $\tilde{\mathbf{u}}(0) \in \mathbb{R}^{n_{\mathbf{u}}}$, all $\tilde{\mathbf{z}}(0) \in \mathbb{R}^{n_{\mathbf{z}}}$, and all $\tilde{\mathbf{m}}(0) \in \mathbb{R}^{n_{\mathbf{u}}+1}$. In addition, for sufficiently small $\epsilon_3, \epsilon_4, \epsilon_6 \in \mathbb{R}_{>0}$ and all $\alpha_{\boldsymbol{\omega}}\lambda_{\mathbf{u}} \leq \eta_{\mathbf{m}}\epsilon_4$, there exist constants $c_{\mathbf{m}1}, ..., c_{\mathbf{m}8} \in \mathbb{R}_{>0}$ such that the solutions $\tilde{\mathbf{m}}$ of system (2.66) satisfy*

$$\begin{aligned} \sup_{t\geq t_1}\|\tilde{\mathbf{m}}(t)\| \leq \sup_{t\geq t_1} \max\Big\{ &c_{\mathbf{m}1}\|\tilde{\mathbf{m}}(t_1)\|, c_{\mathbf{m}2}\frac{\alpha_{\boldsymbol{\omega}}^2\lambda_{\mathbf{u}}}{\eta_{\mathbf{m}}}\|\tilde{\mathbf{u}}(t)\|, \alpha_{\boldsymbol{\omega}}^2 c_{\mathbf{m}3}, c_{\mathbf{m}4}\|\tilde{\mathbf{z}}(t)\|, \\ &\alpha_{\mathbf{z}}\delta_{\mathbf{z}1}c_{\mathbf{m}5}, \alpha_{\mathbf{z}}\delta_{\mathbf{z}2}c_{\mathbf{m}6}\|\tilde{\mathbf{u}}(t)\|^2, \alpha_{\mathbf{z}}\alpha_{\boldsymbol{\omega}}^2\delta_{\mathbf{z}2}c_{\mathbf{m}7}, \sqrt{\sigma_r}\alpha_{\boldsymbol{\omega}}c_{\mathbf{m}8}\|\tilde{\mathbf{u}}(t)\|\Big\}, \end{aligned} \tag{2.67}$$

and

$$\begin{aligned} \limsup_{t\to\infty}\|\tilde{\mathbf{m}}(t)\| \leq \limsup_{t\to\infty} \max\Big\{ &c_{\mathbf{m}2}\frac{\alpha_{\boldsymbol{\omega}}^2\lambda_{\mathbf{u}}}{\eta_{\mathbf{m}}}\|\tilde{\mathbf{u}}(t)\|, \alpha_{\boldsymbol{\omega}}^2 c_{\mathbf{m}3}, c_{\mathbf{m}4}\|\tilde{\mathbf{z}}(t)\|, \\ &\alpha_{\mathbf{z}}\delta_{\mathbf{z}1}c_{\mathbf{m}5}, \alpha_{\mathbf{z}}\delta_{\mathbf{z}2}c_{\mathbf{m}6}\|\tilde{\mathbf{u}}(t)\|^2, \alpha_{\mathbf{z}}\alpha_{\boldsymbol{\omega}}^2\delta_{\mathbf{z}2}c_{\mathbf{m}7}, \sqrt{\sigma_r}\alpha_{\boldsymbol{\omega}}c_{\mathbf{m}8}\|\tilde{\mathbf{u}}(t)\|\Big\}, \end{aligned} \tag{2.68}$$

for all $t \geq t_1$, and all time-varying $\tilde{\mathbf{u}}(t) \in \mathbb{R}^{n_{\mathbf{u}}}$.

Proof. *See Appendix 2.F.* □

The dynamics of $\tilde{\mathbf{u}}$, $\tilde{\mathbf{z}}$, and $\tilde{\mathbf{m}}$ can be seen as feedback-interconnected subsystems for which the solutions satisfy the bounds in Lemmas 2.21, 2.23, and 2.24, respectively. To verify that this feedback-interconnected system exhibits

bounded solutions, the cyclic-small-gain criterion in Liu et al. (2011) is employed. Let us consider arbitrary initial conditions $\mathbf{x}(0) \in \mathbb{R}^{n_{\mathbf{x}}}$, $\mathbf{Q}(0) \in \mathbb{R}^{n_{\mathbf{u}}+1 \times n_{\mathbf{u}}+1}$ symmetric and positive-definite, $\mathbf{z}(0) \in \mathbb{R}^{n_{\mathbf{z}}}$, $\hat{\mathbf{m}}(0) \in \mathbb{R}^{n_{\mathbf{u}}+1}$, an arbitrary large compact set $\mathcal{U}_0 \subset \mathcal{U} \subset \mathbb{R}^{n_{\mathbf{u}}}$ of initial conditions for $\hat{\mathbf{u}}(t)$ with $\mathcal{U}_0 := \{\hat{\mathbf{u}} \in \mathbb{R}^{n_{\mathbf{u}}} : \|\tilde{\mathbf{u}}(t)\| \leq \rho_{\mathbf{u}}\}$ and with $\rho_{\mathbf{u}} \in \mathbb{R}_{>0}$, and $\mathcal{U} := \{\hat{\mathbf{u}} \in \mathbb{R}^{n_{\mathbf{u}}} : \|\tilde{\mathbf{u}}(t)\| \leq L_{\mathbf{u}}\}$ a (arbitrarily large) compact set with some (sufficiently large) constant $L_{\mathbf{u}} \in \mathbb{R}_{>0}$. Later on, we will elaborate more on the role of the constant $L_{\mathbf{u}}$. For now, we consider it to exist, and additionally, we consider $\hat{\mathbf{u}}(t) \in \mathcal{U}$ for all time.

Under the conditions of Theorem 2.16, there exist sufficiently small constants $\epsilon_0, \ldots, \epsilon_6 \in \mathbb{R}_{>0}$, such that the cyclic-small-gain criteria that follow from Lemmas 2.21, 2.23 and 2.24 and given by $c_{\mathbf{u}1}c_{\mathbf{m}2}\epsilon_4 < 1$, $c_{\mathbf{u}1}c_{\mathbf{m}6}\epsilon_1\delta_{\mathbf{z}2}L_{\mathbf{u}} < 1$, $c_{\mathbf{u}1}c_{\mathbf{m}4}c_{\mathbf{z}4}(\epsilon_0, \epsilon_1, \epsilon_3, \epsilon_5, \epsilon_{\mathbf{z}})\epsilon_2 < 1$, $c_{\mathbf{u}1}c_{\mathbf{m}8}\sqrt{\epsilon_6} < 1$ are satisfied, rendering the closed-loop system of the extended plant Σ and the extremum-seeking controller to have bounded solutions. The final property that needs to be validated is that $\hat{\mathbf{u}}(t) \in \mathcal{U}$ for all time. We do this for the two temporal stages of convergence.

First, we consider $0 \leq t \leq t_1$. From the optimizer in (2.40) we have that $\|\dot{\tilde{\mathbf{u}}}(t)\| \leq \eta_{\mathbf{u}}$. For any $\hat{\mathbf{u}}(0) \in \mathcal{U}_0$, it follows that $\sup_{0\leq t\leq t_1} \|\tilde{\mathbf{u}}(t)\| \leq \rho_{\mathbf{u}} + \eta_{\mathbf{u}}t_1$. Under the conditions in Theorem 2.16, sufficiently small $\epsilon_0, \ldots, \epsilon_6 \in \mathbb{R}_{>0}$ such that the cyclic-gain criteria are satisfied, and for any finite time $t_1 \geq 0$, there exist tunable parameters $\eta_{\mathbf{u}}, \alpha_{\boldsymbol{\omega}}, \eta_{\mathbf{m}} \in \mathbb{R}_{>0}$ with $\eta_{\mathbf{u}} \leq \alpha_{\boldsymbol{\omega}}\eta_{\mathbf{m}}\epsilon_5 \leq \epsilon_0^2\epsilon_1\epsilon_2\epsilon_3\epsilon_5$, such that $\sup_{0\leq t\leq t_1} \|\tilde{\mathbf{u}}(t)\| \leq \rho_{\mathbf{u}} + \eta_{\mathbf{u}}t_1 < L_{\mathbf{u}}$ for sufficiently large $L_{\mathbf{u}} \in \mathbb{R}_{>0}$, implying $\hat{\mathbf{u}}(t) \in \mathcal{U}$ for $0 \leq t \leq t_1$.

Secondly, we consider $t \geq t_1$. From (2.56), (2.64), (2.67), and the satisfaction of the cyclic-small-gain criteria we obtain

$$\begin{aligned}\sup_{t\geq t_1}\|\tilde{\mathbf{u}}(t)\| \leq \max\Big\{&\|\tilde{\mathbf{u}}(t_1)\|, \frac{1}{\alpha_{\boldsymbol{\omega}}}c_{\mathbf{u}1}c_{\mathbf{m}1}\|\tilde{\mathbf{m}}(t_1)\|, \alpha_{\boldsymbol{\omega}}c_{\mathbf{u}1}c_{\mathbf{m}3}, \frac{\eta_{\boldsymbol{\omega}}}{\alpha_{\mathbf{z}}}c_{\mathbf{z}2}c_{\mathbf{u}1}c_{\mathbf{m}4},\\ &\frac{1}{\alpha_{\boldsymbol{\omega}}}c_{\mathbf{u}1}c_{\mathbf{m}4}c_{\mathbf{z}1}\|\tilde{\mathbf{z}}(t_1)\|, \alpha_{\boldsymbol{\omega}}c_{\mathbf{u}1}c_{\mathbf{m}4}c_{\mathbf{z}3}, \frac{\alpha_{\mathbf{z}}}{\alpha_{\boldsymbol{\omega}}}\delta_{\mathbf{z}1}c_{\mathbf{u}1}c_{\mathbf{m}5}, \alpha_{\mathbf{z}}\alpha_{\boldsymbol{\omega}}\delta_{\mathbf{z}2}c_{\mathbf{u}1}c_{\mathbf{m}7}\Big\},\end{aligned} \tag{2.69}$$

For the first term in the right-hand side of (2.69) we can make a similar observation as for the case when $0 \leq t \leq t_1$. Furthermore, for sufficiently small $\epsilon_0, \ldots, \epsilon_6 \in \mathbb{R}_{>0}$, there exist tunable parameters $\alpha_{\boldsymbol{\omega}}, \eta_{\boldsymbol{\omega}}, \alpha_{\mathbf{z}}$ with $\alpha_{\boldsymbol{\omega}} \leq \epsilon_0, \alpha_{\mathbf{z}} \leq \alpha_{\boldsymbol{\omega}}\epsilon_1$ and $\eta_{\boldsymbol{\omega}} \leq \alpha_{\mathbf{z}}\epsilon_2$, such that the third, and fifth through eight term in the right-hand side of (2.69) can be made arbitrarily small (smaller than $L_{\mathbf{u}}$). Finally, we can derive expressions for the second and fourth term in the right-hand side of (2.69) using Lemmas 2.23 and 2.24. Under the conditions of Theorem 2.16, for the initial conditions $\mathbf{x}(0)$, $\mathbf{Q}(0)$, $\mathbf{z}(0)$, $\hat{\mathbf{m}}(0)$, and $\hat{\mathbf{u}}(0) \in \mathcal{U}_0$, and sufficiently small constants $\epsilon_0, ..., \epsilon_6 \in \mathbb{R}_{>0}$, there exist tunable parameters $\alpha_{\mathbf{z}}, \alpha_{\boldsymbol{\omega}}, \eta_{\mathbf{u}}, \lambda_{\mathbf{u}}, \eta_{\mathbf{m}}, \eta_{\boldsymbol{\omega}} \in \mathbb{R}_{>0}$ and $\sigma_r \in \mathbb{R}_{\geq 0}$ with $\alpha_{\boldsymbol{\omega}} \leq \epsilon_0$, $\alpha_{\mathbf{z}} \leq \alpha_{\boldsymbol{\omega}}\epsilon_1$, $\eta_{\boldsymbol{\omega}} \leq \alpha_{\mathbf{z}}\epsilon_2$, $\eta_{\mathbf{m}} \leq \eta_{\boldsymbol{\omega}}\epsilon_3$, $\alpha_{\boldsymbol{\omega}}\lambda_{\mathbf{u}} \leq \eta_{\mathbf{m}}\epsilon_4$, $\eta_{\mathbf{u}} \leq \alpha_{\boldsymbol{\omega}}\eta_{\mathbf{m}}\epsilon_5$, and $\sigma_r \leq \epsilon_6$, such that the second and fourth term in the right-hand side of (2.69) can be made arbitrarily small (smaller than $L_{\mathbf{u}}$). As a result, $\hat{\mathbf{u}}(t) \in \mathcal{U}$ for all time.

Finally, from (2.57), (2.65), and (2.68) we obtain

$$\limsup_{t\to\infty} \|\tilde{\mathbf{u}}(t)\| \leq \max\Big\{\alpha_{\boldsymbol{\omega}} c_{\mathbf{u}1} c_{\mathbf{m}3}, \frac{\eta_{\boldsymbol{\omega}}}{\alpha_{\mathbf{z}}} c_{\mathbf{z}2} c_{\mathbf{u}1} c_{\mathbf{m}4}, \alpha_{\boldsymbol{\omega}} c_{\mathbf{u}1} c_{\mathbf{m}4} c_{\mathbf{z}3}, \frac{\alpha_{\mathbf{z}}}{\alpha_{\boldsymbol{\omega}}} \delta_{\mathbf{z}1} c_{\mathbf{u}1} c_{\mathbf{m}5}, \alpha_{\mathbf{z}} \alpha_{\boldsymbol{\omega}} \delta_{\mathbf{z}2} c_{\mathbf{u}1} c_{\mathbf{m}7}\Big\}. \tag{2.70}$$

Concluding, given a (time-varying) disturbance $\mathbf{w} \in \mathcal{W}$ and Assumptions 2.2, 2.6, 2.12, and 2.15. Consider arbitrary initial conditions $\mathbf{x}(0) \in \mathbb{R}^{n_{\mathbf{x}}}$, $\mathbf{Q}(0) \in \mathbb{R}^{n_{\mathbf{u}}+1 \times n_{\mathbf{u}}+1}$ symmetric and positive-definite, $\mathbf{z}(0) \in \mathbb{R}^{n_{\mathbf{z}}}$, $\hat{\mathbf{m}}(0) \in \mathbb{R}^{n_{\mathbf{u}}+1}$, and an arbitrary compact set $\mathcal{U}_0 \subset \mathbb{R}^{n_{\mathbf{u}}}$ of initial conditions for $\hat{\mathbf{u}}(t)$. There exist sufficiently small constants $\epsilon_0, ..., \epsilon_6 \in \mathbb{R}_{>0}$, such that, for all tunable parameters $\alpha_{\mathbf{z}}, \alpha_{\boldsymbol{\omega}}, \eta_{\mathbf{u}}, \lambda_{\mathbf{u}}, \eta_{\mathbf{m}}, \eta_{\boldsymbol{\omega}} \in \mathbb{R}_{>0}$ and $\sigma_r \in \mathbb{R}_{\geq 0}$ with $\alpha_{\boldsymbol{\omega}} \leq \epsilon_0$, $\alpha_{\mathbf{z}} \leq \alpha_{\boldsymbol{\omega}}\epsilon_1$, $\eta_{\boldsymbol{\omega}} \leq \alpha_{\mathbf{z}}\epsilon_2$, $\eta_{\mathbf{m}} \leq \eta_{\boldsymbol{\omega}}\epsilon_3$, $\alpha_{\boldsymbol{\omega}}\lambda_{\mathbf{u}} \leq \eta_{\mathbf{m}}\epsilon_4$, $\eta_{\mathbf{u}} \leq \alpha_{\boldsymbol{\omega}}\eta_{\mathbf{m}}\epsilon_5$, and $\sigma_r \leq \epsilon_6$, the solutions of the closed-loop system are bounded. Moreover, the bound on the solutions $\hat{\mathbf{u}}(t)$ with $\hat{\mathbf{u}}(0) \in \mathcal{U}_0$ in (2.41) follows from (2.70) with $c_1 := \max\{c_{\mathbf{u}1} c_{\mathbf{m}3}, c_{\mathbf{u}1} c_{\mathbf{m}4} c_{\mathbf{z}3}\}$, $c_2 := c_{\mathbf{z}2} c_{\mathbf{u}1} c_{\mathbf{m}4}$, $c_3 := c_{\mathbf{u}1} c_{\mathbf{m}5}$, $c_4 := c_{\mathbf{u}1} c_{\mathbf{m}7}$, which completes the proof of Theorem 2.16. □

2.5 Case study: Performance-optimal nonlinear control strategy for a short-stroke wafer stage

In this section, we consider an industrial case study of the performance-optimal tuning of a variable-gain control (VGC) strategy for a short-stroke wafer stage of a wafer scanner as also studied in Pavlov et al. (2013) and Hunnekens et al. (2012). Wafer scanners are part of the complex machinery used to manufacture integrated circuits (ICs), see, e.g. Fig. 2.4 and some of its crucial elements. Basically, light, emitted by a laser, first passes through a so-called reticle which contains an image of the desired topology of an IC. The image is then projected onto a photo-sensitive layer on a so-called wafer by an optical system. The light in combination with the photo-sensitive layer induces a chemical reaction, resulting in the desired topology being transferred onto the wafer. A wafer typically contains 100 ICs, which requires extremely fast (re-)positioning of the wafer stage in three degrees-of-freedom with *nm*-accuracy to achieve the desired high machine throughput. Achieving *nm*-accuracy and high speeds of the wafer stage are in general realized by high-bandwidth linear controllers. However, due to the well-known waterbed-effect, see, e.g., Freudenberg et al. (2000), increasing the bandwidth further to improve the ability to suppress low-frequency disturbances comes at the expense of an increased sensitivity to high-frequency disturbances and noise. Instead, a variable-gain controller can be used to balance this trade-off in a more desirable manner (Heertjes et al., 2009); it enables a higher bandwidth only when necessary. Although VGC is intuitive in nature, performance-optimal tuning of a variable-gain controller is far from trivial and heavily depends on the disturbance situation at hand. In this section, we employ the ESC method proposed in Section 2.2 to tune the VGC strategy for optimal

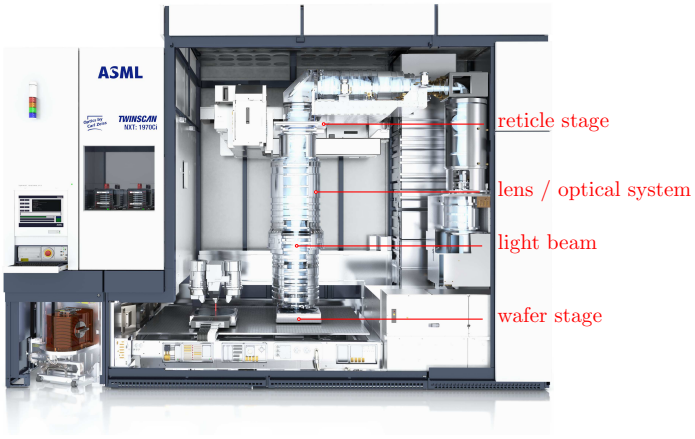

Figure 2.4: Overview of the crucial elements of a wafer scanner.

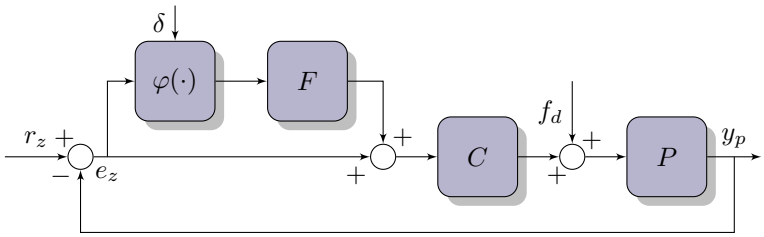

Figure 2.5: The closed-loop variable-gain control scheme.

steady-state performance of a short-stroke wafer stage simulation model, illustrating the effectiveness of the proposed ESC approach.

2.5.1 Variable-gain controlled wafer stage

Nonlinear feedback control scheme

The VGC structure is shown in Fig. 2.5. The scheme consists of a plant P, representing the dynamics of a short-stroke wafer stage in z-direction, and a nominal linear controller C, having transfer functions $P(s)$ and $C(s)$, respectively, with $s \in \mathbb{C}$ being the Laplacian variable, (time-varying) force disturbances $f_d(t)$, a nonlinear control element $\varphi(\cdot,\cdot)$, and a shaping filter $F(s)$. Furthermore, r_z denotes the setpoint in z-direction, and e_z denotes the tracking error in z-direction, which is the performance variable to-be optimized. The setpoint is $r_z = 0$. The nonlinearity $\varphi(e_z, \delta)$, representing the variable-gain element with e_z and δ as inputs, is given by a dead-zone characteristic

$$\varphi(e_z,\delta) = \begin{cases} \alpha(e_z+\delta), & \text{if } e_z < -\delta, \\ 0, & \text{if } |e_z| \le \delta, \\ \alpha(e_z-\delta), & \text{if } e_z > \delta, \end{cases} \tag{2.71}$$

where α and δ denote the so-called additional gain and the dead-zone length, respectively. The plant is modelled as a 4^{th}-order mass-spring-damper-mass system, admitting the following transfer function representation

$$P(s) = \frac{m_1 s^2 + bs + k}{s^2(m_1 m_2 s^2 + b(m_1+m_2)s + k(m_1+m_2))}, \tag{2.72}$$

for which we have used the following numerical values: $m_1 = 5$ kg, $m_2 = 17.5$ kg, $k = 7.5 \cdot 10^7$ N/m, $b = 90$ Ns/m. The nominal, and stabilizing linear controller C consists of a PID-controller C_{pid}, a second-order low-pass filter C_{lp} and a notch filter C_n, i.e. $C(s) = C_{pid}(s)C_{lp}(s)C_n(s)$. The transfer function representation of the filters are as follows:

$$C_{pid}(s) = \frac{k_p(s^2 + (\omega_i + \omega_d)s + \omega_i\omega_d)}{\omega_d s}, \tag{2.73}$$

where $k_p = 6.9 \cdot 10^6$ N/m, $\omega_d = 3.8 \cdot 10^2$ rad/s, and $\omega_i = 3.14 \cdot 10^2$ rad/s,

$$C_{lp}(s) = \frac{\omega_{lp}^2}{s^2 + 2\beta_{lp}\omega_{lp}s + \omega_{lp}^2}, \tag{2.74}$$

where $\omega_{lp} = 3.04 \cdot 10^3$ rad/s, and $\beta_p = 0.08$, and

$$C_n(s) = \frac{s^2 + 2\beta_z\omega_z s + \omega_z^2}{s^2 + 2\beta_p\omega_p s + \omega_p^2}, \tag{2.75}$$

where $\omega_z = 4.39 \cdot 10^3$ rad/s, $\omega_p = 5.03 \cdot 10^3$ rad/s, $\beta_z = 2.7 \cdot 10^{-3}$, and $\beta_p = 0.88$. The transfer function representation of the shaping filter $F(s)$ is given by

$$F(s) = \frac{s^2 + 2\beta_{z,F}\omega_{z,F}s + \omega_{z,F}^2}{s^2 + 2\beta_{p,F}\omega_{p,F}s + \omega_{p,F}^2}, \tag{2.76}$$

with $\omega_{z,F} = \omega_{p,F} = 2 \cdot 10^3$ rad/s, $\beta_{z,F} = 0.6$, $\beta_{p,F} = 4.8$. The bandwidth, i.e., the cross-over frequency of the nominal open-loop frequency response function $C(s)P(s)$, is about 150 Hz.

Remark 2.25. *Assumption 2.2 states that the dynamics of the plant* (2.1) *are twice continuously differentiable with respect to the vector of tunable plant parameters. The use of a dead-zone nonlinearity as presented in* (2.71) *actually violates this assumption. Although it is possible to define a sufficiently smooth nonlinearity $\varphi(\cdot)$, for ease of implementation and the fact that the conclusions with respect to convergence are similar, we use the non-smooth nonlinearity as in* (2.71).

Time-domain performance

The disturbance $f_d(t)$ acting on the system consists of a low-frequency force disturbance contribution induced by (3^{rd}-order) setpoint accelerations in the x- and y-direction of the wafer stage (see Fig. 2.6 for a scaled acceleration profile in y-direction depicted by (--)), and a high-frequency force disturbance contribution, modelled as a signal containing multiple sinusoidal components with both random frequencies between 200-500 Hz and random phases between $[-\pi, \pi]$ rad/s, as similarly done in Pavlov et al. (2013) and Hunnekens et al. (2012). From Theorem 1 in Pavlov et al. (2013), which is based on circle criterion type arguments, it can be concluded that if the additional gain for the dead-zone characteristic in (2.71) is chosen as $\alpha \leq 4.34$, then the closed-loop system satisfies Assumption 2.6, i.e., the closed-loop variable-gain control scheme exhibits globally exponentially stable steady-state solutions. The dead-zone length δ turns out to be a stability-invariant tunable plant parameter; however, the choice for δ does affect significantly the achievable tracking performance as the optimal

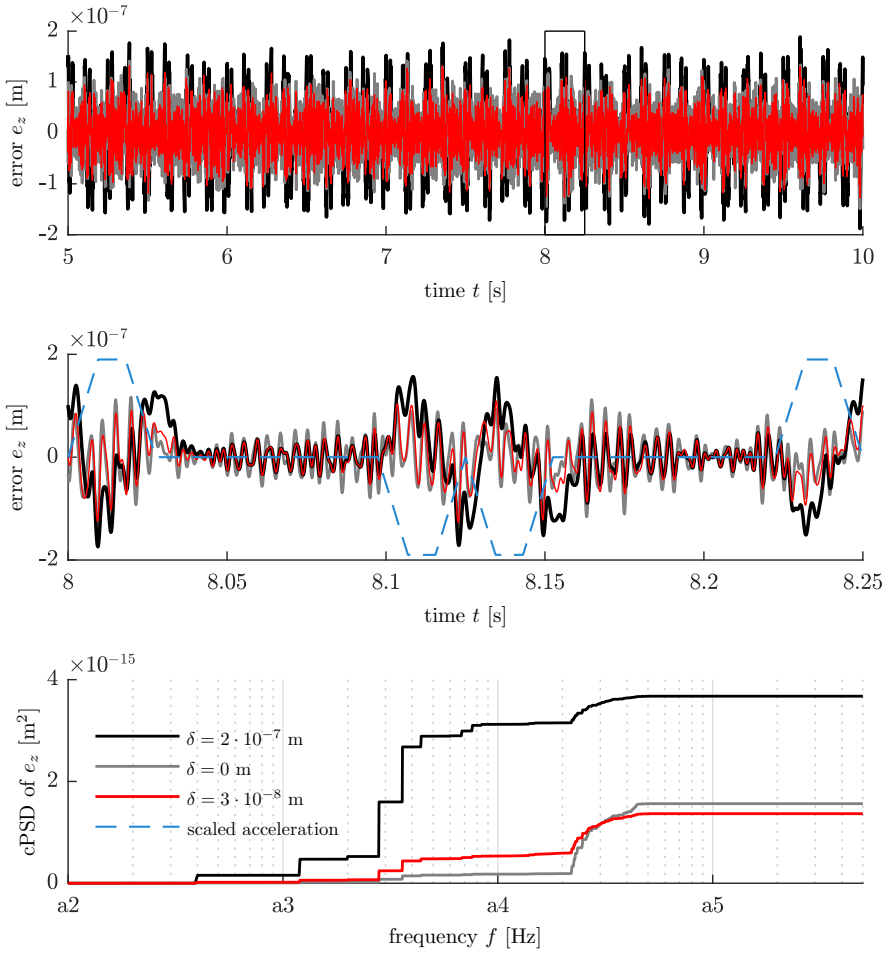

Figure 2.6: The steady-state tracking error (depicted on time window $t \in [5, 10]$ and $t \in [8, 8.25]$) and its cumulative power spectral density for three cases with additional gain $\alpha = 4.33$; i) (—) low-gain linear controller with $\max|e| << \delta = 2 \cdot 10^{-7}$ m, ii) (—) high-gain linear controller with $\delta = 0$ m, and iii) (—) variable-gain controller with $\delta = 3 \cdot 10^{-8}$ m. A scaled acceleration profile in y-direction is depicted by (- -).

value for δ depends heavily on the disturbance situation and performance measure at hand, and is typically chosen in a heuristic manner. Fig. 2.6 shows a time interval of the steady-state tracking error and its cumulative power spectral density plot for three cases of dead-zone length δ with additional gain $\alpha = 4.33$; i) (—) $\delta = 2 \cdot 10^{-7}$, referred to as the nominal low-gain linear controller, ii) (—)

$\delta = 0$, referred to as the high-gain linear controller, and iii) (—) $\delta = 3 \cdot 10^{-8}$, in which VGC is employed. Due to the low-frequency disturbance contribution induced by the reference trajectory, the steady-state responses in Fig. 2.6 behave near periodically with period time $T_{\mathbf{w}} = 0.25$ seconds, which is most apparent in the low-gain control situation. However, due to the high-frequency disturbance contribution having randomly chosen frequencies and phases, the steady-state responses are time-varying rather than periodic. Moreover, periodicity of the responses is not clearly evident in the high-gain control situation. Generally, severe non-periodic behavior may limit extremum-seeking control techniques such as, e.g., in Haring et al. (2013), to achieve optimal system performance. In this case study, we wish to *optimize the tracking error signal e_z by minimizing its power content*. As such, we propose to tune the dead-zone length δ in real-time by the ESC scheme presented in Sections 2.2 and 2.3.

2.5.2 Performance optimization using extremum-seeking control

Here, the working principle of the proposed ESC strategy is illustrated, on the one hand, by optimizing the performance of the variable-gain controlled motion stage, and on the other hand, by exploring the influence of the time-scale of the dynamic cost function and its effect on the convergence speed of the extremum-seeking control scheme.

Identifying the objective function

For the ESC scheme as presented in Sections 2.2 and 2.3, the measured performance variable is the tracking error e_z, and the tunable system parameter is the dead-zone length δ. We choose the cost function as $Z(e_z(t)) = e_z^2(t)$, and the filter Σ_f as a second-order low-pass filter admitting the following state-space formulation

$$\Sigma_f : \begin{cases} \dot{z}_1(t) = \alpha_{\mathbf{z}} z_2(t) \\ \dot{z}_2(t) = \alpha_{\mathbf{z}} \left(y(t) - 2\beta_{\mathbf{z}} z_2(t) - z_1(t) \right) \\ l(t) = z_1(t), \end{cases} \tag{2.77}$$

which is of the form in (2.12). The specific choices for the cost function Z and the filter Σ are motivated by the desire to minimize the power of the tracking error, which ultimately leads to a performance-optimal tracking error. Furthermore, the specific choice of the cost function Z and filter Σ_f with $\alpha_{\mathbf{z}}, \beta_{\mathbf{z}} \in \mathbb{R}_{>0}$, renders the satisfaction of (2.13), (2.15), and Property 2.9. A sufficiently accurate approximation of the objective function $F_{\mathbf{w}}(\delta)$ is obtained through simulation and depicted in Fig. 2.7. Note that, in general, obtaining an approximation of the objective function can be an expensive and time-consuming task.

From the objective function in Fig. 2.7 it can be observed that the optimal dead-zone length δ^* for this specific disturbance situation is approximately

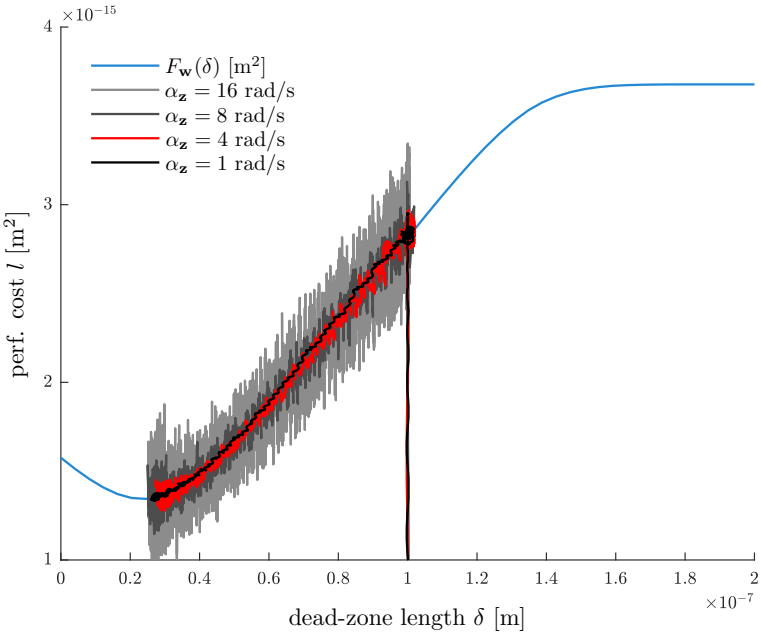

Figure 2.7: Approximation of the objective function $F_{\mathbf{w}}$ obtained through simulation, and the minimization of the performance cost l by adaptation of δ for different values of the filter parameter $\alpha_{\mathbf{z}}$.

$3{\cdot}10^{-8}$ m. In the remainder, extremum-seeking control is used to find the optimal dead-zone length in real-time, without any knowledge about the objective function itself. The nominal tuning of the extremum-seeking controller parameters as used in the simulations is as follows: $\beta_{\mathbf{z}} = \frac{1}{2}\sqrt{2}$, $\alpha_{\boldsymbol{\omega}} = 0.5 \cdot 10^{-9}$ nm, $\alpha_{\mathbf{z}} = 4$ rad/s, $\eta_{\omega} = 5$ rad/s, $\eta_{\mathbf{m}} = 0.5$, $\sigma_r = 1 \cdot 10^{-6}$, $\lambda_{\mathbf{u}} = 1 \cdot 10^{8}$, $\hat{H}(t, \delta) = 0.55$ for all t and δ, and $\eta_{\mathbf{u}} = 1 \cdot 10^{-3}$. The initial conditions are chosen as $\mathbf{z}^{\top}(0) = [0 \quad 0]$, $\hat{\mathbf{m}}^{\top}(0) = [0 \quad 0]$, $\mathbf{Q}(0) = \left[\begin{smallmatrix} 1 & 0 \\ 0 & \frac{2}{1+2\sigma_r} \end{smallmatrix}\right]$, and $\hat{\delta}(0) = 10 \cdot 10^{-8}$.

Convergence to optimal system performance

The extremum-seeking controller is enabled at $t = 0$ seconds. Fig. 2.8 shows the dead-zone length δ and the measured performance cost l as a function of time, and the tracking error e_z for time windows $t \in [10, 10.25]$ seconds and $t \in [149.75, 150]$ seconds for three cases; cases 1 and 2 in which two constant values for δ are used, namely $\delta = 2 \cdot 10^{-7}$ m (low-gain case) and $\delta = 0$ m (high-gain case) and depicted by (—) and (—), respectively, and case 3 in which δ is tuned by an extremum-seeking controller, for which the results are depicted by (—). It can be seen that the plant parameter δ and the corresponding

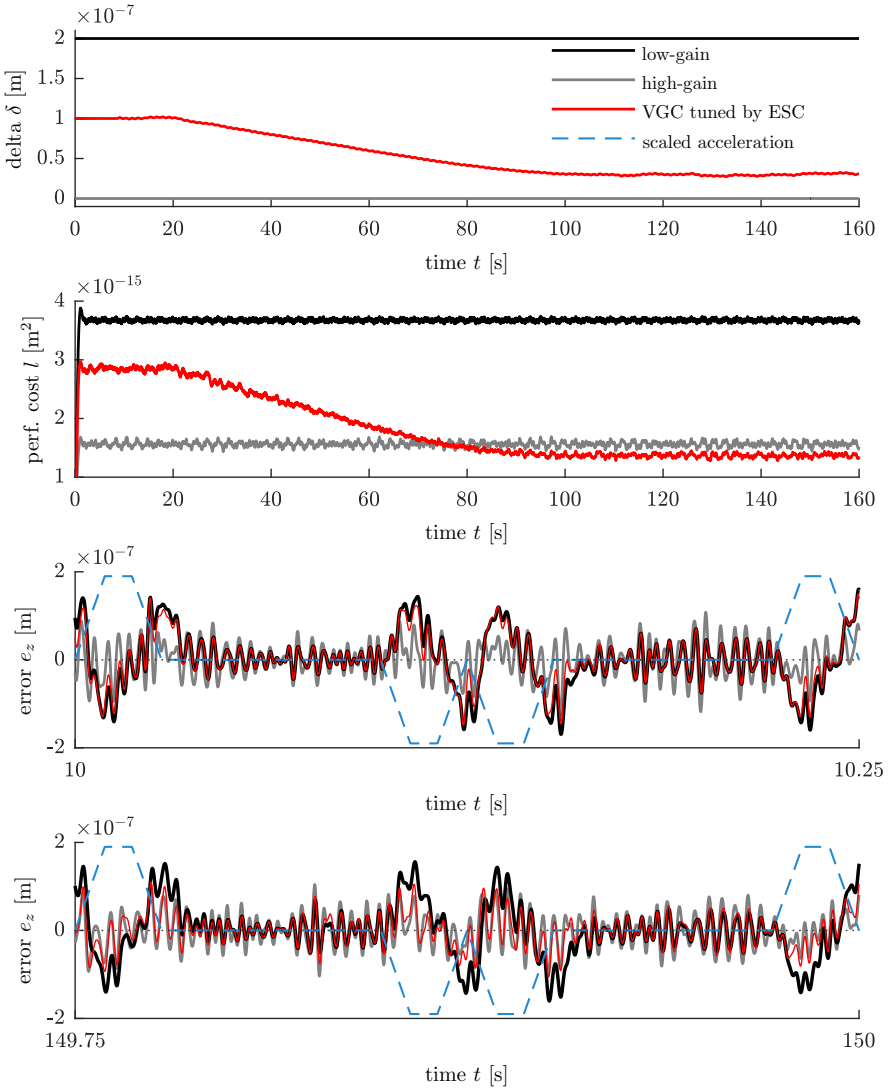

Figure 2.8: The performance cost l as a function of time for two constant values of δ, associated with i) (—) the nominal low-gain linear controller with $\delta = 2 \cdot 10^{-7}$ m, and ii) (—) the high-gain linear controller with $\delta = 0$ m, and iii) (—) the variable-gain controller with the convergence of the tunable parameter δ towards δ^* and corresponding performance cost l using extremum-seeking control. Moreover, the tracking error e_z is depicted for the non-optimal ($t \in [10, 10.25]$ seconds) and optimal dead-zone length settings ($t \in [149.75, 150]$ seconds).

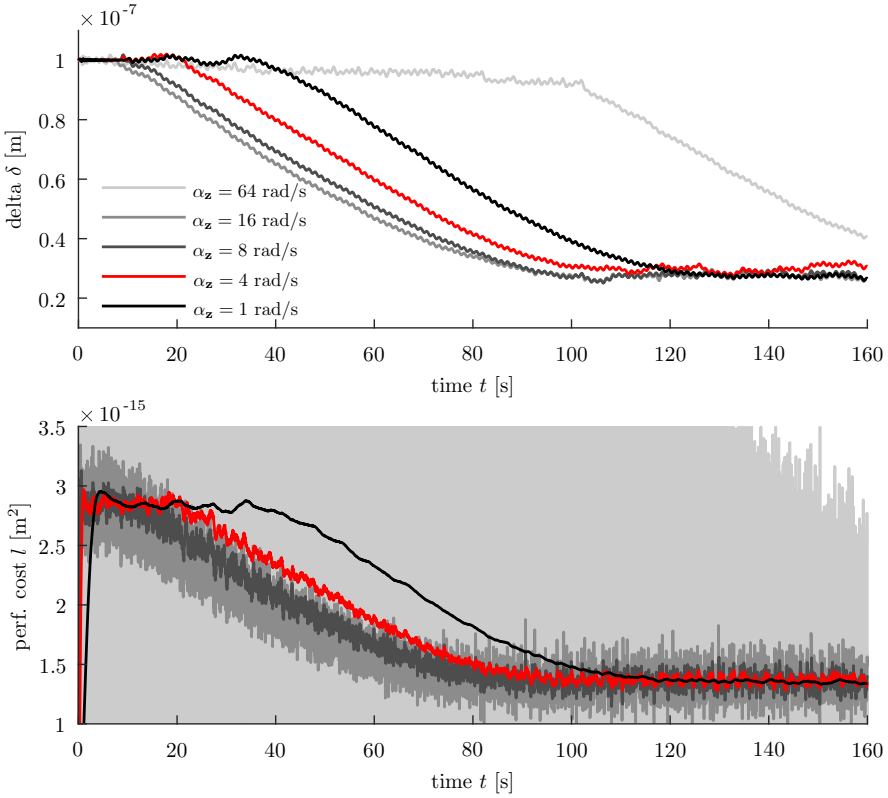

Figure 2.9: Convergence of the tunable parameter δ towards δ^* and the associated performance cost l for different values for $\alpha_{\mathbf{z}}$.

performance cost l converges to the performance-optimal region, which is also illustrated by the convergence of the parameter δ to a neighborhood of the extremum of $F_{\mathbf{w}}(\delta)$ in Fig. 2.7 by (—). Improved tracking error under VGC is clearly shown in the case of optimal settings δ^*; during non-zero accelerations (see the scaled acceleration profile by (- -) in Fig. 2.8) the tracking error behaves similar to the high-gain settings, while during zero accelerations the tracking error behaves similar to the low-gain settings.

Convergence speed and the time-scale of the dynamic cost function

In Fig. 2.9, the effect of the additional time-scale induced by the filter Σ_f is shown for different values for $\alpha_{\mathbf{z}}$. For smaller values of $\alpha_{\mathbf{z}}$ it is expected that the transient response of the extended plant becomes slower, and that the slower time-scale of the filter Σ_f leads to a slower convergence to the optimal

variable-gain controller setting. This behavior can clearly be observed in Fig. 2.9. However, with a smaller value for $\alpha_{\mathbf{z}}$ the extremum-seeking controller suffers less from time-varying system behavior. This can be attributed to the fact that the output of the cost l in steady-state is a more accurate approximation of the objective function $F_{\mathbf{w}}(\delta)$. This can be seen from Fig. 2.7, which shows the convergence of the parameter δ and the corresponding performance cost l to a neighborhood of the extremum of $F_{\mathbf{w}}(\delta)$ for different values of $\alpha_{\mathbf{z}}$. This can be observed from Fig. 2.9 as well, in which the convergence of the parameter δ and the corresponding performance cost l is shown against time. Decreasing the value of $\alpha_{\mathbf{z}}$ further will eventually lead to loss of time-scale separation, unless other parameters of the extremum-seeking controller, e.g., $\eta_{\boldsymbol{\omega}}$ and $\eta_{\mathbf{m}}$ and satisfaction of the associated conditions $\eta_{\boldsymbol{\omega}} \leq \alpha_{\mathbf{z}}\epsilon_2$ and $\eta_{\mathbf{m}} \leq \eta_{\boldsymbol{\omega}}\epsilon_3$ in Theorem 2.16, are properly re-tuned. For larger values of $\alpha_{\mathbf{z}}$, the transient response of the filter decays faster, usually leading to faster convergence of the ESC scheme to the optimal setting δ^*. This is illustrated in Fig. 2.9. However, for even larger values of $\alpha_{\mathbf{z}}$ convergence to the optimal setting is not guaranteed; in such a case the extremum-seeking controller suffers from the time-varying system behavior and is not able to estimate a proper gradient. This behavior is depicted in Fig. 2.9 for the setting $\alpha_{\mathbf{z}} = 64$ rad/s. The results illustrate the necessity of the dynamic cost function in the time-varying setting. However, the dynamic cost function must operate sufficiently slow compared to the time-varying nature of the system responses, and may compromise the convergence speed of the extremum-seeking control scheme. In Chapter 3, a modified extremum-seeking controller design is proposed which is able to enhance convergence speed of the resulting extremum-seeking control scheme.

Convergence speed and the dither amplitude

In Fig. 2.10, the effect of the dither amplitude $\alpha_{\boldsymbol{\omega}}$ is shown for different values for $\alpha_{\boldsymbol{\omega}}$. For smaller values of $\alpha_{\boldsymbol{\omega}}$, it is expected that convergence to the optimal variable-gain controller setting becomes slower. This can clearly be observed in Fig. 2.10. For larger values of $\alpha_{\boldsymbol{\omega}}$, convergence to the optimal setting δ^* is in general faster. However, for larger values of $\alpha_{\boldsymbol{\omega}}$ the neighborhood of the extremum to which the ESC scheme is converging is generally larger, and if the value of $\alpha_{\boldsymbol{\omega}}$ increases even more, convergence to the optimal setting is not guaranteed; in such a case the value of $\alpha_{\mathbf{z}}$ needs to be smaller to cope with the increased time-varying system behavior caused by the increased dither amplitude. This behavior is depicted in Fig. 2.9 for the setting $\alpha_{\boldsymbol{\omega}} = 5 \cdot 10^{-9}$ m.

2.6 Conclusions

In this chapter, a novel ESC method for optimization of time-varying steady-state responses of general nonlinear systems is proposed. The ESC method

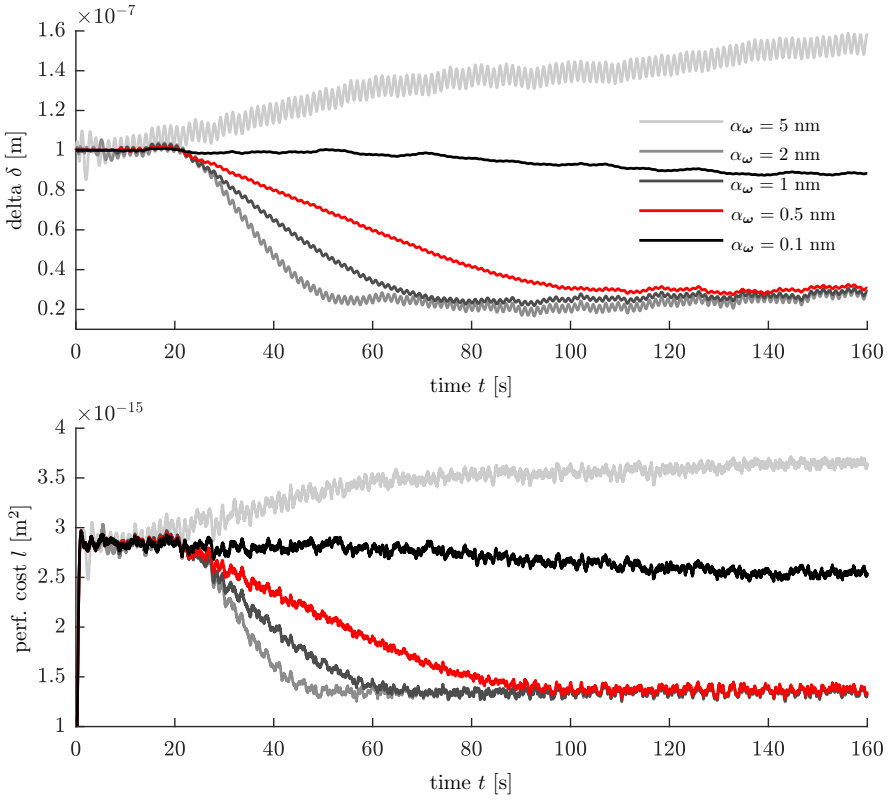

Figure 2.10: Convergence of the tunable parameter δ towards δ^* and the associated performance cost l for different values for the dither amplitude $\alpha_{\boldsymbol{\omega}}$.

utilizes a so-called dynamic cost function which has proven instrumental in the scope of optimization of time-varying system behavior, as it allows for the characterization of a static input-output performance map, despite the presence of time-varying disturbances which induces time-varying steady-state responses. The proposed ESC method is proven to achieve semi-global practical asymptotic stability of the closed-loop scheme in the presence of bounded and time-varying disturbances. An industrial simulation study is provided that shows the steady-state performance optimization of a closed-loop variable-gain controlled motion system subject to a time-varying force disturbance by means of the proposed ESC approach. Moreover, the effect of the time-scale of the dynamic cost function on the convergence of the ESC scheme is illustrated, and illustrates the necessity of the dynamic cost function in the time-varying setting.

2.A Derivation of the least-squares observer in Section 2.3

The least-squares observer in Section 2.3 is obtained by minimizing a quadratic cost function with respect to an exponentially weighted time window of the estimation error (Haring, 2016):

$$\begin{aligned}(t,\hat{\mathbf{m}}) = &\underset{\mathbf{p}(t)\in\mathbb{R}^{n_\mathbf{u}+1}}{\arg\min}\ J(t,\mathbf{p}(t)),\\ \text{subject to: } \dot{\mathbf{p}}(\tau) &= \mathbf{A}(\tau)\mathbf{p}(\tau) + \alpha_{\boldsymbol{\omega}}^2\mathbf{B}\hat{\mathbf{s}}(\tau)\\ \hat{l}(\tau) &= \mathbf{C}(\tau)\mathbf{p}(\tau) + \alpha_{\boldsymbol{\omega}}^2\hat{v}(\tau), \qquad \forall\ \tau\in[0,t],\end{aligned} \tag{2.78}$$

where $\hat{\mathbf{m}}$ denotes the estimate of the state of the observer, and where the quadratic cost function J is given by

$$\begin{aligned}J(t,\mathbf{p}(t)) = \eta_\mathbf{m}\int_0^t e^{-\eta_\mathbf{m}(t-\tau)}\Big(|l(\tau)-\hat{l}(\tau)|^2 + \sigma_r|\mathbf{D}\mathbf{p}(\tau)|^2\Big)d\tau\\ + e^{-\eta_\mathbf{m}t}(\hat{\mathbf{m}}_0-\mathbf{p}_0)^\top\mathbf{Q}_0^{-1}(\hat{\mathbf{m}}_0-\mathbf{p}_0),\end{aligned} \tag{2.79}$$

with $\mathbf{D} = [\mathbf{0}^{n_\mathbf{u}\times 1} \quad \mathbf{I}^{n_\mathbf{u}}\times n_\mathbf{u}]$, $\hat{\mathbf{m}}_0\in\mathbb{R}^{n_\mathbf{u}\times 1}$, with $\mathbf{Q}_0\in\mathbb{R}^{n_\mathbf{u}+1\times n_\mathbf{u}+1}$ a symmetric positive-definite matrix, $l(\tau)$ is the measured output of the extended plant in (2.16), a forgetting factor $\eta_\mathbf{m}\in\mathbb{R}_{>0}$, and a regularization constant $\sigma_r\in\mathbb{R}_{>0}$.

The derivation is as follows. First, we derive the solution for $\mathbf{p}(\tau)$, expressed in terms of $\mathbf{p}(t)$. Second, the equality constraints in (2.78) are substituted into the quadratic cost function in (2.79), and we solve $\frac{\partial J}{\partial \mathbf{p}(t)} = 0$. Third, we determine a set of differential equations for the least-squares observer.

Step 1: Let $\mathbf{P}(\tau)$ be nonsingular for all τ, and define $\mathbf{p}(\tau) = \mathbf{P}(\tau)\boldsymbol{\kappa}(\tau)$ such that

$$\dot{\mathbf{p}}(\tau) = \dot{\mathbf{P}}(\tau)\boldsymbol{\kappa}(\tau) + \mathbf{P}(\tau)\dot{\boldsymbol{\kappa}}(\tau) = \mathbf{A}(\tau)\mathbf{P}(\tau)\boldsymbol{\kappa}(\tau) + \alpha_{\boldsymbol{\omega}}^2\mathbf{B}\hat{\mathbf{s}}(\tau). \tag{2.80}$$

From this equality we obtain the following equivalent system

$$\begin{aligned}\dot{\boldsymbol{\kappa}}(\tau) &= \mathbf{P}(\tau)^{-1}\Big(\mathbf{A}(\tau)\mathbf{P}(\tau) - \dot{\mathbf{P}}(\tau)\Big)\boldsymbol{\kappa}(\tau) + \alpha_{\boldsymbol{\omega}}^2\mathbf{P}(\tau)^{-1}\mathbf{B}\hat{\mathbf{s}}(\tau)\\ \hat{l}(\tau) &= \mathbf{C}(\tau)\mathbf{P}(\tau)\boldsymbol{\kappa}(\tau) + \alpha_{\boldsymbol{\omega}}^2\hat{v}(\tau).\end{aligned} \tag{2.81}$$

Let $\dot{\mathbf{P}}(\tau) = \mathbf{A}(\tau)\mathbf{P}(\tau)$, i.e., $\mathbf{P}(\tau)$ is the so-called fundamental solution matrix, such that

$$\dot{\boldsymbol{\kappa}}(\tau) = \alpha_{\boldsymbol{\omega}}^2\mathbf{P}(\tau)^{-1}\mathbf{B}\hat{\mathbf{s}}(\tau), \tag{2.82}$$

from which we obtain the following equality:

$$\boldsymbol{\kappa}(\tau) = \boldsymbol{\kappa}(t) + \alpha_{\boldsymbol{\omega}}^2\int_t^\tau \mathbf{P}(\sigma)^{-1}\mathbf{B}\hat{\mathbf{s}}(\sigma)d\sigma. \tag{2.83}$$

Define the so-called state transition matrix $\Phi(\tau,t)=\mathbf{P}(\tau)\mathbf{P}^{-1}(t)$. Then from $\mathbf{p}(\tau)=\mathbf{P}(\tau)\boldsymbol{\kappa}(\tau)$ and substitution of (2.83) we obtain the following expressions:

$$\begin{aligned}\mathbf{p}(\tau)=\mathbf{P}(\tau)\boldsymbol{\kappa}(\tau)&=\mathbf{P}(\tau)\boldsymbol{\kappa}(t)+\alpha_{\boldsymbol{\omega}}^2\int_t^\tau\mathbf{P}(\tau)\mathbf{P}(\sigma)^{-1}\mathbf{B}\hat{\mathbf{s}}(\sigma)d\sigma\\&=\Phi(\tau,t)\mathbf{p}(t)-\alpha_{\boldsymbol{\omega}}^2\int_\tau^t\Phi(\tau,\sigma)\mathbf{B}\hat{\mathbf{s}}(\sigma)d\sigma,\end{aligned}\tag{2.84}$$

Step 2: The quadratic cost function in (2.79) can be written as follows:

$$\begin{aligned}J(t,\mathbf{p}(t))=\eta_{\mathbf{m}}\int_0^t&e^{-\eta_{\mathbf{m}}(t-\tau)}\big(l(\tau)-\alpha_{\boldsymbol{\omega}}^2\hat{v}(\tau)\big)^\top\big(l(\tau)-\alpha_{\boldsymbol{\omega}}^2\hat{v}(\tau)\big)\\&-2\mathbf{p}^\top(\tau)\mathbf{C}^\top(\tau)\big(l(\tau)-\alpha_{\boldsymbol{\omega}}^2\hat{v}(\tau)\big)d\tau\\&+\eta_{\mathbf{m}}\int_0^t e^{-\eta_{\mathbf{m}}(t-\tau)}\mathbf{p}^\top(\tau)\big(\mathbf{C}^\top(\tau)\mathbf{C}(\tau)+\sigma_r\mathbf{D}^\top\mathbf{D}\big)\mathbf{p}(\tau)d\tau\\&+e^{-\eta_{\mathbf{m}}t}(\hat{\mathbf{m}}_0-\mathbf{p}_0)^\top\mathbf{Q}_0^{-1}(\hat{\mathbf{m}}_0-\mathbf{p}_0).\end{aligned}\tag{2.85}$$

By substitution of (2.84) in (2.85) we obtain the following expression:

$$\begin{aligned}J(t,\mathbf{p}(t))=\eta_{\mathbf{m}}\int_0^t&e^{-\eta_{\mathbf{m}}(t-\tau)}\Big(\Big(l(\tau)-\alpha_{\boldsymbol{\omega}}^2\hat{v}(\tau)\Big)^\top\Big(l(\tau)-\alpha_{\boldsymbol{\omega}}^2\hat{v}(\tau)\Big)\\&+\alpha_{\boldsymbol{\omega}}^4\Big(\int_\tau^t\Phi(\tau,\sigma)\mathbf{B}\hat{\mathbf{s}}(\sigma)d\sigma\Big)^\top\Big(\mathbf{C}^\top(\tau)\mathbf{C}(\tau)+\sigma_r\mathbf{D}^\top\mathbf{D}\Big)\Big(\int_\tau^t\Phi(\tau,\sigma)\mathbf{B}\hat{\mathbf{s}}(\sigma)d\sigma\Big)\\&+2\alpha_{\boldsymbol{\omega}}^2\Big(\int_\tau^t\Phi(\tau,\sigma)\mathbf{B}\hat{\mathbf{s}}(\sigma)d\sigma\Big)^\top\mathbf{C}^\top(\tau)\Big(l(\tau)-\alpha_{\boldsymbol{\omega}}^2\hat{v}(\tau)\Big)\Big)d\tau\\&+e^{-\eta_{\mathbf{m}}t}\Big(\hat{\mathbf{m}}_0+\alpha_{\boldsymbol{\omega}}^2\int_0^t\Phi(0,\sigma)\mathbf{B}\hat{\mathbf{s}}(\sigma)d\sigma\Big)^\top\mathbf{Q}_0^{-1}\Big(\hat{\mathbf{m}}_0+\alpha_{\boldsymbol{\omega}}^2\int_0^t\Phi(0,\sigma)\mathbf{B}\hat{\mathbf{s}}(\sigma)d\sigma\Big)\\&-2\eta_{\mathbf{m}}\mathbf{p}^\top(t)\int_0^t e^{-\eta_{\mathbf{m}}(t-\tau)}\Phi^\top(\tau,t)\Big(\mathbf{C}^\top(\tau)\big(l(\tau)-\alpha_{\boldsymbol{\omega}}^2\hat{v}(\tau)\big)\\&+\big(\mathbf{C}^\top(\tau)\mathbf{C}(\tau)+\sigma_r\mathbf{D}^\top\mathbf{D}\big)\big(\alpha_{\boldsymbol{\omega}}^2\int_\tau^t\Phi(\tau,\sigma)\mathbf{B}\hat{\mathbf{s}}(\sigma)d\sigma\big)\Big)d\tau\\&+\eta_{\mathbf{m}}\mathbf{p}^\top(t)\int_0^t e^{-\eta_{\mathbf{m}}(t-\tau)}\Phi^\top(\tau,t)\big(\mathbf{C}^\top(\tau)\mathbf{C}(\tau)+\sigma_r\mathbf{D}^\top\mathbf{D}\big)\Phi(\tau,t)d\tau\mathbf{p}(t)\\&-2e^{-\eta_{\mathbf{m}}t}\mathbf{p}^\top(t)\Phi^\top(0,t)\mathbf{Q}_0^{-1}\Big(\hat{\mathbf{m}}_0+\alpha_{\boldsymbol{\omega}}^2\int_0^t\Phi(0,\sigma)\mathbf{B}\hat{\mathbf{s}}(\sigma)d\sigma\Big)\\&+e^{-\eta_{\mathbf{m}}t}\mathbf{p}^\top(t)\Phi^\top(0,t)\mathbf{Q}_0^{-1}\Phi(0,t)\mathbf{p}(t).\end{aligned}\tag{2.86}$$

From $\frac{\partial J}{\partial \mathbf{p}(t)} = 0$ we obtain the following expression:

$$\begin{aligned}
0 = \frac{\partial J(t,\mathbf{p}(t))}{\partial \mathbf{p}(t)} &= -2\eta_{\mathbf{m}} \int_0^t e^{-\eta_{\mathbf{m}}(t-\tau)} \Phi^\top(\tau,t) \Big(\mathbf{C}^\top(\tau) \big(l(\tau) - \alpha_{\boldsymbol{\omega}}^2 \hat{v}(\tau) \big) \\
&+ \big(\mathbf{C}^\top(\tau)\mathbf{C}(\tau) + \sigma_r \mathbf{D}^\top \mathbf{D} \big) \big(\alpha_{\boldsymbol{\omega}}^2 \int_\tau^t \Phi(\tau,\sigma)\mathbf{B}\hat{\mathbf{s}}(\sigma)d\sigma \big) \Big) d\tau \\
&+ 2\eta_{\mathbf{m}} \int_0^t e^{-\eta_{\mathbf{m}}(t-\tau)} \Phi^\top(\tau,t) \big(\mathbf{C}^\top(\tau)\mathbf{C}(\tau) + \sigma_r \mathbf{D}^\top \mathbf{D} \big) \Phi(\tau,t) d\tau \mathbf{p}(t) \\
&- 2e^{-\eta_{\mathbf{m}} t} \Phi^\top(0,t) \mathbf{Q}_0^{-1} \Big(\hat{\mathbf{m}}_0 + \alpha_{\boldsymbol{\omega}}^2 \int_0^t \Phi(0,\sigma)\mathbf{B}\hat{\mathbf{s}}(\sigma)d\sigma \Big) \\
&+ 2e^{-\eta_{\mathbf{m}} t} \Phi^\top(0,t) \mathbf{Q}_0^{-1} \Phi(0,t)\mathbf{p}(t).
\end{aligned} \tag{2.87}$$

From (2.87) and the optimization problem in (2.78), we obtain the state estimate:

$$\hat{\mathbf{m}}(t) = \mathbf{Q}(t)\Psi(t), \tag{2.88}$$

for all $t \in \mathbb{R}_{\geq 0}$, with

$$\begin{aligned}
\mathbf{Q}(t) = \Big(&\eta_{\mathbf{m}} \int_0^t e^{-\eta_{\mathbf{m}}(t-\tau)} \Phi^\top(\tau,t) \big(\mathbf{C}^\top(\tau)\mathbf{C}(\tau) + \sigma_r \mathbf{D}^\top \mathbf{D} \big) \Phi(\tau,t) d\tau \\
&+ e^{-\eta_{\mathbf{m}} t} \Phi^\top(0,t) \mathbf{Q}_0^{-1} \Phi(0,t) \Big)^{-1},
\end{aligned} \tag{2.89}$$

and

$$\begin{aligned}
\Psi(t) = \eta_{\mathbf{m}} &\int_0^t e^{-\eta_{\mathbf{m}}(t-\tau)} \Phi^\top(\tau,t) \Big(\mathbf{C}^\top(\tau) \big(l(\tau) - \alpha_{\boldsymbol{\omega}}^2 \hat{v}(\tau) \big) \\
&+ \big(\mathbf{C}^\top(\tau)\mathbf{C}(\tau) + \sigma_r \mathbf{D}^\top \mathbf{D} \big) \big(\alpha_{\boldsymbol{\omega}}^2 \int_\tau^t \Phi(\tau,\sigma)\mathbf{B}\hat{\mathbf{s}}(\sigma)d\sigma \big) \Big) d\tau \\
&+ e^{-\eta_{\mathbf{m}} t} \Phi^\top(0,t) \mathbf{Q}_0^{-1} \Big(\hat{\mathbf{m}}_0 + \alpha_{\boldsymbol{\omega}}^2 \int_0^t \Phi(0,\sigma)\mathbf{B}\hat{\mathbf{s}}(\sigma)d\sigma \Big).
\end{aligned} \tag{2.90}$$

Step 3: We determine a set of differential equations for the least-squares observer. By differentiating the expression in (2.88) we have that

$$\begin{aligned}
\dot{\hat{\mathbf{m}}}(t) &= \dot{\mathbf{Q}}(t)\Psi(t) + \mathbf{Q}(t)\dot{\Psi}(t) \\
&= \dot{\mathbf{Q}}(t)\mathbf{Q}^{-1}(t)\hat{\mathbf{m}}(t) + \mathbf{Q}(t)\dot{\Psi}(t).
\end{aligned} \tag{2.91}$$

First, we determine $\dot{\mathbf{Q}}(t)$ by differentiation of (2.89) and by using Leibniz's rule

for differentiation:

$$\begin{aligned}
\dot{\mathbf{Q}}(t) &= -\mathbf{Q}(t)\frac{\partial \mathbf{Q}^{-1}(t)}{\partial t}\mathbf{Q}(t) \\
&= -\mathbf{Q}(t)\Big(- \eta_{\mathbf{m}}\eta_{\mathbf{m}} \int_0^t e^{-\eta_{\mathbf{m}}(t-\tau)}\Phi^\top(\tau,t)\big(\mathbf{C}^\top(\tau)\mathbf{C}(\tau) + \sigma_r\mathbf{D}^\top\mathbf{D}\big)\Phi(\tau,t)d\tau \\
&\quad + \eta_{\mathbf{m}}\int_0^t e^{-\eta_{\mathbf{m}}(t-\tau)}\frac{\partial\Phi^\top(\tau,t)}{\partial t}\big(\mathbf{C}^\top(\tau)\mathbf{C}(\tau) + \sigma_r\mathbf{D}^\top\mathbf{D}\big)\Phi(\tau,t)d\tau \\
&\quad + \eta_{\mathbf{m}}\int_0^t e^{-\eta_{\mathbf{m}}(t-\tau)}\Phi^\top(\tau,t)\big(\mathbf{C}^\top(\tau)\mathbf{C}(\tau) + \sigma_r\mathbf{D}^\top\mathbf{D}\big)\frac{\partial\Phi(\tau,t)}{\partial t}d\tau \\
&\quad + \eta_{\mathbf{m}}\big(\mathbf{C}^\top(t)\mathbf{C}(t) + \sigma_r\mathbf{D}^\top\mathbf{D}\big) - \eta_{\mathbf{m}}e^{-\eta_{\mathbf{m}}t}\Phi^\top(0,t)\mathbf{Q}_0^{-1}\Phi(0,t) \\
&\quad + e^{-\eta_{\mathbf{m}}t}\Phi^\top(0,t)\mathbf{A}^\top(t)\mathbf{Q}_0^{-1}\Phi(0,t) + e^{-\eta_{\mathbf{m}}t}\Phi^\top(0,t)\mathbf{Q}_0^{-1}\frac{\partial\Phi(0,t)}{\partial t}\Big)\mathbf{Q}(t) \\
&= \eta_{\mathbf{m}}\mathbf{Q}(t) - \eta_{\mathbf{m}}\mathbf{Q}(t)\big(\mathbf{C}^\top(t)\mathbf{C}(t) + \sigma_r\mathbf{D}^\top\mathbf{D}\big)\mathbf{Q}(t) + \mathbf{Q}(t)\mathbf{A}^\top(t) + \mathbf{A}(t)\mathbf{Q}(t),
\end{aligned} \tag{2.92}$$

where we have used the fact that $\frac{\partial\Phi(\tau,t)}{\partial t} = -\Phi(\tau,t)\mathbf{A}(t)$.

Second, we determine $\dot{\Psi}(t)$ by differentiation of (2.90) and by using Leibniz's rule for differentiation:

$$\begin{aligned}
\dot{\Psi}(t) &= -\eta_{\mathbf{m}}\eta_{\mathbf{m}}\int_0^t e^{-\eta_{\mathbf{m}}(t-\tau)}\Phi^\top(\tau,t)\Big(\mathbf{C}^\top(\tau)\big(l(\tau) - \alpha_{\boldsymbol{\omega}}^2\hat{v}(\tau)\big) \\
&\quad + \alpha_{\boldsymbol{\omega}}^2\big(\mathbf{C}^\top(\tau)\mathbf{C}(\tau) + \sigma_r\mathbf{D}^\top\mathbf{D}\big)\int_\tau^t \Phi(\tau,\sigma)\mathbf{B}\hat{\mathbf{s}}(\sigma)d\sigma\Big)d\tau \\
&\quad - \eta_{\mathbf{m}}e^{-\eta_{\mathbf{m}}t}\Phi^\top(0,t)\mathbf{Q}_0^{-1}\Big(\hat{\mathbf{m}}_0 + \alpha_{\boldsymbol{\omega}}^2\int_0^t\Phi(0,\sigma)\mathbf{B}\hat{\mathbf{s}}(\sigma)d\sigma\Big) \\
&\quad - \eta_{\mathbf{m}}\mathbf{A}^\top(t)\int_0^t e^{-\eta_{\mathbf{m}}(t-\tau)}\Phi^\top(\tau,t)\Big(\mathbf{C}^\top(\tau)\big(l(\tau) - \alpha_{\boldsymbol{\omega}}^2\hat{v}(\tau)\big) \\
&\quad + \alpha_{\boldsymbol{\omega}}^2\big(\mathbf{C}^\top(\tau)\mathbf{C}(\tau) + \sigma_r\mathbf{D}^\top\mathbf{D}\big)\int_\tau^t \Phi(\tau,\sigma)\mathbf{B}\hat{\mathbf{s}}(\sigma)d\sigma\Big)d\tau \\
&\quad - \mathbf{A}^\top(t)e^{-\eta_{\mathbf{m}}t}\Phi^\top(0,t)\mathbf{Q}_0^{-1}\Big(\hat{\mathbf{m}}_0 + \alpha_{\boldsymbol{\omega}}^2\int_0^t\Phi(0,\sigma)\mathbf{B}\hat{\mathbf{s}}(\sigma)d\sigma\Big) \\
&\quad + \eta_{\mathbf{m}}\int_0^t e^{-\eta_{\mathbf{m}}(t-\tau)}\Phi^\top(\tau,t)\big(\mathbf{C}^\top(\tau)\mathbf{C}(\tau) + \sigma_r\mathbf{D}^\top\mathbf{D}\big)\Phi(\tau,t)d\tau\alpha_{\boldsymbol{\omega}}^2\mathbf{B}\hat{\mathbf{s}}(t) \\
&\quad + e^{-\eta_{\mathbf{m}}t}\Phi^\top(0,t)\mathbf{Q}_0^{-1}\Phi(0,t)\alpha_{\boldsymbol{\omega}}^2\mathbf{B}\hat{\mathbf{s}}(t) \\
&\quad + \eta_{\mathbf{m}}\mathbf{C}^\top(t)\big(l(t) - \alpha_{\boldsymbol{\omega}}^2\hat{v}(t)\big) \\
&= -\eta_{\mathbf{m}}\mathbf{Q}^{-1}(t)\hat{\mathbf{m}}(t) - \mathbf{A}^\top\mathbf{Q}^{-1}(t)\hat{\mathbf{m}}(t) + \alpha_{\boldsymbol{\omega}}^2\mathbf{Q}^{-1}(t)\mathbf{B}\hat{\mathbf{s}}(t) \\
&\quad + \eta_{\mathbf{m}}\mathbf{C}^\top(t)\big(l(t) - \alpha_{\boldsymbol{\omega}}^2\hat{v}(t)\big).
\end{aligned} \tag{2.93}$$

Finally, from (2.91), (2.92), and (2.93) we obtain the following differential equation for $\hat{\mathbf{m}}$:

$$\begin{aligned}\dot{\hat{\mathbf{m}}}(t) = (\mathbf{A}(t) - \eta_{\mathbf{m}}\sigma_r\mathbf{Q}(t)\mathbf{D}^\top\mathbf{D})\hat{\mathbf{m}}(t) + \alpha_{\boldsymbol{\omega}}^2\mathbf{B}\hat{\mathbf{s}}(t) \\ + \eta_{\mathbf{m}}\mathbf{Q}(t)\mathbf{C}^\top(t)\big(l(t) - \mathbf{C}(t)\hat{\mathbf{m}}(t) - \alpha_{\boldsymbol{\omega}}^2\hat{v}(t)\big).\end{aligned} \tag{2.94}$$

This completes the derivation of the least-squares observer in (2.38) in Section 2.3.

2.B Proof of Lemma 2.11

Consider some input $\mathbf{v}(\cdot) \in \mathcal{V} \subset \overline{\mathbb{PC}}_{\mathbf{v}}$. Since the $\mathbf{x}$-subsystem of the system in (2.17) is globally exponentially convergent, there exists a steady-state solution $\bar{\mathbf{x}}_{\mathbf{v}}(t)$ that is defined and bounded on $t \in \mathbb{R}$, and GES. Since the $\mathbf{z}$-subsystem of the system in (2.17) is exponentially input-to-state convergent, there exists a steady-state solution $\bar{\mathbf{z}}_{\mathbf{v}}(t)$ corresponding to the input $\bar{\mathbf{x}}_{\mathbf{v}}(t)$. Moreover, $\bar{\mathbf{z}}_{\mathbf{v}}(t)$ is defined and bounded on $t \in \mathbb{R}$, and GES. Let $(\mathbf{x}(t), \mathbf{z}(t))$ be some solution of the cascade system with input $\mathbf{v}(t)$. Denote $\Delta\mathbf{x} := \mathbf{x} - \bar{\mathbf{x}}_{\mathbf{v}}(t)$, and $\Delta\mathbf{z} := \mathbf{z} - \bar{\mathbf{z}}_{\mathbf{v}}(t)$. Then, $\Delta\mathbf{x}$ and $\Delta\mathbf{z}$ satisfy the differential equations

$$\Delta\dot{\mathbf{x}} = \mathbf{F}(\Delta\mathbf{x} + \bar{\mathbf{x}}_{\mathbf{v}}(t), \mathbf{v}(t)) - \mathbf{F}(\bar{\mathbf{x}}_{\mathbf{v}}(t), \mathbf{v}(t)), \tag{2.95}$$

$$\Delta\dot{\mathbf{z}} = \mathbf{G}(\Delta\mathbf{z} + \bar{\mathbf{z}}_{\mathbf{v}}(t), \Delta\mathbf{x} + \bar{\mathbf{x}}_{\mathbf{v}}(t)) - \mathbf{G}(\bar{\mathbf{z}}_{\mathbf{v}}(t), \bar{\mathbf{x}}_{\mathbf{v}}(t)). \tag{2.96}$$

Since the $\mathbf{x}$-subsystem of the system in (2.17) is globally exponentially convergent, the system in (2.95) with input $\mathbf{v}(t)$ is GES. Since the $\mathbf{z}$-subsystem of the system in (2.17) is exponentially input-to-state convergent, the system in (2.96) with input $\Delta\mathbf{x}$ is ISS. As such, there exist class $\mathcal{KL}$-functions $\beta_{\mathbf{x}}$ and $\beta_{\mathbf{z}}$, which are exponentially decaying functions with t, and a class $\mathcal{K}_\infty$-function $\gamma_{\mathbf{z}}$ such that the solutions of (2.95) and (2.96) satisfy

$$\begin{aligned}&\|\mathbf{x}(t) - \bar{\mathbf{x}}_{\mathbf{v}}(t)\| \leq \beta_{\mathbf{x}}(\|\mathbf{x}(s) - \bar{\mathbf{x}}_{\mathbf{v}}(s)\|, t-s), \\ &\|\mathbf{z}(t) - \bar{\mathbf{z}}_{\mathbf{v}}(t)\| \leq \beta_{\mathbf{z}}(\|\mathbf{z}(s) - \bar{\mathbf{z}}_{\mathbf{v}}(s)\|, t-s) + \gamma_{\mathbf{z}}\left(\sup_{s\leq\tau\leq t}\|\Delta\mathbf{x}(\tau)\|\right),\end{aligned} \tag{2.97}$$

where $t \geq s \geq t_0$. Hence, by similar arguments as in Lemma 4.7 in Khalil (2002) the series connection of (2.95) and (2.96) is GES. In the original coordinates $(\mathbf{x}, \mathbf{z})$ this means that the system in (2.17) is GES with respect to the solution $(\bar{\mathbf{x}}_{\mathbf{v}}(t), \bar{\mathbf{z}}_{\mathbf{v}}(t))$. This implies that the system in (2.17) is globally exponentially convergent. □

2.C Proof of Lemma 2.18

The proof of Lemma 2.18 follows a similar line of reasoning as Theorem 4.14 and Lemma 9.8 in Khalil (2002). The structure of the proof is as follows. First, it is shown that the inequalities in (2.47) hold. Second, it is shown that the inequality in (2.48) holds. Third, it is shown that the inequalities in (2.49) hold.

From Assumption 2.6 it follows that the system in (2.1) is globally exponentially convergent for a class of disturbances $\mathbf{w}(\cdot) \in \mathcal{W}$, and for all constant inputs $\mathbf{u} \in \mathbb{R}^{n_{\mathbf{u}}}$, uniformly in $\mathbf{u}$. As such, for each pair $\mathbf{u} \in \mathbb{R}^{n_{\mathbf{u}}}$ and $\mathbf{w}(t) \in \mathcal{W}$, there exist constants $\mu_{\mathbf{x}}, \nu_{\mathbf{x}} \in \mathbb{R}_{>0}$ such that the solutions of the dynamics in (2.46), starting at t_0 with $\tilde{\mathbf{x}}(t_0) \in \mathbb{R}^{n_{\mathbf{x}}}$, satisfy

$$\|\tilde{\mathbf{x}}(t)\| \leq \bar{\mu}_{\mathbf{x}} \|\tilde{\mathbf{x}}(t_0)\| e^{-\underline{\nu}_{\mathbf{x}}(t-t_0)}, \quad \forall\ \tilde{\mathbf{x}}(t_0) \in \mathbb{R}^{n_{\mathbf{x}}},\ t \in \mathbb{R}, \tag{2.98}$$

where $\bar{\mu}_{\mathbf{x}}, \underline{\nu}_{\mathbf{x}} \in \mathbb{R}_{>0}$ denote the maximum of all $\mu_{\mathbf{x}}$ and minimum of all $\nu_{\mathbf{x}}$ for each pair $\mathbf{u}$ and $\mathbf{w}(t)$, respectively.

Let $\phi(\tau; t, \tilde{\mathbf{x}}, \mathbf{u})$ denote the solution of (2.46) for constant inputs $\mathbf{u}$ that starts at $(t, \tilde{\mathbf{x}})$; that is, $\phi(t; t, \tilde{\mathbf{x}}, \mathbf{u}) = \tilde{\mathbf{x}}$. As such, ϕ satisfies the equation

$$\frac{\partial \phi}{\partial \tau}(\tau; t, \tilde{\mathbf{x}}, \mathbf{u}) = \tilde{\mathbf{f}}_{\mathbf{w}}(\tau, \phi(\tau; t, \tilde{\mathbf{x}}, \mathbf{u}), \mathbf{u}), \qquad \phi(t; t, \tilde{\mathbf{x}}, \mathbf{u}) = \tilde{\mathbf{x}}. \tag{2.99}$$

The notation $\phi(\tau; t, \tilde{\mathbf{x}}, \mathbf{u})$ emphasizes the dependence of the solution on the constant input $\mathbf{u}$. Moreover, due to the exponentially decaying bound on the trajectories in (2.98) we can write the following:

$$\|\phi(\tau; t, \tilde{\mathbf{x}}, \mathbf{u})\| \leq \bar{\mu}_{\mathbf{x}} \|\phi(t; t, \tilde{\mathbf{x}}, \mathbf{u})\| e^{-\underline{\nu}_{\mathbf{x}}(\tau - t)}, \quad \forall\ \tau \geq t. \tag{2.100}$$

Define the function

$$V_{\mathbf{x}}(t, \tilde{\mathbf{x}}, \mathbf{u}) := \int_{t}^{t+\delta_x} \phi^T(\tau; t, \tilde{\mathbf{x}}, \mathbf{u}) \phi(\tau; t, \tilde{\mathbf{x}}, \mathbf{u}) d\tau, \tag{2.101}$$

where $\delta_x > 0$ is a positive constant to be chosen. Firstly, we prove that the inequalities in (2.47) hold. Using (2.100), we obtain the following upper bound on $V_{\mathbf{x}}$:

$$V_{\mathbf{x}}(t, \tilde{\mathbf{x}}, \mathbf{u}) \leq \int_{t}^{t+\delta_{\mathbf{x}}} \bar{\mu}_{\mathbf{x}}^2 e^{-2\underline{\nu}_{\mathbf{x}}(\tau - t)} d\tau \|\tilde{\mathbf{x}}\|^2 = \frac{\bar{\mu}_{\mathbf{x}}^2}{2\underline{\nu}_{\mathbf{x}}} \left(1 - e^{-2\underline{\nu}_{\mathbf{x}}\delta_{\mathbf{x}}}\right) \|\tilde{\mathbf{x}}\|^2. \tag{2.102}$$

Next, we construct also a lower bound for $V_{\mathbf{x}}$. From Assumption 2.2, (2.46), and the Mean-Value Theorem, we have

$$\begin{aligned} \|\tilde{\mathbf{f}}_{\mathbf{w}}(t, \tilde{\mathbf{x}}, \mathbf{u})\| &= \|\mathbf{f}(\tilde{\mathbf{x}} + \bar{\mathbf{x}}_{\mathbf{w}}(t, \mathbf{u}), \mathbf{u}, \mathbf{w}) - \mathbf{f}(\bar{\mathbf{x}}_{\mathbf{w}}(t, \mathbf{u}), \mathbf{u}, \mathbf{w})\| \\ &\leq \int_{0}^{1} \left\| \frac{\partial \mathbf{f}}{\partial \mathbf{x}}(\sigma \tilde{\mathbf{x}} + \bar{\mathbf{x}}_{\mathbf{w}}(t, \mathbf{u}), \mathbf{u}, \mathbf{w}) \right\| d\sigma\, \|\tilde{\mathbf{x}}\| = L_{\mathbf{fx}} \|\tilde{\mathbf{x}}\|. \end{aligned} \tag{2.103}$$

By using (2.103) and (2.99) we obtain

$$\begin{aligned}\left|\frac{\partial}{\partial\tau}\left(\|\phi(\tau;t,\tilde{\mathbf{x}},\mathbf{u})\|^2\right)\right| &\leq 2\|\phi(\tau;t,\tilde{\mathbf{x}},\mathbf{u})\|\left\|\tilde{\mathbf{f}}_{\mathbf{w}}(\tau,\phi(\tau;t,\tilde{\mathbf{x}},\mathbf{u}),\mathbf{u})\right\|,\\ &\leq 2L_{\mathbf{fx}}\|\phi(\tau;t,\tilde{\mathbf{x}},\mathbf{u})\|^2,\end{aligned} \tag{2.104}$$

from which we can derive the following bound:

$$\frac{\partial}{\partial\tau}\left(\|\phi(\tau;t,\tilde{\mathbf{x}},\mathbf{u})\|^2\right) \geq -2L_{\mathbf{fx}}\|\phi(\tau;t,\tilde{\mathbf{x}},\mathbf{u})\|^2, \tag{2.105}$$

for all $\tau \geq t$. From the inequality in (2.105) we obtain

$$\frac{\partial}{\partial\tau}\left(\|\phi(\tau;t,\tilde{\mathbf{x}},\mathbf{u})\|^2 e^{2L_{\mathbf{fx}}\tau}\right) \geq 0. \tag{2.106}$$

By integration of both sides with respect to time over the domain $[t,\tau]$, it follows that

$$\|\phi(\tau;t,\tilde{\mathbf{x}},\mathbf{u})\|^2 \geq e^{-2L_{\mathbf{fx}}(\tau-t)}\|\tilde{\mathbf{x}}\|^2. \tag{2.107}$$

Then we obtain, using (2.101) and (2.107), that

$$V_{\mathbf{x}}(t,\tilde{\mathbf{x}},\mathbf{u}) \geq \int_t^{t+\delta_{\mathbf{x}}} e^{-2L_{\mathbf{fx}}(\tau-t)}dt\|\tilde{\mathbf{x}}\|^2 = \frac{1}{2L_{\mathbf{fx}}}\left(1-e^{-2L_{\mathbf{fx}}\delta_{\mathbf{x}}}\right)\|\tilde{\mathbf{x}}\|^2. \tag{2.108}$$

The bounds on $V_{\mathbf{x}}$ in (2.102) and (2.108) imply that the inequalities in (2.47) are satisfied with

$$\gamma_{\mathbf{x}1} = \frac{1}{2L_{\mathbf{fx}}}\left(1-e^{-2L_{\mathbf{fx}}\delta_{\mathbf{x}}}\right), \quad \text{and} \quad \gamma_{\mathbf{x}2} = \frac{\bar{\mu}_{\mathbf{x}}^2}{2\underline{\nu}_{\mathbf{x}}}\left(1-e^{-2\underline{\nu}_{\mathbf{x}}\delta_{\mathbf{x}}}\right), \tag{2.109}$$

and since $L_{\mathbf{fx}}$, $\bar{\mu}_{\mathbf{x}}$, $\underline{\nu}_{\mathbf{x}}$, and $\delta_{\mathbf{x}}$ are positive constants, we have that $\gamma_{\mathbf{x}1} > 0$ and $\gamma_{\mathbf{x}2} > 0$.

Secondly, we prove that the inequality in (2.48) holds. By Leibniz's rule for differentiation, the derivative of $V_{\mathbf{x}}$ along the trajectories of the plant is given as follows:

$$\begin{aligned}\frac{\partial V_{\mathbf{x}}}{\partial t} + \frac{\partial V_{\mathbf{x}}}{\partial\tilde{\mathbf{x}}}\tilde{\mathbf{f}}_{\mathbf{w}}(t,\tilde{\mathbf{x}},\mathbf{u}) &= \phi^T(t+\delta_{\mathbf{x}};t,\tilde{\mathbf{x}},\mathbf{u})\phi(t+\delta_{\mathbf{x}};t,\tilde{\mathbf{x}},\mathbf{u}) - \|\tilde{\mathbf{x}}\|^2\\ &+ \int_t^{t+\delta_{\mathbf{x}}} 2\phi^T(\tau;t,\tilde{\mathbf{x}},\mathbf{u})\left(\frac{\partial\phi}{\partial t}(\tau;t,\tilde{\mathbf{x}},\mathbf{u}) + \frac{\partial\phi}{\partial\tilde{\mathbf{x}}}(\tau;t,\tilde{\mathbf{x}},\mathbf{u})\tilde{\mathbf{f}}_{\mathbf{w}}(t,\tilde{\mathbf{x}},\mathbf{u})\right)d\tau.\end{aligned} \tag{2.110}$$

In order to evaluate the third term in the right-hand side of (2.110), we integrate both sides of (2.99) with respect to time over the domain $[\tau,t]$ such that we obtain

$$\phi(\tau;t,\tilde{\mathbf{x}},\mathbf{u}) = \tilde{\mathbf{x}} + \int_t^{\tau}\tilde{\mathbf{f}}_{\mathbf{w}}(s,\phi(s;t,\tilde{\mathbf{x}},\mathbf{u}),\mathbf{u})ds. \tag{2.111}$$

Taking the partial derivative to t and $\tilde{\mathbf{x}}$, by Leibniz's rule for differentiation we obtain

$$\begin{aligned}\frac{\partial \phi}{\partial t}(\tau;t,\tilde{\mathbf{x}},\mathbf{u}) &= -\tilde{\mathbf{f}}_{\mathbf{w}}(t,\tilde{\mathbf{x}},\mathbf{u}) + \int_t^\tau \frac{\partial \tilde{\mathbf{f}}_{\mathbf{w}}}{\partial \tilde{\mathbf{x}}}(s,\phi(s;t,\tilde{\mathbf{x}},\mathbf{u}),\mathbf{u})\frac{\partial \phi}{\partial t}(s;t,\tilde{\mathbf{x}},\mathbf{u})ds,\\ \frac{\partial \phi}{\partial \tilde{\mathbf{x}}}(\tau;t,\tilde{\mathbf{x}},\mathbf{u}) &= \mathbf{I} + \int_t^\tau \frac{\partial \tilde{\mathbf{f}}_{\mathbf{w}}}{\partial \tilde{\mathbf{x}}}(s,\phi(s;t,\tilde{\mathbf{x}},\mathbf{u}),\mathbf{u})\frac{\partial \phi}{\partial \tilde{\mathbf{x}}}(s;t,\tilde{\mathbf{x}},\mathbf{u})ds.\end{aligned} \tag{2.112}$$

Therefore,

$$\begin{aligned}&\frac{\partial \phi}{\partial t}(\tau;t,\tilde{\mathbf{x}},\mathbf{u}) + \frac{\partial \phi}{\partial \tilde{\mathbf{x}}}(\tau;t,\tilde{\mathbf{x}},\mathbf{u})\tilde{\mathbf{f}}_{\mathbf{w}}(t,\tilde{\mathbf{x}},\mathbf{u}) =\\ &\int_t^\tau \frac{\partial \tilde{\mathbf{f}}_{\mathbf{w}}}{\partial \tilde{\mathbf{x}}}(s,\phi(s;t,\tilde{\mathbf{x}},\mathbf{u}),\mathbf{u})\left(\frac{\partial \phi}{\partial t}(s;t,\tilde{\mathbf{x}},\mathbf{u}) + \frac{\partial \phi}{\partial \tilde{\mathbf{x}}}(s;t,\tilde{\mathbf{x}},\mathbf{u})\tilde{\mathbf{f}}_{\mathbf{w}}(t,\tilde{\mathbf{x}},\mathbf{u})\right)ds.\end{aligned} \tag{2.113}$$

By differentiation of (2.113) with respect to τ, we obtain the following differential equation

$$\begin{aligned}&\frac{\partial}{\partial \tau}\left(\frac{\partial \phi}{\partial t}(\tau;t,\tilde{\mathbf{x}},\mathbf{u}) + \frac{\partial \phi}{\partial \tilde{\mathbf{x}}}(\tau;t,\tilde{\mathbf{x}},\mathbf{u})\tilde{\mathbf{f}}_{\mathbf{w}}(t,\tilde{\mathbf{x}},\mathbf{u})\right) =\\ &\qquad \frac{\partial \tilde{\mathbf{f}}_{\mathbf{w}}}{\partial \tilde{\mathbf{x}}}(\tau,\phi(\tau;t,\tilde{\mathbf{x}},\mathbf{u}),\mathbf{u})\left(\frac{\partial \phi}{\partial t}(\tau;t,\tilde{\mathbf{x}},\mathbf{u}) + \frac{\partial \phi}{\partial \tilde{\mathbf{x}}}(\tau;t,\tilde{\mathbf{x}},\mathbf{u})\tilde{\mathbf{f}}_{\mathbf{w}}(t,\tilde{\mathbf{x}},\mathbf{u})\right),\end{aligned} \tag{2.114}$$

with the initial condition (which follows from (2.112))

$$\frac{\partial \phi}{\partial t}(t;t,\tilde{\mathbf{x}},\mathbf{u}) + \frac{\partial \phi}{\partial \tilde{\mathbf{x}}}(t;t,\tilde{\mathbf{x}},\mathbf{u})\tilde{\mathbf{f}}_{\mathbf{w}}(t,\tilde{\mathbf{x}},\mathbf{u}) = -\tilde{\mathbf{f}}_{\mathbf{w}}(t,\tilde{\mathbf{x}},\mathbf{u}) + \tilde{\mathbf{f}}_{\mathbf{w}}(t,\tilde{\mathbf{x}},\mathbf{u}) = 0. \tag{2.115}$$

From the differential equation in (2.114) and the initial condition in (2.115), it follows that

$$\frac{\partial \phi}{\partial t}(\tau;t,\tilde{\mathbf{x}},\mathbf{u}) + \frac{\partial \phi}{\partial \tilde{\mathbf{x}}}(\tau;t,\tilde{\mathbf{x}},\mathbf{u})\tilde{\mathbf{f}}_{\mathbf{w}}(t,\tilde{\mathbf{x}},\mathbf{u}) = 0, \quad \forall\ \tau \geq t, \tag{2.116}$$

which renders the third term in the right-hand side of (2.110) zero.

In order to evaluate the first term in the right-hand side of (2.110), we use (2.98) from which it follows that

$$\begin{aligned}\phi^T(t+\delta_{\mathbf{x}};t,\tilde{\mathbf{x}},\mathbf{u})\phi(t+\delta_{\mathbf{x}};t,\tilde{\mathbf{x}},\mathbf{u}) &= \|\phi(t+\delta_{\mathbf{x}};t,\tilde{\mathbf{x}},\mathbf{u})\|^2\\ &\leq \bar{\mu}_{\mathbf{x}}^2 e^{-2\underline{\nu}_{\mathbf{x}}\delta_{\mathbf{x}}}\|\phi(t;t,\tilde{\mathbf{x}},\mathbf{u})\|^2 = \bar{\mu}_{\mathbf{x}}^2 e^{-2\underline{\nu}_{\mathbf{x}}\delta_{\mathbf{x}}}\|\tilde{\mathbf{x}}\|^2.\end{aligned} \tag{2.117}$$

By using the results in (2.116) and (2.117), the derivative of $V_{\mathbf{x}}$ along the trajectories of the plant in (2.110) yields

$$\frac{\partial V_{\mathbf{x}}}{\partial t}(t,\tilde{\mathbf{x}},\mathbf{u}) + \frac{\partial V_{\mathbf{x}}}{\partial \tilde{\mathbf{x}}}(t,\tilde{\mathbf{x}},\mathbf{u})\tilde{\mathbf{f}}(t,\tilde{\mathbf{x}},\mathbf{u}) \leq -\left(1-\bar{\mu}_{\mathbf{x}}^2 e^{-2\underline{\nu}_{\mathbf{x}}\delta_{\mathbf{x}}}\right)\|\tilde{\mathbf{x}}\|^2. \tag{2.118}$$

The bound in (2.118) implies that (2.48) is satisfied with $\gamma_{\mathbf{x}3} = \left(1 - \bar{\mu}_{\mathbf{x}}^2 e^{-2\underline{\nu}_{\mathbf{x}}\delta_{\mathbf{x}}}\right)$. To show that $\gamma_{\mathbf{x}3} > 0$, we choose δ_x in (2.101) such that $\delta_x > \frac{\ln(\bar{\mu}_{\mathbf{x}})}{\underline{\nu}_{\mathbf{x}}} > 0$, where $\bar{\mu}_{\mathbf{x}}, \underline{\nu}_{\mathbf{x}} \in \mathbb{R}_{>0}$. Without loss of generality, this implies that

$$1 = \bar{\mu}_{\mathbf{x}}^2 e^{-2\ln(\bar{\mu}_{\mathbf{x}})} > \bar{\mu}_{\mathbf{x}}^2 e^{-2\underline{\nu}_{\mathbf{x}}\delta_{\mathbf{x}}} \geq 0 \tag{2.119}$$

As such, we have that $\gamma_{\mathbf{x}3} > 0$.

To show the validity of the inequality in (2.49), consider the derivative of $V_{\mathbf{x}}$ with respect to $\tilde{\mathbf{x}}$:

$$\frac{\partial V_{\mathbf{x}}}{\partial \tilde{\mathbf{x}}} = \int_t^{t+\delta_{\mathbf{x}}} 2\phi^T(\tau; t, \tilde{\mathbf{x}}, \mathbf{u}) \frac{\partial \phi}{\partial \tilde{\mathbf{x}}}(\tau; t, \tilde{\mathbf{x}}, \mathbf{u}) d\tau. \tag{2.120}$$

Then we obtain

$$\left\| \frac{\partial V_{\mathbf{x}}}{\partial \tilde{\mathbf{x}}} \right\| \leq \int_t^{t+\delta_{\mathbf{x}}} 2 \left\| \phi(\tau; t, \tilde{\mathbf{x}}, \mathbf{u}) \right\| \left\| \frac{\partial \phi}{\partial \tilde{\mathbf{x}}}(\tau; t, \tilde{\mathbf{x}}, \mathbf{u}) \right\| d\tau. \tag{2.121}$$

From (2.100) it follows that

$$\|\phi(\tau; t, \tilde{\mathbf{x}}, \mathbf{u})\| \leq \bar{\mu}_{\mathbf{x}} e^{-\underline{\nu}_{\mathbf{x}}(\tau - t)} \|\tilde{\mathbf{x}}\|, \quad \forall \tau \geq t. \tag{2.122}$$

Moreover, by differentiation of the second equation in (2.112) with respect to τ we obtain

$$\begin{aligned} \frac{\partial}{\partial \tau} \left(\frac{\partial \phi}{\partial \tilde{\mathbf{x}}}(\tau; t, \tilde{\mathbf{x}}, \mathbf{u}) \right) &= \frac{\partial \tilde{\mathbf{f}}_{\mathbf{w}}}{\partial \tilde{\mathbf{x}}}(\tau, \phi(\tau; t, \tilde{\mathbf{x}}, \mathbf{u}), \mathbf{u}) \frac{\partial \phi}{\partial \tilde{\mathbf{x}}}(\tau; t, \tilde{\mathbf{x}}, \mathbf{u}), \\ \frac{\partial \phi}{\partial \tilde{\mathbf{x}}}(t; t, \tilde{\mathbf{x}}, \mathbf{u}) &= \mathbf{I}. \end{aligned} \tag{2.123}$$

Then we obtain the following bound:

$$\left\| \frac{\partial}{\partial \tau} \left(\frac{\partial \phi}{\partial \tilde{\mathbf{x}}}(\tau; t, \tilde{\mathbf{x}}, \mathbf{u}) \right) \right\| \leq \left\| \frac{\partial \tilde{\mathbf{f}}_{\mathbf{w}}}{\partial \tilde{\mathbf{x}}}(\tau, \phi(\tau; t, \tilde{\mathbf{x}}, \mathbf{u}), \mathbf{u}) \right\| \left\| \frac{\partial \phi}{\partial \tilde{\mathbf{x}}}(\tau; t, \tilde{\mathbf{x}}, \mathbf{u}) \right\|. \tag{2.124}$$

Using the fact that

$$\frac{\partial}{\partial \tau} \left\| \frac{\partial \phi}{\partial \tilde{\mathbf{x}}}(\tau; t, \tilde{\mathbf{x}}, \mathbf{u}) \right\| \leq \left\| \frac{\partial}{\partial \tau} \left(\frac{\partial \phi}{\partial \tilde{\mathbf{x}}}(\tau; t, \tilde{\mathbf{x}}, \mathbf{u}) \right) \right\|, \tag{2.125}$$

and that, by Assumption 2.2, we have

$$\begin{aligned} \left\| \frac{\partial \tilde{\mathbf{f}}_{\mathbf{w}}}{\partial \tilde{\mathbf{x}}}(t, \tilde{\mathbf{x}}, \mathbf{u}) \right\| &= \left\| \frac{\partial \mathbf{x}}{\partial \tilde{\mathbf{x}}} \frac{\partial}{\partial \mathbf{x}} \Big(\mathbf{f}(\mathbf{x}, \mathbf{u}, \mathbf{w}) - \mathbf{f}(\bar{\mathbf{x}}_{\mathbf{w}}, \mathbf{u}, \mathbf{w}) \Big) \right\| \\ &= \left\| \frac{\partial \mathbf{f}}{\partial \mathbf{x}}(\mathbf{x}, \mathbf{u}, \mathbf{w}) \right\| \leq L_{\mathbf{fx}}, \end{aligned} \tag{2.126}$$

it follows from (2.124), (2.125), and (2.126) that

$$\frac{\partial}{\partial \tau}\left\|\frac{\partial \phi}{\partial \tilde{\mathbf{x}}}(\tau;t,\tilde{\mathbf{x}},\mathbf{u})\right\| \leq L_{\mathbf{fx}}\left\|\frac{\partial \phi}{\partial \tilde{\mathbf{x}}}(\tau;t,\tilde{\mathbf{x}},\mathbf{u})\right\|. \tag{2.127}$$

The inequality in (2.127) can be rewritten as

$$\frac{\partial}{\partial \tau}\left(\left\|\frac{\partial \phi}{\partial \tilde{\mathbf{x}}}(\tau;t,\tilde{\mathbf{x}},\mathbf{u})\right\| e^{-L_{\mathbf{fx}}\tau}\right) \leq 0. \tag{2.128}$$

By integrating both sides with respect to time over the domain $[t,\tau]$ and using the initial condition in (2.123), we obtain

$$\left\|\frac{\partial \phi}{\partial \tilde{\mathbf{x}}}(\tau;t,\tilde{\mathbf{x}},\mathbf{u})\right\| \leq e^{L_{\mathbf{fx}}(\tau-t)}. \tag{2.129}$$

Using (2.122) and (2.129) in (2.121), we obtain

$$\left\|\frac{\partial V_{\mathbf{x}}}{\partial \tilde{\mathbf{x}}}\right\| \leq \frac{2\bar{\mu}_{\mathbf{x}}}{\underline{\nu}_{\mathbf{x}}-L_{\mathbf{fx}}}\left(1-e^{-(\underline{\nu}_{\mathbf{x}}-L_{\mathbf{fx}})\delta_{\mathbf{x}}}\right)\|\tilde{\mathbf{x}}\|. \tag{2.130}$$

The bound in (2.130) implies that the inequality in (2.49) is satisfied with

$$\gamma_{\mathbf{x}4} = \frac{2\bar{\mu}_{\mathbf{x}}}{L_{\mathbf{fx}}-\underline{\nu}_{\mathbf{x}}}\left(e^{(L_{\mathbf{fx}}-\underline{\nu}_{\mathbf{x}})\delta_{\mathbf{x}}}-1\right). \tag{2.131}$$

Without loss of generality, we assume that $L_{\mathbf{fx}} \neq \underline{\nu}_{\mathbf{x}}$, and given the fact that $L_{\mathbf{fx}}, \bar{\mu}_{\mathbf{x}}, \underline{\nu}_{\mathbf{x}}, \delta_{\mathbf{x}} \in \mathbb{R}_{>0}$, it follows that $\gamma_{\mathbf{x}4} > 0$.

To show the validity of the inequality in (2.50), consider the derivative of $V_{\mathbf{x}}$ with respect to $\mathbf{u}$ which reads

$$\frac{\partial V_{\mathbf{x}}}{\partial \mathbf{u}} = \int_{t}^{t+\delta_{\mathbf{x}}} 2\phi^{T}(\tau;t,\tilde{\mathbf{x}},\mathbf{u})\frac{\partial \phi}{\partial \mathbf{u}}(\tau;t,\tilde{\mathbf{x}},\mathbf{u})d\tau, \tag{2.132}$$

from which it follows that

$$\left\|\frac{\partial V_{\mathbf{x}}}{\partial \mathbf{u}}\right\| \leq \int_{t}^{t+\delta_{\mathbf{x}}} 2\|\phi(\tau;t,\tilde{\mathbf{x}},\mathbf{u})\|\left\|\frac{\partial \phi}{\partial \mathbf{u}}(\tau;t,\tilde{\mathbf{x}},\mathbf{u})\right\| d\tau. \tag{2.133}$$

Differentiation of both sides of (2.111) with respect to $\mathbf{u}$ gives us

$$\begin{aligned}\frac{\partial \phi}{\partial \mathbf{u}}(\tau;t,\tilde{\mathbf{x}},\mathbf{u}) = &\int_{t}^{\tau} \frac{\partial \tilde{\mathbf{f}}_{\mathbf{w}}}{\partial \mathbf{u}}(s,\phi(s;t,\tilde{\mathbf{x}},\mathbf{u}),\mathbf{u}) \\ &+ \frac{\partial \mathbf{f}}{\partial \mathbf{x}}(\phi(s;t,\tilde{\mathbf{x}},\mathbf{u})+\bar{\mathbf{x}}_{\mathbf{w}}(s,\mathbf{u}),\mathbf{u},\mathbf{w})\frac{\partial \phi}{\partial \mathbf{u}}(s;t,\tilde{\mathbf{x}},\mathbf{u})ds.\end{aligned} \tag{2.134}$$

By Assumption 2.2 and (2.126) we have that

$$\begin{aligned}\left\|\frac{\partial \tilde{\mathbf{f}}_{\mathbf{w}}}{\partial \mathbf{u}}(t,\tilde{\mathbf{x}},\mathbf{u})\right\| &= \left\|\frac{\partial \mathbf{f}}{\partial \mathbf{u}}(\mathbf{x},\mathbf{u},\mathbf{w}) - \frac{\partial \mathbf{f}}{\partial \mathbf{u}}(\bar{\mathbf{x}}_{\mathbf{w}},\mathbf{u},\mathbf{w})\right\|, \\ &\leq \left\|\frac{\partial \mathbf{f}}{\partial \mathbf{u}}(\mathbf{x},\mathbf{u},\mathbf{w})\right\| + \left\|\frac{\partial \mathbf{f}}{\partial \mathbf{u}}(\bar{\mathbf{x}}_{\mathbf{w}},\mathbf{u},\mathbf{w})\right\| \leq 2L_{\mathbf{fu}},\end{aligned} \tag{2.135}$$

Then from (2.134) we obtain the following inequality

$$\begin{aligned}\left\|\frac{\partial \phi}{\partial \mathbf{u}}(\tau;t,\tilde{\mathbf{x}},\mathbf{u})\right\| &\leq \int_t^\tau \left(2L_{\mathbf{fu}} + L_{\mathbf{fx}}\left\|\frac{\partial \phi}{\partial \mathbf{u}}(s;t,\tilde{\mathbf{x}},\mathbf{u})\right\|\right) ds, \\ &\leq 2L_{\mathbf{fu}}(\tau - t) + L_{\mathbf{fx}}\int_t^\tau \left\|\frac{\partial \phi}{\partial \mathbf{u}}(s;t,\tilde{\mathbf{x}},\mathbf{u})\right\| ds.\end{aligned} \tag{2.136}$$

By using Grönwall's inequality, it follows that

$$\left\|\frac{\partial \phi}{\partial \mathbf{u}}(\tau;t,\tilde{\mathbf{x}},\mathbf{u})\right\| \leq 2L_{\mathbf{fu}}(\tau - t)e^{L_{\mathbf{fx}}(\tau - t)}. \tag{2.137}$$

Substitution of the exponentially decaying bound on the trajectories in (2.98) and (2.137) in (2.133), and after some computation, it follows that

$$\left\|\frac{\partial V_{\mathbf{x}}}{\partial \mathbf{u}}\right\| \leq \frac{4\bar{\mu}_{\mathbf{x}}L_{\mathbf{fu}}}{(L_{\mathbf{fx}} - \underline{\nu}_{\mathbf{x}})^2}\left(e^{(L_{\mathbf{fx}} - \underline{\nu}_{\mathbf{x}})\delta_{\mathbf{x}}}\big((L_{\mathbf{fx}} - \underline{\nu}_{\mathbf{x}})\delta_{\mathbf{x}} - 1\big) + 1\right)\|\tilde{\mathbf{x}}\| \tag{2.138}$$

The bound in (2.138) implies that the inequality in (2.50) is satisfied with

$$\gamma_{\mathbf{x}5} = \frac{4\bar{\mu}_{\mathbf{x}}L_{\mathbf{fu}}}{(L_{\mathbf{fx}} - \underline{\nu}_{\mathbf{x}})^2}\left(e^{(L_{\mathbf{fx}} - \underline{\nu}_{\mathbf{x}})\delta_{\mathbf{x}}}\big((L_{\mathbf{fx}} - \underline{\nu}_{\mathbf{x}})\delta_{\mathbf{x}} - 1\big) + 1\right). \tag{2.139}$$

Without loss of generality, if $L_{\mathbf{fx}} \neq \underline{\nu}_{\mathbf{x}}$ and with $\bar{\mu}_{\mathbf{x}}$, $\underline{\nu}_{\mathbf{x}}$, $L_{\mathbf{x}}$, $L_{\mathbf{fu}}$, $L_{\mathbf{fx}}$, $\delta_{\mathbf{x}} \in \mathbb{R}_{>0}$, it can be shown that $\gamma_{\mathbf{x}5} > 0$; the fraction in the expression for $\gamma_{\mathbf{x}5}$ is defined and positive whenever $L_{\mathbf{fx}} \neq \underline{\nu}_{\mathbf{x}}$. The expression between brackets is a function of the form $q(x) = 1 + e^x(x-1)$. The derivative of $q(x)$ with respect to x is given by $\frac{dq}{dx} = e^x x$. From this follows that $\frac{dq}{dx} = 0$ if $x = 0$ (the limit $x \to -\infty$ is not considered here). For $x = 0$ it follows that $q(0) = 0$. Furthermore, $\frac{dq}{dx} < 0$ for $x < 0$, and $\frac{dq}{dx} > 0$ for $x > 0$. As such, $q(x)$ is positive for all $x \neq 0$. As a result, if $L_{\mathbf{fx}} \neq \underline{\nu}_{\mathbf{x}}$, then $\gamma_{\mathbf{x}5} > 0$. This completes the proof of Lemma 2.18. □

2.D Proof of Lemma 2.19

By using the function $V_{\mathbf{x}}$ in Lemma 2.18 as a Lyapunov function candidate for the $\tilde{\mathbf{x}}$-dynamics in (2.51) with time-varying inputs $\mathbf{u}(t)$ and generated by (2.28)

and (2.40), we obtain the following expression for $\dot{V}_{\mathbf{x}}$:

$$\dot{V}_{\mathbf{x}} = \frac{\partial V_{\mathbf{x}}}{\partial t} + \frac{\partial V_{\mathbf{x}}}{\partial \tilde{\mathbf{x}}} \tilde{\mathbf{f}}_{\mathbf{w}}(t, \tilde{\mathbf{x}}, \mathbf{u}) + \left(\frac{\partial V_{\mathbf{x}}}{\partial \mathbf{u}} - \frac{\partial V_{\mathbf{x}}}{\partial \tilde{\mathbf{x}}} \frac{\partial \bar{\mathbf{x}}_{\mathbf{w}}}{\partial \mathbf{u}} \right) \dot{\mathbf{u}}, \tag{2.140}$$

for all $\tilde{\mathbf{x}} \in \mathbb{R}^{n_{\mathbf{x}}}$, all time-varying inputs $\mathbf{u}(t) \in \mathbb{R}^{n_{\mathbf{u}}}$, for all t. Note that in (2.140) we have omitted most arguments for notational clarity. Using Assumption 2.2, (2.8) in Assumption 2.6, the inequalities from Lemma 2.18, and Young's inequality, it follows that

$$\dot{V}_{\mathbf{x}} \leq -\frac{\gamma_{\mathbf{x}3}}{2\gamma_{\mathbf{x}2}} V_{\mathbf{x}}(t, \tilde{\mathbf{x}}, \mathbf{u}) + \frac{\left(\gamma_{\mathbf{x}4} L_{\mathbf{xu}} + \gamma_{\mathbf{x}5}\right)^2}{2\gamma_{\mathbf{x}3}} \|\dot{\mathbf{u}}\|^2. \tag{2.141}$$

To find an upper bound for $\|\dot{\mathbf{u}}\|$, it follows from (2.28) that $\dot{\mathbf{u}} = \dot{\hat{\mathbf{u}}} + \alpha_{\boldsymbol{\omega}} \dot{\boldsymbol{\omega}}$. From (2.29), we have that there exists a constant $L_{\boldsymbol{\omega}1} \in \mathbb{R}_{>0}$ such that $\|\dot{\boldsymbol{\omega}}\| \leq \eta_{\boldsymbol{\omega}} L_{\boldsymbol{\omega}1}$. Furthermore, from (2.40) we have that $\|\dot{\hat{\mathbf{u}}}\| \leq \eta_{\mathbf{u}}$. Therefore, we obtain an upperbound on $\|\dot{\mathbf{u}}\|$ which is given by

$$\|\dot{\mathbf{u}}\| \leq \alpha_{\boldsymbol{\omega}} \eta_{\boldsymbol{\omega}} \left(\epsilon_3 \epsilon_5 + L_{\boldsymbol{\omega}1} \right), \tag{2.142}$$

for all $\epsilon_3, \epsilon_5 \in \mathbb{R}_{>0}$, all $\eta_{\mathbf{u}} \leq \alpha_{\boldsymbol{\omega}} \eta_{\mathbf{m}} \epsilon_5$, and all $\eta_{\mathbf{m}} \leq \eta_{\boldsymbol{\omega}} \epsilon_3$ (as guaranteed by the conditions in Theorem 2.16). Substitution of (2.142) in (2.141), and applying the comparison lemma (Khalil, 2002, Lemma 3.4), it follows that

$$\begin{aligned} V_{\mathbf{x}}(t, \tilde{\mathbf{x}}(t), \mathbf{u}(t)) \leq\ & V_{\mathbf{x}}(0, \tilde{\mathbf{x}}(0), \mathbf{u}(0)) e^{-\frac{\gamma_{\mathbf{x}3}}{2\gamma_{\mathbf{x}2}} t} \\ & + \alpha_{\boldsymbol{\omega}}^2 \eta_{\boldsymbol{\omega}}^2 \gamma_{\mathbf{x}2} \frac{\left(\gamma_{\mathbf{x}4} L_{\mathbf{xu}} + \gamma_{\mathbf{x}5}\right)^2}{\gamma_{\mathbf{x}3}^2} \left(\epsilon_3 \epsilon_5 + L_{\boldsymbol{\omega}1} \right)^2, \end{aligned} \tag{2.143}$$

for all $t \geq 0$, all $\tilde{\mathbf{x}}(0) \in \mathbb{R}^{n_{\mathbf{x}}}$, and all time-varying $\mathbf{u}(t) \in \mathbb{R}^{n_{\mathbf{u}}}$. From (2.47) in Lemma 2.18, we obtain

$$\|\tilde{\mathbf{x}}(t)\| \leq \max \left\{ c_{\mathbf{x}1} \|\tilde{\mathbf{x}}(0)\| e^{-\beta_{\mathbf{x}} t}, \alpha_{\boldsymbol{\omega}} \eta_{\boldsymbol{\omega}} c_{\mathbf{x}2} \right\}, \tag{2.144}$$

with positive constants $\beta_{\mathbf{x}} = \frac{\gamma_{\mathbf{x}3}}{4\gamma_{\mathbf{x}2}}$, $c_{\mathbf{x}1} = \sqrt{\frac{2\gamma_{\mathbf{x}2}}{\gamma_{\mathbf{x}1}}}$, and

$$c_{\mathbf{x}2} = \sqrt{\frac{2\gamma_{\mathbf{x}2}}{\gamma_{\mathbf{x}1}}} \frac{\gamma_{\mathbf{x}4} L_{\mathbf{xu}} + \gamma_{\mathbf{x}5}}{\gamma_{\mathbf{x}3}} \left(\epsilon_3 \epsilon_5 + L_{\boldsymbol{\omega}1} \right), \tag{2.145}$$

which completes the proof of Lemma 2.19. □

2.E Proof of Lemma 2.23

By using the function $V_{\mathbf{z}}$ in Lemma 2.22 as a Lyapunov function candidate for the $\tilde{\mathbf{z}}$-dynamics in (2.63) with time-varying inputs $\mathbf{u}(t)$ and generated by (2.28)

and (2.40), we obtain the following expression for $\dot{V}_{\mathbf{z}}$:

$$\begin{aligned}\dot{V}_{\mathbf{z}} = \frac{\partial V_{\mathbf{z}}}{\partial t} + \alpha_{\mathbf{z}}\frac{\partial V_{\mathbf{z}}}{\partial \tilde{\mathbf{z}}}\tilde{\mathbf{h}}_{\mathbf{w}}(t,\tilde{\mathbf{z}},\mathbf{u},\alpha_{\mathbf{z}}) + \alpha_{\mathbf{z}}\frac{\partial V_{\mathbf{z}}}{\partial \tilde{\mathbf{z}}}\Big(\mathbf{h}(\mathbf{z},y) - \mathbf{h}(\mathbf{z},\bar{y}_{\mathbf{w}}(t,\mathbf{u}))\Big) \\ + \left(\frac{\partial V_{\mathbf{z}}}{\partial \mathbf{u}} - \frac{\partial V_{\mathbf{z}}}{\partial \tilde{\mathbf{z}}}\left(\frac{\partial \bar{\mathbf{z}}_{\mathbf{w}}}{\partial \mathbf{u}} - \frac{d\mathbf{q}_{\mathbf{w}}}{d\mathbf{u}} + \frac{d\mathbf{q}_{\mathbf{w}}}{d\mathbf{u}}\right)\right)\dot{\mathbf{u}},\end{aligned} \tag{2.146}$$

for all $\tilde{\mathbf{z}} \in \mathbb{R}^{n_{\mathbf{z}}}$, all time-varying inputs $\mathbf{u}(t) \in \mathbb{R}^{n_{\mathbf{u}}}$, for all t, and all $y, \bar{y}_{\mathbf{w}} \in \mathbb{R}$ satisfying (2.11) and (2.14), respectively. Note that in (2.146) we have omitted most arguments for notational clarity. Using the inequalities from Lemma 2.22 and Assumption 2.12, it follows that

$$\begin{aligned}\dot{V}_{\mathbf{z}} \leq -\alpha_{\mathbf{z}}\gamma_{\mathbf{z}3}\|\tilde{\mathbf{z}}\|^2 + \alpha_{\mathbf{z}}\gamma_{\mathbf{z}4}L_{\mathbf{z}1}\|\tilde{\mathbf{z}}\|\|\dot{\mathbf{u}}\| + \alpha_{\mathbf{z}}\gamma_{\mathbf{z}4}\|\tilde{\mathbf{z}}\|\|\mathbf{h}(\mathbf{z},y) - \mathbf{h}(\mathbf{z},\bar{y}_{\mathbf{w}}(t,\mathbf{u}))\| \\ + \gamma_{\mathbf{z}5}\|\tilde{\mathbf{z}}\|\|\dot{\mathbf{u}}\| + \Big(\gamma_{\mathbf{z}6} + \alpha_{\mathbf{z}}\gamma_{\mathbf{z}4}L_{\mathbf{z}2} + \gamma_{\mathbf{z}4}L_{\mathbf{q}}\Big)\|\mathbf{u} - \mathbf{u}^*_{\mathbf{w}}\|\|\tilde{\mathbf{z}}\|\|\dot{\mathbf{u}}\|.\end{aligned} \tag{2.147}$$

By defining $\tilde{y} := y - \bar{y}_{\mathbf{w}}(t,\mathbf{u})$ and the bounds in (2.15), it follows that

$$\|\mathbf{h}(\mathbf{z},y) - \mathbf{h}(\mathbf{z},\bar{y}_{\mathbf{w}}(t,\mathbf{u}))\| \leq L_{\mathbf{h}y}\|\tilde{y}\|. \tag{2.148}$$

By defining $\tilde{\mathbf{e}} := \mathbf{e} - \bar{\mathbf{e}}_{\mathbf{w}}(t,\mathbf{u})$, using (2.11), (2.14), and the bounds in (2.13), it follows that

$$\begin{aligned}\|\tilde{y}\| \leq L_{Z\mathbf{e}}\|\bar{\mathbf{e}}_{\mathbf{w}}(t,\mathbf{u}) - \bar{\mathbf{e}}_{\mathbf{w}}(t,\mathbf{u}^*_{\mathbf{w}})\|\|\tilde{\mathbf{e}}\| + L_{Z*}\|\tilde{\mathbf{e}}\| \\ + \frac{L_{Z\mathbf{e}}}{2}\|\tilde{\mathbf{e}}\|^2 + L_{Z\mathbf{u}}\|\mathbf{u} - \mathbf{u}^*_{\mathbf{w}}\|\|\tilde{\mathbf{e}}\|,\end{aligned} \tag{2.149}$$

with $L_{Z*} = \left\|\frac{\partial Z}{\partial \mathbf{e}}(\bar{\mathbf{e}}_{\mathbf{w}}(t,\mathbf{u}^*_{\mathbf{w}}),\mathbf{u}^*_{\mathbf{w}})\right\| \in \mathbb{R}_{>0}$. From Assumption 2.2 and (2.8) in Assumption 2.6, it follows that

$$\|\tilde{\mathbf{e}}\| = \|\mathbf{g}(\mathbf{x},\mathbf{u},\mathbf{w}) - \mathbf{g}(\bar{\mathbf{x}}_{\mathbf{w}}(t,\mathbf{u}),\mathbf{u},\mathbf{w})\| \leq L_{\mathbf{gx}}\|\tilde{\mathbf{x}}\|, \tag{2.150}$$

and

$$\|\bar{\mathbf{e}}_{\mathbf{w}}(t,\mathbf{u}) - \bar{\mathbf{e}}_{\mathbf{w}}(t,\mathbf{u}^*_{\mathbf{w}})\| \leq (L_{\mathbf{gu}} + L_{\mathbf{gx}}L_{\mathbf{xu}})\|\mathbf{u} - \mathbf{u}^*_{\mathbf{w}}\|. \tag{2.151}$$

From (2.29), it follows that there exists a constant $L_{\boldsymbol{\omega}2} \in \mathbb{R}_{>0}$ such that $\|\boldsymbol{\omega}\| \leq L_{\boldsymbol{\omega}2}$. From this fact, (2.28), and the coordinate transformation in (2.42), it follows that

$$\|\mathbf{u} - \mathbf{u}^*_{\mathbf{w}}\| \leq \|\tilde{\mathbf{u}}\| + \alpha_{\boldsymbol{\omega}}L_{\boldsymbol{\omega}2}. \tag{2.152}$$

Substitution of (2.148) to (2.152) into (2.147), applying Young's inequality, using the bound on $\|\dot{\mathbf{u}}\|$ in (2.142), and the inequality in (2.59) from Lemma 2.22, results in

$$\begin{aligned}\dot{V}_{\mathbf{z}} \leq -\frac{\alpha_{\mathbf{z}}\gamma_{\mathbf{z}3}}{2\gamma_{\mathbf{z}2}}V_{\mathbf{z}}(t,\tilde{\mathbf{z}},\mathbf{u},\alpha_{\mathbf{z}}) + \frac{9\alpha_{\mathbf{z}}z_1^2}{2\gamma_{\mathbf{z}3}}\|\tilde{\mathbf{x}}\|^4 + \frac{9\alpha_{\mathbf{z}}z_8^2}{2\gamma_{\mathbf{z}3}}\|\tilde{\mathbf{x}}\|^2 + \frac{9\alpha_{\mathbf{z}}\alpha_{\boldsymbol{\omega}}^2 z_9^2}{2\gamma_{\mathbf{z}3}}\|\tilde{\mathbf{x}}\|^2 \\ + \frac{9\alpha_{\mathbf{z}}z_2^2}{2\gamma_{\mathbf{z}3}}\|\tilde{\mathbf{u}}\|^2\|\tilde{\mathbf{x}}\|^2 + \frac{9\alpha_{\boldsymbol{\omega}}^2\eta_{\boldsymbol{\omega}}^2}{2\alpha_{\mathbf{z}}\gamma_{\mathbf{z}3}}z_{10}^2\left(\epsilon_0\epsilon_1 z_4 + z_3\right)^2\|\tilde{\mathbf{u}}\|^2 \\ + \frac{9\alpha_{\boldsymbol{\omega}}^2 z_5^2}{2\alpha_{\mathbf{z}}\gamma_{\mathbf{z}3}}\alpha_{\boldsymbol{\omega}}^2\eta_{\boldsymbol{\omega}}^2 z_{10}^2 + \frac{9\alpha_{\boldsymbol{\omega}}^2\eta_{\boldsymbol{\omega}}^2}{2\alpha_{\mathbf{z}}\gamma_{\mathbf{z}3}}z_{10}^2\left(\epsilon_0\epsilon_1 z_6 + z_7\right)^2,\end{aligned} \tag{2.153}$$

for all $\alpha_{\boldsymbol{\omega}} \leq \epsilon_0$, all $\alpha_{\mathbf{z}} \leq \alpha_{\boldsymbol{\omega}}\epsilon_1$, all $\eta_{\mathbf{m}} \leq \eta_{\boldsymbol{\omega}}\epsilon_3$, and all $\eta_{\mathbf{u}} \leq \alpha_{\boldsymbol{\omega}}\eta_{\mathbf{m}}\epsilon_5$, where we have used that $\epsilon_h^2\epsilon_i^2 z_j^2 + z_k^2 \leq (\epsilon_h\epsilon_i z_j + z_k)^2$ when $\epsilon_h, \epsilon_i, z_j, z_k \in \mathbb{R}_{>0}$, and with $z_{10} = \epsilon_3\epsilon_5 + L_{\boldsymbol{\omega}}1$, and some positive constants $z_1, ..., z_9 \in \mathbb{R}_{>0}$.

From Lemmas 2.19 and 2.21, it follows that, for any finite time $t_1 \geq 0$, the solutions $\tilde{\mathbf{x}}(t)$ and $\tilde{\mathbf{u}}(t)$ are bounded for all $0 \leq t \leq t_1$. As such, the right-hand side of (2.153) is bounded for all $0 \leq t \leq t_1$. Therefore, $V_{\mathbf{z}}(t, \tilde{\mathbf{z}}(t), \tilde{\mathbf{u}}(t), \alpha_{\mathbf{z}})$ is bounded for all $0 \leq t \leq t_1$, and from the bounds in Lemma 2.22 it follows that the solutions $\tilde{\mathbf{z}}(t)$ are bounded for all $0 \leq t \leq t_1$.

From Lemma 2.19, it follows that here exists a time instance $t_1 \geq 0$, such that $\|\tilde{\mathbf{x}}\| \leq \alpha_{\boldsymbol{\omega}}\eta_{\boldsymbol{\omega}}c_{\mathbf{x}2}$. Substitution in (2.153), subsequently applying the comparison lemma and using the inequality (2.59) in Lemma 2.22, we obtain the bound on $\tilde{\mathbf{z}}$ as

$$\sup_{t\geq t_1} \|\tilde{\mathbf{z}}(t)\| \leq \sup_{t\geq t_1} \max \left\{ c_{\mathbf{z}1}\|\tilde{\mathbf{z}}(t_1)\|, \frac{\alpha_{\boldsymbol{\omega}}\eta_{\boldsymbol{\omega}}}{\alpha_{\mathbf{z}}}c_{\mathbf{z}2}, \alpha_{\boldsymbol{\omega}}^2 c_{\mathbf{z}3}, \frac{\alpha_{\boldsymbol{\omega}}\eta_{\boldsymbol{\omega}}}{\alpha_{\mathbf{z}}}c_{\mathbf{z}4}\|\tilde{\mathbf{u}}(t)\| \right\}, \quad (2.154)$$

and

$$\limsup_{t\to\infty} \|\tilde{\mathbf{z}}(t)\| \leq \limsup_{t\to\infty} \max \left\{ \frac{\alpha_{\boldsymbol{\omega}}\eta_{\boldsymbol{\omega}}}{\alpha_{\mathbf{z}}}c_{\mathbf{z}2}, \alpha_{\boldsymbol{\omega}}^2 c_{\mathbf{z}3}, \frac{\alpha_{\boldsymbol{\omega}}\eta_{\boldsymbol{\omega}}}{\alpha_{\mathbf{z}}}c_{\mathbf{z}4}\|\tilde{\mathbf{u}}(t)\| \right\}, \quad (2.155)$$

with

$$\begin{aligned}
c_{\mathbf{z}1} &= \frac{6}{\gamma_{\mathbf{z}3}}\sqrt{\frac{\gamma_{\mathbf{z}2}}{\gamma_{\mathbf{z}1}}}, \\
c_{\mathbf{z}2} &= \frac{6}{\gamma_{\mathbf{z}3}}\sqrt{\frac{\gamma_{\mathbf{z}2}}{\gamma_{\mathbf{z}1}}}\left(z_{10}\left(\epsilon_0\epsilon_1 z_6 + z_7\right) + \epsilon_0\epsilon_1 z_8 c_{\mathbf{x}2}\right), \\
c_{\mathbf{z}3} &= \frac{6}{\gamma_{\mathbf{z}3}}\sqrt{\frac{\gamma_{\mathbf{z}2}}{\gamma_{\mathbf{z}1}}}\epsilon_2\left(z_{10}z_5 + \epsilon_0\epsilon_1 c_{\mathbf{x}2}\left(z_9 + \epsilon_0\epsilon_1\epsilon_2 z_1 c_{\mathbf{x}2}\right)\right), \\
c_{\mathbf{z}4} &= \frac{6}{\gamma_{\mathbf{z}3}}\sqrt{\frac{\gamma_{\mathbf{z}2}}{\gamma_{\mathbf{z}1}}}\left(z_{10}\left(\epsilon_0\epsilon_1 z_4 + z_3\right) + \epsilon_0\epsilon_1 z_2 c_{\mathbf{x}2}\right),
\end{aligned} \quad (2.156)$$

for all $t \geq t_1$, all $\alpha_{\boldsymbol{\omega}} \leq \epsilon_0$, all $\alpha_{\mathbf{z}} \leq \alpha_{\boldsymbol{\omega}}\epsilon_1$, all $\eta_{\boldsymbol{\omega}} \leq \alpha_{\mathbf{z}}\epsilon_2$, all $\eta_{\mathbf{m}} \leq \eta_{\boldsymbol{\omega}}\epsilon_3$, and all $\eta_{\mathbf{u}} \leq \alpha_{\boldsymbol{\omega}}\eta_{\mathbf{m}}\epsilon_5$, which completes the proof of Lemma 2.23. □

2.F Proof of Lemma 2.24

The proof of Lemma 2.24 builds upon the proof of Lemma 2.13 in Haring (2016, Chapter 2). We define the following Lyapunov function candidate for the $\tilde{\mathbf{m}}$-dynamics in (2.66):

$$V_{\mathbf{m}}(\tilde{\mathbf{m}}, \mathbf{Q}) = \tilde{\mathbf{m}}^\top \mathbf{Q}^{-1}\tilde{\mathbf{m}}. \quad (2.157)$$

For notational clarity, from this point on we omit the time argument. We note that

$$\lambda_{min}(\mathbf{Q}^{-1})\|\tilde{\mathbf{m}}\|^2 \leq V_{\mathbf{m}}(\tilde{\mathbf{m}}, \mathbf{Q}) \leq \lambda_{max}(\mathbf{Q}^{-1})\|\tilde{\mathbf{m}}\|^2, \quad (2.158)$$

where $\lambda_{min}(\mathbf{Q}^{-1})$ and $\lambda_{max}(\mathbf{Q}^{-1})$ are the smallest and largest eigenvalue of $\mathbf{Q}^{-1}$, respectively. For further details on $\mathbf{Q}^{-1}$, the reader is referred to Haring (2016, Chapter 2). From the observer in (2.38) and (2.66) we obtain the time derivative of $V_{\mathbf{m}}$ as

$$\begin{aligned}\dot{V}_{\mathbf{m}} &= 2\tilde{\mathbf{m}}^\top \mathbf{Q}^{-1}\dot{\tilde{\mathbf{m}}} - \tilde{\mathbf{m}}^\top \mathbf{Q}^{-1}\dot{\mathbf{Q}}\mathbf{Q}^{-1}\tilde{\mathbf{m}},\\ &= -\eta_{\mathbf{m}}\tilde{\mathbf{m}}^\top \mathbf{Q}^{-1}\tilde{\mathbf{m}} - \eta_{\mathbf{m}}\tilde{\mathbf{m}}^\top \left(\mathbf{C}^\top\mathbf{C} + \sigma_r \mathbf{D}^\top\mathbf{D}\right)\tilde{\mathbf{m}}\\ &\quad + 2\alpha_{\boldsymbol{\omega}}^2 \tilde{\mathbf{m}}^\top \mathbf{Q}^{-1}\mathbf{B}\left(\hat{\mathbf{s}} - \mathbf{s}\right) - 2\eta_{\mathbf{m}}\sigma_r\alpha_{\boldsymbol{\omega}}\tilde{\mathbf{m}}^\top \mathbf{D}^\top \frac{dF_{\mathbf{w}}}{d\mathbf{u}^\top}(\hat{\mathbf{u}})\\ &\quad - 2\eta_{\mathbf{m}}\tilde{\mathbf{m}}^\top \mathbf{C}^\top(\alpha_{\boldsymbol{\omega}}^2\left(\hat{v} - v\right) - r - d),\end{aligned} \tag{2.159}$$

where we have used the fact that $\mathbf{Q}^{-1}$ is real and symmetric, i.e., $\mathbf{Q}^{-1} = \mathbf{Q}^{-T}$, and, given $\mathbf{A}$ in (2.36), that $\tilde{\mathbf{m}}^\top\left(\mathbf{Q}^{-1}\mathbf{A} - \mathbf{A}^\top\mathbf{Q}^{-1}\right)\tilde{\mathbf{m}} = 0$. Furthermore, given $\mathbf{C}$ in (2.36) and $\mathbf{D} = [\mathbf{0}^{n_{\mathbf{u}}\times 1} \quad \mathbf{I}^{n_{\mathbf{u}}\times n_{\mathbf{u}}}]$, using the fact that $-\tilde{\mathbf{m}}^\top\mathbf{C}^\top\mathbf{C}\tilde{\mathbf{m}} = -\left\|\tilde{\mathbf{m}}^\top\mathbf{C}^\top\mathbf{C}\tilde{\mathbf{m}}\right\| = -\left\|\mathbf{C}\tilde{\mathbf{m}}\right\|^2$ and $\left\|\tilde{\mathbf{m}}^\top\mathbf{C}^\top\right\| = \left\|\mathbf{C}\tilde{\mathbf{m}}\right\|$, (2.157), and Young's inequality, we obtain

$$\begin{aligned}\dot{V}_{\mathbf{m}} \leq -\frac{\eta_{\mathbf{m}}}{2}V_{\mathbf{m}}(\tilde{\mathbf{m}},\mathbf{Q}) + \eta_{\mathbf{m}}\sigma_r\alpha_{\boldsymbol{\omega}}^2\left\|\frac{dF_{\mathbf{w}}}{d\mathbf{u}^\top}(\hat{\mathbf{u}})\right\|^2 + \frac{2\alpha_{\boldsymbol{\omega}}^4}{\eta_{\mathbf{m}}}\|\mathbf{Q}^{-1}\|\|\mathbf{B}\|^2\left\|\hat{\mathbf{s}} - \mathbf{s}\right\|^2\\ + 3\eta_{\mathbf{m}}\alpha_{\boldsymbol{\omega}}^4\left|\hat{v} - v\right|^2 + 3\eta_{\mathbf{m}}\left|r\right|^2 + 3\eta_{\mathbf{m}}\left|d\right|^2.\end{aligned} \tag{2.160}$$

From (2.37), (2.39), the bound $\|\hat{\mathbf{H}}(t,\hat{\mathbf{u}}(t))\| \leq L_{\mathbf{H}}$, the definition of $\boldsymbol{\omega}$ in (2.29), which implies that there exists a constant $L_{\boldsymbol{\omega}2} \in \mathbb{R}_{>0}$ such that $\|\boldsymbol{\omega}\| \leq L_{\boldsymbol{\omega}2}$, and the bound in (2.27) we obtain

$$\begin{aligned}\left\|\hat{\mathbf{s}} - \mathbf{s}\right\| &\leq \frac{1}{\alpha_{\boldsymbol{\omega}}}\left(L_{\mathbf{H}} + L_{F2}\right)\|\dot{\hat{\mathbf{u}}}\|,\\ \left|\hat{v} - v\right| &\leq \frac{1}{2}\left(L_{\mathbf{H}} + L_{F2}\right)L_{\boldsymbol{\omega}2}^2.\end{aligned} \tag{2.161}$$

From (2.37) and the bounds in (2.15), it follows that

$$|r| = \left\|\int_0^1 \frac{dk}{d\mathbf{z}}(\sigma\tilde{\mathbf{z}} + \bar{\mathbf{z}}_{\mathbf{w}})d\sigma\tilde{\mathbf{z}}\right\| \leq L_k\|\tilde{\mathbf{z}}\|. \tag{2.162}$$

From (2.152) and by using Young's inequality, it follows that $\|\mathbf{u} - \mathbf{u}_{\mathbf{w}}^*\|^2 \leq 2\|\tilde{\mathbf{u}}\|^2 + 2\alpha_{\boldsymbol{\omega}}^2 L_{\boldsymbol{\omega}2}^2$. From this, (2.32), the bounds in (2.15), and Assumption 2.12, we obtain

$$|d| \leq L_k\alpha_{\mathbf{z}}(\delta_{\mathbf{z}1} + 2\delta_{\mathbf{z}2}\|\tilde{\mathbf{u}}\|^2 + 2\delta_{\mathbf{z}2}\alpha_{\boldsymbol{\omega}}^2 L_{\boldsymbol{\omega}2}^2). \tag{2.163}$$

From the coordinate transformation in (2.42) and the bound in (2.27), we obtain

$$\left\|\frac{dF_{\mathbf{w}}}{d\mathbf{u}}(\hat{\mathbf{u}})\right\| \leq \int_0^1 \left\|\frac{d^2F_{\mathbf{w}}}{d\mathbf{u}d\mathbf{u}^\top}(\sigma\tilde{\mathbf{u}} + \mathbf{u}_{\mathbf{w}}^*)\right\| d\sigma\,\|\tilde{\mathbf{u}}\| = L_{F2}\,\|\tilde{\mathbf{u}}\|. \tag{2.164}$$

By combining (2.160)-(2.164) and since we have from (2.36) that $\|\mathbf{B}\| = 1$, we obtain

$$\begin{aligned}\dot{V}_{\mathbf{m}} \leq & -\frac{\eta_{\mathbf{m}}}{2} V_{\mathbf{m}}(\tilde{\mathbf{m}}, \mathbf{Q}) + \eta_{\mathbf{m}} \sigma_r \alpha_{\boldsymbol{\omega}}^2 L_{F2}^2 \|\tilde{\mathbf{u}}\|^2 + \frac{2\alpha_{\boldsymbol{\omega}}^2}{\eta_{\mathbf{m}}} \left(L_{\mathbf{H}} + L_{F2}\right)^2 \|\mathbf{Q}^{-1}\| \|\dot{\hat{\mathbf{u}}}\|^2 \\ & + 3\eta_{\mathbf{m}} L_k^2 \|\tilde{\mathbf{z}}\|^2 + 9\eta_{\mathbf{m}} L_k^2 \alpha_{\mathbf{z}}^2 (\delta_{\mathbf{z}1}^2 + 4\delta_{\mathbf{z}2}^2 \|\tilde{\mathbf{u}}\|^4 + 4\delta_{\mathbf{z}2}^2 \alpha_{\boldsymbol{\omega}}^4 L_{\boldsymbol{\omega}2}^4) \\ & + \frac{3}{4} \eta_{\mathbf{m}} \alpha_{\boldsymbol{\omega}}^4 \left(L_{\mathbf{H}} + L_{F2}\right)^2 L_{\boldsymbol{\omega}2}^4. \end{aligned} \tag{2.165}$$

From Lemmas 2.21 and 2.22 we have that, for any finite time $t_1 \geq 0$, the solutions $\tilde{\mathbf{u}}$ and $\tilde{\mathbf{z}}$ are bounded for all $0 \leq t \leq t_1$. Moreover, from Lemma 2.20 we have that $\mathbf{Q}^{-1}$ is positive definite and bounded for all $0 \leq t \leq t_1$. From these facts and $\|\dot{\hat{\mathbf{u}}}\| \leq \eta_{\mathbf{u}}$, which follows from (2.40), we obtain that the right-hand side of (2.165) is bounded for all $0 \leq t \leq t_1$. Therefore, $V_{\mathbf{m}}(\tilde{\mathbf{m}}(t), \mathbf{Q}(t))$ will be bounded for all $0 \leq t \leq t_1$, and $\mathbf{Q}^{-1}$ is positive definite and bounded for all $0 \leq t \leq t_1$ as well, it follows from (2.158) that the solutions $\tilde{\mathbf{m}}$ are bounded for all $0 \leq t \leq t_1$.

Define $t_1 \geq 0$ such that from Lemma 2.19 and Lemma 2.20 we have that $\|\tilde{\mathbf{x}}(t)\| \leq \alpha_{\boldsymbol{\omega}} \eta_{\boldsymbol{\omega}} c_{\mathbf{x}2}$ and $\|\tilde{\mathbf{Q}}(t)\| \leq \frac{1}{8}$, for all $t \geq t_1$. From the proof of Lemma 2.11 in Haring (2016, Chapter 2), we have that $\frac{1}{4}\mathbf{I} \preceq \mathbf{Q}^{-1} \preceq \frac{5}{4}\mathbf{I}$ for all $t \geq t_1$, all $\eta_{\mathbf{m}} \leq \eta_{\boldsymbol{\omega}} \epsilon_3$ and all $\sigma_r \leq \epsilon_6$, with ϵ_3 and ϵ_6 sufficiently small. Moreover, it follows that $\frac{1}{4}\|\tilde{\mathbf{m}}\|^2 \leq V_{\mathbf{m}}(\tilde{\mathbf{m}}, \mathbf{Q}) \leq \frac{5}{4}\|\tilde{\mathbf{m}}\|^2$, for all $t \geq t_1$, and $\|\mathbf{Q}^{-1}\| \leq \frac{5}{4}$ for all $t \geq t_1$. From (2.30), (2.40), (2.42), $\|\mathbf{D}\| = 1$, and the bound in (2.27), it follows that $\|\dot{\hat{\mathbf{u}}}\|^2 \leq 8\lambda_{\mathbf{u}}^2 V_{\mathbf{m}}(\tilde{\mathbf{m}}, \mathbf{Q}) + 2\alpha_{\boldsymbol{\omega}}^2 \lambda_{\mathbf{u}}^2 L_{F2}^2 \|\tilde{\mathbf{u}}\|^2$, for all $t_1 \geq 0$. From this, and taking ϵ_4 in Theorem 2.16 sufficiently small, we obtain from (2.165) that

$$\begin{aligned}\dot{V}_{\mathbf{m}} \leq & -\frac{\eta_{\mathbf{m}}}{4} V_{\mathbf{m}}(\tilde{\mathbf{m}}, \mathbf{Q}) + \eta_{\mathbf{m}} \sigma_r \alpha_{\boldsymbol{\omega}}^2 L_{F2}^2 \|\tilde{\mathbf{u}}\|^2 + \frac{5\alpha_{\boldsymbol{\omega}}^4 \lambda_{\mathbf{u}}^2}{\eta_{\mathbf{m}}} \left(L_{\mathbf{H}} + L_{F2}\right)^2 L_{F2}^2 \|\tilde{\mathbf{u}}\|^2 \\ & + \frac{3}{4} \eta_{\mathbf{m}} \alpha_{\boldsymbol{\omega}}^4 \left(L_{\mathbf{H}} + L_{F2}\right)^2 L_{\boldsymbol{\omega}2}^4 + 3\eta_{\mathbf{m}} L_k^2 \|\tilde{\mathbf{z}}\|^2 \\ & + 9\eta_{\mathbf{m}} L_k^2 \alpha_{\mathbf{z}}^2 (\delta_{\mathbf{z}1}^2 + 4\delta_{\mathbf{z}2}^2 \|\tilde{\mathbf{u}}\|^4 + 4\delta_{\mathbf{z}2}^2 \alpha_{\boldsymbol{\omega}}^4 L_{\boldsymbol{\omega}2}^4), \end{aligned} \tag{2.166}$$

for all $t \geq t_1$, and all $\alpha_{\boldsymbol{\omega}} \lambda_{\mathbf{u}} \leq \eta_{\mathbf{m}} \epsilon_4$. From the comparison lemma and the inequality in (2.166), and using (2.158), we obtain

$$\begin{aligned}\sup_{t \geq t_1} \|\tilde{\mathbf{m}}(t)\| \leq \sqrt{32} \sup_{t \geq t_1} \max \Big\{ & \sqrt{\frac{5}{4}} \|\tilde{\mathbf{m}}(t_1)\|, 2\sqrt{5} \frac{\alpha_{\boldsymbol{\omega}}^2 \lambda_{\mathbf{u}}}{\eta_{\mathbf{m}}} \left(L_{\mathbf{H}} + L_{F2}\right) L_{F2} \|\tilde{\mathbf{u}}(t)\|, \\ & 2\sqrt{3} L_k \|\tilde{\mathbf{z}}(t)\|, \sqrt{3} \alpha_{\boldsymbol{\omega}}^2 \left(L_{\mathbf{H}} + L_{F2}\right) L_{\boldsymbol{\omega}2}^2, 2\sqrt{\sigma_r} \alpha_{\boldsymbol{\omega}} L_{F2} \|\tilde{\mathbf{u}}(t)\|, \\ & 12\alpha_{\mathbf{z}} \delta_{\mathbf{z}2} L_k \|\tilde{\mathbf{u}}(t)\|^2, 12\alpha_{\mathbf{z}} \delta_{\mathbf{z}2} \alpha_{\boldsymbol{\omega}}^2 L_k L_{\boldsymbol{\omega}2}^2, 6\alpha_{\mathbf{z}} \delta_{\mathbf{z}1} L_k \Big\}, \end{aligned} \tag{2.167}$$

and

$$\limsup_{t\to\infty} \|\tilde{\mathbf{m}}(t)\| \leq 2\sqrt{6} \limsup_{t\to\infty} \Big\{ 2\sqrt{5}\frac{\alpha_{\boldsymbol{\omega}}^2 \lambda_{\mathbf{u}}}{\eta_{\mathbf{m}}} \left(L_{\mathbf{H}} + L_{F2}\right) L_{F2} \|\tilde{\mathbf{u}}(t)\|, \\ 2\sqrt{3} L_k \|\tilde{\mathbf{z}}(t)\|, \sqrt{3}\alpha_{\boldsymbol{\omega}}^2 \left(L_{\mathbf{H}} + L_{F2}\right) L_{\boldsymbol{\omega}2}^2, 2\sqrt{\sigma_r}\alpha_{\boldsymbol{\omega}} L_{F2} \|\tilde{\mathbf{u}}(t)\|, \\ 12\alpha_{\mathbf{z}}\delta_{\mathbf{z}2} L_k \|\tilde{\mathbf{u}}(t)\|^2, 12\alpha_{\mathbf{z}}\delta_{\mathbf{z}2}\alpha_{\boldsymbol{\omega}}^2 L_k L_{\boldsymbol{\omega}2}^2, 6\alpha_{\mathbf{z}}\delta_{\mathbf{z}1} L_k \Big\}. \tag{2.168}$$

for all $t \geq t_1$, all $\eta_{\mathbf{m}} \leq \eta_{\boldsymbol{\omega}}\epsilon_3$, all $\alpha_{\boldsymbol{\omega}}\lambda_{\mathbf{u}} \leq \eta_{\mathbf{m}}\epsilon_4$, and all $\sigma_r \leq \epsilon_6$. The bounds in (2.67) and (2.68) of Lemma 2.24 follow from (2.167) and (2.168), respectively, which completes the proof of Lemma 2.24. □

Chapter 3

Extremum-seeking control and enhanced convergence speed for optimization of industrial motion systems

Abstract - *In Chapter 2, an extremum-seeking control approach has been developed for optimization of time-varying steady-state responses of general nonlinear systems. A generic filter structure was introduced, the so-called dynamic cost function, which has been instrumental in facilitating the use of extremum seeking in the more generic, time-varying context. The dynamic cost function, however, must operate sufficiently slow compared to the time-varying nature of the system responses, thereby compromising convergence speed of the extremum-seeking control scheme. The first contribution of this chapter is the proposition of a modified extremum-seeking controller design that incorporates explicit knowledge about the user-defined dynamic cost function, enhancing convergence speed of the resulting extremum-seeking control scheme. The second contribution of this chapter is a stability analysis for this extended approach. The third contribution of this chapter is an experimental demonstration of the extremum-seeking controller design in Chapter 2 and the extended design in this chapter for the performance-optimal tuning of a variable-gain control strategy employed on a high-accuracy industrial motion stage set-up, exhibiting generically time-varying steady-state responses. Experiments show that, for the unknown disturbance situation at hand, the variable-gain controller can be automatically tuned using both ESC approaches to achieve optimal system performance. In addition, enhanced convergence speed with the modified extremum-seeking controller design is evidenced experimentally.*

The content of this chapter is based on: L. Hazeleger, J. van de Wijdeven, M. Haring, N. van de Wouw, "Extremum-seeking with enhanced convergence speed for optimization of time-varying steady-state behavior of industrial motion stages", *Submitted for publication in IEEE Transactions on Control Systems Technology*

3.1 Introduction

Extremum-seeking control (ESC) is a data-driven and model-free method for optimizing the steady-state behavior of a stable or stabilized plant in real-time, by automated adaptation of tunable plant parameters. Often in the ESC literature, the general requirement for optimizing a stable or stabilized plant is the existence of a (unknown) time-invariant parameter-to-steady-state performance map, i.e., a *static* input-output relation between tunable plant parameters and the steady-state plant performance, see, e.g., Ariyur and Krstić (2003), Krstić and Wang (2000), Teel and Popović (2001), and Nešić et al. (2010). In those references, the steady-state performance map characterizes the performance of the dynamical plant to-be optimized in an *equilibria* setting. Even in the presence of (high-frequency) noise, convergence towards a neighborhood of the optimum can be achieved, the size of which is often dependent on the noise level, see, e.g., Zhang and Ordónez (2009), Stanković and Stipanović (2010), Tan et al. (2010), and Haring (2016). In cases where *periodic* steady-state behavior characterizes system performance, often induced by periodic references and disturbances acting on the system dynamics, ESC methods have been proposed in Wang and Krstić (2000), Guay et al. (2007), Haring et al. (2013). To cope with a more generic problem setting, in Chapter 2 an ESC method has been proposed to optimize *generically time-varying* steady-state behavior of a class of nonlinear systems, see also (Hazeleger et al., 2018).

Considering generically time-varying disturbances and the resulting to-be-optimized performance in terms of generically time-varying steady-state responses an integral part of the problem formulation for performance optimization of time-varying steady-state plant behavior is essential, especially in practice. Namely, steady-state performance of many industrial applications is related to generically time-varying system responses. For example, time-varying behavior emerges in reference tracking or disturbance attenuation problems, which are encountered, for example, in industrial positioning stages commonly found in pick-and-place systems, robotics, electron microscopes, and wafer scanning systems. Given the fact that accurate knowledge on the disturbances is typically not available and may vary from machine to machine or mode-of-use, ESC is a candidate for data-based performance optimization. Namely, ESC only exploits measured outputs of the system, and as such, can be used to automatically tune system parameters in the presence of arbitrary reference trajectories, unknown external disturbances, and possibly unknown system dynamics.

Other works, which have studied extremum-seeking control in the presence of time-varying system behavior, are, e.g., Scheinker and Krstić (2014), Scheinker and Scheinker (2016) and Scheinker and Krstić (2013). In these references, extremum-seeking controllers are utilized directly as feedback controller, able to, on the one hand, control unstable and time-varying input-affine systems, and on the other hand, optimize steady-state equilibria in the presence of noise.

The methods have been experimentally demonstrated in, e.g., the minimization of reflected input radio frequency (RF) power in RF resonant cavities (Scheinker, 2017), and the minimization of so-called betatron oscillations in particle accelerators (Scheinker et al., 2018). We care to emphasize that, in this chapter, we consider the problem of optimizing time-varying steady-state responses of stable or stabilized plants, which is a different problem from the one considered in Scheinker and Krstić (2014), Scheinker and Scheinker (2016) and Scheinker and Krstić (2013). Moreover, we remark that the methods in Scheinker and Krstić (2014), Scheinker and Scheinker (2016) and Scheinker and Krstić (2013) typically rely on high dither frequencies relative to the time-varying system dynamics, while the ESC method proposed in this chapter can employ small dither frequencies relative to the time-varying system dynamics, even in the presence of high-frequency disturbances. Additionally, in the case of extremum-seeking control for already stable or stabilized systems, the class of systems considered in this chapter is more general.

ESC for slowly time-varying performance maps is considered in, e.g., Grushkovskaya et al. (2017), Sahneh et al. (2012), Cao et al. (2017), Fu and Özgüner (2011), and Rušiti et al. (2019). Herein, optimal plant performance is obtained by tracking optimal, slowly time-varying, plant parameters. We remark that this problem setting is different from the one considered in this chapter. Namely, we consider the problem of optimizing *static* performance maps in the spirit of Hunnekens et al. (2015), Wang and Krstić (2000), and Haring et al. (2013), although more general in terms of the time-varying nature of the disturbances. We propose an ESC method that seeks *constant* plant parameter settings that optimize steady-state plant performance in terms of time-varying steady-state system responses.

To facilitate the use of extremum seeking in the more generic, time-varying context, in Chapter 2 a generic filter structure was introduced, the so-called dynamic cost function. However, to warrant sufficient time-scale separation in the ESC scheme, the dynamic cost function must operate sufficiently slow compared to the time-varying nature of the system responses, thereby compromising convergence speed of the ESC scheme. The first contribution of this chapter is the proposition of a modified extremum-seeking controller design which enables enhanced convergence speed of the ESC scheme compared to the nominal extremum-seeking controller design presented in Chapter 2. By exploiting a particular linear-time-invariant (LTI) filter structure for the user-defined dynamic cost function design and incorporating the explicit knowledge in the extremum-seeking controller design, enhanced convergence speed of the ESC scheme compared to the nominal ESC design is achievable. The effectiveness of the modified extremum-seeking controller design with respect to the nominal ESC approach is shown by means of a simulation example. The second contribution of this chapter is to provide a stability analysis of the closed-loop ESC scheme with the modified extremum-seeking controller design.

The third contribution is the experimental demonstration of both the nominal extremum-seeking controller design as presented in Chapter 2, and the modified extremum-seeking controller design presented in this chapter. In particular, the impact of the tuning of a particular dynamic cost function design on the convergence of the closed-loop ESC scheme will be shown, as well as the effectiveness of the modified extremum-seeking controller design in terms of enhanced convergence speed with respect to the nominal extremum-seeking controller design.

Both ESC approaches are utilized to achieve performance-optimal tuning of a variable-gain control (VGC) strategy applied to an industrial motion stage set-up which is subject to unknown and time-varying (external) disturbances. VGC is a nonlinear control strategy that is able to enhance system performance by balancing the typical tradeoff between the use of low-gain and high-gain feedback control in linear motion control systems, and has been the topic of many studies (Heertjes et al., 2009, 2011; Su et al., 2005; Zheng et al., 2005; van de Wouw et al., 2008; Hespanha and Morse, 2002; Hunnekens et al., 2014). Due to the well-known waterbed-effect, see, e.g., Freudenberg et al. (2000) and Seron et al. (1997), increasing the bandwidth of linear motion control systems by applying high-gain feedback control to improve the ability to suppress low-frequency disturbances comes at the expense of an increased sensitivity to high-frequency disturbances and noise. Instead, VGC enables a higher gain, and thus a higher bandwidth, only when necessary. However, the ability to achieve optimal performance ultimately relies on the tuning of the variable-gain controller, which can be far from trivial as system performance highly depends on the unknown disturbance situation at hand.

Automatic tuning of (nonlinear) control strategies for optimal performance has been studied in many works, see, e.g., Hunnekens et al. (2014), Heertjes et al. (2018), Hjalmarsson et al. (1998), Pavlov et al. (2013), Karimi et al. (2004), Hjalmarsson et al. (1994), Campi et al. (2002), and Bazanella et al. (2012). Here, we pursue the tuning of variable-gain controllers through ESC as an alternative means to achieve optimal performance, which does not require knowledge on the plant model as in, e.g., Hunnekens et al. (2014), Heertjes et al. (2018), Karimi et al. (2004), specific (linear parameterized) controller structures as in, e.g., Campi et al. (2002), specific experiments as in, e.g., Hjalmarsson et al. (1998), Hjalmarsson et al. (1994), or disturbance knowledge as in Pavlov et al. (2013). In Hunnekens et al. (2015), ESC has been applied in the scope of *periodic* steady-state behavior for the adaptive design of a VGC strategy applied to a magnetically levitated industrial motion platform.

The main contributions of this chapter can be summarized as follows. The first contribution is a modified extremum-seeking controller design for the optimization of time-varying steady-state responses of nonlinear systems that enables enhanced convergence speed of the closed-loop ESC scheme. The second contribution is a stability analysis of the closed-loop ESC scheme. The third contribution is the experimental demonstration of both the extremum-seeking controller

design proposed in Chapter 2, and the modified extremum-seeking controller design in this chapter, for the performance-optimal tuning of a variable-gain control strategy employed on a high-accuracy industrial motion stage set-up.

This chapter is organized as follows. In the first part of Section 3.2, the ESC approach for systems with time-varying steady-state responses as proposed in Chapter 2 is briefly described. This will be helpful in the second part of Section 3.2, in which we present the modified extremum-seeking controller design and a closed-loop stability analysis. Section 3.3 presents the industrial motion stage set-up under study. In Section 3.4, the experimental results of both ESC strategies will be discussed for the performance-optimal tuning of variable-gain controllers. Section 3.5 closes with conclusions.

3.2 Extremum-seeking for optimization of generically time-varying steady-state system behavior

In this section, first, we will briefly recap the ESC problem formulation for *generically time-varying* system responses and the extremum-seeking controller design as studied in Chapter 2. Second, we propose a modified extremum-seeking controller design that incorporates explicit knowledge about the dynamic cost function to enhance convergence speed compared to the initial extremum-seeking controller design. Third, we present a stability result of the closed-loop ESC scheme with modified ESC approach.

3.2.1 Extremum-seeking control problem formulation for optimization of time-varying system responses

Here we elaborate on the elements of the so-called extended plant Σ as depicted in Fig. 3.1, i.e., the series connection of a to-be-optimized, nonlinear system Σ_p that may exhibit generically time-varying behavior in steady-state conditions and for which we can measure its output, and a so-called *dynamic cost function*, consisting of a user-defined cost function Z and a user-defined filter Σ_f. This dynamic cost function has proven instrumental to achieve extremum-seeking in the time-varying steady-state setting.

Nonlinear systems

We consider the following generic description of a multiple-input-multiple-output nonlinear system:

$$\Sigma_p : \begin{cases} \dot{\mathbf{x}}(t) = \mathbf{f}(\mathbf{x}(t), \mathbf{u}(t), \mathbf{w}(t)) \\ \mathbf{e}(t) = \mathbf{g}(\mathbf{x}(t), \mathbf{u}(t), \mathbf{w}(t)), \end{cases} \tag{3.1}$$

where $\mathbf{x} \in \mathbb{R}^{n_\mathbf{x}}$ denotes the state of the system, $\mathbf{u} \in \mathbb{R}^{n_\mathbf{u}}$ denotes the input of the system, $\mathbf{e} \in \mathbb{R}^{n_\mathbf{e}}$ denotes the output of the system, $\mathbf{w} \in \mathbb{R}^{n_\mathbf{w}}$ are disturbances,

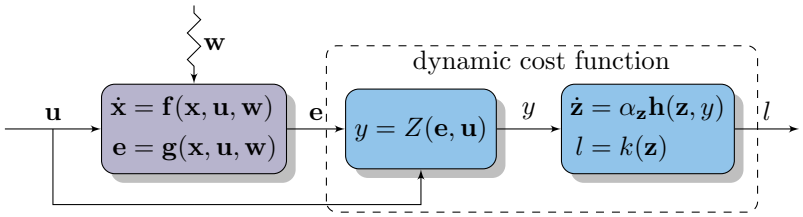

Figure 3.1: The extended plant Σ, i.e., series connection of the nonlinear system Σ_p, the user-defined cost function Z, and the to-be-designed filter Σ_f.

and $t \in \mathbb{R}$ is time. In the context of ESC, Σ_p represents the system to be optimized, where the input $\mathbf{u}$ can be regarded as a vector of tunable system parameters, the output $\mathbf{e}$ can be regarded as a vector of measured performance variables, and $\mathbf{w}$ are piecewise continuous (time-varying and typically unknown) disturbances, defined and bounded on $t \in \mathbb{R}$. We denote this class of disturbances by $\overline{\mathbb{PC}}_{\mathbf{w}}$, and define the following set of disturbances:

$$\mathcal{W} = \{\mathbf{w} \in \overline{\mathbb{PC}}_{\mathbf{w}} : \|\mathbf{w}(t)\| \leq \rho_{\mathbf{w}} \ \forall \ t \in \mathbb{R}\} \tag{3.2}$$

with $\rho_{\mathbf{w}} > 0$. We adopt the following assumption on the system in (3.1), see Assumption 2.6 in Chapter 2.

Assumption 3.1. *The nonlinear system Σ_p in (3.1) is globally uniformly exponentially convergent*[1] *for a class of disturbances $\mathbf{w}(\cdot) \in \mathcal{W}$, and for all constant input $\mathbf{u} \in \mathbb{R}^{n_{\mathbf{u}}}$, uniformly in $\mathbf{u}$. In addition, given a disturbance $\mathbf{w} \in \mathcal{W}$, the globally exponentially stable (GES) steady-state solution, which we denote by $\bar{\mathbf{x}}_{\mathbf{w}}(t, \mathbf{u})$, is twice continuously differentiable in $\mathbf{u}$ and satisfies*

$$\left\| \frac{\partial \bar{\mathbf{x}}_{\mathbf{w}}}{\partial \mathbf{u}}(t, \mathbf{u}) \right\| \leq L_{\mathbf{xu}}, \tag{3.3}$$

for all $t \in \mathbb{R}$, all $\mathbf{u} \in \mathbb{R}^{n_{\mathbf{u}}}$, and some constant $L_{\mathbf{xu}} \in \mathbb{R}_{>0}$.

Given Assumption 3.1, for constant inputs $\mathbf{u} \in \mathbb{R}^{n_{\mathbf{u}}}$ and a given $\mathbf{w} \in \mathcal{W}$, there exists a unique, time-varying steady-state output of the system Σ_p in (3.1), denoted by $\bar{\mathbf{e}}_{\mathbf{w}}(t, \mathbf{u})$, which is given by

$$\bar{\mathbf{e}}_{\mathbf{w}}(t, \mathbf{u}) = \mathbf{g}(\bar{\mathbf{x}}_{\mathbf{w}}(t, \mathbf{u}), \mathbf{u}, \mathbf{w}(t)). \tag{3.4}$$

The aim is to find constant inputs $\mathbf{u}$ that optimize the steady-state performance of the system in (3.1). Common practice (in the ESC literature) is to define

[1] The notion of convergent systems has proven instrumental in the scope of the stability analysis of the ESC scheme with time-varying steady-state responses in Chapter 2. For details on convergent systems, see Pavlov et al. (2006) and Chapter 2.

a cost function in terms of the system responses and inputs that quantifies the performance of interest for the system under study. For example, consider the following performance measure which is adopted from Haring et al. (2013) and exploited in Hunnekens et al. (2015):

$$L_2(t, \mathbf{e}(t)) := \frac{1}{T} \int_{t-T}^{t} \|\mathbf{e}(\tau)\|^2 d\tau \qquad \forall t \geq T, \tag{3.5}$$

where $T \in \mathbb{R}_{>0}$ typically indicates a known performance relevant time-interval. In the case where, for constant inputs $\mathbf{u}$, the steady-state plant outputs $\bar{\mathbf{e}}_{\mathbf{w}}$ in (3.4) are *constant* for all time or *periodic* with period time T, the steady-state output of the cost function in (3.5) is constant for all time as well. Having a constant steady-state output of the cost function for constant inputs $\mathbf{u}$ is one of the basic requirements in the ESC literature that study the data-based optimization of stable (nonlinear) systems by means of extremum seeking control (Krstić and Wang, 2000; Tan et al., 2006; Haring et al., 2013). However, in many (industrial) applications this requirement is not met, as the steady-state plant outputs $\bar{\mathbf{e}}_{\mathbf{w}}(t, \mathbf{u})$ that characterize system performance are generically *time-varying* in nature (also for constant $\mathbf{u}$). In addition, periodicity of the steady-state plant outputs $\bar{\mathbf{e}}_{\mathbf{w}}$ is not evident due to the fact that system responses can be induced by complex, time-varying, possibly non-periodic disturbances and reference trajectories. In those cases, often the neighborhood to which the ESC scheme converges can not be made arbitrarily small, thereby limiting the achievable performance gain.

Dynamic cost function

To deal with the time-varying nature of the system responses, Chapter 2 proposes the series connection of the system Σ_p as in (3.1), and a so-called *dynamic cost function*, i.e., the series connection of a cost function Z of the form

$$y(t) = Z(\mathbf{e}(t), \mathbf{u}(t)), \tag{3.6}$$

where $y \in \mathbb{R}$, and a user-defined filter, denoted by Σ_f, which has the following general form

$$\Sigma_f : \begin{cases} \dot{\mathbf{z}}(t) = \alpha_{\mathbf{z}} \mathbf{h}(\mathbf{z}(t), y(t)) \\ l(t) = k(\mathbf{z}(t)), \end{cases} \tag{3.7}$$

where $\alpha_{\mathbf{z}} \in \mathbb{R}_{>0}$ is a tuning parameter, $\mathbf{z} \in \mathbb{R}^{n_{\mathbf{z}}}$ is the state of the filter, $y \in \mathbb{R}$ is the input of the filter defined by (3.6), and $l \in \mathbb{R}$ is the output of the filter. The function $Z : \mathbb{R}^{n_{\mathbf{e}}} \times \mathbb{R}^{n_{\mathbf{u}}} \to \mathbb{R}$ is designed to be twice continuously differentiable with respect to both arguments. Moreover, we choose Z in such a way that there exist constants $L_{Z\mathbf{e}}$, $L_{Z\mathbf{u}} \in \mathbb{R}_{>0}$ such that

$$\left\| \frac{\partial^2 Z}{\partial \mathbf{e} \partial \mathbf{e}^\top}(\mathbf{e}, \mathbf{u}) \right\| \leq L_{Z\mathbf{e}}, \quad \left\| \frac{\partial^2 Z}{\partial \mathbf{e} \partial \mathbf{u}^\top}(\mathbf{e}, \mathbf{u}) \right\| \leq L_{Z\mathbf{u}}, \tag{3.8}$$

for all $\mathbf{e} \in \mathbb{R}^{n_\mathbf{e}}$, and all $\mathbf{u} \in \mathbb{R}^{n_\mathbf{u}}$. Given a disturbance $\mathbf{w} \in \mathcal{W}$, for all constant inputs $\mathbf{u} \in \mathbb{R}^{n_\mathbf{u}}$, the steady-state output of Z is denoted by $\bar{y}_\mathbf{w}(t, \mathbf{u})$ and reads

$$\bar{y}_\mathbf{w}(t, \mathbf{u}) = Z(\mathbf{g}(\bar{\mathbf{x}}_\mathbf{w}(t, \mathbf{u}), \mathbf{u}, \mathbf{w}(t)), \mathbf{u}). \tag{3.9}$$

The functions $\mathbf{h} : \mathbb{R}^{n_\mathbf{z}} \times \mathbb{R} \to \mathbb{R}^{n_\mathbf{z}}$ and $k : \mathbb{R}^{n_\mathbf{z}} \to \mathbb{R}$ in (2.12) are designed to be twice continuously differentiable with respect to all arguments. Moreover, we design Σ_f in such a way that there exist constants $L_{\mathbf{hz}}$, $L_{\mathbf{h}y}$, $L_k \in \mathbb{R}_{>0}$ such that

$$\left\| \frac{\partial \mathbf{h}}{\partial \mathbf{z}}(\mathbf{z}, y) \right\| \leq L_{\mathbf{hz}}, \left\| \frac{\partial \mathbf{h}}{\partial y}(\mathbf{z}, y) \right\| \leq L_{\mathbf{h}y}, \left\| \frac{dk}{d\mathbf{z}}(\mathbf{z}) \right\| \leq L_k, \tag{3.10}$$

for all $\mathbf{z} \in \mathbb{R}^{n_\mathbf{z}}$, and all $y \in \mathbb{R}$. The design of the dynamic cost function should satisfy the following property.

Property 3.2. *The dynamic cost function consisting of the cascade of Z and Σ_f, given by* (3.6) *and* (3.7)*, respectively, is exponentially input-to-state convergent (for the definition of (exponentially) input-to-state convergence, see, e.g., Pavlov et al. (2006) or Definition 2.5 in Chapter 2) for all constant inputs $\mathbf{u} \in \mathbb{R}^{n_\mathbf{u}}$ and all $\alpha_\mathbf{z} \in \mathbb{R}_{>0}$, uniformly in $\mathbf{u}$.*

Instead of defining system performance in a time-averaged sense as in (3.5) with fixed period time T, the filter Σ_f is introduced to act as an averaging operator on $y(t)$ in (3.6), which quantifies system performance similar to the use of exponentially weighting filters (Wang and Krstić, 2000; Antonello et al., 2009). By tuning $\alpha_\mathbf{z}$ sufficiently small, the solution $\mathbf{z}(t)$ will vary "slowly" in time, i.e., the output of the filter $l(t)$ will be quasi-constant and determined predominantly by the average of $y(t)$. By properly designing cost function Z and tuning $\alpha_\mathbf{z}$ in (3.7) small, the output of the dynamic cost function $l(t)$ is quasi-constant and reflects the performance of the system, while being characterized by the time-varying system response $\mathbf{e}(t)$. Hence, by subsequently minimizing $l(t)$ using ESC, we optimize the time-varying system response $\mathbf{e}(t)$.

Extended plant dynamics

The series connection of the nonlinear plant Σ_p in (3.1) and the dynamic cost function, consisting of the cost function Z in (3.6) and filter Σ_f in (3.7), is referred to as the extended plant Σ and is schematically depicted in Fig. 3.1. The dynamics of the extended plant is given by

$$\Sigma : \begin{cases} \dot{\mathbf{x}}(t) = \mathbf{f}(\mathbf{x}(t), \mathbf{u}(t), \mathbf{w}(t)) \\ \dot{\mathbf{z}}(t) = \alpha_\mathbf{z} \mathbf{h}(\mathbf{z}(t), Z(\mathbf{g}(\mathbf{x}(t), \mathbf{u}(t), \mathbf{w}(t)), \mathbf{u}(t))) \\ l(t) = k(\mathbf{z}(t)). \end{cases} \tag{3.11}$$

In Lemma 2.11 in Chapter 2, it has been shown that, given the nonlinear system and the dynamic cost function described above, the extended plant Σ is globally

uniformly exponentially convergent for a class of disturbances $\mathbf{w}(\cdot) \in \mathcal{W}$, for all constant inputs $\mathbf{u} \in \mathbb{R}^{n_\mathbf{u}}$, uniformly in $\mathbf{u}$. This implies that there exists a unique steady-state solution of Σ_f, denoted by $\bar{\mathbf{z}}_\mathbf{w}(t, \mathbf{u}, \alpha_\mathbf{z})$ and induced by the extended plant, which is defined and bounded on $t \in \mathbb{R}$ and globally exponentially stable (GES). We denote this steady-state solution by $\bar{\mathbf{z}}_\mathbf{w}(t, \mathbf{u}, \alpha_\mathbf{z})$ to emphasize the dependency on time-varying disturbances $\mathbf{w}(t)$, constant inputs $\mathbf{u}$, and the tunable parameter $\alpha_\mathbf{z}$.

Parameter-to-steady-state performance map

Next, we define the objective function $F_\mathbf{w}$ in terms of the steady-state solution $\bar{\mathbf{z}}_\mathbf{w}$ of the extended plant Σ, for which we adopt part of Assumption 2.12 in Chapter 2.

Assumption 3.3. *Given a disturbance $\mathbf{w}(t) \in \mathcal{W}$, there exists a twice continuously differentiable function $\mathbf{q}_\mathbf{w} : \mathbb{R}^{n_\mathbf{u}} \to \mathbb{R}^{n_\mathbf{z}}$, referred to as the constant performance cost, such that*

$$\mathbf{q}_\mathbf{w}(\mathbf{u}) = \lim_{\alpha_\mathbf{z} \to 0} \bar{\mathbf{z}}_\mathbf{w}(t, \mathbf{u}, \alpha_\mathbf{z}), \tag{3.12}$$

for all $t \in \mathbb{R}$, and all $\mathbf{u} \in \mathbb{R}^{n_\mathbf{u}}$. Moreover, there exist constants $\delta_{\mathbf{z}1}, \delta_{\mathbf{z}2} \in \mathbb{R}_{\geq 0}$, related to the disturbance $\mathbf{w}(t)$ and the extended plant Σ, such that the difference between the steady-state solution $\bar{\mathbf{z}}_\mathbf{w}(t, \mathbf{u}, \alpha_\mathbf{z})$ and the function $\mathbf{q}_\mathbf{w}(\mathbf{u})$ satisfies

$$\|\bar{\mathbf{z}}_\mathbf{w}(t, \mathbf{u}, \alpha_\mathbf{z}) - \mathbf{q}_\mathbf{w}(\mathbf{u})\| \leq \alpha_\mathbf{z} \left(\delta_{\mathbf{z}1} + \delta_{\mathbf{z}2} \|\mathbf{u} - \mathbf{u}_\mathbf{w}^*\|^2 \right), \tag{3.13}$$

for all $t \in \mathbb{R}$, all $\mathbf{u} \in \mathbb{R}^{n_\mathbf{u}}$, and all $0 < \alpha_\mathbf{z} \leq \epsilon_\mathbf{z}$ for some constant $\epsilon_\mathbf{z} \in \mathbb{R}_{>0}$, where $\mathbf{u}_\mathbf{w}^*$ denotes the optimal vector of tunable system parameters.

Hence, by Assumption 3.3, under steady-state conditions of the extended plant dynamics in (3.11), in the limit $\alpha_\mathbf{z} \to 0$, and for constant inputs $\mathbf{u}$, we have that the parameter-to-steady-state performance map of the system can be characterized as follows:

$$F_\mathbf{w}(\mathbf{u}) := k(\mathbf{q}_\mathbf{w}(\mathbf{u})), \quad \forall\, \mathbf{u} \in \mathbb{R}^{n_\mathbf{u}}. \tag{3.14}$$

The following assumption on $F_\mathbf{w}$ in (3.14) is adopted from Assumption 2.15 in Chapter 2.

Assumption 3.4. *Given a disturbance $\mathbf{w} \in \mathcal{W}$, the objective function $F_\mathbf{w} : \mathbb{R}^{n_\mathbf{u}} \to \mathbb{R}$ in (3.14) is twice continuously differentiable and exhibits a unique minimum in $\mathbb{R}^{n_\mathbf{u}}$. Let the corresponding optimal input $\mathbf{u}_\mathbf{w}^*$ be defined as*

$$\mathbf{u}_\mathbf{w}^* := \arg\min_{\mathbf{u} \in \mathbb{R}^{n_\mathbf{u}}} F_\mathbf{w}(\mathbf{u}). \tag{3.15}$$

There exist constants $L_{F1}, L_{F2} \in \mathbb{R}_{>0}$ *such that*

$$\frac{dF_{\mathbf{w}}}{d\mathbf{u}}(\mathbf{u} - \mathbf{u}^*_{\mathbf{w}}) \geq L_{F1}\|\mathbf{u} - \mathbf{u}^*_{\mathbf{w}}\|^2, \tag{3.16}$$

and

$$\left\| \frac{d^2 F_{\mathbf{w}}}{d\mathbf{u} d\mathbf{u}^\top} \right\| \leq L_{F2}, \tag{3.17}$$

for all $\mathbf{u} \in \mathbb{R}^{n_{\mathbf{u}}}$.

To optimize the time-varying system behavior $\bar{\mathbf{e}}_{\mathbf{w}}$, we aim to find the system parameter values $\mathbf{u}$ for which the objective function in (3.14) is minimal. Information of the objective function can only be obtained through measured outputs l of the extended plant in (3.11). On the basis of these measured outputs, we aim to steer the inputs $\mathbf{u}$ to their performance optimizing values $\mathbf{u}^*_{\mathbf{w}}$ by using the measured extended plant output $l(t)$ as feedback to an extremum-seeking controller that is introduced next.

3.2.2 Extremum-seeking controller design

The extremum-seeking controller employed in this chapter is based on the one in (Haring, 2016, Chapter 2). A novel ESC design extension will be presented in Section 3.2.3. We will briefly elaborate on 1) the dither signal design, 2) a model of the input-output behavior of the extended plant to be used as a basis for gradient estimation, 3) a least-squares observer to estimate the state of the model (and therewith the gradient of the objective function $F_{\mathbf{w}}$), and 4) a normalized optimizer to steer the system parameters $\mathbf{u}$ to the minimizer $\mathbf{u}^*_{\mathbf{w}}$.

Dither signal

In order to estimate the gradient of the objective function $F_{\mathbf{w}}$ and use this estimated gradient to drive $\mathbf{u}$ towards $\mathbf{u}^*_{\mathbf{w}}$ by an optimizer, we supply the following dither signal:

$$\mathbf{u}(t) = \hat{\mathbf{u}}(t) + \alpha_{\boldsymbol{\omega}}\boldsymbol{\omega}(t), \tag{3.18}$$

where $\alpha_{\boldsymbol{\omega}}\boldsymbol{\omega}$ is a vector of perturbation signals with amplitude $\alpha_{\boldsymbol{\omega}} \in \mathbb{R}_{>0}$, and $\hat{\mathbf{u}}$ is referred to as the nominal system parameter to be generated by the extremum-seeking controller. The vector $\boldsymbol{\omega}$ is defined by $\boldsymbol{\omega}(t) = [\omega_1(t), \omega_2(t), ..., \omega_{n_{\mathbf{u}}}(t)]^\top$, with

$$\omega_i(t) = \begin{cases} \sin\left(\dfrac{i+1}{2}\eta_{\boldsymbol{\omega}} t\right), & \text{if } i \text{ is odd,} \\ \cos\left(\dfrac{i}{2}\eta_{\boldsymbol{\omega}} t\right), & \text{if } i \text{ is even,} \end{cases} \tag{3.19}$$

for $i = \{1, 2, ..., n_{\mathbf{u}}\}$, where $\eta_{\boldsymbol{\omega}} \in \mathbb{R}_{>0}$ is a tuning parameter.

Model of input-output behavior of the extended plant

To obtain an estimate of the gradient of the objective function (3.14), the input-to-output behavior of the extended plant in (3.11), that is, from input $\hat{\mathbf{u}}$ to measured output l, is modelled in a general form. We define the state vector of the model as

$$\mathbf{m}(t) = \begin{bmatrix} F_{\mathbf{w}}(\hat{\mathbf{u}}(t)) \\ \alpha_{\boldsymbol{\omega}} \dfrac{dF_{\mathbf{w}}}{d\mathbf{u}^\top}(\hat{\mathbf{u}}(t)) \end{bmatrix}. \tag{3.20}$$

The measured output of the extended plant l in (3.11) can be written as

$$l(t) = r(t) + F_{\mathbf{w}}(\mathbf{u}(t)) + d(t), \tag{3.21}$$

with the signals $r(t)$ and $d(t)$ defined as

$$\begin{aligned} r(t) &:= k(\mathbf{z}(t)) - k(\bar{\mathbf{z}}_{\mathbf{w}}(t, \mathbf{u}(t), \alpha_{\mathbf{z}})), \\ d(t) &:= k(\bar{\mathbf{z}}_{\mathbf{w}}(t, \mathbf{u}(t), \alpha_{\mathbf{z}})) - k(\mathbf{q}_{\mathbf{w}}(\mathbf{u}(t))). \end{aligned} \tag{3.22}$$

Using Taylor's Theorem and (3.18), the objective function $F_{\mathbf{w}}$ can be written as

$$\begin{aligned} F_{\mathbf{w}}(\mathbf{u}(t)) &= F_{\mathbf{w}}(\hat{\mathbf{u}}(t) + \alpha_{\boldsymbol{\omega}}\boldsymbol{\omega}(t)), \\ &= F_{\mathbf{w}}(\hat{\mathbf{u}}(t)) + \alpha_{\boldsymbol{\omega}} \frac{dF_{\mathbf{w}}}{d\mathbf{u}}(\hat{\mathbf{u}}(t))\boldsymbol{\omega}(t) + \frac{1}{2}\alpha_{\boldsymbol{\omega}}^2 \boldsymbol{\omega}^\top(t)\mathbf{H}(t, \hat{\mathbf{u}}(t))\boldsymbol{\omega}(t), \end{aligned} \tag{3.23}$$

where $\mathbf{H}(t, \hat{\mathbf{u}}(t))$ reads

$$\mathbf{H}(t, \hat{\mathbf{u}}(t)) = 2 \int_0^1 (1-\sigma) \frac{d^2 F_{\mathbf{w}}}{d\mathbf{u} d\mathbf{u}^\top}(\hat{\mathbf{u}}(t) + \sigma\alpha_{\boldsymbol{\omega}}\boldsymbol{\omega}(t)) d\sigma. \tag{3.24}$$

The dynamics of the state vector in (3.20) is governed by

$$\begin{aligned} \dot{\mathbf{m}}(t) &= \mathbf{A}(t)\mathbf{m}(t) + \alpha_{\boldsymbol{\omega}}^2 \mathbf{B}\mathbf{s}(t) \\ l(t) &= \mathbf{C}(t)\mathbf{m}(t) + \alpha_{\boldsymbol{\omega}}^2 v(t) + r(t) + d(t), \end{aligned} \tag{3.25}$$

with the matrices $\mathbf{A}$, $\mathbf{B}$ and $\mathbf{C}$ defined as

$$\begin{aligned} \mathbf{A}(t) &= \frac{1}{\alpha_{\boldsymbol{\omega}}} \begin{bmatrix} 0 & \dot{\hat{\mathbf{u}}}^\top(t) \\ \mathbf{0}^{n_{\mathrm{u}} \times 1} & \mathbf{0}^{n_{\mathrm{u}} \times n_{\mathrm{u}}} \end{bmatrix}, \ \mathbf{B} = \begin{bmatrix} \mathbf{0}^{1 \times n_{\mathrm{u}}} \\ \mathbf{I}^{n_{\mathrm{u}} \times n_{\mathrm{u}}} \end{bmatrix}, \\ \mathbf{C}(t) &= \begin{bmatrix} 1 & \boldsymbol{\omega}^\top(t) \end{bmatrix}, \end{aligned} \tag{3.26}$$

and the signals $\mathbf{s}(t)$ and $v(t)$ defined as follows:

$$\begin{aligned} \mathbf{s}(t) &:= \frac{d^2 F_{\mathbf{w}}}{d\mathbf{u} d\mathbf{u}^\top}(\hat{\mathbf{u}}(t)) \frac{\dot{\hat{\mathbf{u}}}(t)}{\alpha_{\boldsymbol{\omega}}}, \\ v(t) &:= \frac{1}{2}\boldsymbol{\omega}^\top(t)\mathbf{H}(t, \hat{\mathbf{u}}(t))\boldsymbol{\omega}(t). \end{aligned} \tag{3.27}$$

The signals $\mathbf{s}$, v, r, and d can be interpreted as unknown disturbances to the model in (3.25). The influences of $\mathbf{s}$, v, r, and d on the state and output of the model in (3.25) are small if i) $\hat{\mathbf{u}}$ is slowly time varying, if ii) $\alpha_{\boldsymbol{\omega}}$ is small, if iii) the states $\mathbf{x}$ of the system in (3.1) and the states $\mathbf{z}$ of the filter in (3.7) are close to their steady-state values, respectively $\bar{\mathbf{x}}_{\mathbf{w}}$ and $\bar{\mathbf{z}}_{\mathbf{w}}$, and if iv) $\alpha_{\mathbf{z}}$ is sufficiently small.

Extremum-seeking controller design

The state $\mathbf{m}$ in (3.20) contains the gradient of the objective function, scaled by the perturbation amplitude $\alpha_{\boldsymbol{\omega}}$. Hence, an estimate of the gradient of the objective function $F_{\mathbf{w}}$ can be obtained from an estimate of the state $\mathbf{m}$. Here we present a least-squares observer to estimate the state $\mathbf{m}$ of the model in (3.25) based on measured outputs of the extended plant $l(t)$. The least-squares observer, denoted by Σ_o, is given by

$$\Sigma_o : \begin{cases} \dot{\hat{\mathbf{m}}} = \left(\mathbf{A} - \eta_{\mathbf{m}}\sigma_r \mathbf{Q}\mathbf{D}^\top\mathbf{D}\right)\hat{\mathbf{m}} + \alpha_{\boldsymbol{\omega}}^2 \mathbf{B}\hat{\mathbf{s}} \\ \qquad\quad + \eta_{\mathbf{m}}\mathbf{Q}\mathbf{C}^\top(l - \mathbf{C}\hat{\mathbf{m}} - \alpha_{\boldsymbol{\omega}}^2\hat{v}) \\ \dot{\mathbf{Q}} = \eta_{\mathbf{m}}\mathbf{Q} + \mathbf{A}\mathbf{Q} + \mathbf{Q}\mathbf{A}^\top \\ \qquad\quad - \eta_{\mathbf{m}}\mathbf{Q}(\mathbf{C}^\top\mathbf{C} + \sigma_r\mathbf{D}^\top\mathbf{D})\mathbf{Q}, \end{cases} \tag{3.28}$$

with initial conditions $\hat{\mathbf{m}}(0) = \hat{\mathbf{m}}_0 \in \mathbb{R}^{n_{\mathbf{u}}+1}$ and $\mathbf{Q}(0) = \mathbf{Q}_0 \in \mathbb{R}^{n_{\mathbf{u}}+1\times n_{\mathbf{u}}+1}$, where $\mathbf{Q}_0$ is a symmetric and positive definite matrix, $\mathbf{D} = [\mathbf{0}^{n_{\mathbf{u}}\times 1} \quad \mathbf{I}^{n_{\mathbf{u}}\times n_{\mathbf{u}}}]$, $\eta_{\mathbf{m}} \in \mathbb{R}_{>0}$ and $\sigma_r \in \mathbb{R}_{\geq 0}$ are tuning parameters related to the observer, referred to as a forgetting factor and a regularization constant, respectively, and signals $\hat{\mathbf{s}}$ and $\hat{v}$ are defined as

$$\begin{aligned} \hat{\mathbf{s}}(t) &:= \hat{\mathbf{H}}(t, \hat{\mathbf{u}}(t))\frac{\dot{\hat{\mathbf{u}}}(t)}{\alpha_{\boldsymbol{\omega}}}, \\ \hat{v}(t) &:= \frac{1}{2}\boldsymbol{\omega}^\top(t)\hat{\mathbf{H}}(t, \hat{\mathbf{u}}(t))\boldsymbol{\omega}(t), \end{aligned} \tag{3.29}$$

with a user-defined function $\hat{\mathbf{H}} : \mathbb{R} \times \mathbb{R}^{n_{\mathbf{u}}} \to \mathbb{R}^{n_{\mathbf{u}}\times n_{\mathbf{u}}}$ satisfying $\|\hat{\mathbf{H}}(t, \hat{\mathbf{u}})\| \leq L_{\mathbf{H}}$, for all $t \in \mathbb{R}$, all $\hat{\mathbf{u}} \in \mathbb{R}^{n_{\mathbf{u}}}$, and with $L_{\mathbf{H}} \in \mathbb{R}_{>0}$. Note that in order to arrive at the observer design in (3.28), we have considered the signals r and d in (3.25) to be zero. This is justified for steady-state conditions of the extended plant Σ, and sufficiently small $\alpha_{\mathbf{z}}$. The optimizer, denoted by Σ_r, uses the estimated gradient to steer the nominal system inputs $\hat{\mathbf{u}}$ to their performance-optimal values $\mathbf{u}_{\mathbf{w}}^*$. The optimizer Σ_r is given by

$$\Sigma_r : \quad \dot{\hat{\mathbf{u}}}(t) = -\lambda_{\mathbf{u}}\frac{\eta_{\mathbf{u}}\mathbf{D}\hat{\mathbf{m}}(t)}{\eta_{\mathbf{u}} + \lambda_{\mathbf{u}}\|\mathbf{D}\hat{\mathbf{m}}(t)\|}, \tag{3.30}$$

with $\lambda_{\mathbf{u}}$, $\eta_{\mathbf{u}} \in \mathbb{R}_{>0}$ being tuning parameters related to the optimizer. The closed-loop ESC scheme, composed of the extended plant Σ in (3.11), the observer Σ_o in (3.28), and the optimizer Σ_r in (3.30), is depicted in Fig. 2.3.

3.2.3 Extremum-seeking controller design for enhanced convergence speed

The least-squares observer presented in Section 3.2.2, used to obtain a local estimate of the gradient of the objective function $F_{\mathbf{w}}$, is constructed based on a general model of the input-output behavior of the extended plant in (3.11), that is, from input $\hat{\mathbf{u}}$ to measured output l. To be able to obtain an accurate gradient estimate of $F_{\mathbf{w}}(\hat{\mathbf{u}})$, on the one hand, the user-defined filter Σ_f must act on a slow enough time scale to reduce the effect of time-varying behavior in the steady-state output of the filter l, leading to a quasi-static approximation of the objective function $F_{\mathbf{w}}(\hat{\mathbf{u}})$. On the other hand, for this quasi-static approximation of $F_{\mathbf{w}}(\hat{\mathbf{u}})$ to hold in case of dithering, the perturbation of the input $\hat{\mathbf{u}}$ must be even slower. As a result, convergence of the ESC scheme is generally slow.

Convergence speed of the ESC scheme can be improved by increasing the frequency of the perturbation. However, this can lead to a deterioration of the gradient estimation because the quasi-static approximation of $F_{\mathbf{w}}(\hat{\mathbf{u}}(t))$, in the case of high-frequency perturbations, is distorted by the (transient) dynamics of the filter Σ_f. Instead, by taking into account the dynamics of the user-defined filter Σ_f in the observer design, this distortion of quasi-static approximation can be taken into account, improving the convergence speed in cases where the time-scales of the perturbation and filter are similar. We propose an alternative least-squares observer design that incorporates user-defined filters Σ_f of the linear time-invariant (LTI) type, which enables enhanced convergence speed of the resulting ESC scheme. We 1) revisit the model of the input-output behavior with knowledge on Σ_f, and 2) provide the modified ESC design. In Section 3.2.5, the effectiveness of the modified extremum-seeking controller design is shown by means of a simulation example.

Model of input-output behavior and knowledge on the dynamic cost function

The model presented here extends the model in Section 3.2.2. Let us focus on LTI designs of the filter Σ_f in (3.7), given by the following form:

$$\Sigma_f : \begin{cases} \dot{\mathbf{z}}(t) = \alpha_{\mathbf{z}} \left(\mathbf{A}_{\Sigma_f} \mathbf{z}(t) + \mathbf{B}_{\Sigma_f} y(t) \right) \\ l(t) = \mathbf{C}_{\Sigma_f} \mathbf{z}(t), \end{cases} \tag{3.31}$$

with the matrices $\mathbf{A}_{\Sigma_f} \in \mathbb{R}^{n_{\mathbf{z}} \times n_{\mathbf{z}}}$, $\mathbf{B}_{\Sigma_f} \in \mathbb{R}^{n_{\mathbf{z}} \times 1}$, $\mathbf{C}_{\Sigma_f} \in \mathbb{R}^{1 \times n_{\mathbf{z}}}$. Note that if $\mathbf{A}_{\Sigma_f}$ is Hurwitz, then Σ_f is exponentially stable, and Property 3.2 is guaranteed. Define a state $\mathbf{m}_{\mathbf{z}}$ governed by the following dynamics:

$$\dot{\mathbf{m}}_{\mathbf{z}} = \alpha_{\mathbf{z}} \left(\mathbf{A}_{\Sigma_f} \mathbf{m}_{\mathbf{z}}(t) + \mathbf{B}_{\Sigma_f} F_{\mathbf{w}}(\mathbf{u}(t)) \right), \tag{3.32}$$

where $\mathbf{m}_{\mathbf{z}} \in \mathbb{R}^{n_{\mathbf{z}}}$. We can reformulate the output l in (3.31) as follows:

$$l(t) = \mathbf{C}_{\Sigma_f} \mathbf{m}_{\mathbf{z}}(t) + \mathbf{C}_{\Sigma_f} \tilde{\mathbf{m}}_{\mathbf{z}}(t), \tag{3.33}$$

where $\tilde{\mathbf{m}}_\mathbf{z} := \mathbf{z} - \mathbf{m}_\mathbf{z}$, and generated by the following dynamics:

$$\dot{\tilde{\mathbf{m}}}_\mathbf{z} = \alpha_\mathbf{z} \left(\mathbf{A}_{\Sigma_f} \tilde{\mathbf{m}}_\mathbf{z}(t) + \mathbf{B}_{\Sigma_f} (y(t) - F_\mathbf{w}(\mathbf{u}(t))) \right). \tag{3.34}$$

We can define a new state vector which reads

$$\mathbf{m}_f(t) = \begin{bmatrix} \mathbf{m}_\mathbf{z}(t) \\ \mathbf{m}(t) \end{bmatrix} \in \mathbb{R}^{n_{\mathbf{m}_f}}, \tag{3.35}$$

where $n_{\mathbf{m}_f} = n_\mathbf{z} + n_\mathbf{u} + 1$ denotes the dimension of the state vector $\mathbf{m}_f$. By using (3.32), (3.23), and the dynamics of the state vector $\mathbf{m}$ in (3.25), the dynamics governing the state vector in (3.35) is given as follows:

$$\begin{aligned} \dot{\mathbf{m}}_f(t) &= \mathbf{A}_f(t)\mathbf{m}_f(t) + \alpha_{\boldsymbol{\omega}}^2 \mathbf{B}_f \mathbf{s}(t) + \alpha_\mathbf{z} \alpha_{\boldsymbol{\omega}}^2 \mathbf{E}_f v(t) \\ l(t) &= \mathbf{C}_f \mathbf{m}_f(t) + \mathbf{C}_{\Sigma_f} \tilde{\mathbf{m}}_\mathbf{z}(t), \end{aligned} \tag{3.36}$$

with the matrices $\mathbf{A}_f \in \mathbb{R}^{n_{\mathbf{m}_f} \times n_{\mathbf{m}_f}}$, $\mathbf{B}_f \in \mathbb{R}^{n_{\mathbf{m}_f} \times n_\mathbf{u}}$, $\mathbf{C}_f \in \mathbb{R}^{1 \times n_{\mathbf{m}_f}}$, and $\mathbf{E}_f \in \mathbb{R}^{n_{\mathbf{m}_f} \times 1}$, defined as follows:

$$\begin{aligned} \mathbf{A}_f(t) &= \begin{bmatrix} \alpha_\mathbf{z} \mathbf{A}_{\Sigma_f} & \alpha_\mathbf{z} \mathbf{B}_{\Sigma_f} & \alpha_\mathbf{z} \mathbf{B}_{\Sigma_f} \boldsymbol{\omega}^\top(t) \\ \mathbf{0}^{1 \times n_\mathbf{z}} & 0 & \dfrac{\hat{\mathbf{u}}^\top}{\alpha_{\boldsymbol{\omega}}} \\ \mathbf{0}^{n_\mathbf{u} \times n_\mathbf{z}} & 0^{n_\mathbf{u} \times 1} & \mathbf{0}^{n_\mathbf{u} \times n_\mathbf{u}} \end{bmatrix}, \\ \mathbf{B}_f^\top &= \begin{bmatrix} \mathbf{0}^{n_\mathbf{u} \times n_\mathbf{z}} & \mathbf{0}^{n_\mathbf{u} \times 1} & \mathbf{I}^{n_\mathbf{u} \times n_\mathbf{u}} \end{bmatrix}, \\ \mathbf{C}_f &= \begin{bmatrix} \mathbf{C}_{\Sigma_f} & 0 & \mathbf{0}^{1 \times n_\mathbf{u}} \end{bmatrix}, \\ \mathbf{E}_f^\top &= \begin{bmatrix} \mathbf{B}_{\Sigma_f}^\top & 0 & \mathbf{0}^{1 \times n_\mathbf{u}} \end{bmatrix}. \end{aligned} \tag{3.37}$$

Modified extremum-seeking controller design

Inspired by the observer in (3.28), the least-squares observer to estimate $\mathbf{m}_f$ of the model in (3.36), denoted by Σ_{fo}, is given by

$$\Sigma_{fo} : \begin{cases} \dot{\hat{\mathbf{m}}}_f = \left(\mathbf{A}_f - \eta_\mathbf{m} \sigma_r \mathbf{Q}_f \mathbf{D}_f^\top \mathbf{D}_f \right) \hat{\mathbf{m}}_f + \alpha_{\boldsymbol{\omega}}^2 \mathbf{B}_f \hat{\mathbf{s}} \\ \qquad\quad + \alpha_\mathbf{z} \alpha_{\boldsymbol{\omega}}^2 \mathbf{E}_f \hat{v} + \eta_\mathbf{m} \mathbf{Q}_f \mathbf{C}_f^\top (l - \mathbf{C}_f \hat{\mathbf{m}}_f) \\ \dot{\mathbf{Q}}_f = \eta_\mathbf{m} \mathbf{Q}_f + \mathbf{A}_f \mathbf{Q}_f + \mathbf{Q}_f \mathbf{A}_f^\top \\ \qquad\quad - \eta_\mathbf{m} \mathbf{Q}_f (\mathbf{C}_f^\top \mathbf{C}_f + \sigma_r \mathbf{D}_f^\top \mathbf{D}_f) \mathbf{Q}_f, \end{cases} \tag{3.38}$$

with initial conditions $\hat{\mathbf{m}}_f(0) = \hat{\mathbf{m}}_{f0} \in \mathbb{R}^{n_{\mathbf{m}_f}}$ and $\mathbf{Q}_f(0) = \mathbf{Q}_{f0} \in \mathbb{R}^{n_{\mathbf{m}_f} \times n_{\mathbf{m}_f}}$, where $\mathbf{Q}_{f0}$ is a symmetric and positive definite matrix, and the matrix $\mathbf{D}_f$ defined as

$$\mathbf{D}_f = [\mathbf{0}^{n_\mathbf{u} \times n_\mathbf{z}} \quad \mathbf{0}^{n_\mathbf{u} \times 1} \quad \mathbf{I}^{n_\mathbf{u} \times n_\mathbf{u}}]. \tag{3.39}$$

The signals $\hat{\mathbf{s}}$ and $\hat{v}$ are defined in (3.29). To arrive at the observer design in (3.38) we have assumed $\tilde{\mathbf{m}}_\mathbf{z}$ to be zero, similar as for the signals r and d in the

observer design in (3.28). Again, this is justified for steady-state conditions of the extended plant Σ, and sufficiently small $\alpha_{\mathbf{z}}$. The optimizer, denoted by Σ_{fr}, reads as follows:

$$\Sigma_{fr}: \quad \dot{\hat{\mathbf{u}}}(t) = -\lambda_{\mathbf{u}} \frac{\eta_{\mathbf{u}} \mathbf{D}_f \hat{\mathbf{m}}_f(t)}{\eta_{\mathbf{u}} + \lambda_{\mathbf{u}} \|\mathbf{D}_f \hat{\mathbf{m}}_f(t)\|}. \tag{3.40}$$

3.2.4 Closed-loop stability analysis

Next we provide a stability result and supporting stability proof for the closed-loop ESC scheme with the modified extremum-seeking controller proposed in Section 3.2.3. The next result states conditions on tuning parameters under which the ESC scheme with the modified extremum-seeking controller guarantees that $\hat{\mathbf{u}}$ converges to an arbitrarily small set around the optimum $\mathbf{u}^*_{\mathbf{w}}$.

Theorem 3.5. *Consider a (time-varying) disturbance $\mathbf{w} \in \mathcal{W}$ and Assumptions 2.2, 3.1, 3.3, 3.4. Moreover, consider arbitrary initial conditions $\mathbf{x}(0) \in \mathbb{R}^{n_{\mathbf{x}}}$, $\mathbf{Q}_f(0) \in \mathbb{R}^{n_{\mathbf{m}_f} \times n_{\mathbf{m}_f}}$ symmetric and positive-definite, $\mathbf{z}(0) \in \mathbb{R}^{n_{\mathbf{z}}}$, $\hat{\mathbf{m}}_f(0) \in \mathbb{R}^{n_{\mathbf{m}_f}}$, and an arbitrary compact set $\mathcal{U}_0 \subset \mathbb{R}^{n_{\mathbf{u}}}$ of initial conditions for $\hat{\mathbf{u}}(t)$. Then, there exist (sufficiently small) constants $\epsilon_0, ..., \epsilon_5 \in \mathbb{R}_{>0}$, such that, for all tunable parameters $\alpha_{\mathbf{z}}, \alpha_{\boldsymbol{\omega}}, \eta_{\mathbf{u}}, \lambda_{\mathbf{u}}, \eta_{\mathbf{m}}, \eta_{\boldsymbol{\omega}} \in \mathbb{R}_{>0}$ and $\sigma_r \in \mathbb{R}_{\geq 0}$ with $\alpha_{\boldsymbol{\omega}} \leq \epsilon_0$, $\eta_{\boldsymbol{\omega}} \leq \alpha_{\mathbf{z}} \epsilon_1$, $\alpha_{\mathbf{z}} \leq \eta_{\mathbf{m}} \epsilon_2$, $\alpha_{\boldsymbol{\omega}} \lambda_{\mathbf{u}} \leq \eta_{\mathbf{m}} \epsilon_3$, $\eta_{\mathbf{u}} \leq \alpha_{\boldsymbol{\omega}} \eta_{\boldsymbol{\omega}} \epsilon_4$, and $\sigma_r \leq \epsilon_5$, the solutions of the closed-loop system consisting of the extended plant in (3.11) and the modified extremum-seeking controller (consisting of the dither signal in (3.18), the observer Σ_{fo} in (3.38), and the optimizer Σ_{fr} in (3.40)) are bounded for all $t \geq 0$. In addition, there exist constants $c_1, \ldots, c_5 \in \mathbb{R}_{>0}$ such that the solutions $\hat{\mathbf{u}}(t)$ with $\hat{\mathbf{u}}(0) \in \mathcal{U}_0$ satisfy*

$$\limsup_{t \to \infty} \|\hat{\mathbf{u}}(t) - \mathbf{u}^*_{\mathbf{w}}\| \leq \max \left\{ \alpha_{\boldsymbol{\omega}} \eta^2_{\boldsymbol{\omega}} c_1, \alpha_{\mathbf{z}} \alpha_{\boldsymbol{\omega}} \delta_{\mathbf{z}2} c_2, \eta_{\boldsymbol{\omega}} c_3, \frac{\alpha_{\mathbf{z}}}{\alpha_{\boldsymbol{\omega}}} c_4 \delta_{\mathbf{z}1}, \alpha_{\boldsymbol{\omega}} c_5 \right\} \tag{3.41}$$

Proof. The proof of Theorem 3.5 follows similar arguments as the proof of Theorem 14 in Hazeleger et al. (2018) and the proof of Theorem 2.16 in Chapter 2. Different from Theorem 2.16 in Chapter 2 and its proof are the bounds on the solutions of the error dynamics of the novel least-squares observer in (3.38). Here we will present these bounds. Introduce the following coordinate transformation:

$$\begin{aligned} \tilde{\mathbf{m}}_f(t) &= \hat{\mathbf{m}}_f(t) - \mathbf{m}_f(t), \\ \tilde{\mathbf{Q}}_f(t) &= \mathbf{Q}_f^{-1}(t) - \Xi_f^{-1}, \end{aligned} \tag{3.42}$$

with

$$\Xi_f^{-1} = \mathbf{C}_f^\top \mathbf{C}_f + \sigma_r \mathbf{D}_f^\top \mathbf{D}_f. \tag{3.43}$$

From the observer in (3.38), the coordinate transformation in (3.42), and the model of the input-output behavior in (3.36), we have the following state equations for $\tilde{\mathbf{Q}}_f$ and $\tilde{\mathbf{m}}_f$:

$$\dot{\tilde{\mathbf{Q}}}_f = -\eta_{\mathbf{m}} \tilde{\mathbf{Q}}_f - \Xi_f^{-1} \mathbf{A}_f - \mathbf{A}_f^\top \Xi_f^{-1} - \tilde{\mathbf{Q}}_f \mathbf{A}_f - \mathbf{A}_f^\top \tilde{\mathbf{Q}}_f \tag{3.44}$$

and

$$\begin{aligned}\dot{\tilde{\mathbf{m}}}_f = &\left(\mathbf{A}_f - \eta_{\mathbf{m}}\mathbf{Q}_f(\mathbf{C}_f^\top\mathbf{C}_f + \sigma_r\mathbf{D}_f^\top\mathbf{D}_f)\right)\tilde{\mathbf{m}}_f \\ &+ \alpha_{\boldsymbol{\omega}}^2\mathbf{B}_f(\hat{\mathbf{s}} - \mathbf{s}) - \eta_{\mathbf{m}}\sigma_r\alpha_{\boldsymbol{\omega}}\mathbf{Q}_f\mathbf{D}_f^\top\frac{dF_{\mathbf{w}}}{d\mathbf{u}^\top}(\hat{\mathbf{u}}) \\ &+ \alpha_{\mathbf{z}}\alpha_{\boldsymbol{\omega}}^2\mathbf{E}_f(\hat{v} - v) + \eta_{\mathbf{m}}\mathbf{Q}_f\mathbf{C}_f^\top\mathbf{C}_{\Sigma_f}\tilde{\mathbf{m}}_{\mathbf{z}}.\end{aligned} \tag{3.45}$$

Note that we have omitted most arguments of the variables in (3.44) and (3.45) for notational clarity. Firstly, a bound on the solutions $\tilde{\mathbf{Q}}_f(t)$ is presented in Lemma 3.6.

Lemma 3.6. *For any $\epsilon_1, \epsilon_4 \in \mathbb{R}_{>0}$, sufficiently small $\epsilon_2, \epsilon_5 \in \mathbb{R}_{>0}$, and all tunable parameters $\alpha_{\boldsymbol{\omega}}, \eta_{\mathbf{m}} \in \mathbb{R}_{>0}$, there exist constants $c_{\mathbf{Q}}$, $\beta_{\mathbf{Q}} \in \mathbb{R}_{>0}$ such that, for all $\eta_{\boldsymbol{\omega}} \leq \alpha_{\mathbf{z}}\epsilon_1$, $\alpha_{\mathbf{z}} \leq \eta_{\mathbf{m}}\epsilon_2$, all $\eta_{\mathbf{u}} \leq \alpha_{\boldsymbol{\omega}}\eta_{\boldsymbol{\omega}}\epsilon_4$, and all $\sigma_r \leq \epsilon_5$, the solutions $\tilde{\mathbf{Q}}_f$ satisfy*

$$\|\tilde{\mathbf{Q}}_f(t)\| \leq \max\left\{c_{\mathbf{Q}}\|\tilde{\mathbf{Q}}_f(0)\|e^{-\eta_{\mathbf{m}}\beta_{\mathbf{Q}}t}, \frac{1}{8}\right\}, \tag{3.46}$$

for all $t \geq 0$, all $\tilde{\mathbf{Q}}_f(0) \in \mathbb{R}^{n_{\mathbf{m}_f} \times n_{\mathbf{m}_f}}$ for which $\mathbf{Q}_f(0)$ is symmetric and positive definite, and all time-varying $\mathbf{u}(t) \in \mathbb{R}^{n_{\mathbf{u}}}$.

Proof. *See Appendix 3.A.* □

Secondly, a bound on the solutions $\tilde{\mathbf{m}}_f(t)$ for time-varying inputs $\mathbf{u}(t)$ is presented in Lemma 3.7.

Lemma 3.7. *For any $\epsilon_0, \epsilon_1, \epsilon_2, \epsilon_4 \in \mathbb{R}_{>0}$, sufficiently small $\epsilon_5 \in \mathbb{R}_{>0}$, any finite time $t_1 \geq 0$, and any $\delta_{\mathbf{z}1}, \delta_{\mathbf{z}2} \in \mathbb{R}_{\geq 0}$, the solutions $\tilde{\mathbf{m}}_f$ are bounded for all $0 \leq t \leq t_1$, all $\tilde{\mathbf{u}}(0) \in \mathbb{R}^{n_{\mathbf{u}}}$, all $\tilde{\mathbf{m}}_f(0) \in \mathbb{R}^{n_{\mathbf{m}_f}}$, and all $\alpha_{\boldsymbol{\omega}} \leq \epsilon_0, \eta_{\boldsymbol{\omega}} \leq \alpha_{\mathbf{z}}\epsilon_1, \alpha_{\mathbf{z}} \leq \eta_{\mathbf{m}}\epsilon_2, \eta_{\mathbf{u}} \leq \alpha_{\boldsymbol{\omega}}\eta_{\boldsymbol{\omega}}\epsilon_4$, and all $\sigma_r \leq \epsilon_5$. In addition, for sufficiently small $\epsilon_3, \epsilon_5 \in \mathbb{R}_{>0}$ and all $\alpha_{\boldsymbol{\omega}}\lambda_{\mathbf{u}} \leq \eta_{\mathbf{m}}\epsilon_3$, there exist constants $c_{\mathbf{m}1}, ..., c_{\mathbf{m}8}(\epsilon_0), ..., c_{\mathbf{m}10}(\epsilon_2) \in \mathbb{R}_{>0}$ such that the solutions $\tilde{\mathbf{m}}_f$ satisfy*

$$\begin{aligned}\sup_{t\geq t_1}\|\tilde{\mathbf{m}}_f(t)\| \leq \sup_{t\geq t_1}\max\{&c_{\mathbf{m}1}\|\tilde{\mathbf{m}}_f(t_1)\|, \sqrt{\sigma_r}\alpha_{\boldsymbol{\omega}}c_{\mathbf{m}2}\left\|\tilde{\mathbf{u}}(t)\right\|, \\ &\alpha_{\boldsymbol{\omega}}\frac{\alpha_{\boldsymbol{\omega}}\lambda_{\mathbf{u}}}{\eta_{\mathbf{m}}}c_{\mathbf{m}3}\|\tilde{\mathbf{u}}(t)\|, \alpha_{\mathbf{z}}c_{\mathbf{m}4}\delta_{\mathbf{z}2}\|\tilde{\mathbf{u}}(t)\|^2, \alpha_{\boldsymbol{\omega}}\eta_{\boldsymbol{\omega}}c_{\mathbf{m}5}\|\tilde{\mathbf{u}}(t)\|, \\ &\alpha_{\boldsymbol{\omega}}^2\eta_{\boldsymbol{\omega}}^2c_{\mathbf{m}6}, \alpha_{\mathbf{z}}\alpha_{\boldsymbol{\omega}}^2c_{\mathbf{m}7}\delta_{\mathbf{z}2}, \alpha_{\boldsymbol{\omega}}\eta_{\boldsymbol{\omega}}c_{\mathbf{m}8}, \alpha_{\mathbf{z}}c_{\mathbf{m}9}\delta_{\mathbf{z}1}, \alpha_{\boldsymbol{\omega}}^2c_{\mathbf{m}10}\}.\end{aligned} \tag{3.47}$$

and

$$\begin{aligned}\limsup_{t\to\infty}\|\tilde{\mathbf{m}}_f(t)\| \leq \limsup_{t\to\infty}\max\{&\sqrt{\sigma_r}\alpha_{\boldsymbol{\omega}}c_{\mathbf{m}2}\left\|\tilde{\mathbf{u}}(t)\right\|, \\ &\alpha_{\boldsymbol{\omega}}\frac{\alpha_{\boldsymbol{\omega}}\lambda_{\mathbf{u}}}{\eta_{\mathbf{m}}}c_{\mathbf{m}3}\|\tilde{\mathbf{u}}(t)\|, \alpha_{\mathbf{z}}c_{\mathbf{m}4}\delta_{\mathbf{z}2}\|\tilde{\mathbf{u}}(t)\|^2, \alpha_{\boldsymbol{\omega}}\eta_{\boldsymbol{\omega}}c_{\mathbf{m}5}\|\tilde{\mathbf{u}}(t)\|, \\ &\alpha_{\boldsymbol{\omega}}^2\eta_{\boldsymbol{\omega}}^2c_{\mathbf{m}6}, \alpha_{\mathbf{z}}\alpha_{\boldsymbol{\omega}}^2c_{\mathbf{m}7}\delta_{\mathbf{z}2}, \alpha_{\boldsymbol{\omega}}\eta_{\boldsymbol{\omega}}c_{\mathbf{m}8}, \alpha_{\mathbf{z}}c_{\mathbf{m}9}\delta_{\mathbf{z}1}, \alpha_{\boldsymbol{\omega}}^2c_{\mathbf{m}10}\}.\end{aligned} \tag{3.48}$$

Proof. *See Appendix 3.B.* □

On the basis of the proofs of Theorem 2.16 in Chapter 2 and the bounds on the solutions $\tilde{\mathbf{Q}}_f(t)$ and $\tilde{\mathbf{m}}_f(t)$ in Lemmas 3.6 and 3.7, respectively, we obtain the bounds on the solutions $\hat{\mathbf{u}}(t) - \mathbf{u}_{\mathbf{w}}^*$ in (3.41), which completes the proof of Theorem 3.5. □

Remark 3.8. *Tuning guidelines. Under the conditions of Theorem 3.5 it follows that, if we are dealing with constant (or no) disturbances* $\mathbf{w}$*, i.e.,* $\delta_{\mathbf{z}1}, \delta_{\mathbf{z}2} = 0$ *(see Assumption 3.3), the optimizer state* $\hat{\mathbf{u}}$ *converges to an arbitrarily small region of the performance-optimal value* $\mathbf{u}_{\mathbf{w}}^*$ *if the dither parameters* $\alpha_{\boldsymbol{\omega}}$ *and* $\eta_{\boldsymbol{\omega}}$ *are chosen sufficiently small for an arbitrary bounded* $\alpha_{\mathbf{z}}$*. Choosing* $\alpha_{\mathbf{z}}$ *large in general allows faster convergence towards the performance-optimal value* $\mathbf{u}_{\mathbf{w}}^*$*. In the case of time-varying disturbances* $\mathbf{w}(t)$*, i.e.,* $\delta_{\mathbf{z}1}, \delta_{\mathbf{z}2} > 0$*, we subsequently tune* $\alpha_{\boldsymbol{\omega}}$ *small to make the fifth term in the right-hand side of* (3.41) *arbitrarily small, tune* $\alpha_{\mathbf{z}}$ *small to make the second and fourth term arbitrarily small, and finally tune* $\eta_{\boldsymbol{\omega}}$ *small to make the first and third term arbitrarily small.*

Remark 3.9. *Compared to Theorem 2.16 in Chapter 2, Theorem 3.5 and the associated conditions on the tunable parameters under which the ESC schemes converges to a neighborhood of the extremum are different. Namely, the conditions* $\alpha_{\mathbf{z}} \leq \alpha_{\boldsymbol{\omega}}\epsilon_1$ *and* $\eta_{\mathbf{m}} \leq \eta_{\boldsymbol{\omega}}\epsilon_3 \leq \alpha_{\mathbf{z}}\epsilon_2\epsilon_3$ *in Theorem 2.16 are changed to* $\alpha_{\mathbf{z}} \leq \eta_{\mathbf{m}}\epsilon_2$ *in Theorem 3.5. In the first place, the condition* $\alpha_{\mathbf{z}} \leq \alpha_{\boldsymbol{\omega}}\epsilon_1$*, which introduces an upperbound on the tuning of* $\alpha_{\mathbf{z}}$*, is taken care of by the condition* $\alpha_{\mathbf{z}} \leq \eta_{\mathbf{m}}\epsilon_2$*. In the second place,* $\eta_{\mathbf{m}} \leq \eta_{\boldsymbol{\omega}}\epsilon_3 \leq \alpha_{\mathbf{z}}\epsilon_2\epsilon_3$ *is 'the opposite' of the condition* $\alpha_{\mathbf{z}} \leq \eta_{\mathbf{m}}\epsilon_2$*. This can attributed to the fact that in Chapter 2 we require the time-scale of the dynamic cost function, which can be influenced by* $\alpha_{\mathbf{z}}$*, to operate faster than the time-scale of the observer, which can be influenced by* $\eta_{\mathbf{m}}$*. In Chapter 3, this restriction is not needed due to the explicit knowledge about the dynamic cost function embedded in the observer design.*

3.2.5 Illustrative example: Enhanced convergence speed

To illustrate the enhanced convergence speed of the modified extremum-seeking controller, we have adopted the following exemplary dynamical system from Haring et al. (2013):

$$\Sigma_p : \begin{cases} \dot{x}_1(t) = x_2(t) \\ \dot{x}_2(t) = -25x_1(t) - b(u(t))x_2(t) + w(t) \\ e(t) = x_1(t), \end{cases} \tag{3.49}$$

where $b(u) = 10 + 5(u - 10)^2$ is a nonlinear characteristic that depends on the system input $u \in \mathbb{R}$, and $w(t) = 20\sin(2\pi 10t)$ is an input disturbance. In

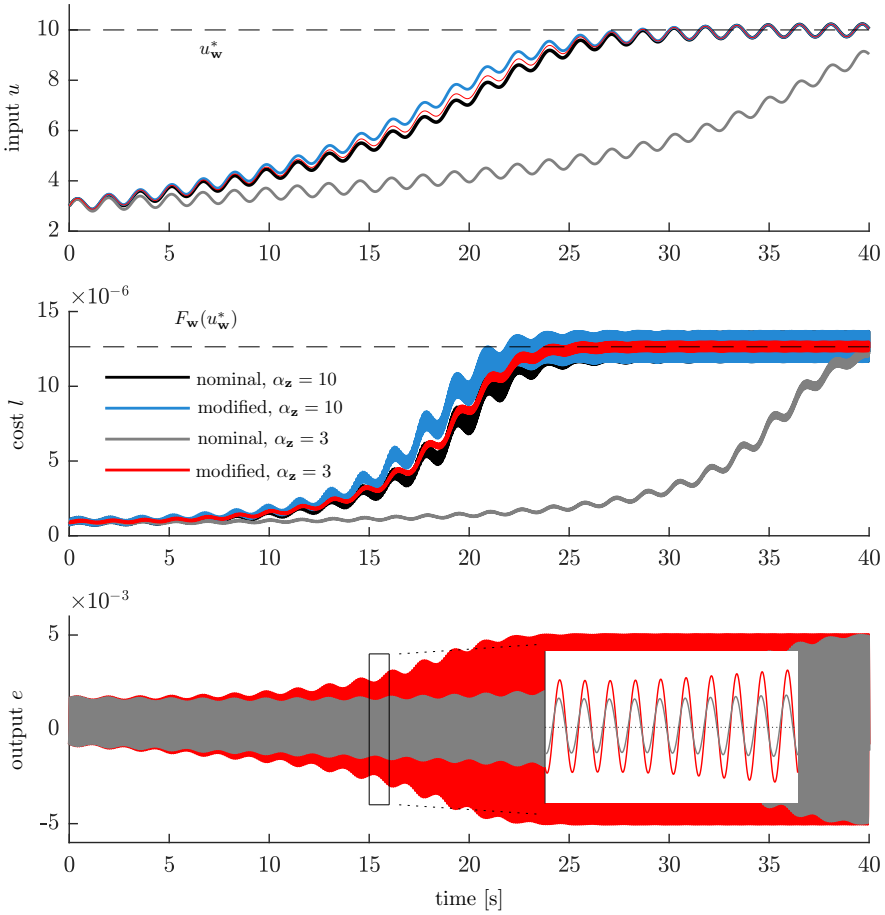

Figure 3.2: Simulation results of both extremum-seeking controllers. By incorporating knowledge on the filter in the observer, faster convergence towards the optimal input $u^*_{\mathbf{w}} = 10$ (see top figure) can be achieved. The improved convergence of the modified extremum-seeking controller is more significant in cases where the value of $\alpha_{\mathbf{z}}$ is relatively small.

this example, the aim is to find the input u that maximizes[2] the amplitude of the steady-state output of the system in (3.49) given the particular disturbance $w(t)$. Note that, for each constant input u, the system in (3.49) is a globally exponentially stable linear system subject to external inputs $w(t)$, which implies that it is globally exponentially convergent, thereby satisfying Assumption 3.1.

We employ the following dynamic cost function, with cost function $Z : y(t) = e(t)^2$, and filter Σ_f given by a low-pass filter $\dot{z}(t) = \alpha_{\mathbf{z}}(y(t) - z(t))$, $l(t) = z(t)$, with $\alpha_{\mathbf{z}}$ the cut-off frequency. Here we employ both ESC strategies given by (3.28)-(3.30) and (3.38)-(3.40), respectively, to investigate the effect of including information of the user-designed filter Σ_f in the observer on the convergence speed. For both extremum-seeking controllers, we employ the following numerical values: $\alpha_{\boldsymbol{\omega}} = 0.25$, $\eta_{\boldsymbol{\omega}} = 4$, $\eta_{\mathbf{m}} = 2$, $\lambda_{\mathbf{u}} = 1.5 \cdot 10^6$, $\eta_{\mathbf{u}} = 0.75$, $\sigma_r = 1 \cdot 10^{-3}$, and $\hat{\mathbf{H}} = -5 \cdot 10^{-7}$. Moreover, we show results for both extremum-seeking controllers with two filter settings: $\alpha_{\mathbf{z}} = 3$ and $\alpha_{\mathbf{z}} = 10$.

Fig. 3.2 presents simulation results that show the convergence of the initial input $u(0) = 3$ to a small neighborhood of the optimal input $u^*_{\mathbf{w}} = 10$ for both filter settings $\alpha_{\mathbf{z}} = 3$ and $\alpha_{\mathbf{z}} = 10$, and both the nominal extremum-seeking controller design, and the modified extremum-seeking controller design. For all settings, it can seen that the input u converges towards $u^*_{\mathbf{w}}$ (top figure), and the amplitude of the output e increases (third sub-figure).

In addition, Fig. 3.2 illustrates the improved convergence speed as a result of incorporating knowledge about Σ_f. For $\alpha_{\mathbf{z}} = 3$, the modified case (—) shows a significantly faster convergence towards $u^*_{\mathbf{w}}$ than the nominal case (—). In case of $\alpha_{\mathbf{z}} = 10$, the convergence speed in the nominal case (see (—) in the first and second sub-figures) is similar to the convergence speed in the modified case (—) in the first and second sub-figures). Concluding, especially in cases where the steady-state plant responses are dominated by time-varying behavior and a relatively small value of $\alpha_{\mathbf{z}}$ is needed, the modified extremum-seeking controller outperforms the nominal case in terms of convergence speed.

3.3 Industrial case study: Performance optimization of an industrial motion stage set-up

In this section, we will give a brief description of the industrial motion stage set-up under study and its nonlinear feedback control design. The industrial motion stage set-up under study, and depicted in Fig. 3.3, represents the short-stroke motion of a wafer stage commonly found in, e.g., complex lithography machinery used to manufacture integrated circuits (ICs); for more details, see Butler (2011). Wafer stages are required to perform fast (re-)positioning in three degrees-of-freedom with *nm*-accuracy to achieve the desired high machine

[2]The extremum-seeking controllers presented in this section are designed for minimization problems. Without loss of generality, we can employ the same controllers for maximization problems by changing the sign of the cost function.

throughput. Achieving *nm*-accuracy and high speeds of the wafer stage are in general realized by high-gain linear feedback controllers. However, due to the well-known waterbed-effect, see, e.g., Freudenberg et al. (2000), increasing the gain further to improve the ability to suppress low-frequency disturbances comes at the expense of an increased sensitivity to high-frequency disturbances and noise. Instead, variable-gain control is able to balance this trade-off in a more desirable manner. The idea of variable-gain control is to schedule an additional gain on the basis of the error signal. A dead-zone nonlinearity is used to perform this scheduling; namely, if the error resides within the dead-zone length the additional gain equals zero and prevents an increased amplification of high frequency disturbances within this regime. If the error is larger than the dead-zone length, which is typically induced by low-frequency disturbances, additional gain will be applied to suppress these low-frequency disturbances.

Although VGC is intuitive in nature, performance-optimal tuning of a variable-gain controller is far from trivial and heavily depends on the disturbance situation at hand. We will use the set-up to experimentally demonstrate both the nominal ESC approach and the modified ESC approach for the optimization of time-varying steady-state responses in Section 3.4. Section 3.3.1 presents the industrial stage set-up. Section 3.3.2 discusses the nominal and nonlinear feedback control designs of the industrial motion stage set-up. In Section 3.3.3, we will discuss the (external) disturbances acting on the system and the system performance measure.

3.3.1 Wafer stage system description

Fig. 3.3 depicts the industrial motion stage set-up under study, which represents the short-stroke motion of a wafer stage commonly found in, e.g., complex lithography machinery used to manufacture integrated circuits (ICs); for more details, see, e.g., Butler (2011). The industrial motion stage set-up, depicted in Fig. 3.3, consist of a base frame ① which is directly connected to the fixed world, force actuators in x-, y-, and z-direction, respectively ⑥, ⑦, and ⑧, which are installed in a force frame ④ that rests on the base frame, encoders in x-, y-, and z-direction ⑨ which are connected to a metrology frame ③ that is isolated from the base frame by means of airmounts ②, and a chuck ④, supported by four passive gravity compensators at the corners ⑧ to achieve a mid-air equilibrium of the chuck. The chuck, being the main component of the set-up, can be controlled in all six DOFs by means of force actuators. The origin of the reference frame is located at the center of gravity of the chuck. Lorentz actuators are used to actuate the chuck in x-, y-, and ϕ_z-direction, and voice coil actuators are used to actuate the chuck in ϕ_x-, ϕ_y-, and z-direction.

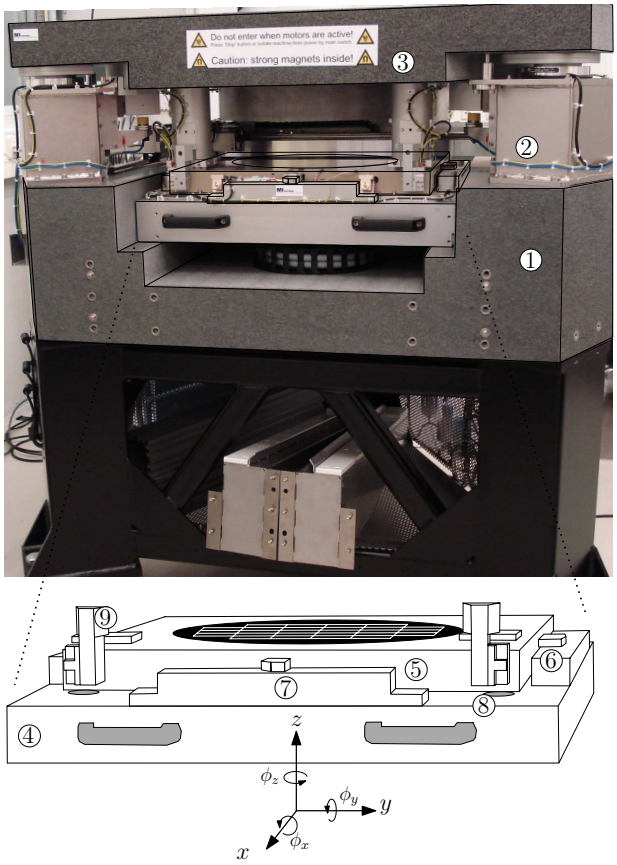

Figure 3.3: Industrial motion stage set-up: ① Base frame, ② Airmounts, ③ Metrology frame, ④ Force frame, ⑤ Chuck, ⑥ x-direction actuators, ⑦ y-direction actuators, ⑧ z-direction actuators, ⑨ sensors.

3.3.2 Nominal and nonlinear feedback control design

Here, we focus on controlling the chuck in the z-direction with the (nonlinear) feedback control loop depicted in Fig. 3.4. Herein $P_z(s)$ represents the (motion) plant dynamics of the actuated chuck (in z-direction), with $s \in \mathbb{C}$ being the Laplace variable. The nonlinear control loop consists of two parts, namely, a nominal linear feedback control part and a VGC part. For the nominal linear feedback control part, transfer function $C_z(s)$ represents the nominal (low-gain) linear controller. The signals r_z, e_z, and f_d denote the setpoint and tracking error in z-direction, and (external, time-varying) disturbances, respectively. Here we consider $r_z = 0$.

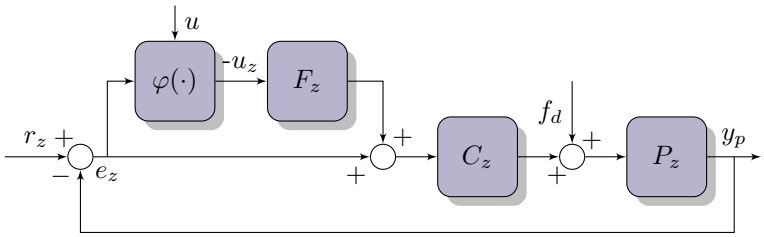

Figure 3.4: The closed-loop variable-gain control scheme.

For the so-called VGC part, $\varphi(\cdot)$ denotes a nonlinear control element, and transfer function $F_z(s)$ is a shaping filter. The nonlinear control element $\varphi(\cdot)$ studied here is given by a dead-zone characteristic:

$$\varphi(e_z(t),u)=\begin{cases}\alpha(e_z(t)+u), & \text{if } e_z(t) < -u,\\ 0, & \text{if } |e_z(t)|\le u,\\ \alpha(e_z(t)-u), & \text{if } e_z(t) > u,\end{cases} \tag{3.50}$$

where α, $u\in\mathbb{R}_{\geq 0}$ are tunable parameters, referred to as the additional gain and the dead-zone length, respectively. From the nonlinearity in (3.50) we can identify three distinct cases:

i) For $u=\infty$, the output of the nonlinear element $\varphi(\cdot)$ is always zero; the VGC part is disabled and only the nominal, low-gain, linear controller $C_z(s)$ is active. This case is referred to as the *low-gain case*.

ii) For $u=0$, the nonlinear element $\varphi(\cdot)$ acts as a gain α, and the VGC part has the transfer $\alpha F_z(s)$. Effectively, this case is referred to as the *high-gain case*; the high-gain linear controller reads $C_z(s)(1+\alpha F_z(s))$.

iii) For $u\in(0,\infty)$, we have nonlinear behavior, where the output of nonlinear element $\varphi(\cdot)$ depends on the amplitude of the tracking error $e_z(t)$. This case is referred to as the *variable-gain case*.

The closed-loop dynamics of the VGC scheme depicted in Fig. 3.4 can be written as a so-called Lur'e-type system, i.e., the feedback connection of a linear dynamical system and a nonlinear element (see, e.g., Khalil (2002, Chapter 7)) having the following state-space form:

$$\Sigma_p:\begin{cases}\dot{\mathbf{x}}(t)=\mathbf{A}_p\mathbf{x}(t)+\mathbf{B}_p u_z(t)+\mathbf{B}_w\mathbf{w}(t)\\ e_z(t)=\mathbf{C}_p\mathbf{x}(t)+\mathbf{D}_w\mathbf{w}(t)\\ u_z(t)=-\varphi(e_z,u),\end{cases} \tag{3.51}$$

with state $\mathbf{x}\in\mathbb{R}^{n_\mathbf{x}}$, and where $\mathbf{w}(t)=[r_z(t)\ f_d(t)]^\top\in\mathbb{R}^{n_\mathbf{w}}$ are all (external) disturbances. To conclude on closed-loop stability of the system in (3.51), we

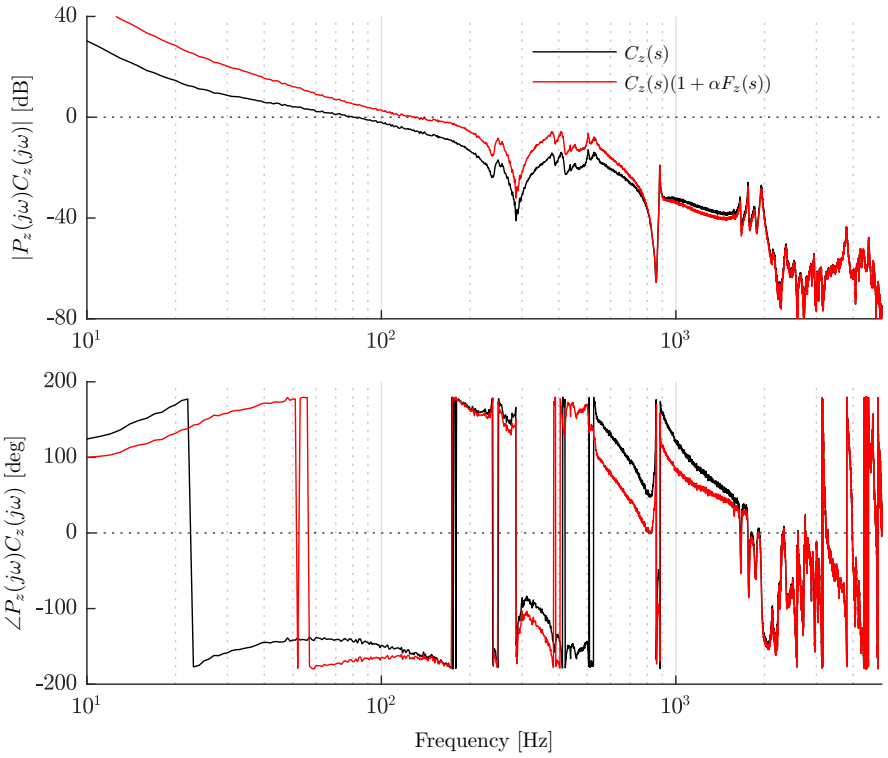

Figure 3.5: Measured open-loop frequency response function with nominal, low-gain linear controller $C_z(s)$ ($u = \infty$, i.e. low-gain case), and the nominal high-gain linear controller $C_z(s)(1 + \alpha F_z(s))$ ($u = 0$, i.e. high-gain case) with the maximum allowable additional gain $\alpha = 6.48$.

denote the transfer from u_z to e_z, i.e., from the output to the input of the nonlinear element $\varphi(\cdot)$, by the following transfer function:

$$G_{eu}(s) = \mathbf{C}_p(s\mathbf{I} - \mathbf{A}_p)^{-1}\mathbf{B}_p = \frac{P_z(s)C_z(s)F_z(s)}{1 + P_z(s)C_z(s)}. \tag{3.52}$$

The following theorem states the conditions under which the dynamics in (3.51) exhibit a unique, time-varying steady-state output that is globally uniformly exponentially stable.

Theorem 3.10. *(van de Wouw et al., 2008) Consider the dynamics in* (3.51)*. Suppose*

- *the matrix* $\mathbf{A}_p$ *is Hurwitz,*

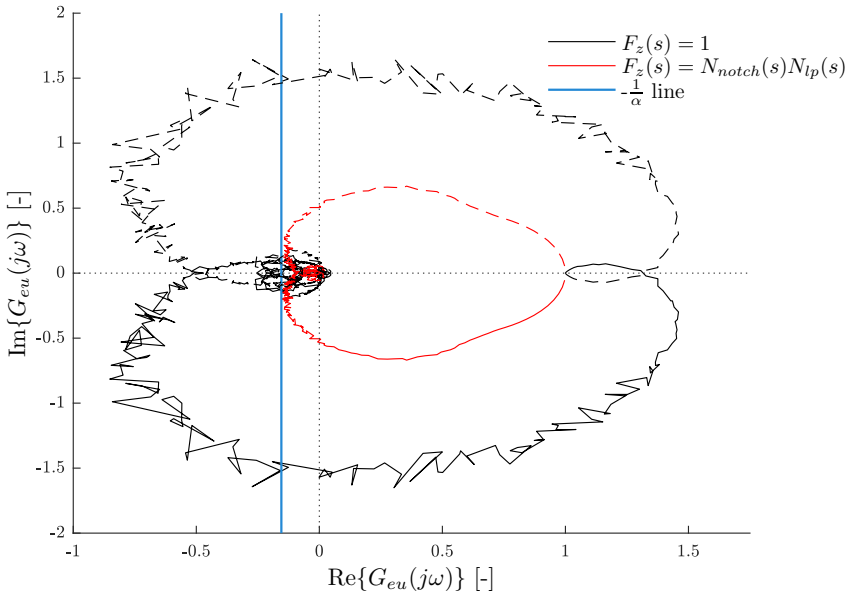

Figure 3.6: Circle-criterion condition based on measured frequency response data, verifying the satisfaction of the third condition of Theorem 3.10; $\mathrm{Re}\{G_{eu}(j\omega)\} > -\frac{1}{\alpha}$ for all $\omega \in \mathbb{R}$. With $F_z(s) = 1$, a maximum allowable additional gain $\alpha = 1.17$ can be achieved. With $F_z(s)$ composed of a notch filter and low-pass filter, a maximum allowable additional gain $\alpha = 6.48$ can be achieved.

- *the nonlinear element $\varphi(e_z, u)$ satisfies the so-called incremental sector condition, which reads as follows:*

$$0 \leq \frac{\varphi(e_1, u) - \varphi(e_2, u)}{e_1 - e_2} \leq \alpha, \tag{3.53}$$

  for all $e_1, e_2 \in \mathbb{R}$, $e_1 \neq e_2$, and all $u \in \mathbb{R}_{\geq 0}$,

- *the transfer function $G_{eu}(s)$ in (3.52) satisfies the following frequency-domain condition:*

$$Re\{G_{eu}(j\omega)\} > -\frac{1}{\alpha} \quad \forall\, \omega \in \mathbb{R}. \tag{3.54}$$

  Then, for any bounded input $\mathbf{w}(t)$, the system in (3.51) has a unique, time-varying steady-state output which is globally exponentially stable.

Based on frequency response measurements of the motion stage set-up, first a stabilizing linear controller $C_z(s)$ is designed using loop-shaping techniques.

The linear controller $C_z(s)$, referred to as the nominal low-gain linear controller, consists of a PID-type controller, low-pass filter, and notch filters, achieving a bandwidth of 80 Hz (see (—) in Fig. 3.5 for the open-loop frequency response function $P_z(j\omega)C_z(j\omega)$).

Having a stabilizing (nominal low-gain) linear controller $C_z(s)$ implies that the first condition of Theorem 3.10 is satisfied. Moreover, from the definition of the nonlinear element in (3.50) follows that the second condition of Theorem 3.10 is satisfied. The third condition of Theorem 3.10 is graphically shown in Fig. 3.6 and can be used to design the additional gain α of the nonlinear element in (3.50) and shaping filter $F_z(s)$. The shaping filter used here is given by $F_z(s) = N_{notch}(s)N_{lp}(s)$ where $N_{notch}(s)$ denotes a notch filter and reads as follows:

$$N_{notch}(s) = \frac{\omega_{pN}^2}{\omega_{zN}^2}\frac{s^2 + 2\beta_{zN}\omega_{zN}s + \omega_{zN}^2}{s^2 + 2\beta_{pN}\omega_{pN}s + \omega_{pN}^2}, \tag{3.55}$$

and N_{lp} denotes a second-order low-pass filter and reads as follows:

$$N_{lp}(s) = \frac{\omega_{lp}^2}{s^2 + 2\beta_{lp}\omega_{lp}s + \omega_{lp}^2}, \tag{3.56}$$

with $\omega_{pN} = \omega_{zN} = 110 \cdot 2\pi$ rad/s, $\beta_{pN} = 3.2$, $\beta_{zN} = 0.4$, $\beta_{lp} = \frac{1}{2}\sqrt{2}$, and $\omega_{lp} = 350 \cdot 2\pi$ rad/s. If we omit the shaping filter, i.e., $F_z(s) = 1$, the maximum allowable additional gain that guarantees closed-loop stability of VGC scheme is $\alpha = 1.17$. With the shaping filter $F_z(s)$ given by (3.55) and (3.56), the maximum allowable additional gain that guarantees closed-loop stability of the VGC scheme is $\alpha = 6.48$, which greatly increases the ability to suppress low-frequency disturbances. In addition, the low-pass filter in (3.56) is employed to attenuate high-frequency content of the large error signal such that the variable-gain controller does not amplify this. Fig. 3.5 depicts the open-loop frequency response functions $P_z(j\omega)C_z(j\omega)$ for the low-gain case and high-gain case, i.e., $C_z(s)$ and $C_z(s)(1 + \alpha F_z(s))$, respectively. In the remainder, we will consider an additional gain $\alpha = 6$ for robustness purposes, which renders the closed-loop system in (3.51) exponentially convergent. Note that this implies the satisfaction of Assumption 3.1, which is a key requirement for the utilization of the proposed ESC.

3.3.3 External disturbances

Although we consider control in the z-direction only, in industrial motion stages the x-, y-, and z-directions are not fully decoupled. For example, in wafer scanning systems the motion of a typical wafer stage in x- and y-direction is usually prescribed by third or fourth-order reference trajectories, denoted by $r_x(t)$ and $r_y(t)$, respectively. Due to cross-coupling between x-, y-, and z-axes, setpoint accelerations in x- and y-direction, denoted by $a_x(t) := \ddot{r}_x(t)$ and $a_y(t) := \ddot{r}_y(t)$,

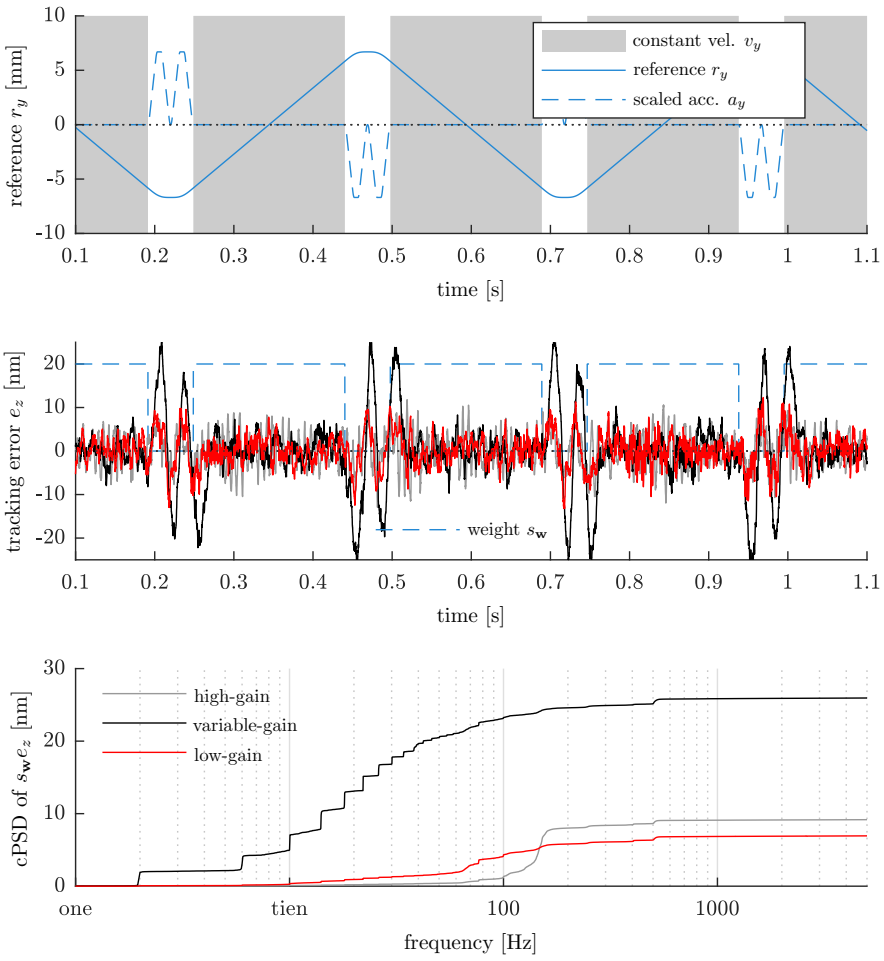

Figure 3.7: Top figure: reference trajectory in y-direction (—), and a scaled acceleration profile in y-direction (- -). Middle figure: tracking error $e_z(t)$ and weighting function $s_{\mathbf{w}}(t)$ (- -). Bottom figure: cumulative power spectral density (PSD) of the weighted error $s_{\mathbf{w}}(t)e_z(t)$. Middle and bottom figure are for the low-gain (—), high-gain (—), and variable-gain case (—), with the additional gain $\alpha = 6$ and dead-zone length $u = 3$ nm.

respectively, induce low-frequency disturbances that affect the positioning accuracy in z-direction among others. The industrial motion stage set-up we consider here has a limited stroke in x- and y-direction. In order to emulate the effect of cross-talk of these setpoint-induced disturbances in x- and y-direction to the

z-direction, we inject a scaled version of the acceleration reference profile in y-direction as an input disturbance in the z-control loop at the location where f_d enters the loop in Fig. 3.4. A scaled version of this acceleration profile in y-direction can be seen in Fig. 3.7 (top figure, (- -)). The grey areas denote regions where the velocity is constant, during which high-accuracy motion stage positioning in the z-direction is desired.

In addition to low-frequency disturbances induced by setpoint accelerations in y-direction, other (high-frequency) effects are disturbing the system as well. These disturbances can be, e.g., vibrational or acoustic disturbances, measurement noise, and amplifier disturbances. Fig. 3.7 (middle figure, (—)) shows a measured tracking error in z-direction for the low-gain case, resulting from these setpoint-induced low-frequency disturbances and other high-frequency effects.

3.3.4 Time-domain performance

In view of the stage disturbances as discussed in the previous section, VGC is introduced to be able to improve the ability to suppress the setpoint-induced low-frequency disturbances in z-direction while limiting the increased sensitivity to high-frequency disturbances under high-gain feedback. This system performance specification can be quantified by the power of a weighted tracking error signal computed over a known performance relevant time-interval $T = 0.5$ seconds. Similar to the one in (3.5), a typical performance measure used to quantify system performance reads:

$$L_2(t, s_{\mathbf{w}} e_z(t)) := \frac{1}{T} \int_{t-T}^{t} (s_{\mathbf{w}}(\tau) e_z(\tau))^2 d\tau, \quad \forall\ t \geq T, \tag{3.57}$$

where we have introduced a weighting function $s_{\mathbf{w}}(t)$ which is defined as follows:

$$s_{\mathbf{w}}(t) = \begin{cases} 0 \text{ if } a_y(t) \neq 0 \\ 1 \text{ if } a_y(t) = 0. \end{cases} \tag{3.58}$$

A scaled version of the specific weighting function used here is depicted in the middle plot of Fig. 3.7 (- -); basically, during non-zero accelerations in y-direction we do not penalize the tracking error, as we are only interested in achieving improved system performance during the constant velocity phase, i.e., zero acceleration in y-direction, see Fig. 3.7. Fig. 3.7 shows the tracking error for the low-gain case ($u = \infty$), high-gain case ($u = 0$), and the variable-gain case with $\alpha = 6$ and $u = 3 \cdot 10^{-9}$ m. In addition, we have depicted a plot of the cumulative power spectral density (cPSD) of the weighted tracking error, analyzed over multiple time-intervals T, which shows the different frequency contributions present in the tracking error. Both plots illustrate the benefit of the variable-gain controller; we can see that, during $s_{\mathbf{w}} \neq 0$, the tracking error response e_z in the VGC case shows "the best of both worlds" in terms of the error responses

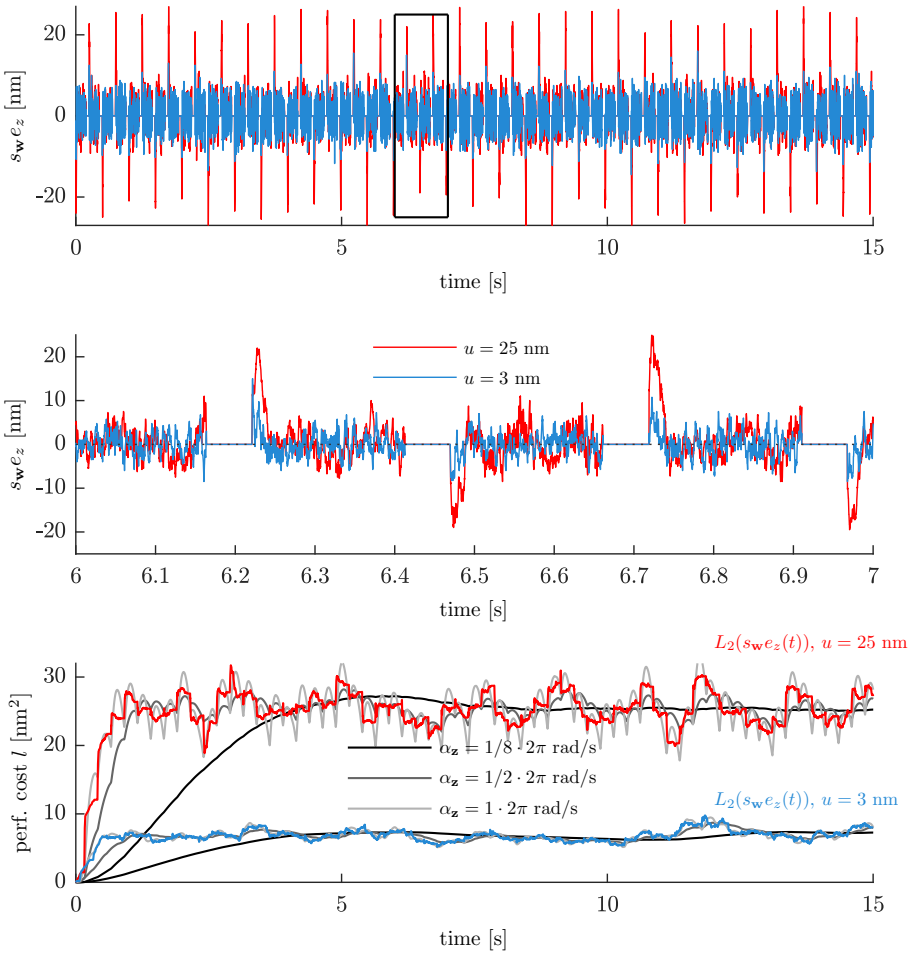

Figure 3.8: Top figure: 2 measurements of the weighted tracking error with $u = 25$ nm and $u = 3$ nm against time. Middle figure: zoomed plot of the weighted tracking error for $t \in [6, 7]$. Bottom figure: response of the dynamic cost function l against time for different values of $\alpha_{\mathbf{z}}$, and the system performance measure in (3.57) for $u = 25$ nm and $u = 3$ nm.

in the low- and high-gain cases. That is, the variable-gain controller is able to suppress low-frequency disturbances similar to the high-gain controller, while the amplification of high-frequency disturbances, especially around 100-200 Hz, is similar to the low-gain controller.

The results in Fig. 3.7 show that there exists a variable-gain controller setting that outperforms the low-gain and high-gain cases in terms of the performance

measure in (3.57). However, we do not know a-priori which value for the dead-zone length u gives the best system performance, as the value of u that minimizes the performance measure in (3.57) depends heavily on the disturbance situation at hand. Since accurate models of the disturbance situation are difficult to obtain, and the disturbance characteristic may slowly change over time, finding the optimal dead-zone length u can be difficult in practice.

In the next section, we will show that, without explicitly using knowledge on the plant and disturbance situation at hand, we can get arbitrarily close to the optimally tuned dead-zone length u by employing the ESC approaches introduced in Section 3.2.

3.4 Experimental results

Here, we will present the experimental results on the performance-optimal tuning of the variable-gain controller applied to the industrial motion stage set-up discussed in Section 3.3 using the ESC approaches discussed in Section 3.2. Section 3.4.1 presents the dynamic cost function design, Section 3.4.2 shows the measured objective function $F_{\mathbf{w}}$ of the industrial motion stage set-up given the particular disturbance situation at hand to help verify the working principles of the ESC approaches. In Sections 3.4.3 and 3.4.4, measurement results are presented of the closed-loop ESC schemes with the nominal ESC design and the modified ESC design, respectively, and Section 3.4.5 presents dedicated tuning guidelines to achieve extremum-seeking for motion stages.

3.4.1 Dynamic cost function

In order to minimize the power of the tracking error, which ultimately leads to a performance-optimal tracking error, the cost function Z in (3.6) is chosen as follows:

$$Z: \; y(t) = (s_{\mathbf{w}}(t)e_z(t))^2, \tag{3.59}$$

with the weighting function $s_{\mathbf{w}}$ defined in (3.58), and the filter Σ_f in (3.7) is designed as a second-order low-pass filter with the following state-space formulation:

$$\Sigma_f : \begin{cases} \dot{z}_1(t) = \alpha_{\mathbf{z}} z_2(t) \\ \dot{z}_2(t) = \alpha_{\mathbf{z}} \left(y(t) - 2\beta_{\mathbf{z}} z_2(t) - z_1(t) \right) \\ \quad l(t) = z_1(t), \end{cases} \tag{3.60}$$

with tunable parameters $\beta_{\mathbf{z}}, \alpha_{\mathbf{z}} \in \mathbb{R}_{>0}$ representing the damping coefficient and cut-off frequency of the second-order low-pass filter, respectively. The top figure of Fig. 3.8 shows two 10 second measurements of the weighted tracking error for two variable-gain cases, respectively $u = 25$ nm (—) and $u = 3$ nm (—). The middle figure shows a zoomed plot for $t \in [6, 6.5]$ seconds. The lower figure shows the response of the dynamic cost function l for different values of $\alpha_{\mathbf{z}}$,

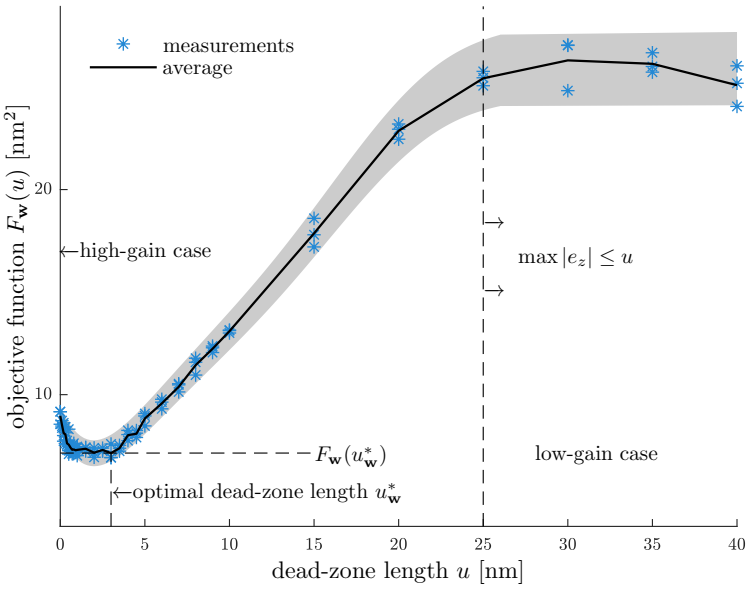

Figure 3.9: Approximation of the objective function $F_{\mathbf{w}}(u)$, averaged over 3 measurements (10 seconds each) with $\alpha_{\mathbf{z}} = \frac{1}{8} \cdot 2\pi$. An average of the last 2 seconds of the measured performance cost l (in steady-state) is used to estimate $F_{\mathbf{w}}(u)$. The grey area indicates an area in which l approximately lies. For smaller values of $\alpha_{\mathbf{z}}$, this area becomes smaller, however a longer measurement time is needed for the transient response to have sufficiently decayed.

and the performance measure in (3.57) for both variable-gain cases. Clearly, the performance measure in (3.57) is time-varying due to the time-varying nature of the measured performnace output, i.e., the weighted tracking error. The output l of the filter Σ_f approximates the performance measure in real time and is also time-varying. However, by selecting a sufficiently small $\alpha_{\mathbf{z}}$, the steady-state output, defined as $\bar{l}_{\mathbf{w}}$, can be made quasi-constant. That is, the filter Σ_f with tunable parameter $\alpha_{\mathbf{z}}$ provides robustness for the ESC scheme against the effect of time-varying system behavior on the performance measure, which can be made arbitrarily small. Note that, for smaller values of $\alpha_{\mathbf{z}}$, it takes a longer time before transient effects are sufficiently decayed. For larger $\alpha_{\mathbf{z}}$ the opposite can be concluded; the effect of time-varying system behavior on the performance measure is larger, while the transients decay faster.

3.4.2 Identifying the objective function

The static parameter-to-steady-state performance map $F_{\mathbf{w}}(u)$ (formalized by (3.14)) of the industrial motion stage set-up and the dynamic cost function is

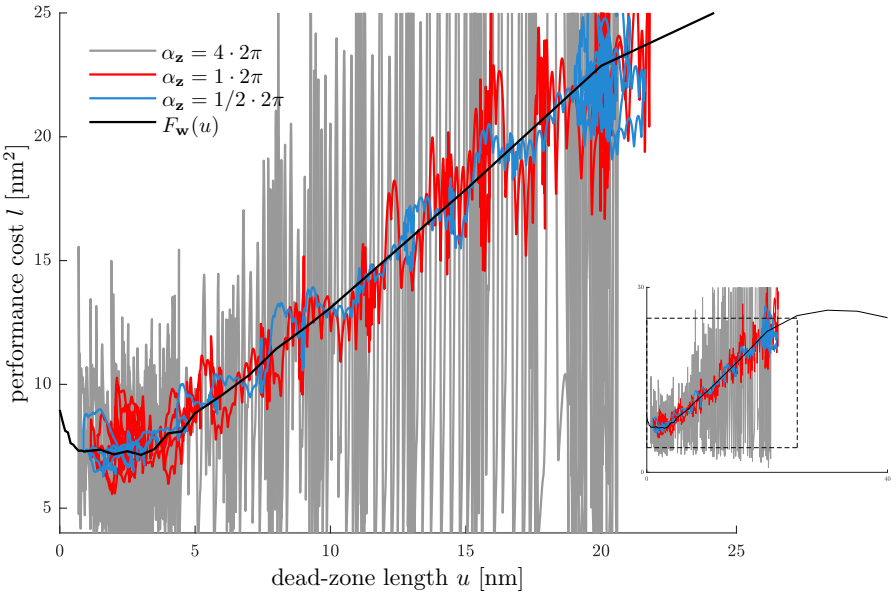

Figure 3.10: Average of measured objective function $F_{\mathbf{w}}(u)$, and a plot of the measured performance cost l against the dead-zone length u for the real-time performance-optimal tuning of the variable-gain controller using the nominal extremum-seeking controller and 3 different values of $\alpha_{\mathbf{z}}$.

experimentally identified through multiple measurements and shown in Fig. 3.9. The objective function clearly shows that there exists an optimal dead-zone length ($u_{\mathbf{w}} \approx 3$ nm) for this particular disturbance situation. Furthermore, the objective function shows the performance corresponding to the low-gain case ($u > 25$ nm), and high-gain case ($u = 0$ nm). The variation between the different measurements for the same dead-zone length can be attributed to multiple causes. The objective function in (3.14) is defined on the limit $\alpha_{\mathbf{z}} \to 0$, however we have used $\alpha_{\mathbf{z}} = 0.25\pi$ to obtain the result in Fig. 3.9. As a result, the steady-state output $\bar{l}_{\mathbf{w}}$ of Σ_f is still time-varying. In addition, the external disturbances and measurement noise present during one experiment can slightly deviate from the disturbance situation during another experiment. We would like to emphasize that the objective function $F_{\mathbf{w}}(u)$ in Fig. 3.9 is typically unknown in practice, and use ESC only to find the optimum of $F_{\mathbf{w}}(u)$. In the remainder, we will only use $F_{\mathbf{w}}(u)$ for verification purposes.

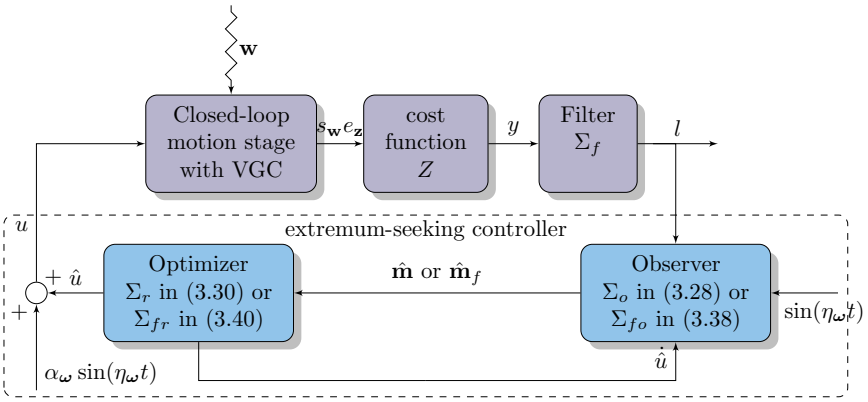

Figure 3.11: The closed-loop ESC scheme composed of the closed-loop motion stage with VGC, the dynamic cost function $Z + \Sigma_f$, the observer Σ_o (or Σ_{fo}), the optimizer Σ_r (or Σ_{fr}), and the dither signal $\alpha_{\boldsymbol{\omega}} \sin(\eta_{\boldsymbol{\omega}} t)$.

3.4.3 Performance optimization using extremum-seeking control

Here we analyze the experimental results obtained using the ESC approaches discussed in Section 3.2. The closed-loop ESC scheme is schematically depicted in Fig. 3.11. The nominal settings and initial conditions of the extremum-seeking controller are displayed in Table 3.1. Fig. 3.12 and Fig. 3.10 show the convergence of the VGC parameter u starting at $u = 20$ nm towards the optimal setting $u^*_{\mathbf{w}} \approx 3$ nm, and thus the optimal system performance $F_{\mathbf{w}}(u^*_{\mathbf{w}})$, in the presence of time-varying system behavior. Moreover, the figures illustrate the convergence and the effect on the convergence speed for different values for the filter parameter $\alpha_{\mathbf{z}}$. The following observations can be made:

- Choosing a larger value for the cut-off frequency $\alpha_{\mathbf{z}}$ results in faster decay of the transient response of the filter Σ_f, which ultimately leads to faster convergence of u towards $u^*_{\mathbf{w}}$, see, e.g., the cases $\alpha_{\mathbf{z}} = 1/2 \cdot 2\pi$ and $\alpha_{\mathbf{z}} = 1 \cdot 2\pi$, depicted by (—) and (—), respectively. Choosing $\alpha_{\mathbf{z}}$ too high deteriorates the convergence of u towards $u^*_{\mathbf{w}}$. For example, see the 'unexpected' slower convergence with $\alpha_{\mathbf{z}} = 4 \cdot 2\pi$ rad/s (—) compared to the case $\alpha_{\mathbf{z}} = 1 \cdot 2\pi$ rad/s (—) in the top figure of Fig. 3.12. From (—) in the bottom figure we can see that the time-varying steady-state response of the extended plant Σ is not quasi-constant, which can lead to poor estimation of the gradient of the objective function by the observer Σ_o, and hence, a deterioration of the convergence of u towards $u^*_{\mathbf{w}}$.

- Choosing $\alpha_{\mathbf{z}}$ too small (much smaller than the dither frequency parameterized by $\eta_{\boldsymbol{\omega}}$) may lead to a deterioration of the convergence of u towards

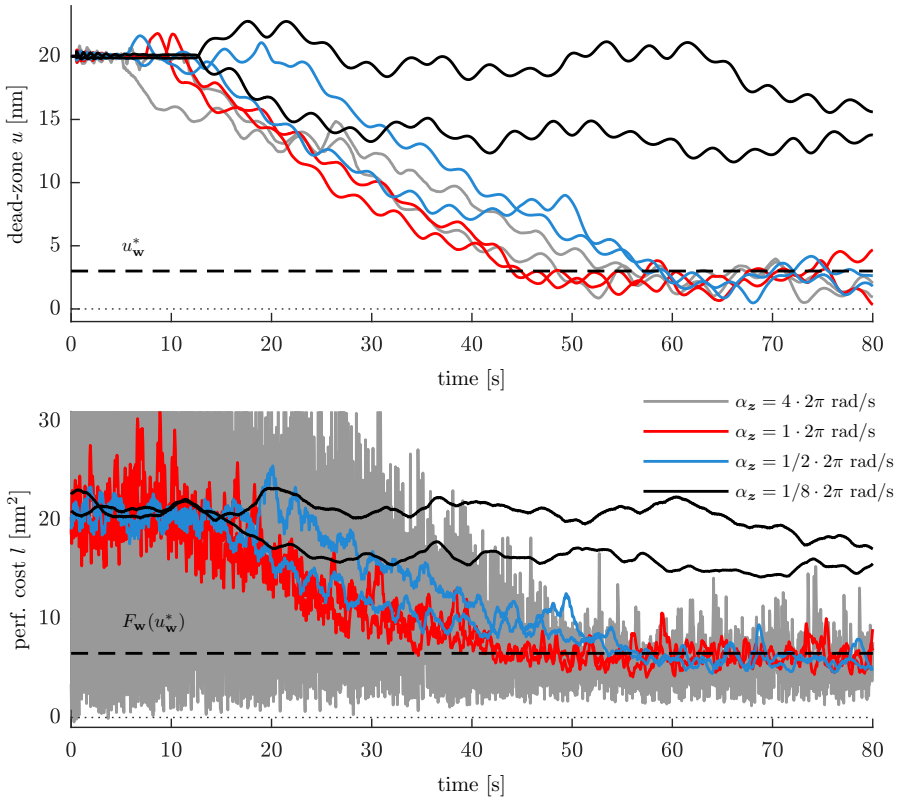

Figure 3.12: Experimental results using the nominal extremum-seeking controller to illustrate the influence of $\alpha_{\mathbf{z}}$ on the convergence of the dead-zone length u towards the optimal input $u^*_{\mathbf{w}}$, and the corresponding performance cost l as a function of time. (−−) indicate the optimal dead-zone length setting $u^*_{\mathbf{w}}$ (top figure) and the corresponding steady-state performance $F_{\mathbf{w}}(u^*_{\mathbf{w}})$ (bottom figure).

$u^*_{\mathbf{w}}$ as well. For example, see the 'convergence' with $\alpha_{\mathbf{z}} = 1/8 \cdot 2\pi$ rad/s in Fig. 3.12 (—). If we choose $\alpha_{\mathbf{z}}$ too low, separation between the time-scales of the filter dynamics and the extremum-seeking controller is insufficient. Re-tuning of the extremum-seeking controller parameters, e.g., decreasing the dither frequency $\eta_{\boldsymbol{\omega}}$, can be necessary to preserve time-scale separation.

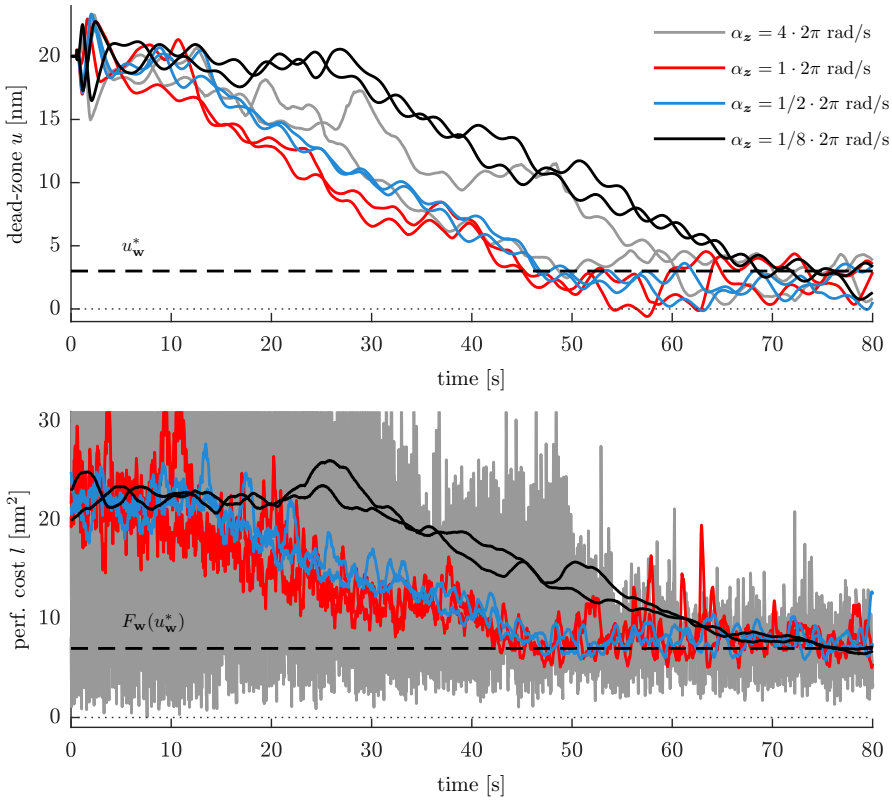

Figure 3.13: Experimental results using the modified extremum-seeking controller to illustrate the influence of the tunable parameter $\alpha_{\mathbf{z}}$ on the convergence of the dead-zone length u towards the optimal input $u^*_{\mathbf{w}}$, and the corresponding performance cost l as a function of time. (−−) indicate the optimal dead-zone length setting $u^*_{\mathbf{w}}$ (top figure) and the corresponding steady-state performance $F_{\mathbf{w}}(u^*_{\mathbf{w}})$ (bottom figure).

3.4.4 Improved convergence speed with modified extremum-seeking controller design

Fig. 3.13 shows the convergence of the VGC parameter u towards the optimal setting $u^*_{\mathbf{w}} \approx 3$ nm for the modified extremum-seeking controller. Moreover, the figure illustrates the convergence and the effect on the convergence speed for different values for the filter parameter $\alpha_{\mathbf{z}}$. The following observations can be made:

- Similar as for the nominal extremum-seeking controller, choosing a larger value for the cut-off frequency $\alpha_{\mathbf{z}}$ results in faster decay of the transient

Table 3.1: Nominal extremum-seeking controller settings

parameter	value	unit
dither amplitude $\alpha_{\boldsymbol{\omega}}$	0.5	[nm]
filter parameter $\alpha_{\mathbf{z}}$	$1 \cdot 2\pi$	[rad/s]
dither frequency $\eta_{\boldsymbol{\omega}}$	$1/4 \cdot 2\pi$	[rad/s]
damping coefficient $\beta_{\mathbf{z}}$	$(1/2)\sqrt{2}$	[-]
forgetting factor $\eta_{\mathbf{m}}$	0.5	[-]
regularization constant σ_r	$1 \cdot 10^{-6}$	[-]
observer parameter $\hat{\mathbf{H}}$	0.25	[-]
optimizer parameter $\eta_{\mathbf{u}}$	$1 \cdot 10^{-3}$	[-]
optimizer parameter $\lambda_{\mathbf{u}}$	$2 \cdot 10^{9}$	[-]
initial condition optimizer $\hat{u}(0)$	20	[nm]
initial condition observer state $\hat{\mathbf{m}}(0)$	$[0\ 0]^\top$	[-]
initial condition observer state $\mathbf{Q}(0)$	$\left[\begin{smallmatrix} 1 & 0 \\ 0 & \frac{2}{1+2\sigma_r} \end{smallmatrix}\right]$	[-]

The nominal ESC settings. Any variations on one of these parameters is indicated in that particular figure.

response of the filter Σ_f, which ultimately leads to faster convergence of u towards $u^*_{\mathbf{w}}$ as well. Moreover, choosing $\alpha_{\mathbf{z}}$ too high deteriorates the convergence of u towards $u^*_{\mathbf{w}}$ (compare again the case $\alpha_{\mathbf{z}} = 4 \cdot 2\pi$ rad/s (—) to the case $\alpha_{\mathbf{z}} = 1 \cdot 2\pi$ rad/s (—) in the top figure of Fig. 3.13).

- The advantage of the modified extremum-seeking controller over the nominal one is particularly evident in case of small values of $\alpha_{\mathbf{z}}$. Where the case $\alpha_{\mathbf{z}} = 1/8 \cdot 2\pi$ rad/s led to a deterioration of the convergence of u towards $u^*_{\mathbf{w}}$ in the nominal case (see (—) in Fig. 3.12), the modified extremum-seeking controller still achieves convergence to the optimal input (see (—) in Fig. 3.13). In general, the improvement of the modified ESC design in terms of convergence speed is more significant in the case of smaller values of $\alpha_{\mathbf{z}}$.

The resulting optimal time-varying steady-state response can be seen in Fig. 3.7 (—).

3.4.5 A note on dedicated tuning guidelines

For the extremum-seeking controller parameters $\alpha_{\boldsymbol{\omega}}$, $\alpha_{\mathbf{z}}$, and $\eta_{\boldsymbol{\omega}}$, we propose dedicated tuning guidelines when optimizing time-varying system behavior of industrial positioning stages.

- The dither amplitude $\alpha_{\boldsymbol{\omega}}$ should be chosen close to the desired accuracy of u to the optimal VGC parameter settings $u^*_{\mathbf{w}}$ when converged, e.g.,

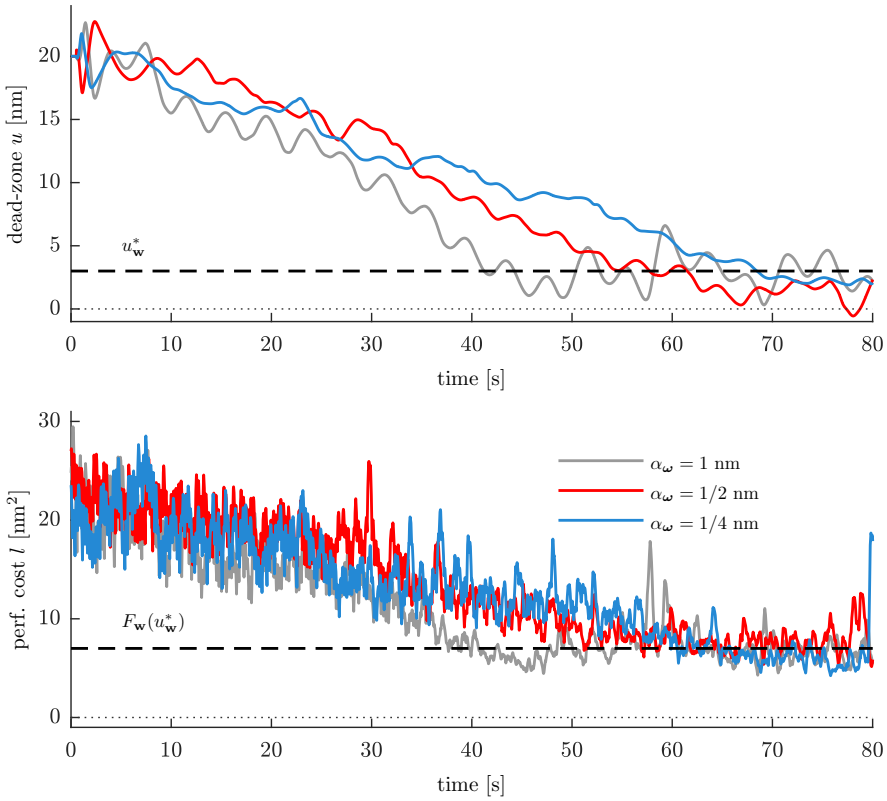

Figure 3.14: Experimental results using the modified extremum-seeking controller to illustrate the influence of the dither amplitude $\alpha_{\boldsymbol{\omega}}$ on the convergence of the dead-zone length u towards the optimal input $u^*_{\mathbf{w}}$, and the corresponding performance cost l as a function of time. $(--)$ indicate the optimal dead-zone length setting $u^*_{\mathbf{w}}$ (top figure) and the corresponding steady-state performance $F_{\mathbf{w}}(u^*_{\mathbf{w}})$ (bottom figure).

$\alpha_{\boldsymbol{\omega}} = 0.5$ nm. Choosing $\alpha_{\boldsymbol{\omega}}$ small may deteriorate the convergence speed of u towards $u^*_{\mathbf{w}}$, see, e.g., Fig 3.14. Choosing $\alpha_{\boldsymbol{\omega}}$ large may result in faster convergence, but the neighborhood of $u^*_{\mathbf{w}}$ to which u converges is in general larger.

- The cut-off frequency $\alpha_{\mathbf{z}}$ of a low-pass filter design for Σ_f should typically be chosen smaller than the lowest significant frequency contribution ω_{low} in the to-be-optimized tracking error, e.g., $\alpha_{\mathbf{z}} = \frac{1}{2}\omega_{low}$. Small values of $\alpha_{\mathbf{z}}$ motivates the use of the modified extremum-seeking controller over the nominal one to prevent slow convergence. In motion stages, the frequency

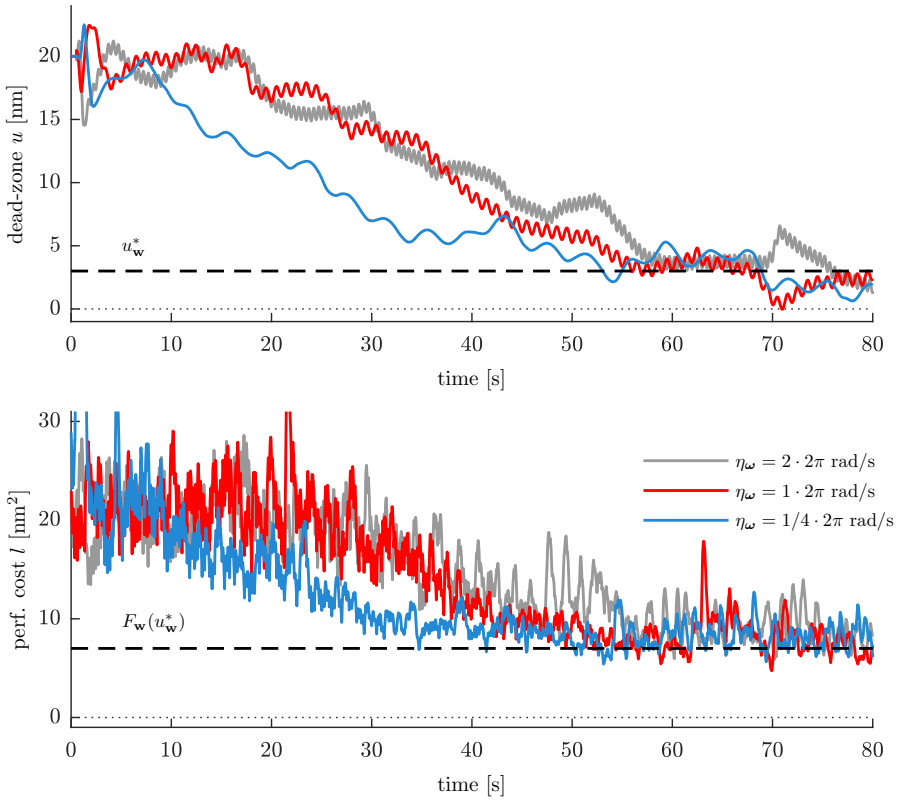

Figure 3.15: Experimental results using the modified extremum-seeking controller to illustrate the influence of the dither frequency $\eta_{\boldsymbol{\omega}}$ on the convergence of the dead-zone length u towards the optimal input $u^*_{\mathbf{w}}$, and the corresponding performance cost l as a function of time. (−−) indicate the optimal dead-zone length setting $u^*_{\mathbf{w}}$ (top figure) and the corresponding steady-state performance $F_{\mathbf{w}}(u^*_{\mathbf{w}})$ (bottom figure).

ω_{low} is usually dictated by the setpoint and the performance-relevant time interval T, i.e., $\omega_{low} = \frac{2\pi}{T}$.

- The dither frequency $\eta_{\boldsymbol{\omega}}$ should be chosen close to or less than $\alpha_{\mathbf{z}}$ to have sufficient excitation and sufficient time-scale separation. Choosing $\eta_{\boldsymbol{\omega}}$ large may deteriorate the convergence speed of u towards $u^*_{\mathbf{w}}$, see, e.g., Fig 3.15. Also, the convergence may be more susceptible to 'unexpected' external disturbances which can be seen around $t = 50$ seconds and $t = 70$ seconds in the case $\eta_{\boldsymbol{\omega}} = 2 \cdot 2\pi$ rad/s (—) (with cut-off frequency $\alpha_{\mathbf{z}} = 1 \cdot 2\pi$ rad/s).

3.5 Conclusions

In this chapter, we have experimentally demonstrated the working principle of a recently developed ESC approach for the optimization of time-varying responses. The (industrial) experimental case study involves optimally tuning parameters of a particular nonlinear control strategy employed on an industrial motion stage set-up, to achieve optimal system performance. The experimental results illustrate the practical applicability of the ESC methodology for the optimization of time-varying steady-state responses of nonlinear systems. Moreover, we have proposed a modified extremum-seeking controller design that incorporates knowledge about the filter Σ_f, and presented a stability analysis of the closed-loop ESC scheme with the modified controller. We have shown via simulations and experiments that the use of the modified extremum-seeking controller leads to an increased convergence speed towards the extremum, especially for small values of the dynamic cost function parameter.

3.A Proof of Lemma 3.6

The proof of Lemma 3.6 follows similar arguments as the proof of Haring (2016, Lemma 2.11). We define the following Lyapunov function candidate for the $\tilde{\mathbf{Q}}_f$-dynamics:

$$V_{\mathbf{Q}_f}(\tilde{\mathbf{Q}}_f(t)) = \mathrm{tr}(\tilde{\mathbf{Q}}_f^2(t)). \tag{3.61}$$

For notational clarity, from this point on we omit the time argument. Note that $\tilde{\mathbf{Q}}_f$ is symmetric because $\mathbf{Q}_f$ and Ξ_f^{-1} are symmetric. From (3.44) we can write the time-derivative of $V_{\mathbf{Q}}$ as follows:

$$\begin{aligned}\dot{V}_{\mathbf{Q}_f}(\tilde{\mathbf{Q}}_f) &= \frac{d}{dt}\mathrm{tr}(\tilde{\mathbf{Q}}_f^2) = \mathrm{tr}(\dot{\tilde{\mathbf{Q}}}_f\tilde{\mathbf{Q}}_f + \tilde{\mathbf{Q}}_f\dot{\tilde{\mathbf{Q}}}_f),\\ &= -2\eta_{\mathbf{m}}\mathrm{tr}(\tilde{\mathbf{Q}}_f^2) - \mathrm{tr}(\mathbf{A}_f^\top\Xi_f^{-1}\tilde{\mathbf{Q}}_f + \tilde{\mathbf{Q}}_f\Xi_f^{-1}\mathbf{A}_f)\\ &\quad - \mathrm{tr}(\Xi_f^{-1}\mathbf{A}_f\tilde{\mathbf{Q}}_f + \tilde{\mathbf{Q}}_f\mathbf{A}_f^\top\Xi_f^{-1}) - 4\mathrm{tr}(\tilde{\mathbf{Q}}_f^2\mathbf{A}_f)\end{aligned} \tag{3.62}$$

where we have used that $\mathrm{tr}(\mathbf{X}+\mathbf{Y}) = \mathrm{tr}(\mathbf{X}) + \mathrm{tr}(\mathbf{Y})$, $\mathrm{tr}(\mathbf{XY}) = \mathrm{tr}(\mathbf{YX})$, and $\mathrm{tr}(\mathbf{X}) = \mathrm{tr}(\mathbf{X}^\top)$. Also, from these, and the fact that $\mathrm{tr}(\mathbf{X}^\top\mathbf{X}) \geq 0$, we obtain the following inequality:

$$\dot{V}_{\mathbf{Q}_f}(\tilde{\mathbf{Q}}_f) \leq -\eta_{\mathbf{m}}\mathrm{tr}(\tilde{\mathbf{Q}}_f^2) - 4\mathrm{tr}(\tilde{\mathbf{Q}}_f^2\mathbf{A}_f) + \frac{4}{\eta_{\mathbf{m}}}\mathrm{tr}(\mathbf{A}_f^\top\Xi_f^{-2}\mathbf{A}_f) \tag{3.63}$$

From the definition of the trace we have the following inequalities:

$$\begin{aligned}\|\tilde{\mathbf{Q}}_f\|^2 \leq V_{\mathbf{Q}_f}(\tilde{\mathbf{Q}}_f) &\leq n_{\mathbf{m}_f}\|\tilde{\mathbf{Q}}_f\|^2,\\ \mathrm{tr}(\tilde{\mathbf{Q}}_f^2\mathbf{A}_f) &\leq n_{\mathbf{m}_f}\|\tilde{\mathbf{Q}}_f\|^2\|\mathbf{A}_f\|,\\ \mathrm{tr}(\mathbf{A}_f^\top\Xi_f^{-2}\mathbf{A}_f) &\leq n_{\mathbf{m}_f}\|\Xi_f^{-1}\|^2\|\mathbf{A}_f\|^2,\end{aligned} \tag{3.64}$$

where $n_{\mathbf{m}_f}$ denotes the dimension of the state $\mathbf{m}_f$. From these inequalities and (3.63) we obtain the following inequality:

$$\dot{V}_{\mathbf{Q}_f}(\tilde{\mathbf{Q}}_f) \leq -\eta_{\mathbf{m}}V_{\mathbf{Q}_f}(\tilde{\mathbf{Q}}_f) + 4n_{\mathbf{m}_f}V_{\mathbf{Q}_f}(\tilde{\mathbf{Q}}_f)\|\mathbf{A}_f\| + \frac{4}{\eta_{\mathbf{m}}}n_{\mathbf{m}_f}\|\Xi_f^{-1}\|^2\|\mathbf{A}_f\|^2. \tag{3.65}$$

The definition of $\boldsymbol{\omega}$ in (3.19) implies that there exists a constant $L_{\boldsymbol{\omega}2} \in \mathbb{R}_{>0}$ such that $\|\boldsymbol{\omega}\| \leq L_{\boldsymbol{\omega}2}$. Moreover, there exist $L_{\mathbf{A}_{\Sigma_f}}, L_{\mathbf{B}_{\Sigma_f}} \in \mathbb{R}_{>0}$ such that $\|\mathbf{A}_{\Sigma_f}\| \leq L_{\mathbf{A}_{\Sigma_f}}$, $\|\mathbf{B}_{\Sigma_f}\| \leq L_{\mathbf{B}_{\Sigma_f}}$, respectively. From (3.37) we obtain the following bound on $\|\mathbf{A}_f\|$:

$$\begin{aligned}\|\mathbf{A}_f\| &\leq \alpha_{\mathbf{z}}\|\mathbf{A}_{\Sigma_f}\| + \alpha_{\mathbf{z}}\|\mathbf{B}_{\Sigma_f}\|\|\boldsymbol{\omega}\| + \frac{\eta_{\mathbf{u}}}{\alpha_{\boldsymbol{\omega}}}\\ &\leq \alpha_{\mathbf{z}}(L_{\mathbf{A}_{\Sigma_f}} + L_{\mathbf{B}_{\Sigma_f}}L_{\boldsymbol{\omega}2}) + \frac{\eta_{\mathbf{u}}}{\alpha_{\boldsymbol{\omega}}}\\ &\leq \alpha_{\mathbf{z}}(L_{\Sigma_f} + \epsilon_1\epsilon_4),\end{aligned} \tag{3.66}$$

for all $\eta_{\boldsymbol{\omega}} \leq \alpha_{\mathbf{z}}\epsilon_1$, and all $\eta_{\mathbf{u}} \leq \alpha_{\boldsymbol{\omega}}\eta_{\boldsymbol{\omega}}\epsilon_4$, and with $L_{\Sigma_f} := L_{\mathbf{A}_{\Sigma_f}} + L_{\mathbf{B}_{\Sigma_f}} L_{\boldsymbol{\omega}2}$. Moreover, without loss of generality, for sufficiently small ϵ_5 and a particular design of $\mathbf{C}_{\Sigma_f}$ (e.g., observable canonical form for Σ_f, such that $\|C_{\Sigma_f}\| = 1$), we have $\|\Xi_f^{-1}\| \leq 2$ for all $\sigma_r \leq \epsilon_5$. Using this, and without loss of generality, for sufficiently small ϵ_2 and ϵ_5, we obtain the following inequality:

$$\dot{V}_{\mathbf{Q}_f}(\tilde{\mathbf{Q}}_f) \leq -\frac{\eta_{\mathbf{m}}}{2} V_{\mathbf{Q}_f}(\tilde{\mathbf{Q}}_f) + \frac{\eta_{\mathbf{m}}}{256}, \tag{3.67}$$

for all $\eta_{\boldsymbol{\omega}} \leq \alpha_{\mathbf{z}}\epsilon_1$, all $\alpha_{\mathbf{z}} \leq \eta_{\mathbf{m}}\epsilon_2$, all $\eta_{\mathbf{u}} \leq \alpha_{\boldsymbol{\omega}}\eta_{\boldsymbol{\omega}}\epsilon_4$, and all $\sigma_r \leq \epsilon_5$. Applying the comparison lemma and using the inequalities in (3.64), we obtain the bound on $\tilde{\mathbf{Q}}_f$ as follows:

$$\|\tilde{\mathbf{Q}}_f(t)\| \leq \max\left\{ e^{-\frac{\eta_{\mathbf{m}}}{4}t}\sqrt{2n_{\mathbf{m}_f}}\|\tilde{\mathbf{Q}}_f(0)\|, \frac{1}{8} \right\}, \tag{3.68}$$

for all $t \geq 0$, all $\tilde{\mathbf{Q}}_f(0) \in \mathbb{R}^{n_{\mathbf{m}_f} \times n_{\mathbf{m}_f}}$, and all time-varying $\mathbf{u}(t) \in \mathbb{R}^{n_{\mathbf{u}}}$, which completes the proof of Lemma 3.6. □

3.B Proof of Lemma 3.7

We define the following Lyapunov function candidate for the $\tilde{\mathbf{m}}_f$-dynamics in (3.45):

$$V_{\mathbf{m}_f}(\tilde{\mathbf{m}}_f, \mathbf{Q}_f) = \tilde{\mathbf{m}}_f^\top \mathbf{Q}_f^{-1} \tilde{\mathbf{m}}_f. \tag{3.69}$$

For notational clarity, from this point on we omit the time argument. We note that

$$\lambda_{min}(\mathbf{Q}_f^{-1})\|\tilde{\mathbf{m}}_f\|^2 \leq V_{\mathbf{m}_f}(\tilde{\mathbf{m}}_f, \mathbf{Q}_f) \leq \lambda_{max}(\mathbf{Q}_f^{-1})\|\tilde{\mathbf{m}}_f\|^2, \tag{3.70}$$

where $\lambda_{min}(\mathbf{Q}_f^{-1})$ and $\lambda_{max}(\mathbf{Q}_f^{-1})$ are the smallest and largest eigenvalue of $\mathbf{Q}_f^{-1}$, respectively. From the observer in (3.38) and (3.45) we obtain the time derivative of $V_{\mathbf{m}_f}$ as follows:

$$\begin{aligned}
\dot{V}_{\mathbf{m}_f} &= 2\tilde{\mathbf{m}}_f^\top \mathbf{Q}_f^{-1} \dot{\tilde{\mathbf{m}}}_f - \tilde{\mathbf{m}}_f^\top \mathbf{Q}_f^{-1} \dot{\mathbf{Q}}_f \mathbf{Q}_f^{-1} \tilde{\mathbf{m}}_f, \\
&= -\eta_{\mathbf{m}} \tilde{\mathbf{m}}_f^\top \mathbf{Q}_f^{-1} \tilde{\mathbf{m}}_f - \eta_{\mathbf{m}} \tilde{\mathbf{m}}_f^\top (\mathbf{C}_f^\top \mathbf{C}_f + \sigma_r \mathbf{D}_f^\top \mathbf{D}_f) \tilde{\mathbf{m}}_f \\
&\quad + 2\alpha_{\boldsymbol{\omega}}^2 \tilde{\mathbf{m}}_f^\top \mathbf{Q}_f^{-1} \mathbf{B}_f (\hat{\mathbf{s}} - \mathbf{s}) - 2\eta_{\mathbf{m}} \sigma_r \alpha_{\boldsymbol{\omega}} \tilde{\mathbf{m}}_f^\top \mathbf{D}_f^\top \frac{dF_{\mathbf{w}}}{d\mathbf{u}^\top}(\hat{\mathbf{u}}) \\
&\quad + 2\alpha_{\mathbf{z}} \alpha_{\boldsymbol{\omega}}^2 \tilde{\mathbf{m}}_f^\top \mathbf{Q}_f^{-1} \mathbf{E}_f (\hat{v} - v) + 2\eta_{\mathbf{m}} \tilde{\mathbf{m}}_f^\top \mathbf{C}_f^\top \mathbf{C}_{\Sigma_f} \tilde{\mathbf{m}}_{\mathbf{z}},
\end{aligned} \tag{3.71}$$

where we have used the fact that $\mathbf{Q}_f^{-1}$ is real and symmetric, i.e., $\mathbf{Q}_f^{-1} = \mathbf{Q}_f^{-\top}$, and, given $\mathbf{A}_f$ in (3.37), that $\tilde{\mathbf{m}}_f^\top \left(\mathbf{Q}_f^{-1} \mathbf{A}_f - \mathbf{A}_f^\top \mathbf{Q}_f^{-1} \right) \tilde{\mathbf{m}}_f = 0$. Furthermore, given $\mathbf{C}_f$ and $\mathbf{D}_f$, using the fact that $-\tilde{\mathbf{m}}_f^\top \mathbf{C}_f^\top \mathbf{C}_f \tilde{\mathbf{m}}_f = -\|\mathbf{C}_f \tilde{\mathbf{m}}_f\|^2 \leq 0$,

$-\tilde{\mathbf{m}}_f^\top \mathbf{D}_f^\top \mathbf{D}_f \tilde{\mathbf{m}}_f = -\|\mathbf{D}_f \tilde{\mathbf{m}}_f\|^2$, and $\left\|\tilde{\mathbf{m}}_f^\top \mathbf{D}_f^\top\right\| = \|\mathbf{D}_f \tilde{\mathbf{m}}_f\|$, (3.69), and Young's inequality, we obtain

$$\begin{aligned}\dot{V}_{\mathbf{m}_f} \leq & -\frac{\eta_{\mathbf{m}}}{2} V_{\mathbf{m}_f}(\tilde{\mathbf{m}}_f, \mathbf{Q}_f) + \eta_{\mathbf{m}} \sigma_r \alpha_{\boldsymbol{\omega}}^2 \left\| \frac{dF_{\mathbf{w}}}{d\mathbf{u}}(\hat{\mathbf{u}}) \right\|^2 \\ & + \frac{4\alpha_{\boldsymbol{\omega}}^4}{\eta_{\mathbf{m}}} \|\mathbf{Q}_f^{-1}\| \|\mathbf{B}_f\|^2 \|\hat{\mathbf{s}} - \mathbf{s}\|^2 + \frac{\eta_{\mathbf{m}}}{4} \|\mathbf{C}_{\Sigma_f} \tilde{\mathbf{m}}_{\mathbf{z}}\|^2 \\ & + \frac{4\alpha_{\mathbf{z}}^2 \alpha_{\boldsymbol{\omega}}^4}{\eta_{\mathbf{m}}} \|\mathbf{Q}_f^{-1}\| \|\mathbf{E}_f\|^2 |\hat{v} - v|^2.\end{aligned} \tag{3.72}$$

From (3.27), (3.29), the bound $\|\hat{\mathbf{H}}(t, \hat{\mathbf{u}}(t))\| \leq L_{\mathbf{H}}$, and the definition of $\boldsymbol{\omega}$ in (3.19), which implies that there exists a constant $L_{\boldsymbol{\omega}2} \in \mathbb{R}_{>0}$ such that $\|\boldsymbol{\omega}\| \leq L_{\boldsymbol{\omega}2}$, we obtain

$$\begin{aligned}\|\hat{\mathbf{s}} - \mathbf{s}\| &\leq \frac{1}{\alpha_{\boldsymbol{\omega}}} \left(L_{\mathbf{H}} + L_{F2}\right) \|\dot{\hat{\mathbf{u}}}\|, \\ |\hat{v} - v| &\leq \frac{1}{2} \left(L_{\mathbf{H}} + L_{F2}\right) L_{\boldsymbol{\omega}2}^2.\end{aligned} \tag{3.73}$$

From Assumption 3.4 we obtain

$$\left\| \frac{dF_{\mathbf{w}}}{d\mathbf{u}}(\hat{\mathbf{u}}) \right\| \leq \int_0^1 \left\| \frac{d^2 F_{\mathbf{w}}}{d\mathbf{u} d\mathbf{u}^\top}(\sigma \tilde{\mathbf{u}} + \mathbf{u}_{\mathbf{w}}^*) \right\| d\sigma \, \|\tilde{\mathbf{u}}\| = L_{F2} \|\tilde{\mathbf{u}}\|. \tag{3.74}$$

Moreover, from the filter design in (3.31) there exist $L_{\mathbf{B}_{\Sigma_f}}, L_{\mathbf{C}_{\Sigma_f}} \in \mathbb{R}_{>0}$ such that $\|\mathbf{B}_{\Sigma_f}\| \leq L_{\mathbf{B}_{\Sigma_f}}$ and $\|\mathbf{C}_{\Sigma_f}\| \leq L_{\mathbf{C}_{\Sigma_f}}$, respectively. Then from (3.37) it follows that $\|\mathbf{E}_f\| = \|\mathbf{B}_{\Sigma_f}\| = L_{\mathbf{B}_{\Sigma_f}}$, and $\|\mathbf{B}_f\| = 1$. Substitution of all these inequalities in (3.72) yields the following inequality:

$$\begin{aligned}\dot{V}_{\mathbf{m}_f} \leq & -\frac{\eta_{\mathbf{m}}}{2} V_{\mathbf{m}_f}(\tilde{\mathbf{m}}_f, \mathbf{Q}_f) + \eta_{\mathbf{m}} \sigma_r \alpha_{\boldsymbol{\omega}}^2 L_{F2}^2 \|\tilde{\mathbf{u}}\|^2 \\ & + \frac{4\alpha_{\boldsymbol{\omega}}^2}{\eta_{\mathbf{m}}} \left(L_{\mathbf{H}} + L_{F2}\right)^2 \|\mathbf{Q}_f^{-1}\| \|\dot{\hat{\mathbf{u}}}\|^2 + \frac{\eta_{\mathbf{m}}}{4} L_{\mathbf{C}_{\Sigma_f}}^2 \|\tilde{\mathbf{m}}_{\mathbf{z}}\|^2 \\ & + \frac{\alpha_{\mathbf{z}}^2 \alpha_{\boldsymbol{\omega}}^4}{\eta_{\mathbf{m}}} L_{\mathbf{B}_{\Sigma_f}}^2 \left(L_{\mathbf{H}} + L_{F2}\right)^2 L_{\boldsymbol{\omega}2}^4 \|\mathbf{Q}_f^{-1}\|.\end{aligned} \tag{3.75}$$

Let us define $\tilde{y} := y - \bar{y}_{\mathbf{w}}(t, \mathbf{u})$. From Property 2.9 we can derive the general solution for (3.34) as follows:

$$\begin{aligned}\tilde{\mathbf{m}}_{\mathbf{z}}(t) = & e^{\alpha_{\mathbf{z}} \mathbf{A}_{\Sigma_f} t} \tilde{\mathbf{m}}_{\mathbf{z}}(0) + \alpha_{\mathbf{z}} \int_0^t e^{\alpha_{\mathbf{z}} \mathbf{A}_{\Sigma_f}(t-\tau)} \mathbf{B}_{\Sigma_f} \tilde{y}(\tau) d\tau \\ & + \alpha_{\mathbf{z}} \int_0^t e^{\alpha_{\mathbf{z}} \mathbf{A}_{\Sigma_f}(t-\tau)} \mathbf{B}_{\Sigma_f} \big(\bar{y}_{\mathbf{w}}(\tau, \mathbf{u}(\tau)) - F_{\mathbf{w}}(\mathbf{u}(\tau))\big) d\tau,\end{aligned} \tag{3.76}$$

for all $t \in \mathbb{R}_{\geq 0}$. The filter Σ_f is designed such that $\alpha_{\mathbf{z}}\mathbf{A}_{\Sigma_f}$ is Hurwitz, i.e., there exist $k, \lambda \in \mathbb{R}_{>0}$ such that $\|e^{\alpha_{\mathbf{z}}\mathbf{A}_{\Sigma_f}(t-\tau)}\| \leq ke^{-\alpha_{\mathbf{z}}\lambda(t-\tau)}$ for all $t \geq \tau$. From this fact, we can bound the second term in (3.76) by $\frac{k}{\lambda}\|\mathbf{B}_{\Sigma_f}\| \sup_{s\in[0,t]} |\tilde{y}(s)|$. For a bound on the third term in (3.76) we exploit Assumption 3.3. By defining $\tilde{\mathbf{e}} := \mathbf{e} - \bar{\mathbf{e}}_{\mathbf{w}}(t, \mathbf{u})$, using (3.6), (3.9), and the bounds in (3.8), it follows that

$$\begin{aligned} |\tilde{y}| \leq{}& L_{Z\mathbf{e}}\|\bar{\mathbf{e}}_{\mathbf{w}}(t,\mathbf{u}) - \bar{\mathbf{e}}_{\mathbf{w}}(t,\mathbf{u}^*_{\mathbf{w}})\|\|\tilde{\mathbf{e}}\| + L_{Z*}\|\tilde{\mathbf{e}}\| \\ &+ \frac{L_{Z\mathbf{e}}}{2}\|\tilde{\mathbf{e}}\|^2 + L_{Z\mathbf{u}}\|\mathbf{u} - \mathbf{u}^*_{\mathbf{w}}\|\|\tilde{\mathbf{e}}\|, \end{aligned} \tag{3.77}$$

with $L_{Z*} = \left\|\frac{\partial Z}{\partial \mathbf{e}}(\bar{\mathbf{e}}_{\mathbf{w}}(t,\mathbf{u}^*_{\mathbf{w}}), \mathbf{u}^*_{\mathbf{w}})\right\| \in \mathbb{R}_{>0}$. Moreover, from Assumption 2.2 we have that

$$\|\tilde{\mathbf{e}}\| = \|\mathbf{g}(\mathbf{x},\mathbf{u},\mathbf{w}) - \mathbf{g}(\bar{\mathbf{x}}_{\mathbf{w}}(t,\mathbf{u}),\mathbf{u},\mathbf{w})\| \leq L_{\mathbf{gx}}\|\tilde{\mathbf{x}}\|, \tag{3.78}$$

and subsequently, from (3.3) in Assumption 2.6 we have that

$$\|\bar{\mathbf{e}}_{\mathbf{w}}(t,\mathbf{u}) - \bar{\mathbf{e}}_{\mathbf{w}}(t,\mathbf{u}^*_{\mathbf{w}})\| \leq (L_{\mathbf{gu}} + L_{\mathbf{gx}}L_{\mathbf{xu}})\|\mathbf{u} - \mathbf{u}^*_{\mathbf{w}}\|. \tag{3.79}$$

From (3.18), it follows that $\|\mathbf{u} - \mathbf{u}^*_{\mathbf{w}}\| \leq \|\tilde{\mathbf{u}}\| + \alpha_{\boldsymbol{\omega}}L_{\boldsymbol{\omega}2}$. Using Young's inequality it follows that $\|\mathbf{u}-\mathbf{u}^*_{\mathbf{w}}\|^2 \leq 2\|\tilde{\mathbf{u}}\|^2 + 2\alpha^2_{\boldsymbol{\omega}}L^2_{\boldsymbol{\omega}2}$. Combining (3.76)-(3.79), we obtain the following bound on $\|\tilde{\mathbf{m}}_{\mathbf{z}}\|$:

$$\begin{aligned} \|\tilde{\mathbf{m}}_{\mathbf{z}}\| \leq \max\big\{ & 2e^{\alpha_{\mathbf{z}}\mathbf{A}_{\Sigma_f}t}\|\tilde{\mathbf{m}}_{\mathbf{z}}(0)\|, c_{mz1}\|\tilde{\mathbf{x}}\|^2 \\ &+ 4\alpha_{\mathbf{z}}\delta_{\mathbf{z}2}\|\tilde{\mathbf{u}}\|^2 + (\alpha_{\boldsymbol{\omega}}c_{mz2} + c_{mz3})\|\tilde{\mathbf{x}}\| \\ &+ c_{mz4}\|\tilde{\mathbf{u}}\|\|\tilde{\mathbf{x}}\| + 2\alpha_{\mathbf{z}}\delta_{\mathbf{z}1} + 4\alpha_{\mathbf{z}}\alpha^2_{\boldsymbol{\omega}}L^2_{\boldsymbol{\omega}2}\delta_{\mathbf{z}2}\big\}, \end{aligned} \tag{3.80}$$

with $c_{mz1}, \ldots, c_{mz4} \in \mathbb{R}_{>0}$ defined as

$$\begin{aligned} c_{mz1} &= 2\frac{L_{Z\mathbf{e}}}{2}\frac{k}{\lambda}L_{\mathbf{B}_{\Sigma_f}}L^2_{\mathbf{gx}}, \\ c_{mz2} &= 2\frac{k}{\lambda}L_{\mathbf{B}_{\Sigma_f}}\left(L_{Z\mathbf{e}}(L_{\mathbf{gu}} + L_{\mathbf{gx}}L_{\mathbf{xu}}) + L_{Z\mathbf{u}}\right)L_{\mathbf{gx}}L_{\boldsymbol{\omega}2} \\ c_{mz3} &= 2\frac{k}{\lambda}L_{\mathbf{B}_{\Sigma_f}}L_{Z*}L_{\mathbf{gx}} \\ c_{mz4} &= 2\frac{k}{\lambda}L_{\mathbf{B}_{\Sigma_f}}\left(L_{Z\mathbf{e}}(L_{\mathbf{gu}} + L_{\mathbf{gx}}L_{\mathbf{xu}})L_{\mathbf{gx}} + L_{Z\mathbf{u}}L_{\mathbf{gx}}\right) \end{aligned} \tag{3.81}$$

From Lemmas 2.19 and 2.21 in Chapter 2 we have that, for any finite time $t_1 \geq 0$, the solutions $\tilde{\mathbf{x}}$ and $\tilde{\mathbf{u}}$ are bounded for all $0 \leq t \leq t_1$. Moreover, from Lemma 3.6 we have that $\mathbf{Q}_f^{-1}$ is positive definite and bounded for all $0 \leq t \leq t_1$. From these facts and $\|\dot{\hat{\mathbf{u}}}\| \leq \eta_{\mathbf{u}}$, which follows from (3.40), we obtain that the right-hand side of (3.75) is bounded for all $0 \leq t \leq t_1$. Therefore, since $V_{\mathbf{m}_f}(\tilde{\mathbf{m}}_f, \mathbf{Q}_f)$ will be bounded for all $0 \leq t \leq t_1$ and $\mathbf{Q}_f^{-1}$ is positive definite and bounded for all $0 \leq t \leq t_1$ as well, it follows from (3.70) that the solutions $\tilde{\mathbf{m}}_f$ are

bounded for all $0 \leq t \leq t_1$. Let us define $t_1 \geq 0$ such that, from Lemma 2.19, Lemma 3.6, and (3.80), we have that $\|\tilde{\mathbf{x}}(t)\| \leq \alpha_{\boldsymbol{\omega}}\eta_{\boldsymbol{\omega}}c_{\mathbf{x}2}$, $\|\tilde{\mathbf{Q}}_f\| \leq \frac{1}{8}$, for all $t \geq t_1$, respectively. Also, $2e^{\alpha_{\mathbf{z}}A_{\Sigma_f}t_1}\|\tilde{\mathbf{m}}_{\mathbf{z}}(0)\|$ in (3.80) is sufficiently decayed for all $t \geq t_1$. In addition, from (3.42) and sufficiently small ϵ_5, we have that $\frac{1}{4}\mathbf{I} \preceq \mathbf{Q}_f^{-1} \preceq \frac{5}{4}\mathbf{I}$ for all $t \geq t_1$, and all $\sigma_r \leq \epsilon_5$. From (3.70), it follows that $\frac{1}{4}\|\tilde{\mathbf{m}}_f\|^2 \leq V_{\mathbf{m}_f}(\tilde{\mathbf{m}}_f, \mathbf{Q}_f) \leq \frac{5}{4}\|\tilde{\mathbf{m}}_f\|^2$, for all $t \geq t_1$, and $\|\mathbf{Q}_f^{-1}\| \leq \frac{5}{4}$ for all $t \geq t_1$. From (3.35), (3.30), (3.42), $\|\mathbf{D}_f\| = 1$, and the bound in (3.17), it follows that $\|\dot{\tilde{\mathbf{u}}}\|^2 \leq 8\lambda_{\mathbf{u}}^2 V_{\mathbf{m}_f}(\tilde{\mathbf{m}}_f, \mathbf{Q}_f) + 2\alpha_{\boldsymbol{\omega}}^2\lambda_{\mathbf{u}}^2 L_{F2}^2\|\tilde{\mathbf{u}}\|^2$, for all $t_1 \geq 0$. From this fact, and taking ϵ_3 in Theorem 2.16 sufficiently small, we obtain

$$
\begin{aligned}
\dot{V}_{\mathbf{m}_f} \leq & -\frac{\eta_{\mathbf{m}}}{4}V_{\mathbf{m}_f}(\tilde{\mathbf{m}}_f, \mathbf{Q}_f) + \eta_{\mathbf{m}}\sigma_r\alpha_{\boldsymbol{\omega}}^2 L_{F2}^2\|\tilde{\mathbf{u}}\|^2 \\
& + 10\eta_{\mathbf{m}}\alpha_{\boldsymbol{\omega}}^2\frac{\alpha_{\boldsymbol{\omega}}^2\lambda_{\mathbf{u}}^2}{\eta_{\mathbf{m}}^2}L_{F2}^2\left(L_{\mathbf{H}} + L_{F2}\right)^2\|\tilde{\mathbf{u}}\|^2 + \frac{6}{4}\eta_{\mathbf{m}}\alpha_{\boldsymbol{\omega}}^4\eta_{\boldsymbol{\omega}}^4 L_{\mathbf{C}_{\Sigma_f}}^2 c_{mz1}^2 c_{\mathbf{x}2}^4 \\
& + 24\eta_{\mathbf{m}}\alpha_{\mathbf{z}}^2 L_{\mathbf{C}_{\Sigma_f}}^2\delta_{\mathbf{z}2}^2\|\tilde{\mathbf{u}}\|^4 + \frac{6}{4}\eta_{\mathbf{m}}\alpha_{\boldsymbol{\omega}}^2\eta_{\boldsymbol{\omega}}^2 L_{\mathbf{C}_{\Sigma_f}}^2\left(\epsilon_0 c_{mz2} + c_{mz3}\right)^2 c_{\mathbf{x}2}^2 \\
& + \frac{6}{4}\eta_{\mathbf{m}}\alpha_{\boldsymbol{\omega}}^2\eta_{\boldsymbol{\omega}}^2 L_{\mathbf{C}_{\Sigma_f}}^2 c_{mz4}^2 c_{\mathbf{x}2}^2\|\tilde{\mathbf{u}}\|^2 + 24\eta_{\mathbf{m}}\alpha_{\mathbf{z}}^2\alpha_{\boldsymbol{\omega}}^4 L_{\mathbf{C}_{\Sigma_f}}^2 L_{\boldsymbol{\omega}2}^4\delta_{\mathbf{z}2}^2 \\
& + 6\eta_{\mathbf{m}}\alpha_{\mathbf{z}}^2 L_{\mathbf{C}_{\Sigma_f}}^2\delta_{\mathbf{z}1}^2 + \frac{5}{4}\eta_{\mathbf{m}}\frac{\alpha_{\mathbf{z}}^2\alpha_{\boldsymbol{\omega}}^4}{\eta_{\mathbf{m}}^2}L_{\mathbf{B}_{\Sigma_f}}^2\left(L_{\mathbf{H}} + L_{F2}\right)^2 L_{\boldsymbol{\omega}2}^4.
\end{aligned}
\tag{3.82}
$$

for all $t \geq t_1$, $\alpha_{\mathbf{z}} \leq \eta_{\mathbf{m}}\epsilon_2$, and all $\alpha_{\boldsymbol{\omega}}\lambda_{\mathbf{u}} \leq \eta_{\mathbf{m}}\epsilon_3$. From the comparison lemma and (3.70) we obtain

$$
\begin{aligned}
\sup_{t\geq t_1}\|\tilde{\mathbf{m}}_f(t)\| \leq 2\sqrt{10}\sup_{t\geq t_1}\max\{ & \sqrt{\frac{5}{4}}\|\tilde{\mathbf{m}}_f(t_1)\|, 2\sqrt{\sigma_r}\alpha_{\boldsymbol{\omega}}L_{F2}\|\tilde{\mathbf{u}}(t)\|, \\
& \sqrt{40}\alpha_{\boldsymbol{\omega}}\frac{\alpha_{\boldsymbol{\omega}}\lambda_{\mathbf{u}}}{\eta_{\mathbf{m}}}L_{F2}\left(L_{\mathbf{H}} + L_{F2}\right)\|\tilde{\mathbf{u}}(t)\|, 4\sqrt{6}\alpha_{\mathbf{z}}L_{\mathbf{C}_{\Sigma_f}}\delta_{\mathbf{z}2}\|\tilde{\mathbf{u}}(t)\|^2, \\
& \sqrt{6}\alpha_{\boldsymbol{\omega}}\eta_{\boldsymbol{\omega}}L_{\mathbf{C}_{\Sigma_f}}c_{mz4}c_{\mathbf{x}2}\|\tilde{\mathbf{u}}(t)\|, \sqrt{6}\alpha_{\boldsymbol{\omega}}^2\eta_{\boldsymbol{\omega}}^2 L_{\mathbf{C}_{\Sigma_f}}c_{mz1}c_{\mathbf{x}2}^2, \\
& 4\sqrt{6}\alpha_{\mathbf{z}}\alpha_{\boldsymbol{\omega}}^2 L_{\mathbf{C}_{\Sigma_f}}L_{\boldsymbol{\omega}2}^2\delta_{\mathbf{z}2}, \sqrt{6}\alpha_{\boldsymbol{\omega}}\eta_{\boldsymbol{\omega}}L_{\mathbf{C}_{\Sigma_f}}\left(\epsilon_0 c_{mz2} + c_{mz3}\right)c_{\mathbf{x}2}, \\
& 2\sqrt{6}\alpha_{\mathbf{z}}L_{\mathbf{C}_{\Sigma_f}}\delta_{\mathbf{z}1}, \sqrt{5}\alpha_{\boldsymbol{\omega}}^2\epsilon_2 L_{\mathbf{B}_{\Sigma_f}}\left(L_{\mathbf{H}} + L_{F2}\right)L_{\boldsymbol{\omega}2}^2\},
\end{aligned}
\tag{3.83}
$$

and

$$
\begin{aligned}
\limsup_{t\to\infty}\|\tilde{\mathbf{m}}_f(t)\| \leq 2\sqrt{10}\limsup_{t\to\infty}\max\{ & 2\sqrt{\sigma_r}\alpha_{\boldsymbol{\omega}}L_{F2}\|\tilde{\mathbf{u}}(t)\|, \\
& \sqrt{40}\alpha_{\boldsymbol{\omega}}\frac{\alpha_{\boldsymbol{\omega}}\lambda_{\mathbf{u}}}{\eta_{\mathbf{m}}}L_{F2}\left(L_{\mathbf{H}} + L_{F2}\right)\|\tilde{\mathbf{u}}(t)\|, 4\sqrt{6}\alpha_{\mathbf{z}}L_{\mathbf{C}_{\Sigma_f}}\delta_{\mathbf{z}2}\|\tilde{\mathbf{u}}(t)\|^2, \\
& \sqrt{6}\alpha_{\boldsymbol{\omega}}\eta_{\boldsymbol{\omega}}L_{\mathbf{C}_{\Sigma_f}}c_{mz4}c_{\mathbf{x}2}\|\tilde{\mathbf{u}}(t)\|, \sqrt{6}\alpha_{\boldsymbol{\omega}}^2\eta_{\boldsymbol{\omega}}^2 L_{\mathbf{C}_{\Sigma_f}}c_{mz1}c_{\mathbf{x}2}^2, \\
& 4\sqrt{6}\alpha_{\mathbf{z}}\alpha_{\boldsymbol{\omega}}^2 L_{\mathbf{C}_{\Sigma_f}}L_{\boldsymbol{\omega}2}^2\delta_{\mathbf{z}2}, \sqrt{6}\alpha_{\boldsymbol{\omega}}\eta_{\boldsymbol{\omega}}L_{\mathbf{C}_{\Sigma_f}}\left(\epsilon_0 c_{mz2} + c_{mz3}\right)c_{\mathbf{x}2}, \\
& 2\sqrt{6}\alpha_{\mathbf{z}}L_{\mathbf{C}_{\Sigma_f}}\delta_{\mathbf{z}1}, \sqrt{5}\alpha_{\boldsymbol{\omega}}^2\epsilon_2 L_{\mathbf{B}_{\Sigma_f}}\left(L_{\mathbf{H}} + L_{F2}\right)L_{\boldsymbol{\omega}2}^2\}.
\end{aligned}
\tag{3.84}
$$

for all $t \geq t_1$, all $\alpha_{\boldsymbol{\omega}} \leq \epsilon_0$, all $\eta_{\boldsymbol{\omega}} \leq \alpha_{\mathbf{z}}\epsilon_1$, all $\alpha_{\mathbf{z}} \leq \eta_{\mathbf{m}}\epsilon_2$, all $\alpha_{\boldsymbol{\omega}}\lambda_{\mathbf{u}} \leq \eta_{\mathbf{m}}\epsilon_3$, all $\eta_{\mathbf{u}} \leq \alpha_{\boldsymbol{\omega}}\eta_{\boldsymbol{\omega}}\epsilon_4$, and all $\sigma_r \leq \epsilon_5$. This completes the proof of Lemma 3.7. $\square$

Part II

Sampled-Data Extremum-Seeking Control

Chapter 4

Sampled-data extremum-seeking control framework for constrained optimization of nonlinear dynamical systems

Abstract - *Most extremum-seeking control (ESC) approaches focus solely on the problem of finding the extremum of some unknown, steady-state input-output map, providing parameter settings that lead to optimal steady-state system performance. However, many industrial applications also have to deal with constraints on operating conditions due to, e.g., actuator limitations, limitations on tunable system parameters, or constraints on measurable variables. In particular, constraints on measurable variables are typically unknown in terms of their relationship with the tunable system parameters. In addition, the constraints on system inputs as a result of the constraints on measurable variables may conflict with the otherwise optimal operational condition, and hence should be taken into account in the data-based optimization approach. In this work, we propose a sampled-data extremum-seeking framework for the constrained optimization of a class of nonlinear dynamical systems with measurable constrained variables. In this framework, barrier function methods are exploited, where both the objective function and constraint functions are available through measurement only. We show, under the assumption that the parametric initialization yield operating conditions that do not violate the constraints, that 1) the resulting closed-loop dynamics is stable, 2) constraint satisfaction of the inputs is guaranteed for all iterations of the optimization process, and 3) constrained optimization is achieved. We illustrate the working principle of the proposed framework by means of an industrial case study of the constrained optimization of extreme ultraviolet light generation in a laser-produced plasma source within a state-of-the-art lithography system.*

The content of this chapter is based on: L. Hazeleger, D. Nešić, N. van de Wouw, "Sampled-data extremum-seeking framework for constrained optimization of nonlinear dynamical systems", *Submitted for publication in Automatica*

4.1 Introduction

Performance optimization of complex nonlinear dynamical systems is a challenging task. Namely, most (numerical) optimization techniques such as, e.g., gradient-descent methods, Newton and quasi-Newton methods, interior-point methods, and Sequential Quadratic Programming (SQP), usually rely on an accurate model of the process to be optimized ((Boyd and Vandenberghe, 2004)), while such a model can be hard or impossible to obtain for complex nonlinear systems. Nevertheless, the steady-state input-output behavior of many of such systems possesses optimal performance under particular operating conditions and we often desire to find such optimal operating conditions. Based solely on output measurements and without using any model knowledge, *extremum-seeking control* (ESC) is able to optimize the performance of such complex systems in real-time by adjusting these operating conditions and driving the system into a neighborhood of its optimal steady-state input-output behavior (Krstić and Wang, 2000; Teel and Popović, 2001).

Along with the pioneering work done in Krstić and Wang (2000) on convergence proofs for continuous-time extremum-seeking schemes based on sinusoidal perturbations, a notable contribution to the field of extremum-seeking control was made in Teel and Popović (2001). In Teel and Popović (2001), it was shown that under assumptions on the asymptotic stability of both the system and on a discrete-time nonlinear programming method used for optimization, extremum seeking can be achieved within a periodic sampled-data framework. This framework allows the use of a wide class of smooth and nonsmooth optimization algorithms for achieving optimization of general nonlinear systems. In Kvaternik and Pavel (2011), closed-loop stability of the sampled-data ESC scheme has been studied from an interconnected systems' theory point-of-view, in which stability results are obtained by imposing stronger conditions on the nonlinear programming methods than done in Teel and Popović (2001).

Extensions of the framework in Teel and Popović (2001) are provided in Khong et al. (2013) and Khong et al. (2013b). The work in Khong et al. (2013) utilizes a trajectory-based approach to prove semi-global practical asymptotic stability of the proposed sampled-data extremum-seeking schemes as opposed to the Lyapunov-type arguments used in Teel and Popović (2001). The former exploits the notion of multi-step consistency (see, e.g., Nešić et al. (1999)) while the latter exploits closeness of solutions of a differential inclusion over a single time step. As such, the framework in Khong et al. (2013) allows to use a broader class of optimization algorithms, including algorithms which do not admit a state-update realization or for which its convergence properties are not encapsulated by a Lyapunov function. Subsequently in Khong et al. (2013b), the framework in Khong et al. (2013) was extended to a more generic framework, which in addition to gradient-based optimization algorithms, also encompasses sampling-based (global) optimization methods capable of non-convex optimiza-

tion, enabling extremum seeking for an even wider class of problems. For example, in Khong et al. (2013a) and Nešić et al. (2013), two sampling-based algorithms are presented that are able to achieve (a weaker type of) convergence to a global optimum.

Most extremum-seeking approaches, whether it is of the continuous-time type as in Krstić and Wang (2000) or the sampled-data type as in Teel and Popović (2001) and Khong et al. (2013), focus solely on the problem of finding the extremum of some unknown steady-state input-output map, providing parameter settings that lead to optimal steady-state system performance. However, many industrial applications also have to deal with constraints on operating conditions due to, e.g., actuator limitations, limitations on design or tunable system parameters, or constraints on measurable signals. The constraints on system inputs as a result of the constraints on measurable variables may conflict with the otherwise optimal operational condition, and hence should be taken into account in the data-based optimization approach.

In terms of dealing with constraints in extremum-seeking schemes, existing approaches can be divided into two main categories: i) approaches that assume a-priori knowledge on constrained operating conditions in the form of explicit constraint functions, and ii) approaches that deal with *unknown* but *measurable constraint functions*. Extremum-seeking approaches that explicitly deal with known constraint functions are considered in, e.g., Tan et al. (2013), DeHaan and Guay (2005), andMills and Krstić (2014). In Tan et al. (2013) and DeHaan and Guay (2005), penalty/barrier functions are employed to adapt the search space so as not to violate the constraints. Another approach proposed in Tan et al. (2013) employs an anti-windup scheme to prevent the optimizer from leaving the known admissible search space. Anti-windup schemes have been applied in, e.g., handling actuator saturation in the optimization of energy efficiency in heating, ventilating, and air conditioning systems (Mu et al., 2016; Li et al., 2010). In Mills and Krstić (2014), constraint satisfaction is achieved by employing a projection operator in the extremum-seeking scheme. Although not aimed at constrained optimization, the sampling-based algorithms in Khong et al. (2013a) and Nešić et al. (2013) operate in an a-priori defined compact (input) set, i.e., these allow incorporation of *known* (input) constraints to adjust the search space.

Extremum-seeking approaches for (strictly) convex optimization problems with unknown but measurable constraint functions are considered in, e.g., Srinivasan et al. (2008), Guay et al. (2015), Labar et al. (2019), Atta et al. (2019), Dürr et al. (2013), van der Weijst et al. (2019), Ramos et al. (2017) and Liao et al. (2019), albeit in the continuous-time extremum-seeking setting. In Srinivasan et al. (2008), Labar et al. (2019), and Guay et al. (2015), a combined barrier/penalty function approach is employed to transform the constrained optimization problem into an unconstrained problem using an augmented cost. The methods allow small violations of the constraints (during transients) to avoid dif-

ficulties in practical applications, e.g., due to the presence of uncertainty and disturbances, or to relax the choice of initial, possibly inadmissible, inputs. Optimization is accomplished by estimation of the gradient of the augmented cost and a gradient-based optimization algorithm. In Dürr et al. (2013), a combination of the classical extremum-seeking approach as in Krstić and Wang (2000) and so-called saddle point algorithms as in Dürr and Ebenbauer (2011) are used to find the constrained minimizer. In van der Weijst et al. (2019), Atta et al. (2019), Ramos et al. (2017) and Liao et al. (2019), gradient-based extremum-seeking approaches are employed that combines the gradients of the objective function and the constraint functions to deal with measurable constraints. In van der Weijst et al. (2019), Ramos et al. (2017) and Liao et al. (2019), a so-called transition function is designed that enables a gradient-based optimizer to switch smoothly between the gradient of the to-be-optimized objective function, typically when constraints are not violated, and the gradient of the constraint functions when the constraints are violated. In van der Weijst et al. (2019), this method has been experimentally validated for optimization of fuel efficiency in combustion engines with constraints on emission of NOx particles. In Atta et al. (2019), a projection operator is employed that finds a feasible direction without constraint violation.

In this chapter, we focus on sampled-data extremum-seeking schemes as in Teel and Popović (2001), as opposed to continuous-time extremum-seeking schemes as in Krstić and Wang (2000). Namely, sampled-data schemes are compelling given the potential of including diverse types of optimization algorithms, see, e.g., Teel and Popović (2001), Teel (2000), Khong et al. (2013b) and Teel (2000). In particular, the main focus of this chapter is the extension we provide to the class of smooth and nonsmooth optimization algorithms in Teel and Popović (2001) to achieve extremum-seeking in the presence of unknown but measurable constraints by employing barrier function methods as presented. Moreover, we solve the problem of finding optimal system inputs for which (steady-state) constraint satisfaction can only be assessed on the basis of measurable constraint functions.

The main contributions of this chapter can be summarized as follows. The first contribution is the extension of the class of optimization problems as studied in Teel and Popović (2001) to a class of constrained optimization problems, for which we consider a class of dynamical systems where both a to-be-optimized objective function and constraint functions are available through measurement only. The second contribution is the extension of the class of smooth and nonsmooth optimization algorithms as studied in Teel and Popović (2001) to facilitate extremum-seeking in the presence of unknown but measurable constraints by employing barrier function methods. The third contribution is to 1) provide a closed-loop stability analysis of the interconnection between the class of dynamical systems and the proposed class of constrained optimization algorithms. 2) show strict constraint satisfaction for all iterations of the optimization process,

and 3) show that constrained optimization is achieved. The fourth contribution is an illustration of the working principle of the proposed framework by means of a representative industrial case study of the constrained optimization of extreme ultraviolet (EUV) light generation in a laser produced plasma (LPP) source within a state-of-the-art lithography system.

The chapter is organized as follows. Section 4.2 presents the class of dynamical systems and the constrained optimization problem formulation. Section 4.3 presents the class of extremum seeking algorithms to facilitate constrained optimization. In Section 4.4, a closed-loop stability analysis is provided. Section 4.5 presents the industrial case study. Section 4.6 closes with conclusions.

We use the following notations:

- A function $\gamma : \mathbb{R}_{\geq 0} \to \mathbb{R}_{\geq 0}$ is of class $\mathcal{K}$ (denoted as $\gamma \in \mathcal{K}$) if it is continuous, strictly increasing, and $\gamma(0) = 0$. If γ is also unbounded, then $\gamma \in \mathcal{K}_\infty$.
- A continuous function $\beta : \mathbb{R}_{\geq 0} \times \mathbb{R}_{\geq 0} \to \mathbb{R}_{\geq 0}$ is of class $\mathcal{KL}$, if, for each fixed t, $\beta(\cdot, t) \in \mathcal{K}$ and, for each s, $\beta(s, \cdot)$ is decreasing to zero.
- Let $\mathcal{X}$ be a Banach space whose norm is denoted by $\|\cdot\|$. Given any subset $\mathcal{Y}$ of $\mathcal{X}$, i.e. $\mathcal{Y} \subset \mathcal{X}$, and a point $x \in \mathcal{X}$, the distance of x from $\mathcal{Y}$ is defined as $\|x\|_{\mathcal{Y}} := \inf_{a \in \mathcal{Y}} \|x - a\|$.
- $\mathcal{A} + \epsilon\bar{\mathcal{B}}$ is an ϵ-neighborhood of $\mathcal{A}$, and $\bar{\mathcal{B}}$ can be identified with the closed unit ball.
- We use the following simplified notation for discrete systems, e.g., $u_{k+1} \in F(u_k) \to u^+ \in F(u)$.
- Let $\lfloor \cdot \rfloor$ denote the floor operator.
- The function $\mathrm{id}(\cdot)$ denotes the identity function.

4.2 Class of dynamical systems and constrained optimization problem formulation

In this section, we introduce the class of nonlinear, possibly infinite-dimensional, systems having multiple measurable outputs. In particular, we consider system outputs that are related to 1) a measurable (to-be-optimized) cost and 2) measurable constraints. Depending on the output constraints at hand, parameter settings that optimize the measurable cost may not satisfy the output constraints. Therefore, this section introduces the constrained optimization problem for that class of systems.

4.2.1 Class of dynamical systems

The following definition of the class of systems is based on the ones from Teel and Popović (2001) and Khong et al. (2013b).

Definition 4.1. *The dynamical system Σ_p is time-invariant, with state $x \in \mathcal{X}$, where $\mathcal{X}$ is a Banach space with norm $\|\cdot\|$. The input to the system is denoted by $u \in \mathbb{R}^{n_u}$. We consider the system to have $n_z + 1$ measurable outputs, separated into two channels, denoted by $y \in \mathbb{R}$, and $z \in \mathbb{R}^{n_z}$, and referred to as the cost output and the constraint outputs, respectively. Given any constant input $u \in \mathbb{R}^{n_u}$ and initial state $x_0 \in \mathcal{X}$, let $x(\cdot, x_0, u)$ be the state trajectory of the dynamical system starting at x_0 with input u. Let $\mathcal{S}(x_0, u)$ be the set of all possible trajectories starting at x_0 and with constant input u.*

In the context of ESC, Σ_p in Definition 4.1 represents the dynamical system to-be optimized, where the input u can be regarded as a vector of tunable system parameters, and the outputs y and z can be regarded as a measurable performance variable and a vector of measurable constrained variables, respectively. The following assumption states properties that the class of systems described in Definition 4.1 must possess, and is largely aligned with the assumptions in Teel and Popović (2001, Assumption 1) and Khong et al. (2013b, Assumption 2).

Assumption 4.2. *Given a system Σ_p described by Definition 4.1, we assume that the following properties hold:*

- *For each constant input u the system's trajectory converges to a uniquely defined attractor, i.e., for each constant input $u \in \mathcal{T} \subseteq \mathbb{R}^{n_u}$, with $\mathcal{T}$ a nonempty (and possibly unknown) set, there exists only one, closed and nonempty set $\mathcal{A}(u) \subset \mathcal{X}$, such that*

$$\lim_{t \to \infty} \|x(t, x_0, u)\|_{\mathcal{A}(u)} = 0. \tag{4.1}$$

  This defines a set-valued mapping $\mathcal{A}(\cdot)$ from $\mathcal{T}$ to subsets of $\mathcal{X}$.

- *There exist (unknown) continuous functions $h : \mathcal{X} \to \mathbb{R}$ and $g : \mathcal{X} \to \mathbb{R}^{n_z}$ that map the state evolution $x(\cdot, x_0, u)$ of the system, starting at $x_0 \in \mathcal{X}$ with constant input $u \in \mathcal{T}$, to the evolution of output channels y and z of the system, as follows:*

$$y(t) := h(x(t, x_0, u)) \quad \forall\ t \geq 0, \tag{4.2}$$

  and

$$z(t) := g(x(t, x_0, u)) \quad \forall\ t \geq 0, \tag{4.3}$$

  which are defined for any input $u \in \mathcal{T}$ and $x_0 \in \mathcal{X}$. Moreover, for any $x_1, x_2 \in \mathcal{A}(u)$, it is assumed that $h(x_1) = h(x_2)$ and $g(x_1) = g(x_2)$. Since the set-valued mapping $\mathcal{A}(u)$ is a uniquely defined attractor for any $x \in \mathcal{S}(x_0, u)$, and both h and g are continuous, for any constant $u \in \mathcal{T}$ and $x_0 \in \mathcal{X}$, we have that

$$Q(u) := \lim_{t \to \infty} h(x(t, x_0, u)) \tag{4.4}$$

and

$$G(u) := \lim_{t\to\infty} g(x(t, x_0, u)) \tag{4.5}$$

for some $x_l \in \mathcal{A}(u)$, which are well-defined (unknown) steady-state input-output maps on $\mathcal{T}$.

- *We assume the (unknown) steady-state input-output mappings Q and G to be locally Lipschitz on $\mathcal{T}$.*
- *For any $\epsilon_1, \epsilon_2, \Delta_{\mathcal{X}_0} \in \mathbb{R}_{>0}$, there exists a so-called waiting time $T > 0$ such that*

$$\|x(t, x_0, u)\|_{\mathcal{A}(u)} \leq \epsilon_1 \|x_0\|_{\mathcal{A}(u)} + \epsilon_2, \tag{4.6}$$

for all $t \geq T$, all constant $u \in \mathcal{T}$, and all $\|x_0\|_{\mathcal{A}(u)} \leq \Delta_{\mathcal{X}_0}$.

4.2.2 Constrained optimization problem formulation

The steady-state input-output mappings Q and G as defined in Assumption 4.2 represent the (unknown) steady-state cost function and the steady-state constraint functions of the plant Σ_p, respectively. Based on these steady-state input-output mappings, we can formulate the steady-state *constrained* optimization problem as follows:

$$\begin{aligned} &\min_{u\in\mathcal{T}} Q(u) \\ &\text{subject to } G(u) \leq 0. \end{aligned} \tag{4.7}$$

For the existence of a solution to the constrained optimization problem in (4.7) and the ability to find this solution, we adopt the following assumption.

Assumption 4.3. *The nonempty (and possibly unknown) set $\mathcal{T}$ in Assumption 4.2 is defined as $\mathcal{T} := \{u \in \mathbb{R}^{n_u} \mid G(u) \leq 0\}$. We call the set $\mathcal{T}$ the* admissible set. *The steady-state input-output mapping Q takes its (global) constrained minimum value in a nonempty, compact set $\mathcal{C}_\mathcal{T} \subset \mathcal{T}$, i.e., there exist system inputs $u^* \in \mathcal{C}_\mathcal{T} \subset \mathcal{T}$ such that for all $u \in \mathcal{T}$, $Q(u) \geq Q(u^*)$. In addition, there exists an admissible initialization set $\mathcal{V}$, which is a nonempty,* known *compact subset of $\mathcal{T}$.*

Remark 4.4. *First, Assumption 4.3 states that there exist some system input that solves the constrained optimization problem in* (4.7)*. This assumption requires that the optimization problem is well-defined. Second, Assumption 4.3 states that we have some limited knowledge about the admissible set $\mathcal{T}$, namely, the known admissible initialization set $\mathcal{V}$, such that we can initialize well within this admissible set. This is a reasonable assumption in practice since we usually have some knowledge about where we can initialize our system without violating the constraints immediately. For example, this assumption is satisfied in our industrial case study in Section 4.5.*

In this work, we will solve the steady-state constrained optimization problem in (4.7) by finding a near-optimal system input u^* for the class of dynamical systems as in Definition 4.1, which satisfies Assumptions 4.2, and 4.3, i.e., we will solve the problem by finding a near-optimal system input for which constraint satisfaction ($G(u) \leq 0$) is achieved in steady-state, and which can only be assessed on the basis of measurable constraint functions. Thereto, in the next section we will present a class of algorithms that exploits barrier function methods and that provides an arbitrarily close solution to the constrained optimization problem in (4.7), based on output measurements y and z, and generated by the system in Definition 4.1.

Remark 4.5. *Examples of often studied dynamical systems in the extremum-seeking literature are, for example, dynamical systems with steady-state equilibria, see, e.g., Krstić and Wang (2000), Tan et al. (2006), and dynamical systems with periodically time-varying steady-state responses, see, e.g., Haring et al. (2013). The presented class of systems covers these examples in the presence of multiple measurable outputs, in which one output is related to a to-be-optimized measurable cost and all other outputs are related to measurable constraint functions.*

4.3 Class of extremum-seeking algorithms for constrained optimization problems using barrier function methods

In this section, firstly, we discuss classical barrier function methods to address constrained optimization problems of the form in (4.7), see, e.g., Fiacco and McCormick (1968). Secondly, in the spirit of the class of algorithms for unconstrained optimization problems presented in Teel and Popović (2001), we introduce a mathematical description of a class of algorithms that enables constrained optimization by means of barrier function methods.

4.3.1 Constrained optimization using barrier function methods

The barrier function method is a well-known approach to address constrained optimization problems. Namely, it allows to approximate constrained optimization problems of the form in (4.7) by an unconstrained *modified* optimization problem. The approximation of the actual constrained optimization problem can be attributed to the nature of the barrier function method. In particular, barrier functions establish a barrier on the boundary of the admissible set $\mathcal{T}$, thereby preventing any optimization algorithm that starts well within the admissible set to reach the boundary of the admissible set. We adopt the following definition.

Definition 4.6. *Let $\mathcal{T}$ be the admissible set as defined in Assumption 4.3. Let $\mathcal{T}^o$ and $\partial\mathcal{T}$ denote the interior and the boundary of the admissible set $\mathcal{T}$, re-*

spectively. For each $\mu \in \mathbb{R}_{>0}$, called the barrier parameter, a barrier function $B : \mathcal{T}^o \times \mathbb{R}_{>0} \to \mathbb{R}$, is defined on $\mathcal{T}^o$ such that

- *$B(u, \mu)$ is continuous for $u \in \mathcal{T}^o$ and $\mu \in \mathbb{R}_{>0}$,*
- *$B(u, \mu) \to 0$ for $u \in \mathcal{T}^o$ and $\mu \to 0$,*
- *$B(u, \mu) \to \infty$ for $\|u\|_{\partial\mathcal{T}} \to 0$ and $\mu \in \mathbb{R}_{>0}$.*

Barrier functions that satisfy Definition 4.6 are, for example, the so-called logarithmic barrier function, given by

$$B(u, \mu) = -\mu \sum_{i=1}^{n_z} \log(-G_i(u)), \tag{4.8}$$

and the so-called inverse barrier function, given by

$$B(u, \mu) = -\mu \sum_{i=1}^{n_z} \frac{1}{G_i(u)}, \tag{4.9}$$

where the barrier parameter μ is usually taken sufficiently small, and G_i denotes the ith element of the constraint functions G.

By exploiting barrier functions as defined in Definition 4.6, we can approximate the constrained optimization problem in (4.7) by the following unconstrained modified optimization problem:

$$\min_{u \in \mathcal{T}^o} \tilde{Q}(u, \mu), \tag{4.10}$$

with $\tilde{Q}(u, \mu) := Q(u) + B(u, \mu)$ the so-called modified objective function. We call the solution to (4.10) an *approximate minimizer*, where $\tilde{\mathcal{C}}_{\mathcal{T}}$ denotes the set of approximate minimizers, i.e., for any $\mu \in \mathbb{R}_{>0}$ there exist system inputs $u^* \in \tilde{\mathcal{C}}_{\mathcal{T}} \subset \mathcal{T}^o$ such that for all $u \in \mathcal{T}^o$, $\tilde{Q}(u, \mu) \geq \tilde{Q}(u^*, \mu)$. The fact that, for constrained optimization problems, a barrier function method only provides approximate solutions is particulary evident in cases where solutions to the actual constrained optimization problem in (4.7) are located on the boundary of the admissible set $\partial\mathcal{T}$, i.e., when the intersection of the boundary of the admissible set and the set of exact minimizers is nonempty, i.e., $\partial\mathcal{T} \cap \mathcal{C}_{\mathcal{T}}$ is nonempty. Namely, in cases where optimization algorithms employ barrier functions, we have that the boundary of the admissible set and the set of approximate minimizers do not intersect, i.e., $\partial\mathcal{T} \cap \tilde{\mathcal{C}}_{\mathcal{T}} = \emptyset$. Nevertheless, we would like to stress that, in practice, the set of approximate minimizers $\tilde{\mathcal{C}}_{\mathcal{T}}$ can be made arbitrarily close to the actual set of minimizers $\mathcal{C}_{\mathcal{T}}$ by having a sufficiently small barrier parameter μ. Namely, for a sufficiently small $\mu \in \mathbb{R}_{>0}$ and $u \in \mathcal{T}^o$, from Definition 4.6 it follows that $B(u, \mu) \approx 0$, and thus $\tilde{Q}(u, \mu) \approx Q(u)$. Next, we will mathematically describe the class of algorithms that enables constrained optimization by means of barrier function methods.

4.3.2 Characterization of constrained optimization algorithms

In this section, we introduce a class of algorithms, inspired by barrier function methods, and designed to induce convergence to the set of approximate minimizers $\tilde{\mathcal{C}}_{\mathcal{T}}$. The class of algorithms that is described here is based on *exact* evaluation of the steady-state input-output mappings Q and G in (4.4) and (4.5), respectively, that is, the outputs y and z are not affected by system dynamics, leading to exact evaluation of the steady-state system performance Q and steady-state constraint functions G, respectively. Moreover, we consider the evaluation of Q and G for a particular input u to be readily available. Later in Section 4.4, we will show how to exploit the introduced class of algorithms in an extremum-seeking control context, in which 1) the evaluation of the steady-state input-output mappings Q and G is obtained sequentially, and 2) the output measurements are affected by (transient) dynamical behavior of the system. Therein, we consider the steady-state system performance Q and steady-state constraint functions G to be available approximately only through measurable outputs y and z.

Let us consider optimization algorithms described by the following difference inclusion (see also, e.g., Teel and Popović (2001)):

$$\Sigma : \qquad u^+ \in F(u, Y(u), Z(u)), \tag{4.11}$$

where $F : \mathbb{R}^{n_u} \times \mathbb{R}^{n_v} \times \mathbb{R}^{n_v \times n_z} \to \mathbb{R}^{n_u}$ is a set-valued map for which the update u^+ can be any element of the set, the function $Y \in \mathbb{R}^{n_v}$ contains all information regarding (the gradient of) the cost near u, and the function $Z \in \mathbb{R}^{n_v \times n_z}$ carries all information about (the gradient of) the constraint functions near u. In particular, Y and Z are respectively defined as follows:

$$Y(u) := \begin{bmatrix} Q(u + v_1(u)) \\ \vdots \\ Q(u + v_{n_v}(u)) \end{bmatrix}, \tag{4.12}$$

and

$$Z(u) := \begin{bmatrix} G_1(u + v_1(u)) & \dots & G_{n_z}(u + v_1(u)) \\ \vdots & \ddots & \vdots \\ G_1(u + v_{n_v}(u)) & \dots & G_{n_z}(u + v_{n_v}(u)) \end{bmatrix}, \tag{4.13}$$

where v_j, with $j = 1, \dots, n_v$, are dither functions, $Q(\cdot)$ and $G(\cdot)$ are the steady-state input-output maps from Assumption 4.2, and G_i denotes the ith element of G. We will adopt the following assumption on optimization algorithms as in (4.11)-(4.13), which can be seen as a generalization of the assumptions on the class of algorithms used in Teel and Popović (2001).

Assumption 4.7. *Let $\mathcal{T}$ be the admissible set as defined in Assumption 4.3, with $\mathcal{T}^o$ and $\partial\mathcal{T}$ the interior and the boundary of the admissible set $\mathcal{T}$, respectively. Let $\tilde{\mathcal{C}}_{\mathcal{T}}$ be the set of approximate constrained minimizers. Let us adopt the following assumption:*

- *For each input $u \in \mathcal{T}^o$, the set $F(u, Y(u), Z(u))$ in (4.11) is nonempty and compact. Moreover, the set F is an upper semi-continuous function of u.*
- *We assume that there exist a locally Lipschitz function $V_\Sigma : \mathbb{R}^{n_u} \to \mathbb{R}_{\geq 0}$, which is radially unbounded on the admissible set $\mathcal{T}$, a nonnegative constant $\delta \in \mathbb{R}_{\geq 0}$, and $\mathcal{K}_\infty$-functions $\alpha(\cdot)$ and $\rho(\cdot)$, such that*

$$\begin{aligned} V_\Sigma(u) &= 0 && \forall\ u \in \tilde{\mathcal{C}}_{\mathcal{T}}, \\ \alpha(\|u\|_{\tilde{\mathcal{C}}_{\mathcal{T}}}) \leq V_\Sigma(u) & && \forall\ u \in \mathcal{T}^o, \\ V_\Sigma(u) &\to \infty && \text{for } \|u\|_{\partial\mathcal{T}} \to 0, \end{aligned} \tag{4.14}$$

and

$$\max_{w \in F(u,Y(u),Z(u))} V_\Sigma(w) - V_\Sigma(u) \leq -\rho(V_\Sigma(u)) + \delta \quad \forall\ u \in \mathcal{T}^o. \tag{4.15}$$

- *We assume that the constant $\delta \in \mathbb{R}_{\geq 0}$ can be made arbitrarily small by tuning the parameters of the optimization algorithm F in (4.11).*

Remark 4.8. *The existence of a function V_Σ satisfying the associated conditions stated in Assumption 4.7 are motivated by converse Lyapunov theorems for stability of discrete-time systems on arbitrary sets, see, e.g., Teel, A.R. and Praly, L. (2000), Kellett and Teel (2004), Kellett (2015). Moreover, radial unboundedness of V_Σ on the admissible set $\mathcal{T}$ is motivated by the use of barrier functions in the constrained optimization problem. Also note that the first and third condition in (4.14) imply that the set of approximate minimizers $\tilde{\mathcal{C}}_{\mathcal{T}}$ and the boundary of the admissible set $\partial\mathcal{T}$ do not intersect.*

Remark 4.9. *In Assumption 4.7, the size of the nonnegative constant δ in (4.15) can typically be influenced by tunable parameters of the optimization algorithm F described by the class of algorithms in (4.11)-(4.13). To motivate this further, consider, for example, the minimization of a convex and differentiable function $\tilde{Q}(u)$ on $\mathcal{T}^o$, with $\tilde{Q}(u) \to \infty$ for $\|u\|_{\partial\mathcal{T}} \to 0$. Moreover, for any $u \in \bar{\mathcal{T}}$, with $\bar{\mathcal{T}}$ a strict subset of $\mathcal{T}^o$, suppose there exists an $M > 0$ such that $\|\nabla^2 \tilde{Q}(u)\| \leq M$ for all $u \in \bar{\mathcal{T}}$. Let us employ, a gradient descent optimization algorithm F for which the gradient is estimated based on a central difference scheme and exact evaluation of the function $\tilde{Q}$ as follows:*

$$F(u, Y(u), Z(u)) := u - \lambda \left(\frac{\tilde{Q}(u + c_v) - \tilde{Q}(u - c_v)}{2c_v} \right), \tag{4.16}$$

with $c_v, \lambda \in \mathbb{R}_{>0}$. *Let us take function* $V_\Sigma(u) := \tilde{Q}(u) - \tilde{Q}(u^*)$, *with* u^* *the extremum for which it holds that* $\nabla\tilde{Q}(u^*) = 0$. *This* $V_\Sigma(u)$ *satisfies the conditions in* (4.14). *With this* $V_\Sigma(u)$, *we obtain the following for the condition in* (4.15)*:*

$$\begin{aligned} V_\Sigma(u^+) - V_\Sigma(u) &= \tilde{Q}(u^+) - \tilde{Q}(u) \\ &\leq \nabla\tilde{Q}(u)(u^+ - u) + \frac{M}{2}\|u^+ - u\|^2 \\ &\leq -\lambda(\nabla V_\Sigma(u))^2 + \delta, \end{aligned} \tag{4.17}$$

with $\delta := M^3\lambda^2 c_v^2$, $\lambda \in (0, \frac{1}{M})$. *The constant* δ *can be made arbitrarily small by selecting sufficiently small* λ *and* c_v.

In the next section, we will analyze the dynamic behavior of the interconnection of a dynamical system described in Definition 4.1, and an optimization algorithm of the form in (4.11)-(4.13) in an online extremum-seeking control implementation.

4.4 Stability of the interconnected class of dynamical systems and a class of constrained extremum seeking algorithms

In this section, we aim to investigate the dynamic behavior of a discrete-time system that describes the closed-loop feedback interconnection of the class of dynamical systems from Section 4.2, denoted by Σ_p, and the class of algorithms discussed in Section 4.3, denoted by Σ, in an extremum-seeking context. In particular, we consider the interconnection of a dynamical system Σ_p and an optimization algorithm Σ through a T-periodic sampler, and a zero-order-hold (ZOH) element, see Fig. 4.1.

We analyze the dynamic behavior of the closed-loop feedback interconnection in the case where the elements of the functions Y and Z in (4.12) and (4.13), respectively, 1) can only be obtained sequentially by performing n_v experiments and evaluating the steady-state input-output mappings Q and G after each experiment, and 2) can only be based on (periodically) sampling the outputs y and z, providing mere approximations of the steady-state input-output mappings Q and G, respectively.

Next, we describe the extremum-seeking algorithm performing n_v experiments to realize one update of the system input u, based on a so-called waiting time T that prescribes the duration of each experiment, and on approximations of the steady-state input-output mappings Q and G obtained via the collection of the corresponding output measurements each T seconds.

Algorithm 4.10. *Suppose that the waiting time* T, *the number of experiments* n_v *to realize one iteration of the optimization algorithm, and the initial algorithm state* u_0 *are specified. Let us define the ideal periodic sampling operation* $x_i :=$

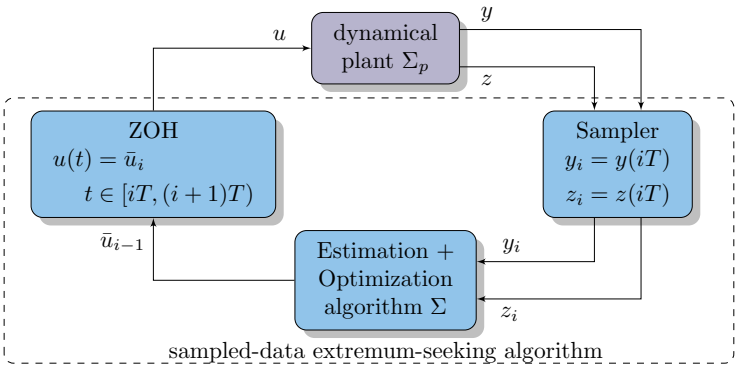

Figure 4.1: Sampled-data extremum-seeking control framework with multiple output channels.

$x(iT)$:

$$y_i := y(iT) \quad \forall\ i = 0, 1, ..., \tag{4.18}$$

and

$$z_i := z(iT) \quad \forall\ i = 0, 1, ..., \tag{4.19}$$

where y_i and z_i are the collected measurements as used by the optimization algorithm, where $i \in \mathbb{N}$ denotes the sampling index. Define the zero-order-hold (ZOH) operation as follows:

$$u(t) := \bar{u}_i \quad \forall\ t \in [iT, (i+1)T), \tag{4.20}$$

with sampling index $i = 0, 1, ...,$, waiting time $T > 0$, and step input parameter $\bar{u}_i$. For sampling index i, the step input parameter $\bar{u}_i$ is determined by the state of the optimization algorithm u_k as follows:

$$\bar{u}_i := u_k + v_{j(i)}(u_k), \quad \forall\ i = 0, 1, ..., \tag{4.21}$$

with $k \in \mathbb{N}$ the optimization algorithm index, u_0 the initial algorithm state, and dither functions $v_{j(i)}$ with $j(i) := (i \bmod n_v) + 1$.

The optimization algorithm index k is related to the sampling index i and number of experiments n_v through $k = \left\lfloor \frac{i}{n_v} \right\rfloor$. The optimization algorithm is characterized by the mapping F given in (4.11), which exploits the collected measurements y_i and z_i:

$$u_{k+1} \in F(u_k, \tilde{Y}(u_k), \tilde{Z}(u_k)), \quad \forall\ k = 0, 1, ..., \tag{4.22}$$

with functions $\tilde{Y}(u_k)$ and $\tilde{Z}(u_k)$ defined as follows:

$$\tilde{Y}(u_k) := \begin{bmatrix} h(x_{kn_v+1}) \\ \vdots \\ h(x_{(k+1)n_v}) \end{bmatrix} = \begin{bmatrix} y_{kn_v+1} \\ \vdots \\ y_{(k+1)n_v} \end{bmatrix}, \tag{4.23}$$

and

$$\tilde{Z}(u_k) := \begin{bmatrix} g_1(x_{kn_v+1}) & \dots & g_{n_z}(x_{kn_v+1}) \\ \vdots & \ddots & \vdots \\ g_1(x_{(k+1)n_v}) & \dots & g_{n_z}(x_{(k+1)n_v}) \end{bmatrix} = \begin{bmatrix} z_{kn_v+1}^\top \\ \vdots \\ z_{(k+1)n_v}^\top \end{bmatrix}, \tag{4.24}$$

which are approximations of the functions $Y(u_k)$ and $Z(u_k)$ in (4.12) *and* (4.13)*, respectively.*

Remark 4.11. *To illustrate the sequence of inputs generated by Algorithm 4.10 for the case $n_v = 3$, consider the initial algorithm state u_0, and the number of experiments $n_v = 3$ to perform one update of the state of the optimization algorithm. The sequence of inputs, the corresponding output measurements, and the algorithm state are provided in Table 4.1.*

Table 4.1: Illustration of a sequence of parameter inputs $\bar{u}_i$ for $t \in [iT, (i+1)T)$ and generated by Algorithm 4.10 for the case $n_v = 3$, the corresponding collected measurements y_i and z_i at $t = iT$, the algorithm state u_k, with $k = \left\lfloor \frac{i}{n_v} \right\rfloor$ and functions $\tilde{Y}(u_k)$ and $\tilde{Z}(u_k)$ defined in (4.23) and (4.24), respectively.

sampling index i	outputs y_i, z_i	parameter input $\bar{u}_i$	algorithm state u_k, $k := \left\lfloor \frac{i}{n_v} \right\rfloor$
0	-	$\bar{u}_0 = u_0 + v_1(u_0)$	u_0 is user-defined
1	y_1, z_1	$\bar{u}_1 = u_0 + v_2(u_0)$	u_0
2	y_2, z_2	$\bar{u}_2 = u_0 + v_3(u_0)$	u_0
3	y_3, z_3	$\bar{u}_3 = u_1 + v_1(u_1)$	$u_1 \in F(u_0, \tilde{Y}(u_0), \tilde{Z}(u_0))$
4	y_4, z_4	$\bar{u}_4 = u_1 + v_2(u_1)$	u_1
5	y_5, z_5	$\bar{u}_5 = u_1 + v_3(u_1)$	u_1
6	y_6, z_6	$\bar{u}_6 = u_2 + v_1(u_2)$	$u_2 \in F(u_1, \tilde{Y}(u_1), \tilde{Z}(u_1))$
$\vdots$	$\vdots$	$\vdots$	$\vdots$

To account for the discrepancy between the steady-state input-output mappings $Q(u)$ and $G(u)$ and the actual measurements y and z, we need the following additional assumption, partially adopted from Teel and Popović (2001).

Assumption 4.12. *For the plant Σ_p described in Definition 4.1, it holds that*

- *for each $\Delta_{\mathcal{U}}, \Delta_{\mathcal{X}} \in \mathbb{R}_{>0}$ there exist $L_H, L_G \in \mathbb{R}_{>0}$ such that, for any input $u \in \mathcal{T}$ with $\|u\|_{\tilde{\mathcal{C}}_{\mathcal{T}}} \leq \Delta_{\mathcal{U}}$, and any $\|x\|_{\mathcal{A}(u)} \leq \Delta_{\mathcal{X}}$, we have the following inequalities:*

$$\|h(x) - Q(u)\| \leq L_H \|x\|_{\mathcal{A}(u)}, \tag{4.25}$$

and

$$\|g(x) - G(u)\| \leq L_G \|x\|_{\mathcal{A}(u)}. \tag{4.26}$$

- *the set-valued map $\mathcal{A}(\cdot)$ is locally Lipschitz; in particular, for each $\Delta_{\mathcal{U}} > 0$, there exists an $L_{\mathcal{A}} > 0$ such that*

$$\max\{\|u_1\|_{\tilde{\mathcal{C}}_{\mathcal{T}}}, \|u_2\|_{\tilde{\mathcal{C}}_{\mathcal{T}}}\} \leq \Delta_{\mathcal{U}} \Rightarrow \mathcal{A}(u_1) \subseteq \mathcal{A}(u_2) + L_{\mathcal{A}}\|u_1 - u_2\|\bar{\mathcal{B}}, \quad (4.27)$$

with $u_1, u_2 \in \mathcal{T}$.

For the optimization algorithm F as described in (4.11) *which satisfies the properties stated in Assumption 4.7, the following assumptions hold:*

- *Take any $u_{\tilde{F}}$ generated by $F(u, \tilde{Y}(u), \tilde{Z}(u))$, and let u_F be its closest point in the set $F(u, Y(u), Z(u))$. Then, for each $\Delta_{\mathcal{U}}, \Delta \in \mathbb{R}_{>0}$, there exist $L_Y, L_Z \in \mathbb{R}_{>0}$ such that for any input $u \in \mathcal{T}^o$ with $\|u\|_{\tilde{\mathcal{C}}_{\mathcal{T}}} \leq \Delta_{\mathcal{U}}$, and $\|\tilde{Y}\|, \|\tilde{Z}\| \leq \Delta$, we have*

$$\|u_{\tilde{F}} - u_F\| \leq L_Y\|\tilde{Y}(u) - Y(u)\| + L_Z\|\tilde{Z}(u) - Z(u)\|. \quad (4.28)$$

- *For the perturbation functions $v_j(\cdot)$ we assume that, for each $\Delta_{\mathcal{U}} \in \mathbb{R}_{>0}$ and for any $u \in \bar{\mathcal{T}}$, with $\bar{\mathcal{T}}$ an arbitrary (large) strict subset of $\mathcal{T}^o$ and $\|u\|_{\tilde{\mathcal{C}}_{\mathcal{T}}} \leq \Delta_{\mathcal{U}}$, there exist (sufficiently small) constants $M_v, c_v \in \mathbb{R}_{\geq 0}$ such that, for each $j = 1, \ldots, n_v$, we have that*

$$\|v_j(u)\| \leq M_v\|u\|_{\tilde{\mathcal{C}}_{\mathcal{T}}} + c_v. \quad (4.29)$$

The next lemma states the outcome of the interconnected discrete-time system after one update of the optimization algorithm, i.e., one sequence of inputs generated by Algorithm 4.10. In particular, define a state $\bar{x}_k := x_{kn_v}$ denoting the state of Σ_p at the beginning of the $(k+1)$th sequence of inputs, where k denotes the optimization algorithm index. The outcome of one sequence of inputs as considered in Lemma 4.13 is an important stepping stone in the proof of Theorem 2.16 to show 1) convergence of the algorithm state u_k to a neighborhood of the set of approximate minimizers $\tilde{\mathcal{C}}_{\mathcal{T}}$ and 2) steady-state constraint satisfaction for all system inputs, over multiple input sequences.

Lemma 4.13. *Suppose that the system Σ_p and the algorithm Σ satisfy Assumptions 4.2, 4.3. 4.7 and 4.12. Let the system Σ_p and algorithm Σ be connected as described in Algorithm 4.10. Then, for any $\epsilon_1 \in (0, 1]$, any $\epsilon_2, \Delta_{\mathcal{X}}, \Delta_{\mathcal{U}} \in \mathbb{R}_{>0}$, and an arbitrary (large) strict subset $\bar{\mathcal{T}} \subset \mathcal{T}^o$, there exists a waiting time $T^* \geq T$, with T as in Assumption 4.2, such that, for any $\bar{x} \in \mathcal{X}$ with $\|\bar{x}\|_{\mathcal{A}(u+v_{n_v}(u))} \leq \Delta_{\mathcal{X}}$ and $u \in \bar{\mathcal{T}}$ with and $\|u\|_{\tilde{\mathcal{C}}_{\mathcal{T}}} \leq \Delta_{\mathcal{U}}$, respectively being the states of the plant and the algorithm at the beginning of the current input sequence, the states of the system and algorithm at the beginning of the next input sequence are given as*

follows:

$$\begin{aligned} u^+ &\in F(u, \tilde{Y}(u), \tilde{Z}(u)) \\ \psi^+ &= u \\ \bar{x}^+ &\in \mathcal{A}(u + v_{n_v}(u)) + \Bigg(\epsilon_1 \Bigg(\|\bar{x}\|_{\mathcal{A}(u+v_{n_v}(u))} \\ &\qquad + L_{\mathcal{A}} \sum_{j=1}^{n_v} \|v_j(u) - v_{j-1}(u)\| \Bigg) + n_v \epsilon_2 \Bigg) \overline{\mathcal{B}}. \end{aligned} \tag{4.30}$$

where ψ is a memory state, $\tilde{Y}(u)$ and $\tilde{Z}(u)$ are given in (4.23), and $v_0(u) := v_{n_v}(u)$.

Proof. *The proof of Lemma 4.13 can be found in Appendix 4.A.* □

For the purpose of the stability analysis let us now define the following function:

$$W(\psi, \bar{x}, u) := V_{\Sigma_p}(\psi, \bar{x}) + 2V_{\Sigma}(u), \tag{4.31}$$

where $V_{\Sigma_p}(\psi, \bar{x}) := \sigma \|\psi\|_{\tilde{\mathcal{C}}_{\mathcal{T}}} + \|\bar{x}\|_{\mathcal{A}(\psi + v_{n_v}(\psi))}$ with some constant $\sigma \in \mathbb{R}_{>0}$. Let us define the following increments:

$$\begin{aligned} \Delta W(\psi, \bar{x}, u) &:= W(\psi^+, \bar{x}^+, u^+) - W(\psi, \bar{x}, u), \\ \Delta V_{\Sigma_p}(\psi, \bar{x}) &:= V_{\Sigma_p}(\psi^+, \bar{x}^+) - V_{\Sigma_p}(\psi, \bar{x}), \\ \Delta V_{\Sigma}(u) &:= V_{\Sigma}(u^+) - V_{\Sigma}(u). \end{aligned} \tag{4.32}$$

The next result states conditions on the initial conditions and parameters of the ESC algorithm (such as the waiting time), such that the system input u converges to an arbitrarily small neighborhood of the set of approximate minimizers $\tilde{\mathcal{C}}_{\mathcal{T}}$, while steady-state constraint satisfaction is guaranteed all along the evolution of the optimization iterations.

Theorem 4.14. *Suppose that the system Σ_p and the algorithm Σ satisfy Assumptions 4.2, 4.3. 4.7 and 4.12. Let the system Σ_p and algorithm Σ be interconnected as described in Algorithm 4.10. For any $u_0, \psi_0 \in \mathcal{V} \subset \bar{\mathcal{T}}$ with $\bar{\mathcal{T}}$ an arbitrary (large) strict subset of $\mathcal{T}^o$ and $\bar{x}_0 \in \mathcal{X}$, with $\|u_0\|_{\tilde{\mathcal{C}}_{\mathcal{T}}} \leq \Delta_{\mathcal{U}}$,$\|\psi_0\|_{\tilde{\mathcal{C}}_{\mathcal{T}}} \leq \Delta_{\mathcal{U}}$, and $\|\bar{x}_0\|_{\mathcal{A}(\psi + v_{n_v}(\psi_0))} \leq \Delta_{\mathcal{X}}$ with some $\Delta_{\mathcal{U}}, \Delta_{\mathcal{X}} \in \mathbb{R}_{>0}$, there exists a sufficiently large waiting time $T^* \geq T$, with T as in Assumption 4.2, and $\mathcal{K}_\infty$-function $\tilde{\gamma}(\cdot)$ such that we obtain the following increment:*

$$\Delta W(\psi, \bar{x}, u) \leq -\tilde{\gamma}(W(\psi, \bar{x}, u)) + 2\delta + \gamma + \delta_V, \tag{4.33}$$

for arbitrarily small $\delta, \gamma \in \mathbb{R}_{>0}$, and any small $\delta_V \in \mathbb{R}_{>0}$. Moreover, there exists $\Delta_W \in \mathbb{R}_{\geq 0}$, $\mathcal{K}_\infty$-function $\hat{\rho}(\cdot)$, and $\mathcal{KL}$-function $\hat{\beta}(\cdot, \cdot)$, such that

$$W(\psi_k, \bar{x}_k, u_k) \leq \max\{\hat{\beta}(W(\psi_0, \bar{x}_0, u_0), k), \tilde{\gamma}^{-1} \circ \hat{\rho}^{-1}(2\delta + \gamma + \delta_V)\}, \tag{4.34}$$

holds for all $k \in \mathbb{N}$*, with* $W(\psi_0, \bar{x}_0, u_0) \leq \Delta_W$*, and for arbitrarily small* $\delta, \gamma \in \mathbb{R}_{>0}$.

As a consequence:

- $V_\Sigma(u_k)$ *is bounded for all* $k \in \mathbb{N}$*, which implies that* $u_k \in \mathcal{T}^o$ *for all* $k \in \mathbb{N}$*, i.e., steady-state constraint satisfaction is guaranteed and*
- *the solutions of the closed-loop system converge to a set* $\mathcal{Y}_u := \{u \in \mathcal{T}^o \mid \|u\|_{\tilde{\mathcal{C}}_\mathcal{T}} \leq \frac{1}{2}\alpha^{-1}\big(\frac{1}{2}\tilde{\gamma}^{-1} \circ \hat{\rho}^{-1}(2\delta + \gamma + \delta_V)\big)\}$*, with* $\alpha \in \mathcal{K}_\infty$ *defined in Assumption 4.7, where this set can be made arbitrarily small.*

Proof. *The proof of Theorem 4.14 can be found in Appendix 4.B.* □

Remark 4.15. *The set* $\mathcal{Y}_u$ *can be made arbitrarily small. Namely, 1)* $\delta_V \in \mathbb{R}_{>0}$ *can be any arbitrarily small constant, 2) we can make* γ *arbitrarily small by choosing a sufficiently large waiting time* $T \in \mathbb{R}_{>0}$*, and 3)* δ*, which is defined in Assumption 4.7, can typically be tuned sufficiently small by tuning the parameters of the optimization algorithm* F *(see also Assumption 4.7 and Remark 4.9).*

Remark 4.16. *Inequality* (4.34) *also expresses a decaying bound on the transient solutions of the closed-loop system. Since* W *expresses both the distance of the plant response to the steady state and the distance of the input* u *to the minimizer in a combined fashion we do not provide a transient bound on these effects individually.*

Remark 4.17. *The result presented in Theorem 4.14 is focused on achieving the optimal input that satisfies the output constraints in steady-state. We emphasize that, under the conditions of Theorem 4.14, constraint satisfaction is also guaranteed during the transients of the extremum seeker if the plant output would be on its steady-state response. Constraint satisfaction on the output responses during the transient of the plant itself is, however, not guaranteed. To accomplish this, additional assumptions on the class of plants would be required. In particular, system properties would need to be defined on compact subsets, and additional assumptions on initial data and on the transient behavior of the plant are required. This extended problem setting is not considered in this work.*

4.5 Industrial case study: Constrained optimization of extreme ultraviolet light generation in a Laser Produced Plasma source system

The semiconductor industry continues to develop lithographic technologies which are able to realize ever-smaller integrated circuit dimensions. Extreme ultraviolet lithography, a next-generation lithography technology, is able to produce sub-nanometer features by exposing substrates, such as silicon wafers, to extreme ultraviolet (EUV) light. The necessary EUV light is typically produced

by a so-called Laser Produced Plasma (LPP) source, which is the most promising approach for providing power output that is scalable to meet the needs of high volume production exposure tools. However, achieving and maintaining optimal EUV light generation is a challenging task. In this section, we provide a description of a typical LPP source and discuss the constrained optimization problem associated to its performance. Moreover, we present a representative LPP source model, and employ the constrained sampled-data extremum-seeking approach proposed in this chapter to achieve optimal EUV light generation.

4.5.1 Laser Produced Plasma source system description

LPP sources produce EUV light by converting a material that has emission lines in the EUV spectrum, e.g., lithium or tin, into a plasma state that ultimately emits the desired EUV photons. Fig. 4.2 schematically depicts a typical LPP source system and its most crucial components: 1) a CO_2 laser generator, 2) a laser beam delivery system, 3) a vacuum chamber, 4) a droplet generator, 5) a spherical mirror, the so-called collector, and 6) an intermediate focus (IF). Inside the vacuum chamber, the EUV-emitting plasma is generated by irradiating droplets of material with a high-energy pulsating CO_2 laser beam. The droplet generator fires small droplets at a rate of 50 kHz into the vacuum chamber. The beam delivery system orients and focusses the high-energy pulsating CO_2 laser beam in such a way that it hits the traveling droplets inside the vacuum chamber. If the droplets are hit correctly, EUV photons are generated by the irradiated material, reflected by the collector, and transmitted towards the IF. Here, the transmitted EUV photons enter the EUV lithography scanner and enable the patterning of sub-nanometer features on a silicon wafer.

To cope with the various losses of EUV intensity within the lithography scanner, and still enable patterning of sub-nanometer features on a silicon wafer using the lithography scanner, the EUV light generated by the light source needs to be maximized. The intensity of the generated EUV light highly depends on the position of the laser beam with respect to the droplet. Due to the complex (plasma) physics involved, the complex interactions between the droplets, laser and plasma, and the difficulty of accurately measuring the position of the laser beam relative to the droplet (amongst other challenges), models of the LPP system based on first-principles tend to be inaccurate in describing the actual system behavior. As such, employing the optimal laser position obtained from such a first principle model on the actual system is likely to yield sub-optimal EUV intensity. Instead, data-based methods such as ESC can be employed to adjust the laser position in y- and z-direction (see Fig. 4.2) in real-time to optimize the EUV intensity, based on real-time measurements of the EUV intensity.

[1]The image is acquired from https://www.asml.com/en/investors/financial-calendar/past-events-and-presentations, June 24th 2019 UBS Investor Forum presentation

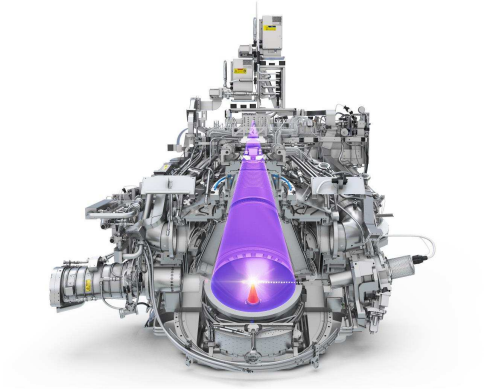

(a) Artist impression[1]

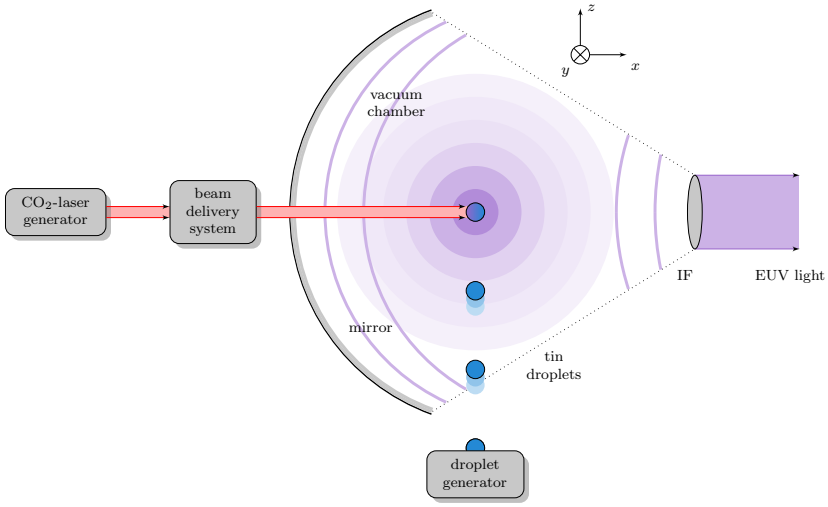

(b) Schematic representation of an LPP source system with the laser-to-droplet (L2D) relative coordinate frame

Figure 4.2: EUV light source system within ASML's lithography system.

Optimizing average EUV light generation using classical (continuous-time, unconstrained) ESC was proposed in Frihauf et al. (2013). That approach, however, does not take into account any (unknown) disturbances, which can lead to undesirably high peak-to-peak variations in the generated EUV intensity for certain laser orientations. In addition, laser light that is being reflected back to the CO_2 laser generator itself, referred to as the back-reflection and

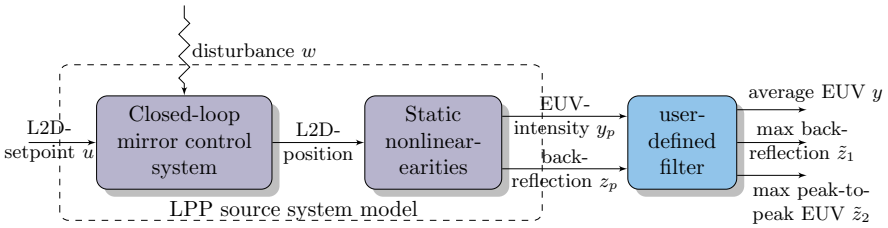

Figure 4.3: Model of the LPP source system.

which is continuously being monitored, can damage the LPP source if it exceeds some threshold value. The conventional approach would be to shut down the machine to prevent excessive damage, and perform a time-consuming and costly re-calibration procedure. Therefore, we employ the developed constrained sampled-data extremum-seeking control strategy to maximize the average EUV intensity while avoiding 1) large variations of EUV intensity, and 2) excessive back-reflection.

4.5.2 Laser Produced Plasma source model

The LPP system under study is modelled[1] by a linear-time-invariant (LTI) dynamical system, representing a closed-loop mirror control system (modelling the beam delivery system in Fig 4.2), followed by an experimentally obtained static nonlinear model for the effect of the laser positioning on the EUV intensity and the laser back reflection (capturing the complex plasma physics of the source). We emphasize that especially the latter part of the model is typically hard (and time-consuming) to obtain in practice, which motivates the use of a data-based approach such as ESC for performance optimization. Here, we employ such experimentally obtained model in support of the simulation study. Finally, and user-defined filters are included to obtain as measured outputs the average EUV intensity, the peak-to-peak EUV intensity, and the laser back reflection signal to be used as input for the extremum-seeking controller, see Fig. 4.3 for a schematic overview of the model.

Closed-loop mirror control system

The closed-loop mirror control system basically comprises the laser orientation part of the beam delivery system of the LPP source. The laser orientation part of the beam delivery system consists of (a set of) adjustable mirrors, able to adjust the laser-to-droplet (L2D) positioning in the y- and z-direction on the

[1] to protect the company's interests, a more detailed description of the LPP model than the one presented here, and units of certain variables, are omitted. Moreover, values of variables are normalized or scaled.

basis of a stable feedback control design. The feedback controller uses the L2D-positions, measured indirectly using data obtained through various sensors, and user-defined L2D-setpoints to minimize the L2D-setpoint errors. The closed-loop mirror control system model takes into account laser-droplet interactions, various external (high- and low-frequency) disturbances ranging from $1 \cdot 10^{-3} - 300$ Hz such as, e.g., CO_2-laser variations, interaction with pulsating laser beam and droplets, plasma oscillations in the vacuum chamber, and white noise, that affect the L2D-position measurements. The disturbances are modelled as T_w-periodic external disturbances w which are supplied to the closed-loop mirror control system, with $T_w = 2$ seconds.

Static nonlinearities

The static nonlinearities in the LPP source model provide mappings from the L2D-position to 1) the EUV intensity, denoted by y_p, and 2) the back-reflection, denoted by z_p. These output nonlinearities are experimentally obtained from an industrial LPP source system for the purpose of modelling. Fig. 4.4 depicts the EUV intensity y_p and the back-reflection signal z_p as a function of time for two particular L2D-setpoints, obtained using the simulation model. Due to the T_w-periodic nature of the external disturbances, the measured outputs are T_w-periodic as well.

User-defined filtering

On the basis of the measurable EUV intensity y_p and back-reflection z_p, and the T_w-periodic nature of these outputs, the following filters are defined that determine the average EUV intensity y, the maximum back-reflection signal $\tilde{z}_1$, and the peak-to-peak EUV variation $\tilde{z}_2$ as follows:

$$\begin{aligned} y(t) &:= \frac{1}{T_w} \int_{t-T_w}^{t} y_p(\tau) d\tau, \\ \tilde{z}_1(t) &:= \max_{\tau \in [t-T_w, t)} z_p(\tau), \\ \tilde{z}_2(t) &:= \max_{\tau \in [t-T_w, t)} y_p(\tau) - \min_{\tau \in [t-T_w, t)} y_p(\tau), \end{aligned} \tag{4.35}$$

for all $t \geq T_w$.

4.5.3 Constrained optimization problem formulation

From simulation, steady-state input-output relations between the L2D-setpoints with

$$u := \begin{bmatrix} \text{L2D}_y\text{-setpoint} \\ \text{L2D}_z\text{-setpoint} \end{bmatrix}, \tag{4.36}$$

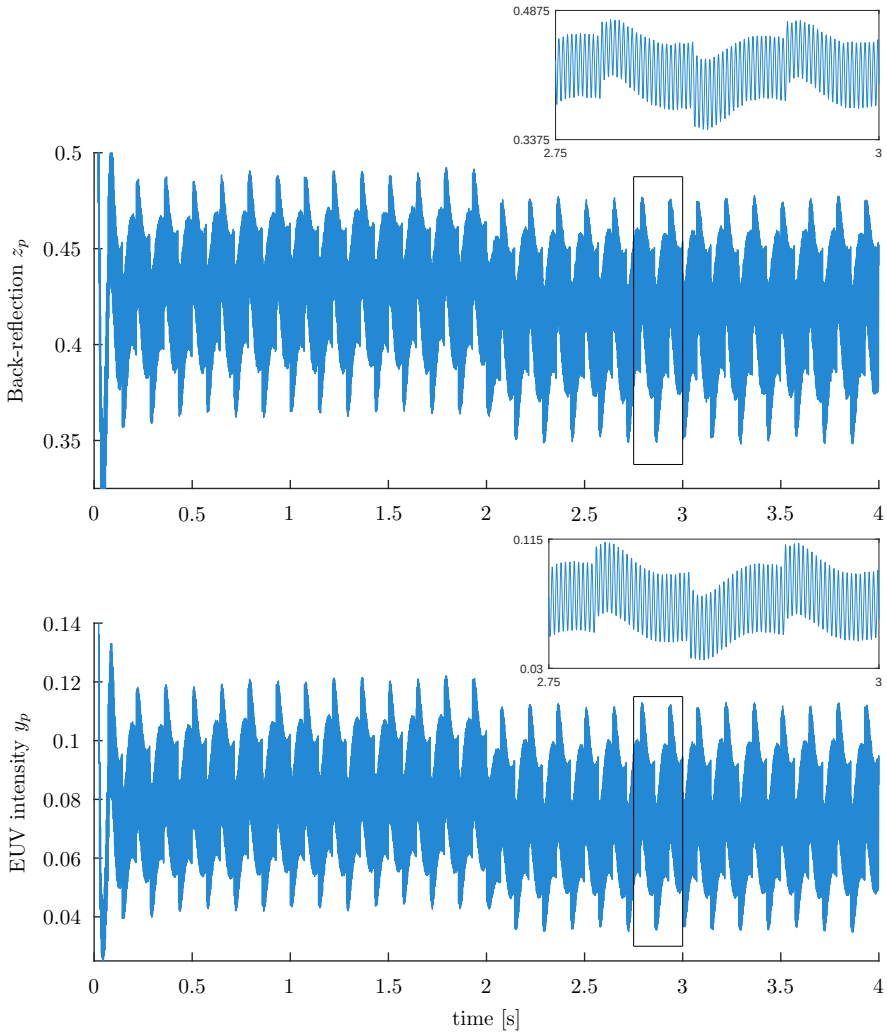

Figure 4.4: The EUV intensity (top) and the back-reflection signal (bottom) as a function of time for two L2D-setpoints; 1) $\text{L2D}_y = -0.225$ [normalized] and $\text{L2D}_z = 0.4$ [normalized] during $t \in [0, 2]$ s, and 2) $\text{L2D}_y = -0.275$ [normalized] and $\text{L2D}_z = 0.4$ [normalized] during $t \in (2, 4]$ s.

and 1) the average EUV intensity y, 2) the maximum back-reflection $\tilde{z}_1$, and 3) the peak-to-peak variations in EUV intensity $\tilde{z}_2$, denoted by $Q(u)$, $\tilde{G}_1(u)$, and $\tilde{G}_2(u)$, can be obtained, and are shown in Figures 4.5, 4.6, 4.7, respectively. Knowledge of these mappings is not exploited in the remainder of this section,

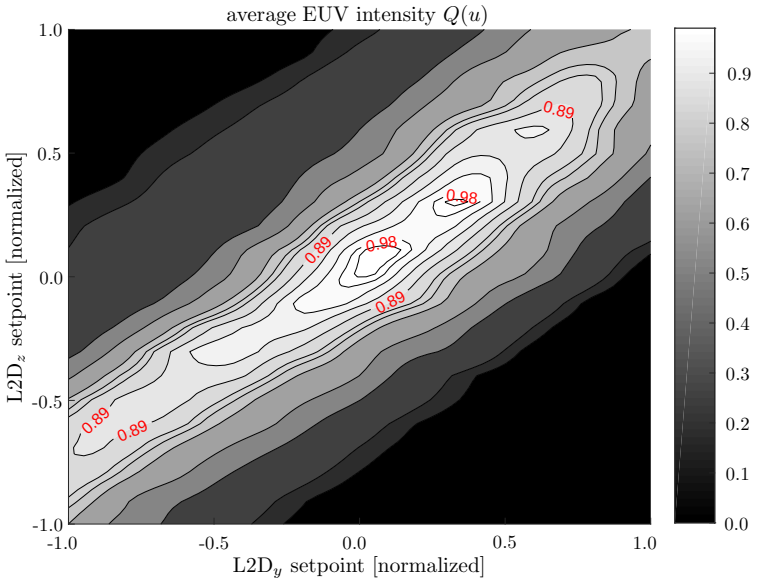

Figure 4.5: Steady-state input-output map from L2D-setpoints to average EUV intensity.

and is presented merely for verification purposes.

From Figures 4.5 to 4.7, it can be that a maximum average EUV intensity is achievable when the L2D-setpoints in y- and z-direction are around zero. In the case when the L2D-setpoints are zero, the maximum back-reflection signal exceeds 0.8, causing excessive damage to the LPP source. This excessive damage can be prevented by keeping the back-reflection signal below a value of $\gamma_{back} = 0.8$. In addition, the peak-to-peak EUV intensity variation is required to remain below $\gamma_{pp} = 0.28$ which guarantees stable EUV light generation for usage in the lithography scanner. To achieve this goal, we formulate the following constrained optimization problem for the LPP source system:

$$\begin{aligned} &\max_{u \in \mathcal{T}} \; Q(u), \\ &\text{subject to } G(u) := \begin{bmatrix} \tilde{G}_1(u) - \gamma_{back} \\ \tilde{G}_2(u) - \gamma_{pp} \end{bmatrix} \leq 0, \end{aligned} \tag{4.37}$$

with $\mathcal{T} := \{u \in \Omega : G(u) \leq 0\}$, and Ω denoting the physical range of the laser-to-droplet position. We assume no knowledge of $Q(u)$ and $G(u)$, and we obtain information on performance and constraint satisfaction only through periodically sampling the outputs $y(t)$ and $z(t)$, where the output $z(t)$ is defined as follows:

$$z(t) := \begin{bmatrix} \tilde{z}_1(t) - \gamma_{back} \\ \tilde{z}_2(t) - \gamma_{pp} \end{bmatrix}. \tag{4.38}$$

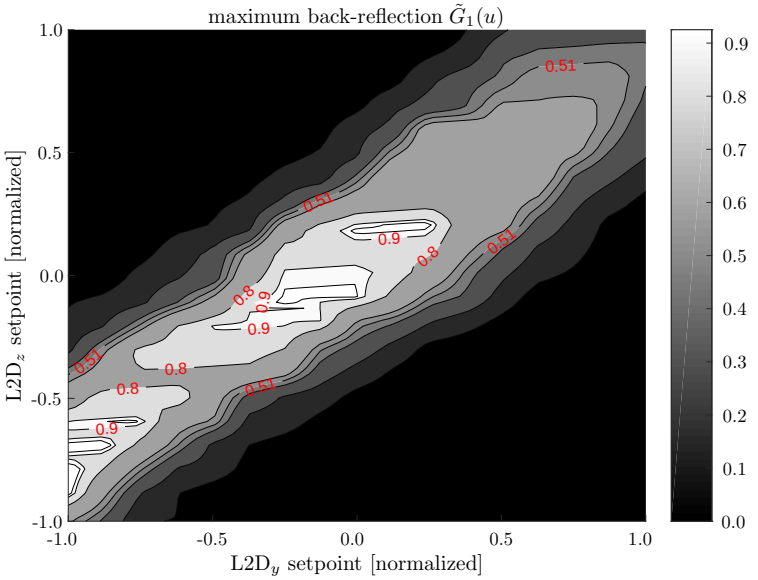

Figure 4.6: Steady-state input-output map from L2D-setpoints to maximum back-reflection.

4.5.4 Gradient-based sampled-data extremum-seeking algorithm with barrier functions

To solve the constrained optimization problem in (4.37), we transform the problem to an unconstrained optimization problem by using logarithmic barrier functions $B(u, \mu)$. The resulting unconstrained optimization problem reads

$$\max_{u \in \mathcal{T}^o} \tilde{Q}(u, \mu) := Q(u) - B(u, \mu), \tag{4.39}$$

with $\tilde{Q}$ the modified objective function, and $\mathcal{T}^o$ denoting the interior of the admissible set $\mathcal{T} = \{u \in \Omega \mid G(u) \leq 0\}$. We employ an extremum-seeking algorithm such as described in Algorithm 4.10, in which we utilize a gradient-based optimization algorithm. The algorithm exploits an estimate of the gradient of the to-be-optimized modified objective function, determined through a central difference computation, and for which we need to perform $n_v = 4$ experiments for each update of the optimization algorithm. A waiting time $T = 2$ seconds is chosen, and $T_w = 2$ seconds is chosen in (4.35).

The gradient-based optimization algorithm F in (4.22) is given as follows:

$$F(u, \tilde{Y}(u), \tilde{Z}(u)) := u + \lambda \nabla \tilde{Q}(u, \mu), \tag{4.40}$$

with so-called optimizer gain λ, and where $\nabla \tilde{Q}(u, \mu)$ denotes the gradient of the modified objective function $\tilde{Q}(u, \mu)$. The actual gradient is unknown

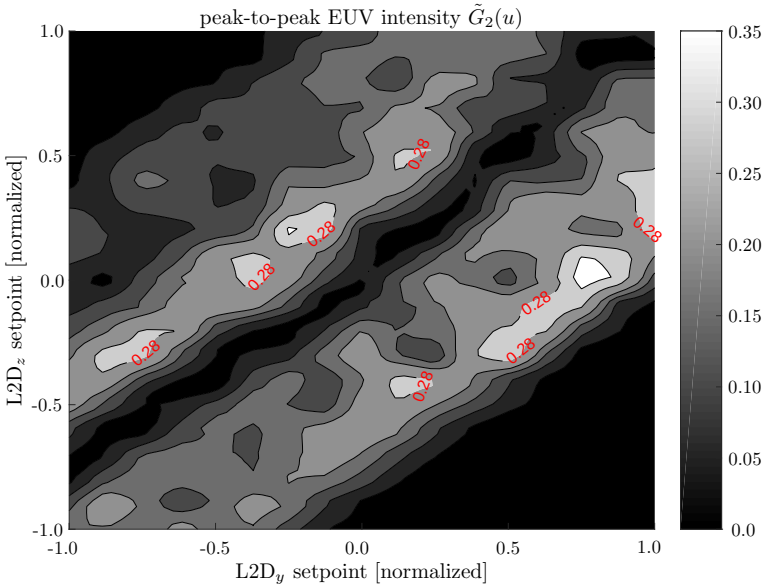

Figure 4.7: Steady-state input-output map from L2D-setpoints to peak-to-peak EUV variation.

since the modified objective function is not analytically known. The gradient is estimated based on the functions $\tilde{Y}(u)$ and $\tilde{Z}(u)$, containing the collected output measurements, and through a central difference computation as follows:

$$\nabla\tilde{Q}(u,\mu) := \frac{1}{2\tau}\begin{bmatrix} 1 & -1 & 0 & 0 \\ 0 & 0 & 1 & -1 \end{bmatrix}\hat{\tilde{Q}}(u,\mu), \tag{4.41}$$

with so-called step size τ, and the measured modified objective function $\hat{\tilde{Q}}(u,\mu) := \tilde{Y}(u) - B(u,\mu)$, with $\tilde{Y}(u)$ as in (4.23), and the barrier function $B(u,\mu)$ defined as follows:

$$B(u,\mu) := -\mu\begin{bmatrix} \sum_{j=1}^{2}\log(-\tilde{Z}_{1j}(u)) \\ \vdots \\ \sum_{j=1}^{2}\log(-\tilde{Z}_{4j}(u)) \end{bmatrix}, \tag{4.42}$$

with $\mu \in \mathbb{R}_{>0}$ the so-called barrier parameter, and where $\tilde{Z}_{ij}$ denotes the ith element from the jth column of the function $\tilde{Z}(u)$ in (4.24). To facilitate the estimation of the gradient through measurements, the dither functions are chosen as follows: $v_1^\top := [\tau\ 0]$, $v_2^\top := [-\tau\ 0]$, $v_3^\top := [0\ \tau]$, and $v_4^\top = [0\ -\tau]$.

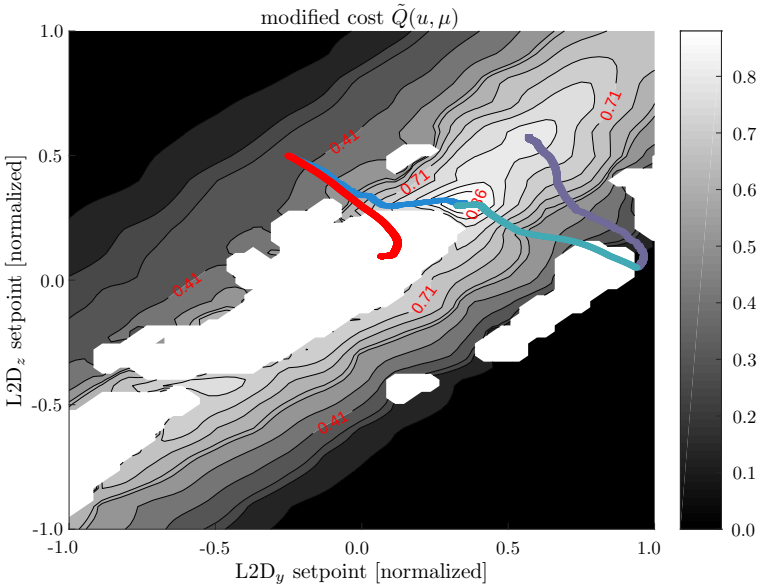

Figure 4.8: The modified objective function $\tilde{Q}$. The white areas indicate regions where $\tilde{Q}$ is undefined (i.e., outside the set of constraint satisfaction).

For illustration purposes only, the modified objective function $\tilde{Q}(u,\mu)$ using barrier functions is visualized in Fig. 4.8, with $\mu = 0.03$.

4.5.5 Simulation results

To obtain the results presented here, we have used the following numerical values for the algorithm: step-size $\tau = 0.005$ [normalized], optimizer gain $\lambda = \begin{bmatrix} 2\cdot 10^{-12} & 0 \\ 0 & 2\cdot 10^{-10} \end{bmatrix}$, and two initial L2D-setpoints, $u_0^{(1)} = [-0.25 \quad 0.5]^\top$ [normalized] and $u_0^{(2)} = [-0.25 \quad 0.5]^\top$ [normalized]. Fig. 4.9 shows the evolution of the laser-to-droplet setpoint position in y- and z-direction as a function of the sampling index starting from the two initial L2D-setpoints $u_0^{(1)}$ and $u_0^{(2)}$, and the corresponding outputs that reflect 1) the average EUV intensity, 2) the maximum back-reflection, and 3) the peak-to-peak EUV intensity. In particular, Fig. 4.9 shows iteration-domain results in the unconstrained optimization case ($\mu = 0.0$) starting from L2D-setpoints $u_0^{(1)}$ (—) and $u_0^{(2)}$ (—), and the constrained optimization case ($\mu = 0.03$) starting from L2D-setpoints $u_0^{(1)}$ (—) and $u_0^{(2)}$ (—), and Fig. 4.8 shows the corresponding trajectories in the input space.

In the case when $\mu = 0.0$, constraint violation occurs. In particular, the optimal operating conditions obtained with the extremum-seeking algorithm

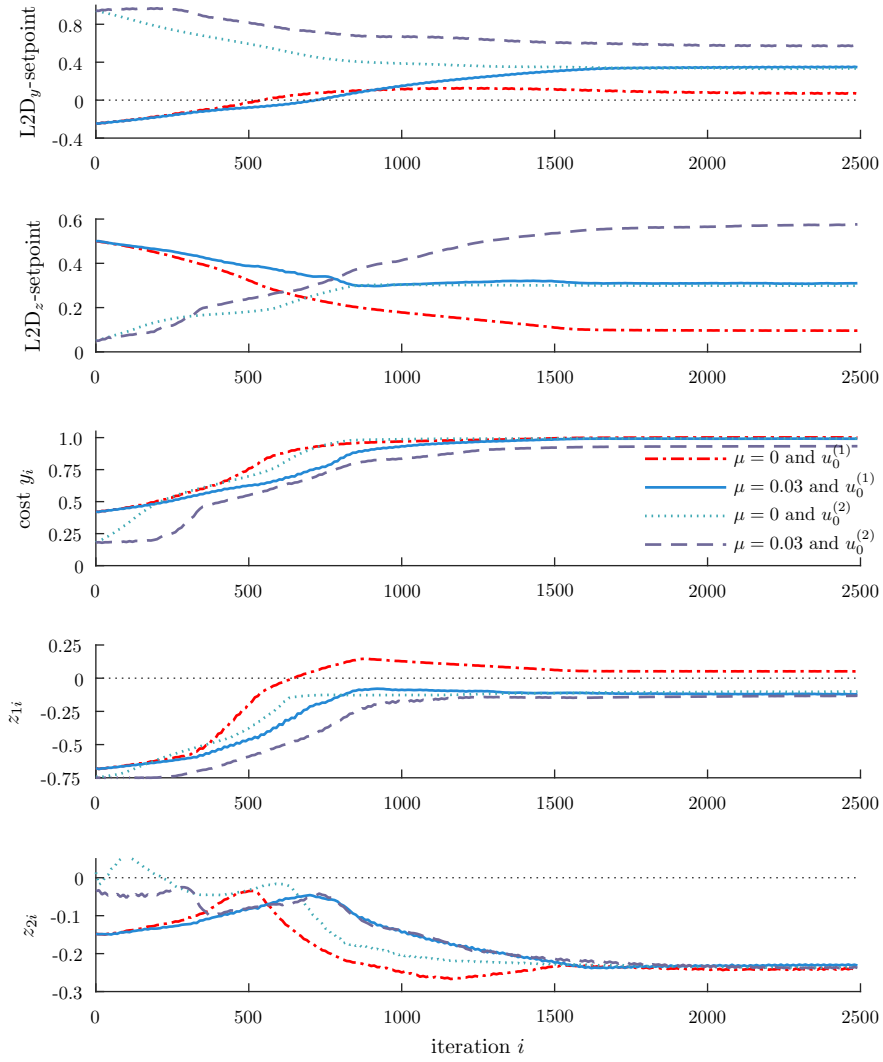

Figure 4.9: Evolution of the laser setpoint position in y- and z-direction as a function of the sampling index, and the corresponding average EUV intensity, maximum back-reflection, and peak-to-peak EUV intensity. In the case when $\mu = 0.0$, constraint violation occurs. In the case when $\mu = 0.03$, the average EUV intensity is similarly optimized, however the imposed constraints are satisfied.

initialized at $u_0^{(1)}$ and $\mu = 0.0$ (—), leading to an average EUV intensity of approximately 1, violate the constraint on the maximum back-reflection signal γ_{back}. This can be seen by (—) in Fig. 4.8 and the fourth sub-figure in Fig 4.9. When the extremum-seeking algorithm is initialized at $u_0^{(2)}$ and $\mu = 0.0$ (—), leading to an average EUV intensity of approximately 1, violation of the constraint on the peak-to-peak EUV variation γ_{pp} occurs. This can be seen by (—) in Fig. 4.8 and the fifth sub-figure in Fig 4.9.

In the case when $\mu = 0.03$, i.e., when the proposed constrained extremum-seeking is in operation and initialized at $u_0^{(1)}$ (—), the average EUV intensity achieved is approximately 1 as well, and the constraint on the maximum back-reflection signal is satisfied. When the extremum-seeking algorithm is initialized at $u_0^{(2)}$ and $\mu = 0.03$ (—), the average EUV intensity is approximately 0.93, while the constraint on the peak-to-peak EUV variation is satisfied.

Fig 4.10 shows the optimization of the EUV intensity y_p and the monitored back-reflection signal z_p as a function of time while using an unconstrained gradient-based extremum-seeking method (—), and the constrained gradient-based extremum-seeking method (—).

Remark 4.18. *Note that, given the non-convexity of the modified cost function $\tilde{Q}(u, \mu)$, see Fig 4.8, and given the fact that we employ a gradient-based extremum-seeking algorithm, convergence to the global optimum is not guaranteed. For example, this occurs in the case when the extremum-seeking algorithm is initialized at $u_0^{(2)}$ and $\mu = 0.03$ (—), as it converges towards a local minimum. Nevertheless, the proposed constrained optimization procedure leads to the satisfaction of the steady-state constraints, and in practice the gradient-based extremum-seeking algorithm can be combined with a multi-start routine as part of a calibration procedure.*

4.6 Conclusions

We have proposed a sampled-data extremum-seeking framework for constrained optimization of dynamical systems using barrier function methods, where both the to-be-optimized objective function and the constraint functions are available through output measurements only. We have shown that for the interconnection of a class of dynamical systems and a class of optimization algorithms, given a sufficiently long waiting time and parameter initialization well within the admissible set, 1) steady-state constraint satisfaction is achieved, and 2) the closed loop is practically asymptotically stable. Finally, we have demonstrated the proposed approach by means of a representative industrial simulation study of the constrained optimization of EUV light generation in an LPP source.

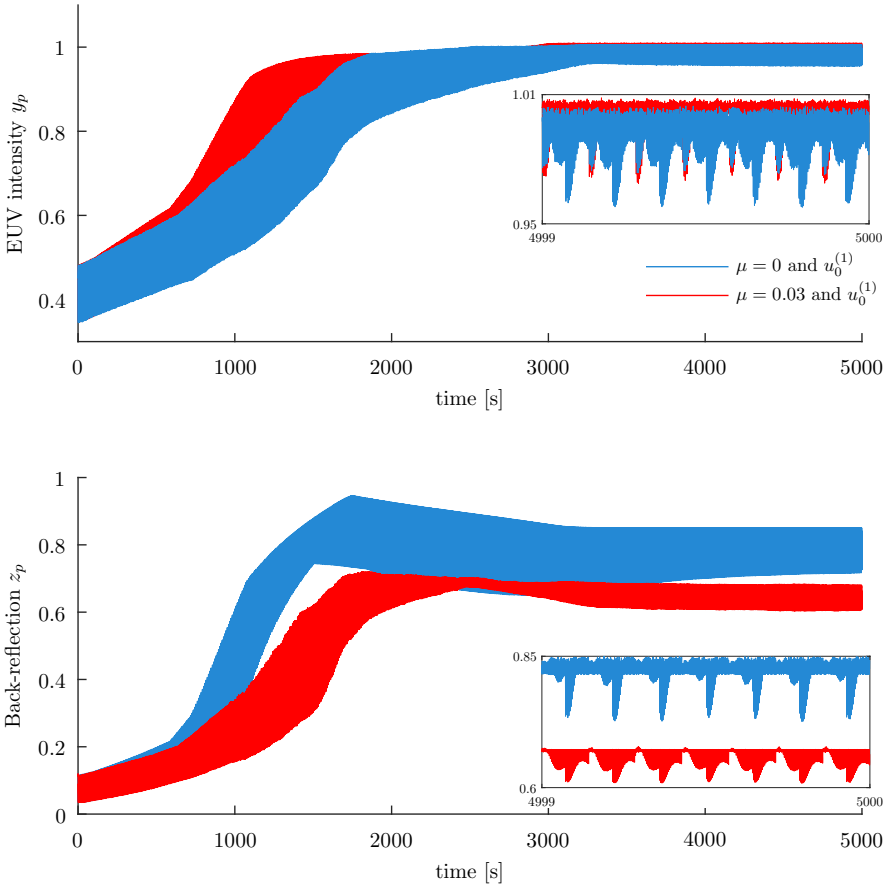

Figure 4.10: The EUV intensity (top) and the back-reflection signal (bottom) as a function of time using an unconstrained gradient-based extremum-seeking method (—), and the constrained gradient-based extremum-seeking method (—).

4.A Proof of Lemma 4.13

The proof of Lemma 4.13 exploits the line of reasoning of the proof of Theorem 1 in Teel and Popović (2001). From Assumption 4.2 we have that, for any $\epsilon_1, \epsilon_2, \Delta_{\mathcal{X}_0} \in \mathbb{R}_{>0}$, there exist a waiting time $T > 0$ such that

$$\|x(t, x_0, u)\|_{\mathcal{A}(u)} \leq \epsilon_1 \|x_0\|_{\mathcal{A}(u)} + \epsilon_2, \tag{4.43}$$

for all $t \geq T$, all $u \in \mathcal{T}$, and all $\|x_0\|_{\mathcal{A}(u)} \leq \Delta_{\mathcal{X}_0}$. Consider an arbitrary system state x_i with sampling index i during some sequence of inputs k, with algorithm

state u_k. Without loss of generality, take $k = 0$. For any $i = 1, ..., n_v$, with n_v the number of experiments for one algorithm index update, and waiting time $T^* > T$, we have

$$\|x_i\|_{\mathcal{A}(u_0+v_i(u_0))} \leq \epsilon_1 \|x_{i-1}\|_{\mathcal{A}(u_0+v_i(u_0))} + \epsilon_2, \tag{4.44}$$

for $\|x_{i-1}\|_{\mathcal{A}(u_0+v_i(u_0))} \leq \Delta_{\mathcal{X}_0}$, with the state $x_i := x(T^*, x_{i-1}, u_0+v_i(u_0))$. From item 2 of Assumption 4.12 it follows that for any $\Delta_{\mathcal{U}} > 0$ there exists a constant $L_{\mathcal{A}} \in \mathbb{R}_{>0}$ such that we have the following inequality:

$$\mathcal{A}(u_0 + v_i(u_0)) \subseteq \mathcal{A}(u_0 + v_{i-1}(u_0)) + L_{\mathcal{A}} \|v_i(u_0) - v_{i-1}(u_0)\| \overline{\mathcal{B}}, \tag{4.45}$$

with $\max\{\|u_0 + v_i(u_0)\|_{\tilde{\mathcal{C}}_{\mathcal{T}}}, \|u_0 + v_{i-1}(u_0)\|_{\tilde{\mathcal{C}}_{\mathcal{T}}}\} \leq \Delta_{\mathcal{U}}$ for $i = 1, ..., n_v$, and with $v_0(\cdot) := v_{n_v}(\cdot)$ (as defined in Lemma 4.13). Let us now employ the following lemma from Teel and Popović (2001).

Lemma 4.19. *Let $x \in \mathcal{X}$, let $\mathcal{A}_1$ and $\mathcal{A}_2$ be closed subsets of $\mathcal{X}$ and suppose $c \geq 0$ is such that $\mathcal{A}_1 \subseteq \mathcal{A}_2 + c\overline{\mathcal{B}}$. Under these conditions, $\|x\|_{\mathcal{A}_1} \leq \|x\|_{\mathcal{A}_2} + c$.*

From Lemma 4.19 and (4.45), we obtain the following inequality:

$$\|x_{i-1}\|_{\mathcal{A}(u_0+v_i(u_0))} \leq \|x_{i-1}\|_{\mathcal{A}(u_0+v_{i-1}(u_0))} + L_{\mathcal{A}} \|v_i(u_0) - v_{i-1}(u_0)\|. \tag{4.46}$$

Combining (4.46) and (4.44), and by using item 4 of Assumption 4.12, for any input $u \in \bar{\mathcal{T}}$ with $\bar{\mathcal{T}}$ an arbitrary (large) strict subset of $\mathcal{T}^o$ and $\|u\|_{\tilde{\mathcal{C}}_{\mathcal{T}}} \leq \Delta_{\mathcal{U}}$, and any $i = 1, ..., n_v$, we obtain the following inequality:

$$\begin{aligned} \|x_i\|_{\mathcal{A}(u_0+v_i(u_0))} \leq \epsilon_1 \big(& \|x_{i-1}\|_{\mathcal{A}(u_0+v_{i-1}(u_0))} \\ & + L_{\mathcal{A}} \|v_i(u_0) - v_{i-1}(u_0)\| \big) + \epsilon_2, \end{aligned} \tag{4.47}$$

for $\|x_{i-1}\|_{\mathcal{A}(u_0+v_{i-1}(u_0))} \leq \Delta_{\mathcal{X}_0} - 2L_{\mathcal{A}}(M_v \Delta_{\mathcal{U}} + c_v)$, such that $\|x_{i-1}\|_{\mathcal{A}(u+v_i(u))} \leq \Delta_{\mathcal{X}_0}$, and with $v_0(\cdot) := v_{n_v}(\cdot)$. Now, let us determine the distance of the system state x_{n_v} to the attractor $\mathcal{A}(u_0 + v_{n_v}(u_0))$ at the end of the current sequence of inputs, as a function of the distance of the state x_0 to $\mathcal{A}(u_0 + v_{n_v}(u_0))$ at the beginning of the current sequence of inputs (i.e., end of the previous sequence

of inputs), with $\|x_0\|_{\mathcal{A}(u_0+v_{n_v}(u_0))} \leq \Delta_{\mathcal{X}}$:

$$\begin{aligned}
\|x_i\|_{\mathcal{A}(u_0+v_i(u_0))} &\leq \epsilon_1 \Big(\|x_{i-1}\|_{\mathcal{A}(u_0+v_{i-1}(u_0))} \\
&\quad + L_{\mathcal{A}} \|v_i(u_0) - v_{i-1}(u_0)\| \Big) + \epsilon_2, \\
&\leq \epsilon_1 \Big(\epsilon_1 \|x_{i-2}\|_{\mathcal{A}(u_0+v_{i-2}(u_0))} \\
&\quad + \epsilon_1 L_{\mathcal{A}} \|v_{i-1}(u_0) - v_{i-2}(u_0)\| \\
&\quad + L_{\mathcal{A}} \|v_i(u_0) - v_{i-1}(u_0)\| \Big) + \epsilon_1\epsilon_2 + \epsilon_2, \\
&\quad \vdots \\
&\leq \epsilon_1 \Big(\epsilon_1^{i-1} \|x_0\|_{\mathcal{A}(u_0+v_{n_v}(u_0))} \\
&\quad + L_{\mathcal{A}} \sum_{j=1}^{i} (\epsilon_1^{i-j} \|v_j(u_0) - v_{j-1}(u_0)\|) \Big) + \epsilon_2 \sum_{j=1}^{i} \epsilon_1^{i-j},
\end{aligned} \tag{4.48}$$

for all $i = 1, \ldots, n_v$ and with $v_0(\cdot) := v_{n_v}(\cdot)$. By considering $\epsilon_1 \in (0, 1]$, which can be accomplished by having a sufficiently long waiting time T, see, e.g., Assumption 4.2, we obtain the following inequality:

$$\begin{aligned}
\|x_i\|_{\mathcal{A}(u_0+v_i(u_0))} &\leq \epsilon_1 \Big(\|x_0\|_{\mathcal{A}(u_0+v_{n_v}(u_0))} \\
&\quad + L_{\mathcal{A}} \sum_{j=1}^{i} (\|v_j(u_0) - v_{j-1}(u_0)\|) \Big) + n_v \epsilon_2,
\end{aligned} \tag{4.49}$$

for all $i = 1, \ldots, n_v$, and with $v_0(\cdot) := v_{n_v}(\cdot)$. Define $\bar{x} := x_0$ the state of the plant at the beginning of the current sequence of inputs, and $\bar{x}^+ := x_{n_v}$ the new state of the plant at the end of the current sequence of inputs. Moreover, let $u := u_0$ be the current state of the algorithm. From (4.49) and for $i = n_v$, for any $\Delta_{\mathcal{X}}, \Delta_{\mathcal{U}}, \epsilon_2 \in \mathbb{R}_{>0}$ and $\epsilon_1 \in (0, 1]$, there exists a sufficiently long waiting time $T^* \geq T$ such that for any $\bar{x} \in \mathcal{X}$ with $\|\bar{x}\|_{\mathcal{A}(u+v_{n_v}(u))} \leq \Delta_{\mathcal{X}}$ and any $u \in \bar{\mathcal{T}}$ with $\bar{\mathcal{T}}$ an arbitrary (large) strict subset of $\mathcal{T}^o$ and with $\|u\|_{\bar{\mathcal{C}}_{\mathcal{T}}} \leq \Delta_{\mathcal{U}}$, we can write the following inequality:

$$\begin{aligned}
\|\bar{x}^+\|_{\mathcal{A}(u+v_{n_v}(u))} &\leq \epsilon_1 \Big(\|\bar{x}\|_{\mathcal{A}(u+v_{n_v}(u))} \\
&\quad + L_{\mathcal{A}} \sum_{j=1}^{n_v} \|v_j(u) - v_{j-1}(u)\| \Big) + n_v \epsilon_2,
\end{aligned} \tag{4.50}$$

or

$$\begin{aligned}\bar{x}^+ \in \mathcal{A}(u+v_{n_v}(u)) + \Bigg(\epsilon_1\Bigg(\|\bar{x}\|_{\mathcal{A}(u+v_{n_v}(u))} \\ + L_{\mathcal{A}}\sum_{j=1}^{n_v}\|v_j(u)-v_{j-1}(u)\|\Bigg) + n_v\epsilon_2\Bigg)\overline{\mathcal{B}},\end{aligned} \tag{4.51}$$

with $v_0(\cdot) := v_{n_v}(\cdot)$. This concludes the proof of Lemma 4.13. □

4.B Proof of Theorem 4.14

The structure of the proof is as follows. First, a bound on $\Delta V_\Sigma(u)$ is derived. Second, a bound on $\Delta V_{\Sigma_p}(\psi,\bar{x})$ is derived. Third, a bound on $\Delta W(\psi,\bar{x},u)$ is derived. Fourth, we show 1) constraint satisfaction and 2) the convergence of u to a region around the set of approximate minimizers $\tilde{\mathcal{C}}_{\mathcal{T}}$.

Step 1: Let us derive a bound on $\Delta V_\Sigma(u) := V_\Sigma(u^+) - V_\Sigma(u)$, where u^+ is generated by (4.30) in Lemma 4.13, i.e., $u^+ \in F(u,\tilde{Y}(u),\tilde{Z}(u))$. Let $\tilde{u} \in F(u,Y(u),Z(u))$ be the closest point to $u^+ \in F(u,\tilde{Y}(u),\tilde{Z}(u))$. From Assumption 4.7, it follows that for any $u \in \bar{\mathcal{T}}$ with $\bar{\mathcal{T}}$ an arbitrary (large) strict subset of $\mathcal{T}^o$, there exist constants $L_V \in \mathbb{R}_{>0}$ and $\delta \in \mathbb{R}_{\geq 0}$, and a $\mathcal{K}_\infty$-function $\rho(\cdot)$, such that we can write

$$\begin{aligned}\Delta V_\Sigma(u) &= V_\Sigma(u^+) - V_\Sigma(u) \\ &= V_\Sigma(u^+) - V_\Sigma(\tilde{u}) + V_\Sigma(\tilde{u}) - V_\Sigma(u) \\ &\leq V_\Sigma(u^+) - V_\Sigma(\tilde{u}) - \rho(V_\Sigma(u)) + \delta \\ &\leq L_V\|u^+ - \tilde{u}\| - \rho(V_\Sigma(u)) + \delta.\end{aligned} \tag{4.52}$$

From Assumption 4.12, it follows that

$$\begin{aligned}\|u^+ - \tilde{u}\| &= \|u^+\|_{F(u,Y(u),Z(u))} \\ &\leq L_Y\|\tilde{Y}(u) - Y(u)\| + L_Z\|\tilde{Z}(u) - Z(u)\|,\end{aligned} \tag{4.53}$$

which, together with (4.52), leads to the following inequality:

$$\begin{aligned}\Delta V_\Sigma(u) \leq L_V L_Y\|\tilde{Y}(u) - Y(u)\| \\ + L_V L_Z\|\tilde{Z}(u) - Z(u)\| - \rho(V_\Sigma(u)) + \delta.\end{aligned} \tag{4.54}$$

From Assumption 4.12 and after one sequence of inputs it also follows that

$$\begin{aligned}\|\tilde{Y}(u) - Y(u)\| &\leq L_H\begin{bmatrix}\|x_1\|_{\mathcal{A}(u+v_1(u))} \\ \vdots \\ \|x_{n_v}\|_{\mathcal{A}(u+v_{n_v}(u))}\end{bmatrix} \\ &\leq n_v L_H\|\bar{x}^+\|_{\mathcal{A}(u+v_{n_v}(u))},\end{aligned} \tag{4.55}$$

and similarly

$$\begin{aligned}\|\tilde{Z}(u) - Z(u)\| &\leq L_G \begin{bmatrix} \|x_1\|_{\mathcal{A}(u+v_1(u))} \\ \vdots \\ \|x_{n_v}\|_{\mathcal{A}(u+v_{n_v}(u))} \end{bmatrix} \\ &\leq n_v L_G \|\bar{x}^+\|_{\mathcal{A}(u+v_{n_v}(u))}.\end{aligned} \tag{4.56}$$

Let us define $\tilde{L} := n_v L_V (L_Y L_H + L_Z L_G)$. As such, from (4.54)-(4.56) we obtain the following inequality:

$$\Delta V_\Sigma(u) \leq \tilde{L}\|\bar{x}^+\|_{\mathcal{A}(u+v_{n_v}(u))} - \rho(V_\Sigma(u)) + \delta. \tag{4.57}$$

Step 2: Let us derive a bound on $\Delta V_{\Sigma_p}(\psi, \bar{x}) := V_{\Sigma_p}(\psi^+, \bar{x}^+) - V_{\Sigma_p}(\psi, \bar{x})$. Since $V_{\Sigma_p}(\psi, \bar{x}) := \sigma\|\psi\|_{\tilde{\mathcal{C}}_\mathcal{T}} + \|\bar{x}\|_{\mathcal{A}(\psi+v_{n_v}(\psi))}$ with $\sigma \in \mathbb{R}_{>0}$, we obtain the following equation:

$$\Delta V_{\Sigma_p}(\psi, \bar{x}) = \|\bar{x}^+\|_{\mathcal{A}(u+v_{n_v}(u))} - \|\bar{x}\|_{\mathcal{A}(\psi+v_{n_v}(\psi))} + \sigma\|u\|_{\tilde{\mathcal{C}}_\mathcal{T}} - \sigma\|\psi\|_{\tilde{\mathcal{C}}_\mathcal{T}}, \tag{4.58}$$

where we used that $\psi^+ = u$.

Step 3: From (4.57) and (4.58) and $W(\psi, \bar{x}, u)$ in (4.31), it follows that

$$\begin{aligned}\Delta W(\psi, \bar{x}, u) &= \Delta V_{\Sigma_p}(\psi, \bar{x}) + 2\Delta V_\Sigma(u) \\ &\leq \bar{L}\|\bar{x}^+\|_{\mathcal{A}(u+v_{n_v}(u))} - \|\bar{x}\|_{\mathcal{A}(\psi+v_{n_v}(\psi))} \\ &\quad + \sigma\|u\|_{\tilde{\mathcal{C}}_\mathcal{T}} - \sigma\|\psi\|_{\tilde{\mathcal{C}}_\mathcal{T}} - 2\rho(V_\Sigma(u)) + 2\delta,\end{aligned} \tag{4.59}$$

with $\bar{L} := 1 + 2\tilde{L}$. By using Lemma 4.13 and (4.29) in Assumption 4.12, we obtain the following inequality:

$$\begin{aligned}\Delta W(\psi, \bar{x}, u) &\leq \bar{L}\epsilon_1\|\bar{x}\|_{\mathcal{A}(u+v_{n_v}(u))} - \|\bar{x}\|_{\mathcal{A}(\psi+v_{n_v}(\psi))} \\ &\quad + \bar{L}\epsilon_1 L_\mathcal{A} \sum_{j=1}^{n_v} \|v_j(u) - v_{j-1}(u)\| + \bar{L}n_v\epsilon_2 \\ &\quad + \sigma\|u\|_{\tilde{\mathcal{C}}_\mathcal{T}} - \sigma\|\psi\|_{\tilde{\mathcal{C}}_\mathcal{T}} - 2\rho(V_\Sigma(u)) + 2\delta \\ &\leq \bar{L}\epsilon_1\big(\|\bar{x}\|_{\mathcal{A}(u+v_{n_v}(u))} - \|\bar{x}\|_{\mathcal{A}(\psi+v_{n_v}(\psi))}\big) \\ &\quad + (\sigma + 2\bar{L}\epsilon_1 L_\mathcal{A} n_v M_v)\|u\|_{\tilde{\mathcal{C}}_\mathcal{T}} + 2\bar{L}\epsilon_1 L_\mathcal{A} n_v c_v \\ &\quad + \bar{L}n_v\epsilon_2 - (1 - \bar{L}\epsilon_1)\|\bar{x}\|_{\mathcal{A}(\psi+v_{n_v}(\psi))} \\ &\quad - \sigma\|\psi\|_{\tilde{\mathcal{C}}_\mathcal{T}} - 2\rho(V_\Sigma(u)) + 2\delta,\end{aligned} \tag{4.60}$$

The following lemma is adopted from Teel and Popović (2001) and will be used below.

Lemma 4.20. *Under Assumptions 4.2 and 4.12, the value*

$$\kappa := \inf\{\hat{\kappa} \in \mathbb{R}_{\geq 0} : \mathcal{A}(u_1) \subseteq \mathcal{A}(u_2) + \hat{\kappa}\overline{\mathcal{B}}, \forall\ u_1, u_2 \in \tilde{\mathcal{C}}_\mathcal{T}\}, \tag{4.61}$$

is well-defined, and for all $\Delta_{\mathcal{U}} > 0$, there exists $L_{\mathcal{A}} \in \mathbb{R}_{>0}$ such that

$$\begin{aligned} &\max\{\|u_1\|_{\tilde{\mathcal{C}}_{\mathcal{T}}}, \|u_2\|_{\tilde{\mathcal{C}}_{\mathcal{T}}}\} \leq \Delta_{\mathcal{U}} \Rightarrow \\ &\mathcal{A}(u_1) \subseteq \mathcal{A}(u_2) + L_{\mathcal{A}}(\|u_1\|_{\tilde{\mathcal{C}}_{\mathcal{T}}} + \|u_2\|_{\tilde{\mathcal{C}}_{\mathcal{T}}} + \kappa)\overline{\mathcal{B}}. \end{aligned} \tag{4.62}$$

From Lemmas 4.20 and 4.19, there exists a $\kappa \in \mathbb{R}_{\geq 0}$ such that we obtain the following inequality:

$$\begin{aligned} &\|\bar{x}\|_{\mathcal{A}(u+v_{n_v}(u))} - \|\bar{x}\|_{\mathcal{A}(\psi+v_{n_v}(\psi))} \leq \\ &L_{\mathcal{A}}\bigg(\|u\|_{\tilde{\mathcal{C}}_{\mathcal{T}}} + \|\psi\|_{\tilde{\mathcal{C}}_{\mathcal{T}}} + \|v_{n_v}(u)\| + \|v_{n_v}(\psi)\| + \kappa\bigg) \\ &\leq L_{\mathcal{A}}\bigg((1+M_v)\|u\|_{\tilde{\mathcal{C}}_{\mathcal{T}}} + (1+M_v)\|\psi\|_{\tilde{\mathcal{C}}_{\mathcal{T}}} + 2c_v + \kappa\bigg). \end{aligned} \tag{4.63}$$

From substitution of (4.63) into (4.60), and using Assumption 4.7, we obtain the following inequality:

$$\begin{aligned} \Delta W(\psi, \bar{x}, u) \leq &-(\sigma - \bar{L}\epsilon_1 L_{\mathcal{A}}(1+M_v))\|\psi\|_{\tilde{\mathcal{C}}_{\mathcal{T}}} \\ &+ 2\bar{L}\epsilon_1 L_{\mathcal{A}} c_v + \bar{L}\epsilon_1 L_{\mathcal{A}}\kappa + 2\bar{L}\epsilon_1 L_{\mathcal{A}} n_v c_v + \bar{L} n_v \epsilon_2 \\ &+ (\sigma + \bar{L}\epsilon_1 L_{\mathcal{A}}(2n_v M_v + 1 + M_v))\|u\|_{\tilde{\mathcal{C}}_{\mathcal{T}}} \\ &- (1 - \bar{L}\epsilon_1)\|\bar{x}\|_{\mathcal{A}(\psi+v_{n_v}(\psi))} - 2\rho(V_\Sigma(u)) + 2\delta, \end{aligned} \tag{4.64}$$

For any (arbitrarily small) $\gamma \in \mathbb{R}_{>0}$, we ensure that $2\bar{L}\epsilon_1 L_{\mathcal{A}} c_v + \bar{L}\epsilon_1 L_{\mathcal{A}}\kappa \leq \frac{1}{2}\gamma$ and $2\bar{L}\epsilon_1 L_{\mathcal{A}} n_v c_v + \bar{L} n_v \epsilon_2 \leq \frac{1}{2}\gamma$ by designing $\epsilon_1 \in (0, 1]$ and $\epsilon_2 \in \mathbb{R}_{>0}$ sufficiently small, which can be achieved by selecting a sufficiently long waiting time T, see the last item of Assumption 4.2. As such, we obtain the following inequality:

$$\begin{aligned} \Delta W(\psi, \bar{x}, u) \leq &-(\sigma - \bar{L}\epsilon_1 L_{\mathcal{A}}(1+M_v))\|\psi\|_{\tilde{\mathcal{C}}_{\mathcal{T}}} \\ &+ (\sigma + \bar{L}\epsilon_1 L_{\mathcal{A}}(2n_v M_v + 1 + M_v))\|u\|_{\tilde{\mathcal{C}}_{\mathcal{T}}} \\ &- (1 - \bar{L}\epsilon_1)\|\bar{x}\|_{\mathcal{A}(\psi+v_{n_v}(\psi))} - 2\rho(V_\Sigma(u)) + 2\delta + \gamma, \end{aligned} \tag{4.65}$$

Moreover, for any $\sigma \in \mathbb{R}_{>}0$, we ensure that $\bar{L}\epsilon_1 \leq \frac{1}{2}$, $\bar{L}\epsilon_1 L_{\mathcal{A}}(1+M_v) \leq \frac{1}{2}\sigma$, and $2\bar{L}\epsilon_1 L_{\mathcal{A}} n_v M_v \leq \frac{1}{2}\sigma$ by designing $\epsilon_1 \in (0, 1]$ sufficiently small. This can be achieved by selecting a sufficiently long waiting time T, see the last item of Assumption 4.2. This leads to the following inequality:

$$\begin{aligned} \Delta W(\psi, \bar{x}, u) \leq &-\frac{1}{2}\|\bar{x}\|_{\mathcal{A}(\psi+v_{n_v}(\psi))} - \frac{1}{2}\sigma\|\psi\|_{\tilde{\mathcal{C}}_{\mathcal{T}}} \\ &+ 2\sigma\|u\|_{\tilde{\mathcal{C}}_{\mathcal{T}}} - 2\rho(V_\Sigma(u)) + 2\delta + \gamma, \end{aligned} \tag{4.66}$$

With $V_{\Sigma_p}(\psi, \bar{x}) := \sigma\|\psi\|_{\tilde{\mathcal{C}}_{\mathcal{T}}} + \|\bar{x}\|_{\mathcal{A}(\psi+v_{n_v}(\psi))}$, we obtain the following inequality from (4.66):

$$\begin{aligned} \Delta W(\psi, \bar{x}, u) \leq &-\frac{1}{2}V_{\Sigma_p}(\psi, \bar{x}) - \rho(V_\Sigma(u)) \\ &+ 2\sigma\|u\|_{\tilde{\mathcal{C}}_{\mathcal{T}}} - \rho(V_\Sigma(u)) + 2\delta + \gamma, \end{aligned} \tag{4.67}$$

Let us define a $\mathcal{K}_\infty$-function $\bar{\gamma}(\cdot) := \min\{\rho(\cdot), (\cdot)\}$. This implies that $\bar{\gamma}(\cdot) \leq \rho(\cdot)$, and $\bar{\gamma}(\cdot) \leq (\cdot)$. As such, $-\frac{1}{2}V_{\Sigma_p}(\psi, \bar{x}) \leq -\bar{\gamma}(\frac{1}{2}V_{\Sigma_p}(\psi, \bar{x}))$, and $-\rho(V_\Sigma(u)) \leq -\bar{\gamma}(V_\Sigma(u))$. This yields the following inequality:

$$\begin{aligned}\Delta W(\psi, \bar{x}, u) \leq -\bar{\gamma}\left(\frac{1}{2}V_{\Sigma_p}(\psi, \bar{x})\right) - \bar{\gamma}(V_\Sigma(u)) \\ + 2\sigma\|u\|_{\tilde{\mathcal{C}}_\mathcal{T}} - \rho(V_\Sigma(u)) + 2\delta + \gamma,\end{aligned} \tag{4.68}$$

Moreover, given the fact that $\bar{\gamma}(\cdot) \in \mathcal{K}_\infty$, it follows that

$$\bar{\gamma}\left(\frac{1}{2}(\frac{1}{2}V_{\Sigma_p}(\psi, \bar{x}) + V_\Sigma(u))\right) \leq \bar{\gamma}\left(\frac{1}{2}V_{\Sigma_p}(\psi, \bar{x})\right) + \bar{\gamma}\left(V_\Sigma(u)\right),$$

see, e.g., Kellett (2014), resulting in the following inequality:

$$\begin{aligned}\Delta W(\psi, \bar{x}, u) \leq -\bar{\gamma}\left(\frac{1}{4}(V_{\Sigma_p}(\psi, \bar{x}) + 2V_\Sigma(u))\right) \\ + 2\sigma\|u\|_{\tilde{\mathcal{C}}_\mathcal{T}} - \rho(V_\Sigma(u)) + 2\delta + \gamma.\end{aligned} \tag{4.69}$$

Let us define a function $\tilde{\gamma}(\cdot) \in \mathcal{K}_\infty$ such that

$$\tilde{\gamma}\left(V_{\Sigma_p}(\psi, \bar{x}) + 2V_\Sigma(u)\right) := \bar{\gamma}\left(\frac{1}{4}\left(V_{\Sigma_p}(\psi, \bar{x}) + 2V_\Sigma(u)\right)\right). \tag{4.70}$$

From this definition and (4.31), it follows that

$$\Delta W(\psi, \bar{x}, u) \leq -\tilde{\gamma}\left(W(\psi, \bar{x}, u)\right) + 2\delta + \gamma + 2\sigma\|u\|_{\tilde{\mathcal{C}}_\mathcal{T}} - \rho(V_\Sigma(u)). \tag{4.71}$$

From item 2 in Assumption 4.7, we have that there exists a function $\alpha \in \mathcal{K}_\infty$ such that $\alpha(\|u\|_{\tilde{\mathcal{C}}_\mathcal{T}}) \leq V_\Sigma(u)$. From this fact and $\rho \in \mathcal{K}_\infty$, we obtain that $-\rho(V_\Sigma(u)) \leq -\rho(\alpha(\|u\|_{\tilde{\mathcal{C}}_\mathcal{T}}))$. For any $\alpha, \rho \in \mathcal{K}_\infty$, we have that $\tilde{\rho}(\cdot) := \rho(\alpha(\cdot)) \in \mathcal{K}_\infty$, which implies that $-\rho(V_\Sigma(u)) \leq -\tilde{\rho}(\|u\|_{\tilde{\mathcal{C}}_\mathcal{T}})$. For any $\Delta_\mathcal{U} \in \mathbb{R}_{>0}$ and any small $\delta_V \in \mathbb{R}_{>0}$, there exists a $c \in \mathbb{R}_{>0}$ such that $-\tilde{\rho}(\|u\|_{\tilde{\mathcal{C}}_\mathcal{T}}) \leq -c\|u\|_{\tilde{\mathcal{C}}_\mathcal{T}} + \delta_V$ for $u \in \bar{\mathcal{T}}$ and with $\|u\|_{\tilde{\mathcal{C}}_\mathcal{T}} \leq \Delta_\mathcal{U}$. From (4.71) we obtain the following inequality:

$$\Delta W(\psi, \bar{x}, u) \leq -\tilde{\gamma}\left(W(\psi, \bar{x}, u)\right) + 2\delta + \gamma + \delta_V - (c - 2\sigma)\|u\|_{\tilde{\mathcal{C}}_\mathcal{T}}, \tag{4.72}$$

with any small $\delta_V \in \mathbb{R}_{>0}$. Let $\sigma := \frac{c}{2}$. From (4.72) we obtain the following inequality:

$$\Delta W(\psi, \bar{x}, u) \leq -\tilde{\gamma}(W(\psi, \bar{x}, u)) + 2\delta + \gamma + \delta_V. \tag{4.73}$$

Step 4: Next, we will use the inequality in (4.73) to 1) show constraint satisfaction and 2) the convergence of u to a neighborhood of the set of approximate minimizers $\tilde{\mathcal{C}}_\mathcal{T}$. Let $\hat{\rho} \in \mathcal{K}_\infty$ such that $(\mathrm{id} - \hat{\rho}) \in \mathcal{K}_\infty$. For any

$\hat{\rho} \circ \tilde{\gamma}(W(\psi, \bar{x}, u)) \geq 2\delta + \gamma + \delta_V$ we obtain that

$$\begin{aligned} \Delta W(\psi, \bar{x}, u) &\leq -\tilde{\gamma}(W(\psi, \bar{x}, u)) + 2\delta + \gamma + \delta_V \\ &\leq -(\mathrm{id} - \hat{\rho}) \circ \tilde{\gamma}(W(\psi, \bar{x}, u)) \\ &\quad - \hat{\rho} \circ \tilde{\gamma}(W(\psi, \bar{x}, u)) + 2\delta + \gamma + \delta_V \\ &\leq -(\mathrm{id} - \hat{\rho}) \circ \tilde{\gamma}(W(\psi, \bar{x}, u)). \end{aligned} \tag{4.74}$$

From (4.74) and the comparison lemma, see, e.g., Lemma 4.3 in Jiang and Wang (2002), we have that there exists some $\mathcal{KL}$-function $\hat{\beta}$ such that

$$W(\psi_k, \bar{x}_k, u_k) \leq \max\{\hat{\beta}(W(\psi_0, \bar{x}_0, u_0), k), \tilde{\gamma}^{-1} \circ \hat{\rho}^{-1}(2\delta + \gamma + \delta_V)\}, \tag{4.75}$$

for all $k \in \mathbb{N}$. This shows the validity of inequality (4.34) in the theorem. Based on this inequality we can now validate the two statements in the theorem on constraint satisfaction and the convergence to a neighborhood of the approximate constrained minimizer set:

- For any $u_0, \psi_0 \in \mathcal{V} \subset \bar{\mathcal{T}}$ with $\bar{\mathcal{T}}$ an arbitrary (large) strict subset of $\mathcal{T}^o$ and $\bar{x}_0 \in \mathcal{X}$ with $\|u_0\|_{\tilde{\mathcal{C}}_\mathcal{T}} \leq \Delta_\mathcal{U}$, $\|\psi_0\|_{\tilde{\mathcal{C}}_\mathcal{T}} \leq \Delta_\mathcal{U}$, and $\|\bar{x}_0\|_{\mathcal{A}(\psi_0 + v_{n_v}(\psi_0))} \leq \Delta_\mathcal{X}$ with some $\Delta_\mathcal{U}, \Delta_\mathcal{X} \in \mathbb{R}_{\geq 0}$, we have that $W(\psi_0, \bar{x}_0, u_0)$ is bounded, i.e., $W(\psi_0, \bar{x}_0, u_0) \leq \Delta_W$ for some $\Delta_W \in \mathbb{R}_{\geq 0}$. From (4.75) we obtain that $W(\psi_k, \bar{x}_k, u_k)$ is bounded for all $k \geq 0$. Next, boundedness of $W(\psi_k, \bar{x}_k, u_k)$ for all $k \geq 0$ implies that $V_\Sigma(u_k)$ is bounded for all $k \geq 0$. As such, from Assumption 4.7 and boundedness of $V_\Sigma(u_k)$ it follows that $u_k \in \mathcal{T}^o$ for all $k \geq 0$, i.e., steady-state constraints satisfaction is guaranteed for all $k \geq 0$.

- From the inequality in (4.75), we have the following ultimate bound for W:

  $$\lim_{k \to \infty} W(\psi_k, \bar{x}_k, u_k) = \tilde{\gamma}^{-1} \circ \hat{\rho}^{-1}(2\delta + \gamma + \delta_V). \tag{4.76}$$

  Given the fact that $2V_\Sigma(u) \leq W(\psi, \bar{x}, u)$, and $\alpha(\|u\|_{\tilde{\mathcal{C}}_\mathcal{T}}) \leq V_\Sigma(u)$ which follows from item 2 in Assumption 4.7, we have that the solutions converge to the following set:

  $$\mathcal{Y}_u := \{u \in \mathcal{T}^o \mid \|u\|_{\tilde{\mathcal{C}}_\mathcal{T}} \leq \alpha^{-1}\big(\frac{1}{2}\tilde{\gamma}^{-1} \circ \hat{\rho}^{-1}(2\delta + \gamma + \delta_V)\big)\}. \tag{4.77}$$

The set $\mathcal{Y}_u$ can be made arbitrarily small. Namely, 1) $\delta_V \in \mathbb{R}_{>0}$ can be any arbitrarily small constant, 2) we can make γ arbitrarily small by choosing a sufficiently large waiting time $T \in \mathbb{R}_{>0}$, and 3) δ, which is defined in Assumption 4.7, can be made sufficiently small by tuning the parameters of the particular optimization algorithm F, as discussed in Assumption 4.7 and Remark 4.9. This completes the proof of Theorem 4.14. □

Chapter 5

Sampled-data extremum-seeking control for high-accuracy repetitive positioning of frictional motion systems

Abstract - *Classical proportional-integral-derivative (PID) control is exploited widely in industrial motion systems with dry friction, motivated by the intuitive, and easy-to-use design and tuning tools available. However, classical PID control suffers from severe performance limitations. In particular, friction-induced limit cycling (i.e., hunting) is observed when integral control is employed on frictional systems that suffer from the Stribeck effect, thereby compromising setpoint stability. In addition, the resulting time-domain behavior, such as, e.g., rise-time, overshoot, settling time, and positioning accuracy, highly depends on the particular frictional characteristic, which is typically unknown or uncertain. On the other hand, omitting integral control can lead to constant non-zero setpoint errors (i.e., stick). To achieve superior setpoint performance for frictional motion systems in a repetitive motion setting, we propose a PID-based feedback controller with a time-varying integrator gain design. To ensure optimal setpoint positioning accuracy and enable transient performance optimization, a data-based sampled-data extremum-seeking architecture is employed to obtain an optimal time-varying integrator gain design on the basis of a user-defined basis function parametrization. The proposed approach does not rely on knowledge on the system, and in particular, its friction characteristic. Finally, the effectiveness of the proposed approach is evidenced experimentally by application to an industrial nano-positioning motion stage set-up of a high-end electron microscope.*

The content of this chapter is based on: L. Hazeleger, R. Beerens, N. van de Wouw, "Proportional-Integral-Derivative-based learning control for high-accuracy repetitive positioning of frictional motion systems", *Provisionally accepted for publication in IEEE Transactions on Control Systems Technology*

5.1 Introduction

Many industrial motion systems perform repetitive tasks, e.g., repetitive motion profiles in pick-and-place machines (van Loon et al., 2016, Sec. 5), large-scale transferring of circuit topology to silicon wafers in lithography systems (Butler, 2011), and automated scanning procedures in electron microscopes. Due to demands on hardware cost reduction in the design phase or wear in the operational phase, friction is commonly present in such high-precision positioning systems, thereby limiting the achievable positioning accuracy.

Various control solutions have been presented throughout the literature to cope with frictional effects in motion systems. Model-based compensation techniques (see, e.g., Makkar et al. (2007) and Freidovich et al. (2010)), exploit parametric models in the control loop to compensate for friction. However, as friction characteristics are commonly unknown, uncertain, and (slowly) time-varying, model-based methods are prone to modeling errors, ultimately compromising positioning accuracy. Non-model-based methods, e.g., impulsive control (van de Wouw and Leine, 2012), dithering-based techniques (Iannelli et al., 2006), and sliding-mode control (Bartolini et al., 2003), may result in stability of the setpoint. In general, these non-model-based control techniques have a common disadvantage. Namely, the persistent injection of high-frequency control signals may excite unmodeled high-frequency system dynamics, which is highly undesirable in motion systems. Moreover, tuning and implementation of such controllers is not straightforward. Therefore, these techniques are not appealing for industrial applications.

Despite the existence of the above control techniques, the vast majority of the high-precision industry still employs classical proportional-integral-derivative (PID) control, since control practitioners are often well-trained in linear control design (loop-shaping). Moreover, it is well-known that integral action in PID control is capable of compensating for *unknown* static friction in motion systems, see, e.g., Bisoffi et al. (2018), Beerens et al. (2019) and Putra et al. (2007). However, PID control is prone to performance limitations as well. For example, solutions settle on a persistent oscillation around the setpoint when integral control is employed on systems where the friction characteristic includes the velocity-weakening (Stribeck) effect, so that stability of the setpoint is not achieved (this phenomenon is also called friction-induced limit cycling or *hunting*, see Hensen et al. (2003) and Section 5.2). Even if stability can be warranted, rise-time, overshoot, settling time (Beerens et al., 2019), and positioning accuracy depend on the particular friction characteristic, which is highly uncertain in practice. Hence, despite the popularity of the PID controller in industry, friction is a performance- and reliability-limiting factor in PID-controlled motion systems. This motivates the development of a more advanced control strategy, while preserving the benefits and intuition of classical PID feedback control design.

In this chapter, a PID-based learning controller is proposed in order to achieve a high setpoint accuracy for motion systems subject to unknown static and velocity-dependent friction, including the Stribeck effect, and tailored for repetitive motion tasks within a finite time interval. The PID-based learning controller consists of two elements. First, a PID control architecture with a *time-varying integrator gain* design is proposed, facilitating a tailored design for the repetitive motion and friction characteristic at hand. In this manner, friction-induced limit cycles can be avoided, and high accuracy repetitive setpoint positioning and improved transient behavior can be achieved instead. In addition, similar robustness properties as classical PD control at the desired setpoint can be achieved. Second, we propose a data-driven, model-free optimization strategy, in order to iteratively find the optimal time-varying integrator gain, in the presence of unknown friction. Such a data-driven tuning procedure yields optimal setpoint accuracy and improved transient behavior.

In this chapter, the finite-horizon optimization problem of finding the optimal time-varying integrator gain for repetitive motion tasks is formulated in terms of a model-free sampled-data extremum-seeking control (ESC) problem (see, e.g., Teel and Popović (2001), Kvaternik and Pavel (2011), and Khong et al. (2013b)). This is achieved by exploiting a linear spline basis function parametrization of the time-varying integrator gain. The extremum seeking mechanism is then designed to iteratively improve system performance by adaptive tuning of the parameters of this basis function parametrization. This learning mechanism has resemblance with iterative feedback tuning (see, e.g., Lequin et al. (2003), Heertjes et al. (2016), and Hjalmarsson et al. (1998)) and iterative learning control (ILC, see, e.g., Bristow et al. (2006) and Wang et al. (2009)). These iterative methods have proven merit in a linear motion control setting. However, for the nonlinear setting in this chapter, employing an extremum-seeking approach instead is beneficial. Namely, ESC is able to deal with unknown, uncertain, time-varying, and general nonlinear systems, and is therefore suitable to be used in the presence of unknown nonlinear frictional effects.Moreover, the potential of ESC in the context of iterative learning control and optimizing transient behavior has been shown in, e.g., Khong et al. (2016); Benosman (2016); Killingsworth and Krstic (2006), and Ren et al. (2012). However, it must be noted that the extremum-seeking strategy to iteratively improve the system's transient behavior proposed in this work is different. Namely, we iteratively learn *time-varying* feedback controller gains using ESC, where, e.g., in Killingsworth and Krstic (2006) and Benosman (2016), ESC is used for iterative tuning of PID controllers having constant gains, and in, e.g., in Khong et al. (2016) and Ren et al. (2012), (sampled-data) ESC is employed to iteratively tune a system input signal.

The main contributions of this chapter can be summarized as follows. The first contribution is a time-varying integrator gain design for PID-based feedback control of motion systems with unknown static and velocity dependent friction,

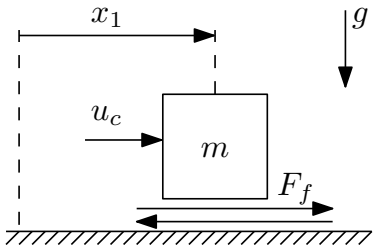

Figure 5.1: Schematic representation of the motion system subject to a friction force F_f.

the latter possibly including the Stribeck effect. The second contribution is an automatic controller tuning procedure based on a sampled-data extremum-seeking framework, facilitated by a basis function parametrization of the time-varying integrator gain. The third contribution is an experimental case study on an industrial high-precision motion stage of an electron microscope.

The chapter is organized as follows. We formalize the control problem in Section 5.2, and we present the PID-based controller with time-varying integrator gain in Section 5.3. In Section 5.4, we present the extremum-seeking-based iterative learning mechanism. Section 5.5 provides an implementation summary. In Section 5.6, we experimentally show the working principles of the proposed PID-based learning controller, applied to an industrial nano-positioning motion stage. Conclusions are presented in Section 5.7.

Notation: Sign$(\cdot)$ (with an upper-case S) denotes the *set-valued* sign function, i.e., Sign$(y) := 1$ for $y > 0$, Sign$(y) := -1$ for $y < 0$, and Sign$(y) := [-1, 1]$ for $y = 0$. $\mathbb{B}$ denotes the closed unit ball of appropriate dimensions, in the Euclidean norm.

5.2 Control problem formulation for frictional motion systems

In this section, we first present a PID-controlled motion system with (Stribeck) friction, to illustrate the shortcomings of P(I)D control for frictional motion systems. Second, we state the control problem formulation for repetitive positioning of frictional motion systems.

5.2.1 PID-controlled single mass system with Stribeck friction

Consider a single-degree-of-freedom motion system, consisting of a mass m sliding on a horizontal plane, with measurable position x_1, velocity x_2, control input u_c (i.e., the actuation force as determined by a motion control algorithm). The mass is subject to a friction force F_f (as schematically depicted in Fig. 5.1) belonging to a friction *set* $\Phi(x_2)$ for a velocity x_2, where $x_2 \rightrightarrows \Phi(x_2)$ is a set-valued

mapping. The set-valued friction characteristic Φ consists of a Coulomb friction component with (unknown) static friction F_s, a viscous contribution γx_2 (where $\gamma \geq 0$ is the viscous friction coefficient), and a nonlinear velocity-dependent friction component f, encompassing the Stribeck effect, i.e.,

$$F_f \in \Phi(x_2) := -F_s \text{Sign}(x_2) - \gamma x_2 + f(x_2), \tag{5.1}$$

We pose the following assumption on the velocity-dependent friction component f.

Assumption 5.1. *The function $f : \mathbb{R} \to \mathbb{R}$ is continuously differentiable and satisfies*

(i) $|f(v)| \leq F_s$ *for all* v*;*

(ii) $vf(v) \geq 0$ *for all* v*;*

(iii) f *is globally Lipschitz with Lipschitz constant* $L > 0$*.*

The dynamics of the motion system with friction are governed by the following differential inclusion:

$$\begin{aligned} \dot{x}_1 &= x_2, \\ m\dot{x}_2 &\in \Phi(x_2) + u_c. \end{aligned} \tag{5.2}$$

Consider a classical PID controller for input u_c in (5.2), i.e.,

$$\begin{aligned} u_c &= k_p e + k_d \dot{e} + k_i x_3, \\ \dot{x}_3 &= e, \end{aligned} \tag{5.3}$$

where $e := r - x_1$ denotes the setpoint error with r the reference signal, x_3 the integrator state, and k_p, k_d, and k_i the proportional, derivative, and integral controller gains, respectively. For frictional motion systems, the presence of an integrator action in (5.3) is motivated by the fact that it is able to compensate for unknown static friction, due to the build-up of control force by integrating the position error. In general motion control systems, integrator action is widely used to improve low-frequency disturbance rejection properties and shorten rise-times, the latter being beneficial for machine throughput. As an illustration, consider a constant reference r, i.e., a point-to-point motion, so that the resulting set of equilibria of closed-loop system (5.1)-(5.3) is given by

$$\mathcal{E}_{pid} = \{(e, \dot{e}, x_3) \in \mathbb{R}^3 : e = 0,\ \dot{e} = 0,\ |x_3| \leq F_s/k_i\}, \tag{5.4}$$

which is globally asymptotically stable for closed-loop system dynamics (5.1)-(5.3) only when $f(\cdot) = 0$, i.e., in the absence of the velocity-weakening (Stribeck) effect, see, Bisoffi et al. (2018). In the presence of the Stribeck effect, however, $\mathcal{E}_{pid}$ is not stable and limit cycling (*hunting*) occurs. Although static friction

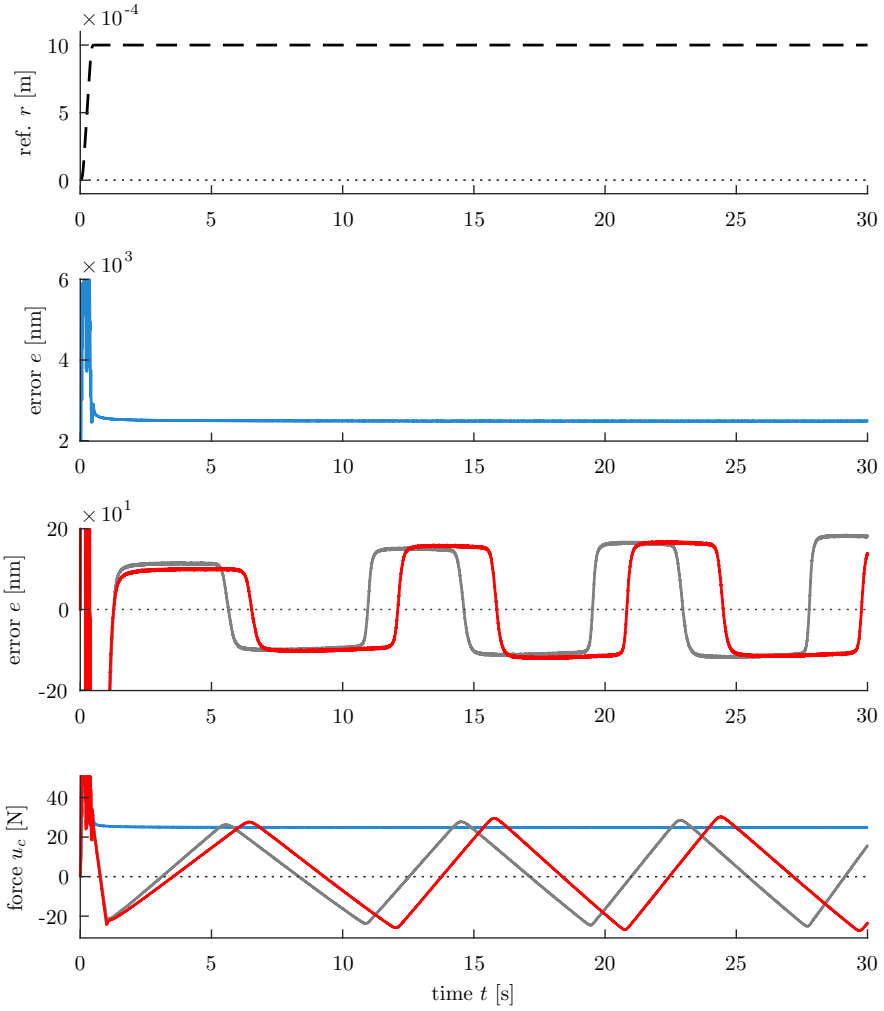

Figure 5.2: Measured error responses of an industrial nano-positioning motion stage set-up subject to a third-order reference trajectory (– –), (for details about the set-up, see Section 5.6) and the corresponding control forces of a PD controller (—), and a PID controller with fixed integrator gain $k_i = 1 \cdot 10^8$ (—) and (—). The PD controller yields a non-zero steady-state positioning error, and the PID controller induces *hunting*.

is eventually compensated by the integrator action, friction is overcompensated in the slip phase that follows due to the velocity-weakening effect, resulting in

overshoot of the setpoint. This process repeats and results in stick-slip limit cycling, compromising setpoint stability. This phenomenon is illustrated experimentally in the third subplot in Fig. 5.2. In particular, Fig. 5.2 presents the reference trajectory employed (subplot 1), the measured error response when using solely PD control (subplot 2), two measured error responses using PID control (subplot 3), and the corresponding control forces generated by the PD and PID controllers (subplot 4) of an industrial nano-positioning motion stage setup (the motion stage setup will be discussed in more detail in Section 5.6). A relatively large positioning error of about 200 nm is obtained when using linear PID control. Omission of the integrator action (i.e., PD control for input u_c in (5.2)) results in the set of equilibria for (5.1)-(5.3) given by

$$\mathcal{E}_{pd} = \{(e, \dot{e}) \in \mathbb{R}^2 : |e| \leq F_s/k_p,\ \dot{e} = 0\}, \tag{5.5}$$

which is stable (see Putra et al. (2007)), but does not guarantee zero steady-state error, as also illustrated in Fig. 5.2. In particular, the size of the achievable steady-state error depends inversely on the proportional gain k_p, which cannot be chosen arbitrarily large for stability purposes. The drawbacks of P(I)D control for frictional motion systems motivate the design of a more suitable control architecture. Respecting the popularity of PID control in industry, we propose a time-varying PID-based controller in Section 5.3 after formalizing the control problem in the next section.

5.2.2 Control problem formulation

In this chapter, we focus on achieving high-accuracy positioning for frictional motion systems that perform a user-defined *T-repetitive* motion. We consider, for the position x_1, a desired repetitive reference r, defined on the time interval $[0, T]$, where the system starts and ends at rest. Specifically, we separate the time interval $[0, T]$ into two particular parts, specified as follows:

i) $t \in [0, T_B)$; the so-called *transient time window*, during which the system is allowed to move from 0 to r;

ii) $t \in [T_B, T]$; the so-called *standstill time window*, during which standstill at r is required. The time interval $[T_B, T]$ is typically used by the industrial machine, of which the motion system is part, to perform a certain machining operation, for which accurate positioning is required.

Respecting the popularity of PID control in industry, and taking into account the advantages of classical P(I)D control, in this chapter we address the following setpoint control problem.

Problem 5.2. *Design a PID-based control strategy for motion systems of the form* (5.1), (5.2)*, that perform a repetitive motion profile and are subject to unknown static and velocity-dependent friction, such that 1) high-accuracy setpoint*

positioning during the standstill time window, and 2) optimal transient behavior during the transient time window is achieved.

The desired performance, i.e., an optimal transient response on $[0, T_B)$, and optimal setpoint accuracy on $[T_B, T]$, can be captured by the following cost function J to be minimized:

$$J(e) := \int_0^T |w(t)e(t)|^2 dt, \tag{5.6}$$

where we have introduced a weighting function $w(t)$ which is defined as follows:

$$w(t) := \begin{cases} w_1 & \text{if} \quad t \in [0, T_B) \\ w_2 & \text{if} \quad t \in [T_B, T] \end{cases}, \tag{5.7}$$

with $w_1, w_2 \in \mathbb{R}$ suitable weighting factors, trading off the emphasis on transient performance versus setpoint accuracy. Other (transient) performance relevant variables, such as the control effort u_c, or the velocity x_2 of the mass can be taken into account in (5.6) as well, if accurate velocity measurements are available.

5.3 A time-varying integrator gain design for PID-based control of frictional motion systems

In this section, first the time-varying integrator design is presented, and subsequently the achievable performance benefits are shown in a numerical example.

5.3.1 Time-varying integrator gain design

The limit-cycle present in the case of PID control with *constant* integrator gain, see, e.g., Fig 5.2, is caused by the build-up of integrator action (during transients and the stick phase) in interplay with the friction characteristic. This observation motivates the design of a novel *time-varying* integrator gain $k_i(t)$ for point-to-point motion for the following reasons:

1. the presence of integrator action still allows the system to escape undesired stick phases,
2. overcompensation of friction due to, e.g., a severe Stribeck effect, can be avoided, by altering $k_i(t)$ during the slip phase,
3. zero integral action can be enforced at the setpoint when standstill of the system is required, such that robustness against other force disturbances is provided by the static friction.

The resulting controller is then given by

$$u_c = k_p e + k_d \dot{e} + k_i(t) x_3, \tag{5.8a}$$

$$\dot{x}_3 = \varsigma(t) e, \tag{5.8b}$$

with $\varsigma(t) \in \{0, 1\}$ a to-be-designed switching function that prevents uncontrolled growth of x_3. Furthermore, the to-be-designed time-varying integral gain $k_i(t)$ should be bounded, i.e., $|k_i(t)| < +\infty$ for all $t \in [0, T]$. Here, we opt to employ a time-varying integrator gain $k_i(t)$, instead of an appropriate feedforward control signal in combination with a constant integrator gain k_i as commonly done in iterative learning control to, e.g., counteract recurring disturbances (Bristow et al., 2006; Wang et al., 2009). This choice is motivated by the fact that, with the proposed controller, we are able to 1) escape undesired stick phases by enabling $k_i(t) \neq 0$ during the transient time window $t \in [0, T_B)$, and 2) create robustness to other force disturbances close to the setpoint, by enforcing $k_i(t) = 0$ during the standstill time window $t \in [T_B, T]$. Integrator action is then disabled, so that the system remains in standstill since build up of control force is prevented. Indeed, robustness to force disturbances is obtained as the proportional action is low, compared to the static friction, due to the anticipated small position error close to the setpoint and achieved by the PID control with time-varying integrator gain during the transient.

Remark 5.3. *Note that the presented engineering intuition here only applies when the integrator gain k_i is placed at the right-hand side in* (5.8a)*, instead of at the right-hand side in* (5.8b)*. Indeed, in the latter case, $k_i = 0$ would still yield a constant integral control force in u_c.*

We now propose a parametric design for $k_i(t)$, parameterized by a finite set of basis functions $\varphi^{(j)}$, $j \in \{1, 2, \ldots, b\}$, as follows:

$$k_i(t) := \sum_{j=1}^{b} \varphi^{(j)}(p, t), \tag{5.9}$$

where b denotes the number of basis functions, and $p \in \mathbb{R}^{n_p}$ is a to-be-designed parameter vector. Next, we give two examples of basis function parametrizations that can be employed to facilitate solving Problem 5.2.

Example 5.4. *Step-like basis functions, i.e., $\varphi^{(j)}(p, t) := p^{(j)}\Psi^{(j)}(t)$ with $\Psi^{(j)}(t)$ defined as follows:*

$$\Psi^{(j)}(t) := \begin{cases} 1, & t \in [(j-1)t_s, jt_s) \\ 0, & t \notin [(j-1)t_s, jt_s) \end{cases} \quad \text{for } j = 1, \ldots, b, \tag{5.10}$$

where t_s satisfies $T = bt_s$, and the to-be-designed parameter vector $p \in \mathbb{R}^{n_p}$, with $n_p = b$.

Example 5.5. *Linear spline basis functions, i.e., $\varphi^{(j)}(p, t) := [p^{(j)}\ p^{(j+1)}]\Psi^{(j)}(t)$*

with $\Psi^{(j)}(t)$ *defined as follows:*

$$\Psi^{(j)}(t) := \begin{cases} \begin{bmatrix} 1 - \frac{t-(j-1)t_s}{t_s} \\ \frac{t-(j-1)t_s}{t_s} \end{bmatrix}, & t \in [(j-1)t_s, jt_s) \\ \begin{bmatrix} 0 & 0 \end{bmatrix}^\top, & t \notin [(j-1)t_s, jt_s) \end{cases} \tag{5.11}$$
$$\text{for } j = 1, \ldots, b,$$

where t_s *satisfies* $T = bt_s$*, and the parameter vector* $p \in \mathbb{R}^{n_p}$*, with* $n_p = b + 1$*.*

Remark 5.6. *Other types of basis function designs can be adopted from the iterative learning control literature. For example, polynomial bases (see, e.g., van de Wijdeven and Bosgra (2010) and van der Meulen et al. (2008)) and rational bases (see, e.g., Bolder and Oomen (2015)) can similarly be exploited.*

In the remainder of this chapter, we opt for a linear spline basis function parametrization of $k_i(t)$, as illustrated in Example 5.5, as it yields a *continuous* control signal. In contrast, the step-like basis function parametrization, as illustrated in Example 5.4 (see also Hazeleger et al. (2019)), results in discontinuities in the control signal, risking excitation of high-frequency system dynamics, which is also a well-known drawback in reset control and impulsive control strategies developed for the control of frictional systems.

The switching function $\varsigma(t)$ in (5.8) is analogously designed as

$$\varsigma(t) := \begin{cases} 1, & t \in [0, T_B), \\ 0, & t \in [T_B, T], \end{cases} \tag{5.12}$$

so that the evolution of the integrator state is disabled on the interval $[T_B, T]$. Summarizing, the resulting closed-loop system with the proposed design for the time-varying integrator gain is given by (5.1), (5.2), (5.8), (5.9), (5.11), and (5.12).

The next proposition presents some properties of the resulting closed-loop system, which will be instrumental in the data-based sampled-data extremum seeking architecture presented in Section 5.4. In particular, the following proposition asserts that each bounded realization of $k_i(t)$ results in a *unique* solution $x = (x_1, x_2, x_3)^\top$ of the closed-loop system, which is *bounded* on the interval $[0, T]$.

Proposition 5.7. *Under Assumption 5.1, for any constant* r*, each bounded realization of* $k_i(t)$ *in* (5.8) *satisfying* $k_i(t) = 0$ *for* $t \in [T_B, T]$*, each initial condition satisfying* $x(0) \in K_1\bar{\mathcal{B}}$ *with* $K_1 \geq 0$*, and* $\varsigma(t)$ *as in* (5.12)*, solutions* $x(t)$ *to closed-loop system* (5.1), (5.2), (5.8), (5.9), (5.11), (5.12) *are unique, and satisfy* $x(t) \in K_2\bar{\mathcal{B}}$ *for some bounded* $K_2 > 0$*, for all* $t \in [0, T]$*.*

Proof. *See Appendix 5.A.*

5.3.2 Illustrative example

We illustrate the potential of the proposed time-varying integrator gain by means of a numerical example. Consider closed-loop system (5.1), (5.2), (5.8), (5.9), (5.11), (5.12), where we adopt the following numerical values: $m = 1$, $k_p = 18$ N/m, $k_d = 2$ Ns/m, $F_s = 0.981$ N, and $\gamma = 0.5$. The Stribeck contribution of the friction f is given by

$$f(x_2) = \left((F_s - F_c)\eta x_2\right)\left(1 + \eta|x_2|\right)^{-1}, \tag{5.13}$$

where F_c the Coulomb friction force, and η the Stribeck shape parameter. The motion profile interval is characterized by $T = 1.5$ s, and $T_B = 0.75$ s. For the time-varying integrator gain design, we take $b = 6$, and the parameter vector p is given by $p = [p^{(1)}\ p^{(2)}\ p^{(3)}\ 0\ 0\ 0\ 0]^\top$. Moreover, $p^{(1)}$ is kept *fixed* to $p^{(1)} = 25$ N/(ms), which enables integral action at least for $t \in [0, t_s)$ to escape a potential initial stick phase. The parameters $p^{(2)}$ and $p^{(3)}$ are tunable, and affect the error response of the closed-loop system, as illustrated next.

We illustrate the potential performance benefits of the controller by considering two cases with different friction characteristics, i.e., 1) $F_c = F_s/2$, $\eta = 20$, $\gamma = 0$, and, 2) $F_c = F_s/3$, $\eta = 60$, $\gamma = 1$. Consider Fig. 5.3, where, for each column, the top subplot depicts the friction characteristic, the middle subplot depicts four different position error evolutions, and the bottom subplot depicts the four corresponding designs for the time-varying integrator gain $k_i(t)$. For both friction cases, the error response with a *classical* PID controller (i.e., with a fixed integrator gain $k_i = 25$ N/(ms) and depicted by (—)), leads to significant overshoot, and eventually limit cycling (the latter explicitly visible for case 2, see also Fig. 5.2 for such limit-cycling effect). We now perform three different simulations for both cases by selecting different pairs of values for the parameters $p^{(2)}$ and $p^{(3)}$, which yield different error responses. The first simulation in friction case 1 (– –) results in significant overshoot, and the second simulation in friction case 1 (-·-) in undershoot. The optimal choice for $p^{(2)}$ and $p^{(3)}$ instead results in zero error in friction case 1, see the third simulation (—). The friction characteristic in case 2 has a more severe Stribeck effect compared to the characteristic in case 1 (see the top subplot), whereby the optimal settings for $p^{(2)}$ and $p^{(3)}$ become negative, but zero steady-state error is still achieved, see (—) in the second and lower subplot. The proposed time-varying PID controller is hence capable of achieving optimal positioning performance, despite the presence of friction, by proper tuning of the parameters in v.

Since the friction characteristic Φ in (5.2) is generally unknown, uncertain, and can change (slowly) in time, the optimal design for the tunable parameters in v is challenging, or even impossible using a model-based approach only. Therefore, we propose a data-based extremum-seeking-based (learning) algorithm in the next section, to learn the optimal $k_i(t)$ by adaptive tuning of the parameter vector p, on the basis of measured error responses.

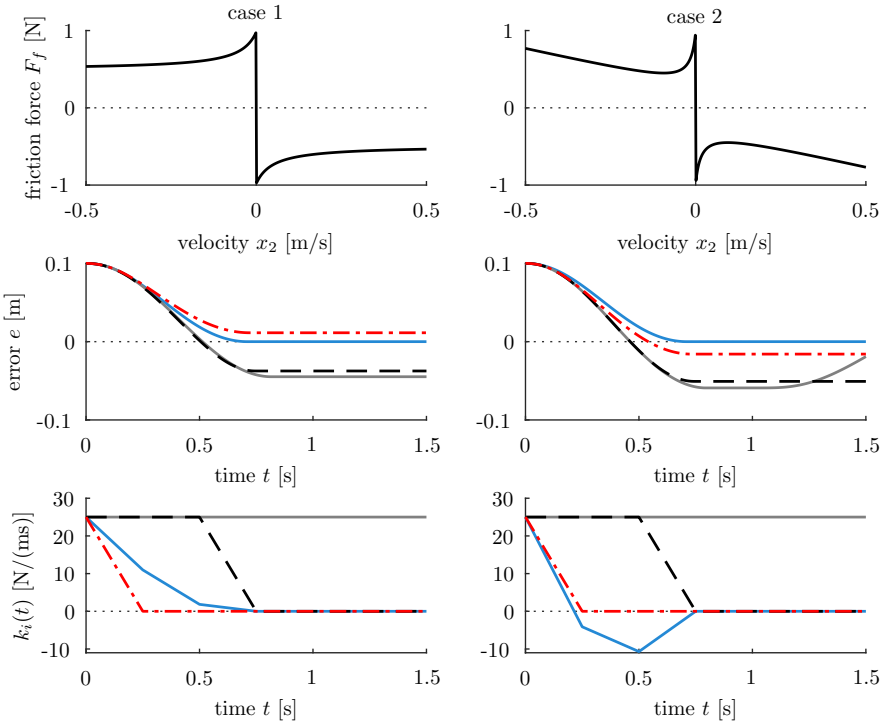

Figure 5.3: Simulation results, where each column presents from top to bottom the friction characteristic, error response, and time-varying integrator gain for case 1 and 2, respectively. The different error responses in the middle subplots correspond to simulations with different realizations of the time-varying integrator gain as in the lower subplots, and the classical PID responses with constant k_i are indicated by (—).

5.4 Sampled-data extremum-seeking for iterative learning in repetitive setpoint positioning

In this section, we propose a sampled-data extremum seeking strategy, akin to iterative learning control and extensively treated in Chapter 4, to optimize the time-varying integrator gain design presented in Section 5.3 to achieve high-accuracy setpoint positioning. Specifically, given the cost function in (5.6) and (linear spline) basis function parametrization of the time-varying integrator gain in (5.9), we can formulate the finite horizon optimization problem as a model-free sampled-data extremum seeking problem (see, e.g., Teel and Popović (2001), Khong et al. (2013b), and Khong et al. (2016)). Namely,

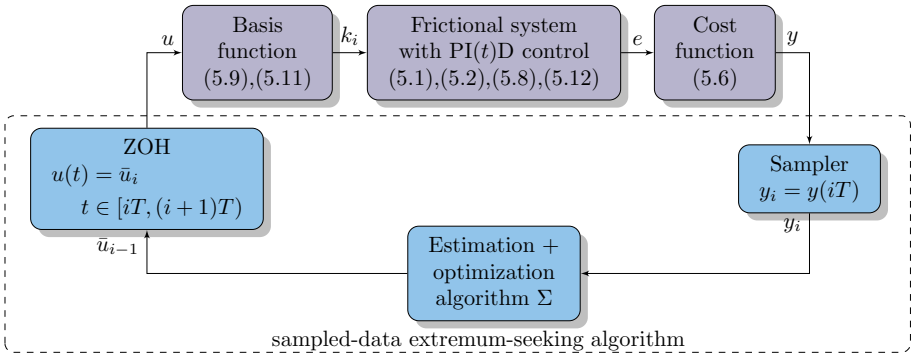

Figure 5.4: The sampled-data extremum-seeking framework based on sampled-data control law with periodic sampling time T, and sampler and zero-order hold elements.

consider the cascade connection of the PID-controlled motion system given by (5.1), (5.2), (5.8), (5.9), (5.11), (5.12), and the cost function J in (5.6). In addition, we consider the to-be-designed parameter vector to be decomposed as follows: $p = p_0 + Cu$, where $p_0 \in \mathbb{R}^{n_p}$ is a user-defined parameter vector, $C \in \mathbb{R}^{n_p \times n_u}$ is a user-defined selection matrix, and $u \in \mathbb{R}^{n_u}$ is the vector of to-be-optimized parameters by the extremum-seeking algorithm. This cascade connection yields the following *unknown* static input-output map $Q : \mathbb{R}^{n_u} \to \mathbb{R}$ for the cascaded system (5.1), (5.2), (5.8), (5.9), (5.11), (5.12), and (5.6):

$$Q(u) := \int_0^T |w(t)e(t)|^2 dt, \tag{5.14}$$

where the weighting function $w(t)$ is defined in (5.7). It must be noted that periodic re-initialization of the states to fixed values, in combination with Proposition 5.7, is needed for extremum seeking control to be applicable in an iterative learning context, i.e., $x(iT) = x_0$ for all $i = 1, 2, \ldots$. Only under these conditions (re-initialization and uniqueness provided by Proposition 5.7), Q in (5.14) is uniquely defined, see also Remark 5.10 below. In addition, the fact that solutions to the closed-loop system remain bounded by Proposition 5.7 guarantees that $Q(u)$ is bounded.

Based solely on output measurements, which we use to compute Q in (5.14), extremum-seeking control is exploited to adaptively find parameters u that minimize Q. Here we focus on a periodically sampled-data extremum-seeking framework, similar as exploited in Chapter 4. Fig. 5.4 schematically depicts the sampled-data extremum-seeking framework, i.e., the interconnection of the PID-based controlled frictional motion system with a basis function parametrization (5.1), (5.2), (5.8), (5.9), (5.11), (5.12), and the cost function J in (5.6)

implemented as follows:

$$y(t) := J(e(t)) = \int_{t-T}^{t} |w(s)e(s)|^2 ds, \tag{5.15}$$

where $e(s) = 0$ for $s \in [-T, 0)$, and with the weighting function implemented as follows:

$$w(t) := \begin{cases} w_1 & \text{if} \quad \text{mod}(t,T) \in [0, T_B) \\ w_2 & \text{if} \quad \text{mod}(t,T) \in [T_B, T] \end{cases}, \tag{5.16}$$

with a T-periodic sampler, an optimization algorithm Σ, and a zero-order hold (ZOH) element. Next, we describe an extremum-seeking algorithm performing n_v experiments to realize one update of the system input u, similar to Algorithm 4.10 in Chapter 4. Different from Algorithm 4.10 in Chapter 4 is how the sampling period T of the sampled-data extremum-seeking algorithm, i.e., the waiting time T, is utilized. Namely, in the iterative learning context, by choosing the waiting time T conform the period time of the repetitive motion profile and satisfaction of the re-initialization condition, the output $y(t)$, as determined by (5.15), and sampled on the sampling instances $y(iT)$ for $i = 1, 2, ...$, coincide with the static input-output map in (5.14).

Algorithm 5.8. *Suppose that the waiting time T, the number of experiments n_v to realize one iteration of the optimization algorithm, and the initial algorithm state u_0 are specified. Let us define the ideal periodic sampling operation $x_i := x(iT)$:*

$$y_i := y(iT) \quad \forall\ i = 0, 1, ..., \tag{5.17}$$

where y_i is the collected measurement as used by the optimization algorithm, and where $i \in \mathbb{N}$ denotes the sampling index. We assume re-initialization of the states to fixed values, i.e., $x(iT) = x_0$ for all $i = 1, 2, ...$ Define the zero-order-hold (ZOH) operation as follows:

$$u(t) := \bar{u}_i \quad \forall\ t \in [iT, (i+1)T), \tag{5.18}$$

with sampling index $i = 0, 1, ...,$, waiting time $T > 0$, and step input parameter $\bar{u}_i$. For sampling index i, the step input parameter $\bar{u}_i$ is determined by the state of the optimization algorithm u_k as follows:

$$\bar{u}_i := u_k + v_{j(i)}(u_k), \quad \forall\ i = 0, 1, ..., \tag{5.19}$$

with $k \in \mathbb{N}$ the optimization algorithm index, u_0 the initial algorithm state, and dither functions $v_{j(i)}$ with $j(i) := (i \bmod n_v) + 1$.

The optimization algorithm index k is related to the sampling index i and number of experiments n_v through $k = \left\lfloor \frac{i}{n_v} \right\rfloor$. The optimization algorithm is characterized by the mapping F given in (4.11), which exploits the collected measurements y_i and z_i:

$$u_{k+1} \in F(u_k, Y(u_k)), \quad \forall\ k = 0, 1, ..., \tag{5.20}$$

with function $\tilde{Y}(u_k)$ *defined as follows:*

$$Y(u_k) := \begin{bmatrix} y_{kn_v+1} \\ \vdots \\ y_{(k+1)n_v} \end{bmatrix} = \begin{bmatrix} Q(\bar{u}_{kn_v}) \\ \vdots \\ Q(\bar{u}_{(k+1)n_v-1}) \end{bmatrix}, \tag{5.21}$$

which is a collection of the objective function Q *in* (5.14) *in terms of* T*-periodically sampled outputs in* (5.15)*.*

Remark 5.9. *In most (sampled-data) extremum-seeking literature,* Q *reflects the* steady-state *behavior of the dynamical system. In those cases, the sampling period* T*, or so-called waiting time* T*, needs to be chosen sufficiently large by the user such that the closed-loop extremum-seeking scheme is robust against inexact measurements of the cost* Q *due to the* transient *behavior of the system, see, e.g., Teel and Popović (2001), Khong et al. (2013b), and Kvaternik and Pavel (2011). Here,* Q *in* (5.14) *actually incorporates the transient behavior of the system, which ultimately determines positioning accuracy. As such, the role of the waiting time* T *is different here, and is conveniently chosen equal to the period time* T *of the repetitive motion profile.*

Remark 5.10. *A common requirement in the extremum-seeking literature is that the input-output mapping* Q *is independent of initial conditions. Here, the transient behavior is partly determined by the initial conditions, and re-initialization after each setpoint operation is theoretically required for an input-output mapping* Q *as in* (5.14) *to be uniquely defined. Re-initialization for transient performance optimization is also a well-known and commonly accepted requirement in the iterative learning control literature, see, e.g., Norrlöf and Gunnarsson (2002) and Bristow et al. (2006).*

In Algorithm 5.8, we consider optimization algorithms that can be described by a difference inclusion, similar to the class of algorithms in Chapter 4 and Teel and Popović (2001) for which its convergence properties are encapsulated by Lyapunov function. In the periodic sampled-data extremum seeking framework in Khong et al. (2013b), other sampling-based algorithms from the optimization literature can be employed as well to achieve (a weaker type of) convergence to the extremum of Q. In particular, the so-called DIRECT and Shubert algorithms (see Jones et al. (1993) and Shubert (1972), respectively) can be employed to find the global extremum of Q, which are not described by a difference inclusion. Nevertheless, if finding a local optima suffices or if Q possesses only a single (global) extremum, gradient-based optimization methods such as the classical gradient descent or Newton method can be used (see, e.g., Boyd and Vandenberghe (2004)). In Section 5.6, we employ such a gradient-based optimization algorithm for F within Algorithm 5.8, to optimally tune the time-varying integrator gain to achieve high-accuracy repetitive positioning of an industrial nano-positioning stage.

5.5 Implementation summary

In this section, a brief summary of the design procedure for achieving high-accuracy repetitive setpoint positioning of frictional motion systems is provided. We would like to emphasize that, in this chapter, we have mainly focussed on frictional motion systems, stabilized by a linear PID feedback controller, that suffer from the Stribeck effect. However, the following design procedure can also prove useful to improve transient behavior of motion control systems performing repetitive positioning tasks in the absence of (severe) frictional effects, and by iteratively adapting (other) performance relevant tunable parameters.

A priori, we assume that a (stabilizing) linear PID controller has been designed for the (unknown) frictional motion system at hand is, and its settings are assumed to be known. Typically, such a linear PID controller has been designed on the basis of measured frequency response functions which do not take into account the Stribeck effect. The (Stribeck) friction characteristic at hand is considered to be unknown. The system is required to perform a known T-repetitive motion with a desired (step) reference from the initial position 0 to position r. Moreover, the standstill time instance T_B and the period time T are provided, which define the transient time window $[0, T_B)$ during which the system is allowed to move from 0 to r, and the standstill time window $[T_B, T]$, during which standstill at r is required. To achieve high-accuracy setpoint positioning in this motion setting, the following design procedure can be employed:

1) Design a cost function (see, e.g., (5.6) and implemented through (5.15)) that captures the desired performance, and define appropriate weights or penalties w_1 and w_2, associated with the transient time window $[0, T_B)$, and the standstill time window $[T_B, T]$, respectively.

2) Replace the linear PID feedback controller in (5.3) by the time-varying PID feedback controller in (5.8) with switching function $\varsigma(t)$ in (5.12):

   a) use the same values for the parameters k_p and k_d.

   b) Parameterize the time-varying integrator gain $k_i(t)$ by a set of basis functions, see (5.9), and choose the type of basis functions, see, e.g., Examples 5.4 or 5.5.

   c) Given the choice of basis functions, choose the number of basis functions b. This determines the size of the to-be-designed parameter vector $p \in \mathbb{R}^{n_p}$, with n_p the number of elements. A large amount of basis functions allows a more flexible design for $k_i(t)$, however it requires more parameters to be tuned later on. This may yield a more complex objective function with many local minima which is not desired when using gradient-based optimization methods. Moreover, visualization of the objective function becomes increasingly difficult or impossible with $n_u 3$, and more parameters to-be-designed typically leads to slower convergence which can be undesired.

3) Decompose the to-be-designed parameter vector p as $p = p_0 + Cu$:

   a) design the initial parameter vector $p_0 \in \mathbb{R}^{n_p}$, having n_p components. A good choice for the first element of p_0 would be to use the value for k_i used in the linear case. A value of 0 for the elements that correspond to the standstill time window is a good choice as well.

   b) select the specific parameters to-be-optimized through the user-defined selection matrix $C \in \mathbb{R}^{n_p \times n_u}$, with n_u the amount of parameters to-be-optimized, and u the vector of to-be-optimized parameters by the extremum-seeking algorithm.

4) Implement the extremum-seeking controller, i.e., a ZOH element in (5.18), a periodic sampler in (5.17), and an extremum-seeking algorithm to optimize the input vector u. The extremum-seeking algorithm can be of the gradient-descent type.

In the next section, this design procedure has been employed to demonstrate the working principle and the effectiveness of the proposed PID-based learning controller on an industrial nano-positioning stage.

5.6 Industrial case study: PID-based learning control for high-accuracy positioning of an industrial motion stage system

In this section, we demonstrate the working principle and the effectiveness of the proposed PID-based learning controller on an industrial nano-positioning stage. The considered stage represents a sample manipulation stage of an electron microscope, exhibiting significant and unknown frictional effects.

5.6.1 Motion stage system description

The experimental setup is presented in Fig. 5.5. The setup consists of a Maxon RE25 DC servo motor ① connected to a spindle ② via a coupling ③ that is stiff in the rotational direction while being flexible in the translational direction. The spindle drives a nut ④, transforming the rotary motion of the spindle to a translational motion of the attached carriage ⑤, with a ratio of $7.96 \cdot 10^{-5}$ m/rad. A coiled spring ⑧ connects the carriage to the fixed world to eliminate any backlash between the spindle and the nut. The position of the carriage is measured by a linear Renishaw encoder ⑥ with a resolution of 1 nm (and peak noise level of 4 nm).

For frequencies up to 200 Hz, the system dynamics can be well described by the model in (5.2). The mass $m = 172.6$ kg consists of the transformed (rotational) inertia of the motor and the spindle (with an *equivalent* mass of 171 kg), and of the mass of the carriage (1.6 kg).

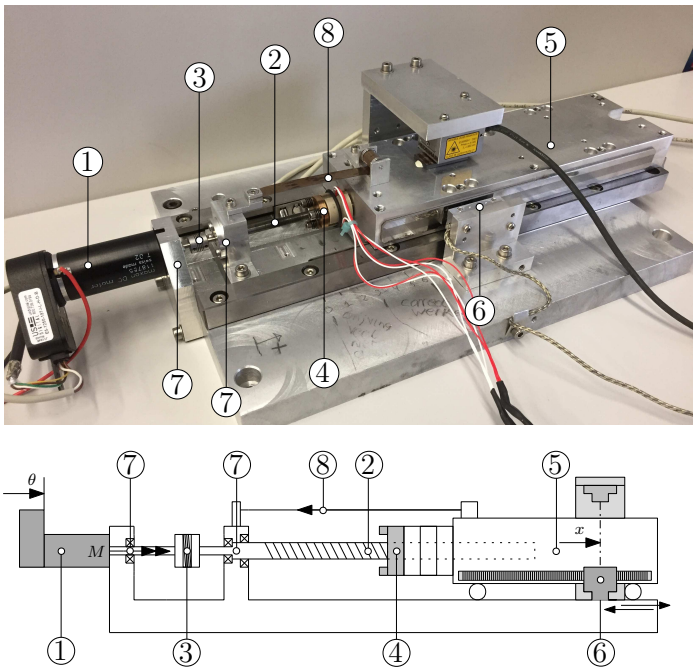

Figure 5.5: Industrial nano-positioning motion stage set-up: ① Maxon RE25 DC servo motor, ② spindle, ③ coupling, ④ nut, ⑤ carriage, ⑥ linear Renishaw encoder, ⑦ bearings, ⑧ coiled spring.

The friction characteristic for Φ in (5.2) is dominated by the bearings supporting the motor axis and the spindle (see ⑦ in Fig. 5.5), and by the contact between the spindle and the nut ④. The latter contact is lubricated, which induces a Stribeck effect. Since the system is rigid and behaves as a single mass for frequencies up to 200 Hz, these friction forces can be summed up to provide a single net friction characteristic as Φ in (5.2).

Remark 5.11. *The experimental setup is the same as the setup in (Beerens et al., 2019, Sec. 5), where dominantly Coulomb and viscous friction was present. For the experimental study in this chapter, a different carriage position and spindle orientation, and different lubrication conditions result in a significant Stribeck effect instead, as illustrated in Fig. 5.2 and the experimental results below.*

According to standard operation of the nano-positioning stage in an electron microscope, we can only use a higher-order reference trajectory. Therefore, the step reference $r = 1$ mm is mimicked by a fast third-order reference trajectory. We require the carriage to be in standstill at $r = 1$ mm at $T_B = 1.5$ s, and the

setpoint operation ends at $T = 3$ s. After each setpoint operation, the system is re-initialized to its starting position $x_1 = 0$ mm using an internal homing procedure.

5.6.2 Controller settings and ESC-based optimal tuning

The design of the PID-based controller with time-varying integrator gain used in the experiments is discussed in Section 5.3. First, the PID-controller gains are tuned using linear loop-shaping techniques (Franklin et al., 2001), resulting in $k_p = 10^7$ N/m, and $k_d = 2 \cdot 10^3$ Ns/m. The time-varying integrator gain is parameterized by (5.9) with $b = 6$ linear spline basis functions as in Example 5.5, from which follows that $t_s = \frac{T}{b} = 0.5$ seconds. We select 2 parameters to-be-optimized. The parameter vector $p = p_0 + Cu$, with initial parameter vector $p_0 = [1 \cdot 10^8 \ 0 \ 0 \ 0 \ 0 \ 0 \ 0]^\top$, and a selection matrix $C = \begin{bmatrix} 0 & 1 & 0 & 0 & 0 & 0 & 0 \\ 0 & 0 & 1 & 0 & 0 & 0 & 0 \end{bmatrix}^\top$. The first element of vector p_0 is equal to the constant integrator gain of a *classical* PID controller, as obtained by the loop-shaping procedure (Fig. 5.2 shows the measured responses with these settings). The vector $u \in \mathbb{R}^{2\times 1}$ will be determined by Algorithm 5.8, and the performance of the control system in the sense of (5.14) depends on the value of these parameters.

For the current case study, we focus on setpoint accuracy rather than transient performance. Therefore, we define the system's performance by the objective function Q in (5.14) and implemented by (5.15), where we have taken $w_1 = 0$ and $w_2 = 1 \cdot 10^8$ in (5.16). Moreover, we augment Q with a logarithmic *barrier function* in order to restrict the values of the parameter values found by the extremum-seeking controller, such that $k_i(t)$ remains bounded for all $t \in [0, T]$. In particular, $k_i(t)$ then satisfies $\underline{k}_i \geq k_i(t) \leq \overline{k}_i$, with $\underline{k}_i = -0.2 \cdot 10^8$, and $\overline{k}_i = 1.2 \cdot 10^8$. The augmented objective function is then given by

$$\tilde{Q}(u, \mu) := Q(u) + \mu B(u), \tag{5.22}$$

with $Q(u, \mu)$ as in (5.14), $\mu = 1 \cdot 10^{-4}$ the barrier parameter, and the logarithmic barrier function B given by

$$B(u) := -\sum_{i=1}^{4} \log(-G_i(u)), \tag{5.23}$$

with $G_1(u) = u^{(1)} - \overline{k}_i$, $G_2(u) = \underline{k}_i - u^{(1)}$, $G_3(u) = u^{(2)} - \overline{k}_i$, $G_4(u) = \underline{k}_i - u^{(2)}$.

Remark 5.12. *Different from the discussion on constrained optimization in Chapter 4, in this case study the constraints on the inputs are explicitly known, while in Chapter 4 explicit constraints on inputs are considered unknown and we can only measure the constraint outputs. Nevertheless, we can use the barrier*

function approach in a similar way as done in Chapter 4, and consider the functions $G_1(u), ..., G_4(u)$ as the 'measurable' constraint functions.

To minimize $\tilde{Q}$, we employ Algorithm 5.8 with the following gradient descent algorithm for F:

$$F(u, Y(u)) := u + \lambda \nabla \tilde{Q}(u, \mu), \tag{5.24}$$

with so-called optimizer gain λ, and where $\nabla \tilde{Q}(u, \mu)$ denotes the gradient of the modified objective function $\tilde{Q}(u, \mu)$. The gradient is estimated based on the function $Y(u)$, containing the collected output measurements taken after each repetition, and through a finite difference computation as follows:

$$\nabla \tilde{Q}(u, \mu) := \frac{1}{\tau} \begin{bmatrix} 1 & -1 & 0 \\ 1 & 0 & -1 \end{bmatrix} Y(u), \tag{5.25}$$

with

$$Y(u_k) := \begin{bmatrix} \tilde{Q}(\bar{u}_{kn_v}, \mu) \\ \vdots \\ Q(\bar{u}_{(k+1)n_v - 1}, \mu) \end{bmatrix}, \tag{5.26}$$

and with so-called step size τ. To facilitate the estimation of the gradient through measurements, the dither functions are chosen as follows: $v_1^\top := [0\ 0]$, $v_2^\top := [\tau\ 0]$, and $v_3^\top := [0\ \tau]$. We use the following numerical values; step size $\tau = 0.25 \cdot 10^7$, and gain $\lambda = 2 \cdot 10^{16}$, unless stated otherwise.

5.6.3 Experimental results

Identifying the objective function

The dependence of the achievable setpoint accuracy, captured by the performance metric $\tilde{Q}$ in (5.22) to be minimized, on the vector u is depicted by means of an measured input-output mapping $\tilde{Q}$ in Fig. 5.6. We use this mapping to verify the time-domain results presented later on. Two regions are observed where $\tilde{Q}$ is small, indicating integrator gain settings that can lead to a high setpoint accuracy. Such a static input-output mapping, however, is in general time-consuming to obtain, can vary (slowly) over time, and can vary from machine to machine. Hence, such an offline, brute-force approach to determine performance-optimal settings is not feasible in practice. Therefore, the optimal parameter settings are iteratively obtained by the online ESC algorithm, solely based on real-time output measurements.

Time-domain results obtained by extremum seeking

Consider Fig. 5.7, which shows the measured augmented performance cost $\tilde{Q}(u_k)$ as in (5.22) and the corresponding vector of parameters u_k as determined by the extremum-seeking controller, as a function of the controller updates, starting

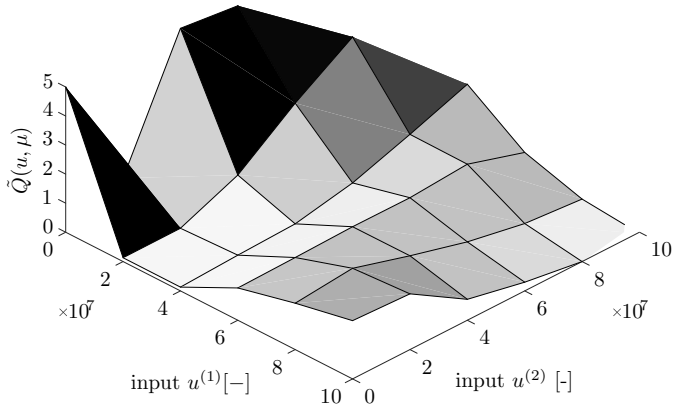

(a) Three-dimensional plot

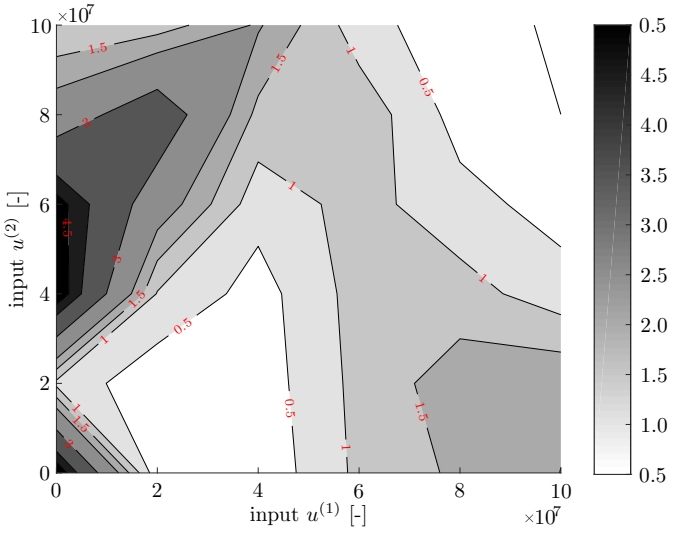

(b) Contour plot

Figure 5.6: Experimentally obtained input-output mapping $\tilde{Q}(u,\mu)$, which shows two regions where $\tilde{Q}(u,\mu)$ is small, indicating integrator gain settings that yield accurate setpoint positioning.

with initial parameter vector $u_0 = [0.85,\ 0.175]^\top \cdot 10^8$. Moreover, Fig. 5.8 depicts the setpoint error $e(t)$, the corresponding time-varying integrator gain design $k_i(t)$, and the resulting control force u_c for four different controller updates

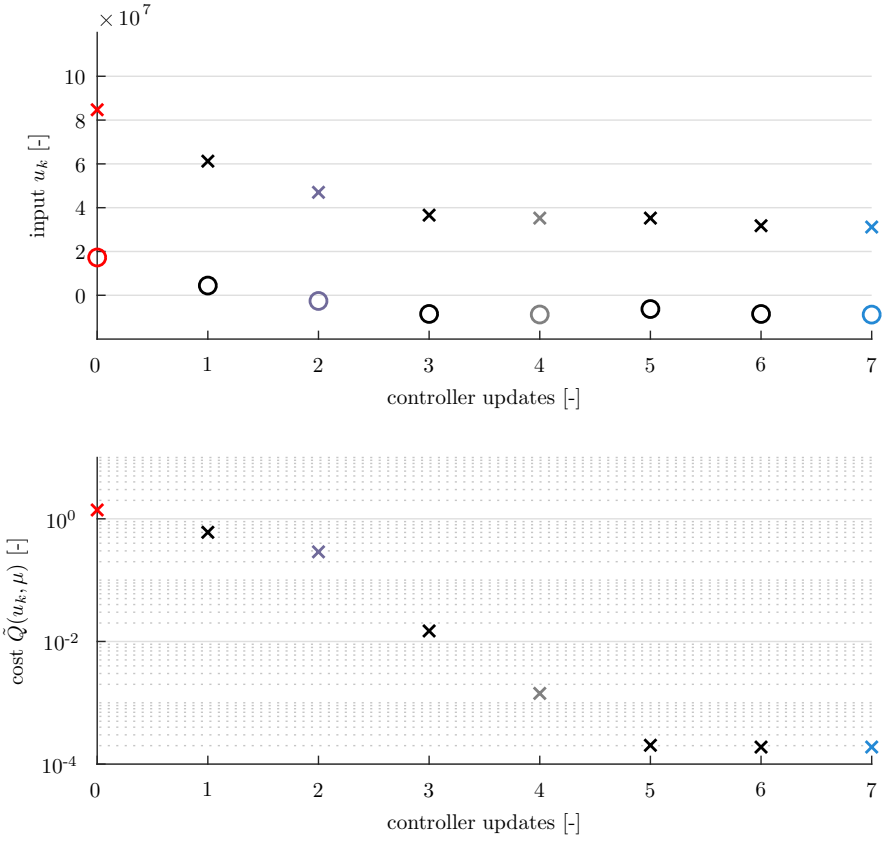

Figure 5.7: Experimental results of the PID-based learning controller applied to the industrial nano-positioning motion stage, illustrating the minimization of the augmented performance cost $\tilde{Q}$ (bottom) and the corresponding parameter vector u_k (top) ('×' and '∘' denote the first and second parameter of the vector u_k, respectively), as a function of the controller updates. Fig. 5.8 depict the setpoint error, and the corresponding time-varying integrator gain $k_i(t)$, and control force u_c, corresponding to the initial parameter setting $u_0 = [0.85\ 0.175]^\top$ (—), the 2nd (—), 4th (—), and 7th (—) extremum seeking controller update.

(final and three intermediate). Additionally, Table 5.1 shows the root-mean-square (rms) value of the setpoint error during the standstill window $t \in [T_B, T]$

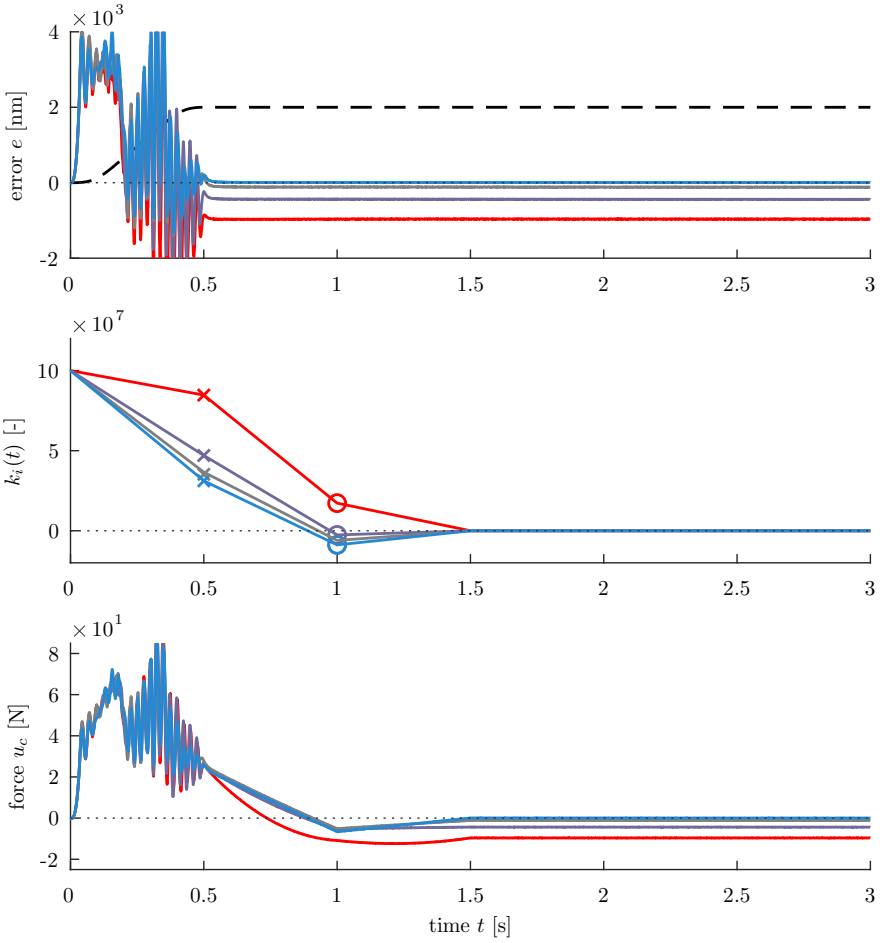

Figure 5.8: Experimental results of the PID-based learning controller applied to the industrial nano-positioning motion stage, illustrating the optimization of the setpoint error (for $t > 1.5$) by adaptation of $k_i(t)$. The error and corresponding $k_i(t)$ and u_c are shown after the initial parameter setting $u_0 = [0.85,\ 0.175]^\top \cdot 10^8$ (—), the 2nd (—), 4th (—), and 7th (—) extremum seeking controller update. The achieved accuracy for $t > 1.5$ after the 7th update is about 5 nm.

for all controller updates, and is computed as follows:

$$e_{rms} := \sqrt{\frac{1}{T - T_B} \int_{T_B}^{T} |e(t)|^2 dt}. \tag{5.27}$$

Table 5.1: The root-mean-square (rms) values of the setpoint error during the standstill window $t \in [T_B, T]$ for all controller updates in the case of initial parameter setting $u_0 = [0.85,\ 0.175]^\top \cdot 10^8$ (left) and $u_0 = [0.9,\ 0.4]^\top \cdot 10^8$ (right).

updates	rms value [nm]
0	$6.42 \cdot 10^2$
1	$4.23 \cdot 10^2$
2	$2.93 \cdot 10^2$
3	66.3
4	20.5
5	7.75
6	7.49
7	7.50

updates	rms value [nm]
0	$4.39 \cdot 10^2$
1	$2.85 \cdot 10^2$
2	$2.52 \cdot 10^2$
3	$1.93 \cdot 10^2$
4	$1.29 \cdot 10^2$
5	65.0
6	41.9
7	27.0
8	21.2

It can be observed that limit cycling is indeed prevented since $k_i(t) = 0$ for all $t \in [T_B, T]$, and we only observe one interval of stick (during the standstill time window, as desired). Moreover, the extremum-seeking controller iteratively finds controller parameters u_k that result in a relatively small time-varying integrator gain design $k_i(t)$ on $t \in [0, 1.5)$, yielding a position error in the range of $4 - 6$ nm, depicted by (—). In contrast, the classical PID controller for this particular measurement yields an absolute error of about 100 nm on the same time interval (see Fig. 5.2), and does not provide robustness during the standstill time window. This clearly illustrates the performance benefits of the proposed PID-based learning controller in terms of the ability to cope with Stribeck friction and achieving superior setpoint positioning accuracy. The parameter evolution of this experiment is visualized by (- -) in the input-output mapping in Fig. 5.11.

Another interesting optimization experiment and resulting time-domain response is depicted in Fig. 5.9, which shows the measured augmented performance cost $\tilde{Q}(u_k)$ as in (5.22) and the corresponding vector of parameters u_k as determined by the extremum-seeking controller, as a function of the controller updates, starting with initial parameter vector $u_0 = [0.9,\ 0.4]^\top \cdot 10^8$. Moreover, Fig. 5.10 depicts the setpoint error $e(t)$, the corresponding time-varying integrator gain design $k_i(t)$, and the resulting control force u_c for four different controller updates (final and three intermediate). Additionally, Table 5.1 shows the root-mean-square (rms) value of the setpoint error during the standstill window $t \in [T_B, T]$ for all controller updates. Again, the parameter evolution of this experiment is visualized by (-·-) in the input-output mapping in Fig. 5.11. The parameters now converge towards the local minimum in the upper right corner of the input-output mapping in Fig. 5.11. The existence of this particular (local) minimum can be explained by considering the upper two subplots

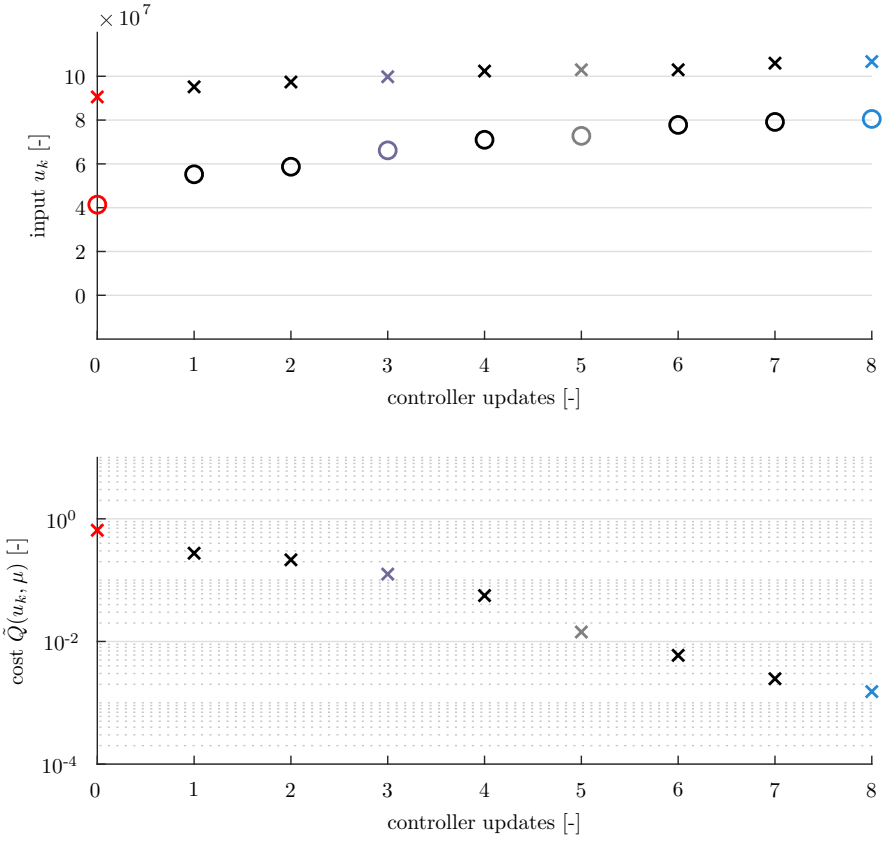

Figure 5.9: Experimental results of the PID-based learning controller applied to the industrial nano-positioning motion stage, illustrating the minimization of the augmented performance cost $\tilde{Q}$ (bottom) and the corresponding parameter vector u_k (top) ('×' and '○' denote the first and second parameter of the vector u_k, respectively), as a function of the controller updates. Fig. 5.8 depict the setpoint error, and the corresponding time-varying integrator gain $k_i(t)$, and control force u_c, corresponding to the initial parameter setting $u_0 = [0.9\ 0.4]^\top$ (—), the 2nd (—), 4th (—), and 7th (—) extremum seeking controller update.

of Fig. 5.10, depicting the position error and time-varying integrator gain design $k_i(t)$, respectively. Due to the relatively large time-varying integrator gain $k_i(t)$ for $t \in [0, 1.5)$ obtained by the extremum-seeking controller and depicted by (—), the associated integral action during the transient results in significant overshoot of the setpoint. The significant overshoot can be attributed to the weight $w_1 = 0$, chosen during the transient time window, which implies that

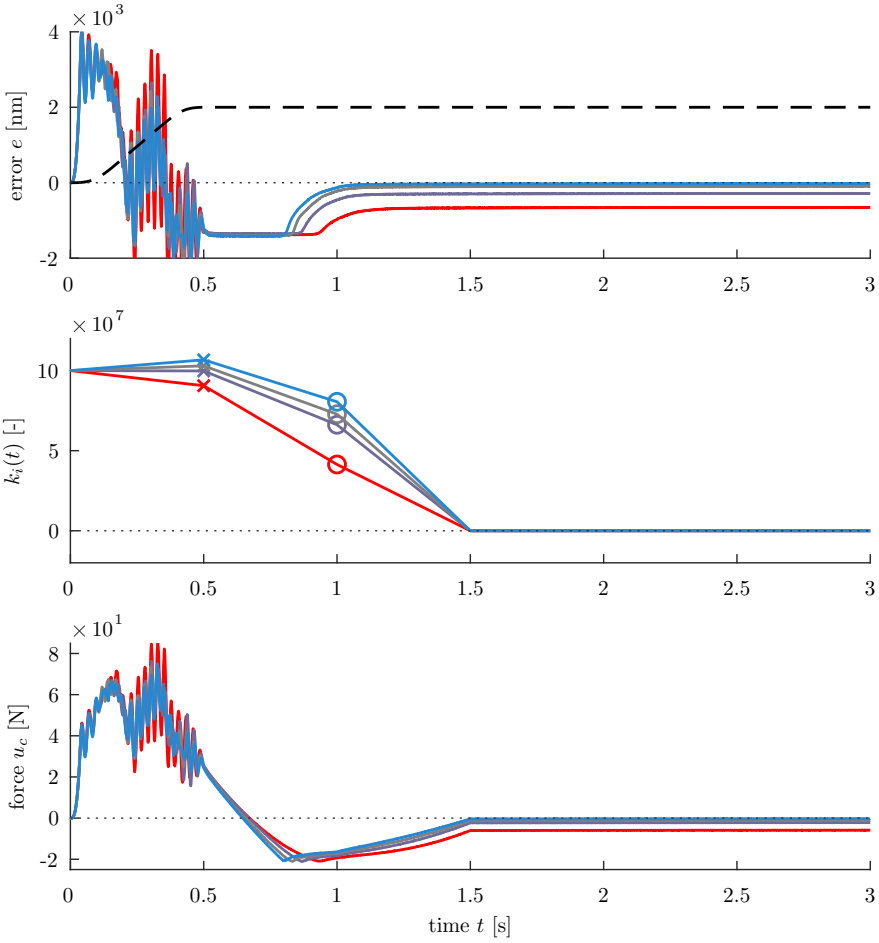

Figure 5.10: Experimental results of the PID-based learning controller applied to the industrial nano-positioning motion stage, illustrating the optimization of the setpoint error (for $t > 1.5$) by adaptation of $k_i(t)$. The error and corresponding $k_i(t)$ and u_c are shown after the initial parameter setting $u_0 = [0.9,\ 0.4]^\top \cdot 10^8$ (—), the 2nd (—), 4th (—), and 7th (—) extremum seeking controller update. The achieved accuracy for $t > 1.5$ after the 7th update is about 25 nm.

large transients are not penalized. The system then arrives in a stick phase, where control force is built up by the integrator action. Eventually the system slips and, due to the Stribeck effect in combination with the particular decreasing integrator gain, the system arrives in a stick phase again close to the setpoint,

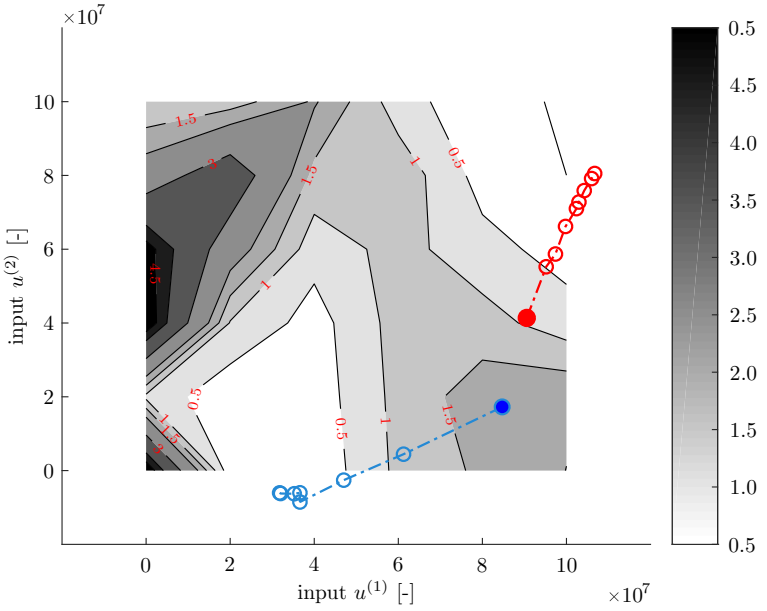

Figure 5.11: Input-output mapping $\tilde{Q}(u)$. The figure shows the convergence to optimal integrator gain settings starting from two different initial conditions u_0, namely $u_0 = [0.85\ 0.175]^\top \cdot 10^8$ (- -) and $u_0 = [0.9\ 0.4]^\top \cdot 10^8$ (-·-). The starting point of both trajectories is denoted by the solid dot.

yielding a position error in the range of 25 nm.

Fig. 5.12 shows the time-domain results after the final extremum seeking controller update for both cases, illustrating the achieved position error. Moreover, for comparison, Fig. 5.12 contains the experimental results of the linear PID feedback controller as well, which shows a significant setpoint error of 100 nm at $t = 3$ seconds. From the zoom plots in Fig. 5.12 it follows that the system is not completely at rest during $t \in [1.5, 3]$. This can be attributed to other microscopic frictional effects that play a role, which are not treated here as they are beyond the scope of this chapter. Nevertheless, the experimental results show that the proposed time-varying PID controller results in superior positioning accuracy (compared to classical PID control), and that the extremum-seeking controller successfully finds the optimal tuning of the time-varying integrator gain, regardless of the initial values of u, for the unknown frictional situation at hand.

5.7 Conclusions

We have presented a novel time-varying integrator gain design for motion systems with unknown Coulomb and velocity-dependent friction (including the Stribeck effect), performing a repetitive motion profile. The proposed controller is capable of achieving a high positioning accuracy, in contrast to classical PID control, which often leads to limit cycling, i.e., loss of setpoint stability. The time-varying integrator gain is parameterized by linear basis functions, resulting in a continuous control signal. The specific tuning of the time-varying integrator gain, that results in a high setpoint accuracy in the presence of unknown friction, is iteratively obtained by employing a sampled-data extremum-seeking framework. The performance benefits of the proposed control architecture are experimentally demonstrated on a nano-positioning stage in an electron microscope, illustrating its superior performance over classical PID control.

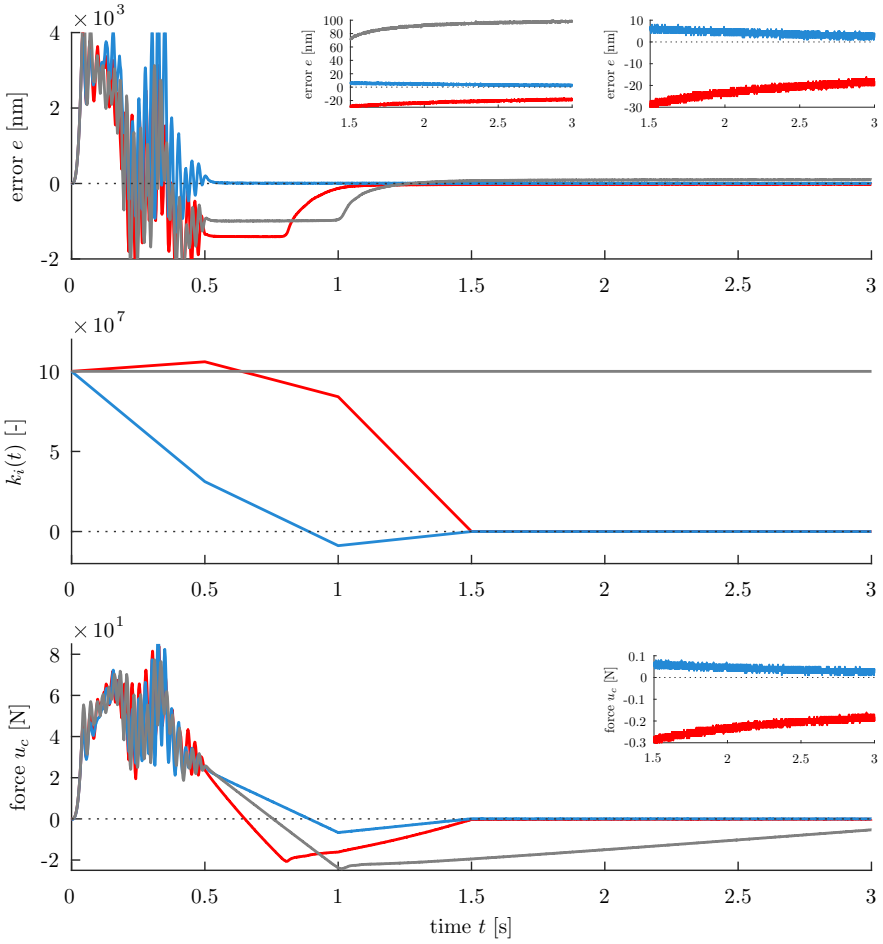

Figure 5.12: Experimental results of the PID-based learning controller applied to the industrial nano-positioning motion stage. The figure illustrates the resulting setpoint errors $e(t)$ and corresponding $k_i(t)$ and $u_c(t)$ after the final extremum seeking controller update, for 2 different experiments and depicted by (—) and (—). The experimental results for a fixed integrator gain are depicted by (—). The initial parameter settings u_0 and the corresponding trajectories are depicted in Fig 5.11 by the corresponding colored plots (-·-) and (- -).

5.A Proof of Proposition 5.7

Without loss of generality, consider $r = 0$ (which implies $e = -x_1$ in (5.8)), and we consider the intervals $[0, T_B)$ and $[T_B, T]$ separately.

By design, we have $\varsigma = 1$ on the interval $[0, T_B)$. Then, with state vector $x := [x_1, x_2, x_3]^\top$, for all $t \in [0, T_B)$, we rewrite the closed-loop system (5.1), (5.2), (5.8) as

$$\dot{x} \in A(t)x - e_2(F_s\mathrm{Sign}(x_2) - f(x_2)) \tag{5.28}$$

with

$$A(t) = \begin{bmatrix} 0 & 1 & 0 \\ -k_p & -k_d - \gamma & -k_i(t) \\ 1 & 0 & 0 \end{bmatrix}, \quad e_2 = \begin{bmatrix} 0 \\ 1 \\ 0 \end{bmatrix}. \tag{5.29}$$

Define $f_L(x_2) := Lx_2 - f(x_2)$, which satisfies $f_L(x_{2,a}) \leq f_L(x_{2,b})$ for each $x_{2,a} < x_{2,b}$ and $L > 0$ by Assumption 5.1(iii), i.e., $f_L(x_2)$ is nondecreasing. Next, define $\Phi_L(x_2) := F_s\mathrm{Sign}(x_2) + f_L(x_2)$, and rewrite (5.28) as

$$\begin{aligned} \dot{x} &\in \begin{bmatrix} 0 & 1 & 0 \\ -k_p & L - k_d - \gamma & k_i(t) \\ -1 & 0 & 0 \end{bmatrix} x - e_2\Phi_L(x_2) \\ &=: A_L(t)x - e_2\Phi_L(x_2). \end{aligned} \tag{5.30}$$

Existence of solutions[1] to (5.30) follows from Filippov (1988, Sec. 7, Thm. 1) because the set-valued mapping in (5.30) is outer semicontinuous and locally bounded with nonempty compact convex values. Consider then two solutions x_a and x_b to (5.30) with $x_a(0) = x_b(0)$, and define $\delta := x_a - x_b$. For almost all $t \in [0, T_B)$,

$$\dot{\delta} \in A_L(t)\delta - e_2(\Phi_L(x_{2,a}) - \Phi_L(x_{2,b})).$$

Since $k_i(t)$ is bounded by design, there exists $M_1 > 0$ such that $|A(t)| \leq M_1$ for all $t \in [0, T_B)$, with $|A(t)|$ the (induced) 2-norm of matrix $A(t)$. Then, we have

$$\begin{aligned} \frac{1}{2}\frac{d}{dt}|\delta|^2 &\in \delta^\top A_L(t)\delta + \delta_2^\top(\Phi_L(x_{2,b}) - \Phi_L(x_{2,a})) \\ &\leq M_1|\delta|^2 + \max_{\substack{f_b \in \Phi_L(x_{2,a}(t) - \delta_2(t)) \\ f_a \in \Phi_L(x_{2,a}(t))}} \delta_2(f_b - f_a) \\ &=: M_1|\delta|^2 + N(t). \end{aligned} \tag{5.31}$$

Whether $x_{2,a}(t)$ and $x_{2,a}(t) - \delta_2(t)$ are positive, zero, or negative, inspection of all cases reveals that $N(t) \leq 0$ for all $t \in [0, T_B)$ because f_L is nondecreasing, which implies that Φ_L is nondecreasing. As a result, (5.31) satisfies

$$\frac{1}{2}\frac{d}{dt}|\delta|^2 \leq M_1|\delta(t)|^2, \tag{5.32}$$

[1] A solution to (5.30) is any locally absolutely continuous function x that satisfies (5.28) for almost all $t \in [0, T_B)$.

for almost all $t \in [0, T_B)$. Then, $\delta(0) = 0$ implies $\delta(t) = 0$ for all $t \in [0, T_B)$ by standard comparison theorems (e.g., Khalil (2002, Lemma 3.4)).

On $[T_B, T]$, we have $\dot{x}_3 = \varsigma x_1 = 0$ because, by design, the switching function $\varsigma = 0$ on the considered interval, so that $x_3(t) = x_3(T_B)$ for all $t \in [T_B, T]$. Moreover, $k_i(t) = 0$ for $t \in [T_B, T]$. With

$$\begin{aligned} \dot{x} &\in \begin{bmatrix} 0 & 1 & 0 \\ -k_p & L - k_d - \gamma & 0 \\ 0 & 0 & 0 \end{bmatrix} x - e_2 \Phi_L(x_2) \\ &=: A_{L_2}(t) x - e_2 \Phi_L(x_2). \end{aligned} \tag{5.33}$$

we obtain analogously to the previous case

$$\frac{1}{2} \frac{d}{dt} |\delta|^2 \leq M_2 |\delta(t)|^2, \tag{5.34}$$

for almost all $t \in [T_B, T]$, with $M_2 := \lambda(A_{L_2})$ the largest singular value of A_{L_2}. Using absolute continuity of solutions, and the fact that $\delta(t) = 0$ for all $t \in [0, T_B)$ (as established above), we have that $\delta(T_B) = 0$, and (5.34) implies that $\delta(t) = 0$ for all $t \in [T_B, T]$. Uniqueness of solutions on $[0, T]$ is then proven.

We now turn to proving that solutions to the closed-loop system remain bounded on $[0, T]$. Let x_a be a generic solution to the closed-loop system, with $x_a(0) \in K_1 \bar{\mathcal{B}}$ and $K_1 \geq 0$, and take $x_b(0) = (0, 0, 0)$, so that $x_b(t) = 0$ for all $t \in [0, T]$, and $\delta(0) \in K_1 \bar{\mathcal{B}}$. The solutions x_a and x_b satisfy (5.32) and (5.34) on $[0, T_B)$ and $[T_B, T]$, respectively. In both inequalities, the right-hand side is bounded for all t in its domain, which excludes finite escape times for δ on $[0, T]$. Hence, there exists $K_2 > 0$ such that $\delta(t) \in K_2 \bar{\mathcal{B}}$ for all $t \in [0, T]$. Since $x_b(t) = 0$ for all $t \in [0, T]$, we have $x_a(t) \in K_2 \bar{\mathcal{B}}$ for all $t \in [0, T]$, which completes the proof. □

Part III

Closing

Chapter 6

Conclusions and Recommendations

6.1 Conclusions

Achieving top-level system performance by means of automatic control in the high-tech industry is still largely realized by skillful control engineers on the basis of accurate system models and expert knowledge. However, the increasing complexity in terms of uncertainty, non-stationary nature of system dynamic properties and disturbances, and mode-of-use dependent performance specifications in current high-tech systems and future engineering developments will progressively challenge the sole usage of purely model-based approaches in achieving *optimal* system performance. To account for changing, uncertain, or unknown dynamics and disturbance characteristics, and to enable the satisfaction of increasing accuracy and robustness demands, a lot can be gained by combining or supporting model-based control engineering in future complex high-tech systems with *data-based*, *automated* and *adaptive* performance optimization techniques.

In this dissertation, data-based automated performance optimization of high-tech systems is addressed by an adaptive control technique known as *extremum-seeking control*. For data-based performance optimization in the context of high-tech systems, the state-of-practice extremum-seeking control methods face a number of challenges. To this end, the following objectives have been addressed in this dissertation.

Objective 1. *Develop an extremum-seeking control method for the data-based optimization of time-varying steady-state responses of general nonlinear systems, which is applicable for the optimization of time-varying behavior in industrial high-tech systems.*

Objective 2. *Develop a sampled-data extremum-seeking control framework for data-based constrained optimization of nonlinear dynamical systems, in which information on system performance and constraints on system inputs is solely obtainable through output measurements.*

Objective 3. *Develop a sampled-data extremum-seeking control method for op-*

timization of transient system behavior, inspired by and applicable to optimization of time-varying, repetitive tasks in high-tech positioning systems.

Objective 4. *Implementation and validation of the developed extremum-seeking control methods in industrially-relevant case studies.*

The five main contributions of this dissertation are directly related to the four objectives mentioned above. In particular, the following two contributions are devoted to addressing **Objective 1**.

- *Chapter 2* presents a novel *extremum-seeking control approach for optimization of generically time-varying steady-state behavior of nonlinear dynamical systems*. This chapter provides an extension of the class of extremum-seeking problems from those involving equilibria solutions or periodic time-varying steady-state responses, to those involving systems exhibiting generically time-varying steady-state responses. In particular, generically time-varying disturbances and the resulting to-be-optimized performance, characterized in terms of generically time-varying steady-state system responses, are considered an integral part in the extremum-seeking control problem formulation. The convergent systems property, being the time-varying analogue of the common global exponential stability property for systems with equilibria solutions, has been essential in this time-varying extremum-seeking context and the extremum-seeking problem formulation. To facilitate the use of extremum seeking control in this more generic and time-varying context, a user-defined, generic filter structure, the so-called dynamic cost function, is introduced. By adopting an observer-based extremum-seeking control strategy, semi-global practical asymptotic stability of the closed-loop extremum-seeking control scheme is proven in the presence of bounded and time-varying external disturbances. The neighborhood of convergence can be made arbitrarily small by selecting sufficiently small values for tunable parameters for the extremum-seeking controller and the dynamic cost function. The working principle of the extremum-seeking control method is illustrated by means of the real-time performance optimal tuning of a nonlinear control strategy for a motion control application.
- *Chapter 3* presents a novel extension of the observer-based extremum-seeking control strategy as exploited in Chapter 2. In particular, the extension involves the incorporation of explicit knowledge about the user-defined dynamic cost function into the observer-based extremum-seeking controller design, which facilitates enhance convergence speed of the resulting extremum-seeking control scheme. On the basis of Chapter 2, semi-global practical asymptotic stability of the closed-loop extremum-seeking control scheme with the extended approach is proven in the presence of bounded and time-varying external disturbances. The effectiveness

of both the nominal extremum-seeking control design in Chapter 2 and the extended design in Chapter 3 are evidenced experimentally by an application to an industrial motion stage set-up which represents the short-stroke motion of a wafer stage system commonly found within lithography systems.

The following contribution is devoted to addressing **Objective 2**.

- *Chapter 4* presents a *sampled-data extremum-seeking control framework for the constrained optimization of a class of nonlinear dynamical systems.* In particular, this chapter provides an extension of the sampled-data extremum-seeking framework in Teel and Popović (2001) in two ways. Namely, the proposed framework considers 1) a class of nonlinear, possibly infinite-dimensional, dynamical systems for which the relations between tunable system parameters and to-be-optimized objective function and the constraint functions are unknown and available through measurement only, and 2) a class of smooth and nonsmooth optimization algorithms to facilitate extremum-seeking in the presence of unknown but measurable objective function and constraints functions, inspired by the use of barrier function methods. Under the assumption that the system initialization yields satisfactory operating conditions that satisfy the constraints in steady-state, the resulting closed-loop dynamics is proven to be stable, steady-state constraint satisfaction is guaranteed for all iterations of the optimization process, and constrained optimization is achieved. The working principle of the proposed framework is illustrated by means of a representative industrial case study of constrained optimization of extreme ultraviolet light generation in a laser produced plasma source within a state-of-the-art lithography system.

The following contribution is devoted to addressing **Objective 3**.

- *Chapter 5* presents an *iterative learning control strategy based on extremum-seeking control for high-accuracy repetitive setpoint control of frictional motion systems.* In particular, a novel proportional-integral-derivative-based controller with a time-varying integrator gain design is proposed that facilitates improved time-domain behavior in terms of overshoot and setpoint accuracy over classical proportional-integral-derivative control for repetitive motion in frictional motion systems with unknown friction. On the basis of a suitable basis function parametrization, the optimal time-varying integrator gain design is obtained through an automatic iterative controller tuning procedure based on a sampled-data extremum-seeking algorithm, ensuring optimal setpoint positioning accuracy despite the unknown friction characteristics and unknown disturbances. The effectiveness of the proposed approach is evidenced experimentally by application to an industrial nano-positioning motion stage set-up of a high-end electron microscope.

The following contribution is devoted to addressing **Objective 4**.

- The working principle of the developed extremum-seeking method for optimization of time-varying steady-state system behavior in Chapter 2, and described in Contribution 1, is illustrated in simulation by means of the real-time performance optimal tuning of a nonlinear control strategy for a motion control application. The effectiveness of the extremum-seeking control methods for optimization of time-varying steady-state system behavior in Chapters 2 and 3, and described in Contributions 1 and 2, respectively, are both evidenced experimentally in Chapter 3 by application to an industrial motion stage set-up which represents the short-stroke motion of a wafer stage system commonly found within lithography systems. The working principle of the proposed sampled-data extremum-seeking framework for constrained optimization in Chapter 4, and described in Contribution 3, is illustrated by means of a representative industrial case study of constrained optimization of extreme ultraviolet light generation in a laser produced plasma source system within a state-of-the-art lithography system. The effectiveness of the proposed approach for transient performance optimization in Chapter 5, and described in Contribution 4, is evidenced experimentally by application to an industrial nano-positioning motion stage set-up of a high-end electron microscope.

Summarizing, this dissertation presents novel extremum-seeking control methods that enable data-based performance optimization for a richer class of optimization problems, such as i) the data-based optimization of generic time-varying system behavior, ii) data-based, constrained optimization on the basis of measurable to-be-optimized objective function and constraint functions, and iii) data-based, transient performance optimization for repetitive system operations on fixed-time intervals. The developments in data-based optimization through extremum-seeking control are inspired by a large variety of industrially relevant optimization problems, and are experimentally and numerically demonstrated to illustrate their value to industrial high-tech systems.

6.2 Recommendations for future research

In this section, recommendations for future research in extremum-seeking control for data-based optimization of high-tech systems are provided.

- In most extremum-seeking control methods, perturbations are added to the extremum-seeking control scheme such that, on the basis of these known perturbations and the resulting (steady-state) output measurements, information can be obtained to optimize the performance of the system (Krstić and Wang, 2000; Tan et al., 2006; Nešić et al., 2010; Teel and Popović, 2001; Khong et al., 2013b). Supplying perturbations to the system is not always desired, or necessary. For example, in the industrial

case study discussed in Chapter 4 on the (constrained) optimization of extreme ultraviolet (EUV) light generation in a laser-produced-plasma (LPP) source within a next-generation lithography system, many (periodic) disturbances affect the measurable laser-to-droplet position (which we have not exploited in Chapter 4) and measurable EUV light intensity generated by the LPP source. Instead of supplying a perturbation to the nominal laser-to-droplet setpoint and correlating these perturbations with the resulting EUV light intensity measurements, an interesting industrial case study would be to exploit the measurable laser-to-droplet position without additional perturbations to the laser-to-droplet setpoint (which is a sufficiently rich signal due to many disturbances) in optimizing the EUV light generation in the LPP source system using extremum-seeking control. From an extremum-seeking control perspective, this case study may provide interest in self-driving extremum-seeking schemes such as in Carnevale et al. (2009), Hunnekens et al. (2014), and Haring (2016, Chapter 4), or perturbation-based extremum-seeking control without externally applied perturbations.

- The sampled-data extremum-seeking framework for constrained optimization presented in Chapter 4 is useful in industrial applications in which we can monitor various signals, and use optimization methods that solely operate in the admissible set of operating conditions, e.g., optimization algorithms in combination with barrier function methods, to prevent damage to the system during steady-state operation. However, in other cases in which the requirement to operate strictly in the admissible set is not needed, other constrained optimization methods can be explored, for example, sequential quadratic programming (SQP) or other numerical constrained optimization algorithms in the literature. Therefore, an interesting extension to the framework presented in Chapter 4 can be to consider a class of constrained extremum-seeking algorithms in which we are allowed to sample in the infeasible region and expand upon the sampled-data extremum-seeking control framework in Khong et al. (2013b). Namely, their framework relies on the notion of attractivity as opposed to asymptotic stability for the extremum-seeking algorithms, which may allow to include a broader class of constrained optimization problems.
- In Chapter 2, we have employed an observer-based extremum-seeking control method with a so-called dynamic cost function to optimize system performance in the presence of time-varying system behavior. The presence of the dynamic cost function enables the use of extremum-seeking control, however, in the case of small values of the tunable parameters of the dynamic cost function to cope with time-varying system behavior, a deterioration of the convergence speed due to the additional time-scale can occur. In Chapter 3, we provided an extended approach in which we embed linear-time invariant (LTI) structures for the dynamic cost function

in the observer-based extremum-seeking controller to enhance convergence speed of the resulting extremum-seeking control scheme. In cases where accurate knowledge about the system is available, for example, accurate models for linear motion systems, it would be interesting if these models can be exploited in a similar fashion as the dynamic cost function, and achieve even better convergence speed in those cases.

- Investigate combining contributions of Chapter 2 and Chapter 4, i.e., expand the class of nonlinear, possibly infinite-dimensional, systems in the sampled-data extremum-seeking control context to a class which i) allows for time-varying steady-state system behavior in the spirit of Chapter 2, and ii) includes a dynamical cost function in its description to cope with said time-varying steady-state system behavior.
- In Chapter 5, we have experimentally evidenced the effectiveness of employing a proportional-integral-derivative based controller with an iterative learning mechanism based on a sampled-data extremum-seeking control architecture to achieve high positioning accuracy for a frictional motion system. However, depending on, e.g., the choice of the basis function parametrization, the number of basis functions, and the friction characteristic at hand, there exist multiple local minima of the resulting objective function. In order for the extremum-seeking controller to arrive at the global optimum, thereby achieving optimally tuning of the time-varying integrator gain, *global* optimization methods can be explored instead, such as the so-called DIRECT and Shubert algorithms (see Jones et al. (1993) and Shubert (1972), respectively) for non-convex optimization problems as studied in Khong et al. (2013a) and Nešić et al. (2013). Additionally, a different basis function parametrization for the time-varying integrator gain design, as well as a different number of basis functions to-be optimized, can be more suitable in terms of robustness and sensitivity against varying friction characteristics, which has not been studied in detail. Finally, it may be useful to study the robustness to variations in the re-initialization of the system, which is theoretically required for iterative learning control and can be a stringent condition in complex high-tech systems.

Bibliography

Aangenent, W. H. T. M., Witvoet, G., Heemels, W. P. M. H., van de Molengraft, M. J. G., and Steinbuch, M. (2010). Performance analysis of reset control systems. *International Journal of Robust and Nonlinear Control*, 20(11):1213–1233.

Antonello, R., Oboe, R., Prandi, L., and Biganzoli, F. (2009). Automatic mode matching in mems vibrating gyroscopes using extremum-seeking control. *IEEE Trans. Ind. Electron.*, 56(10):3880–3891.

Ariyur, K. and Krstić, M. (2003). *Real Time Optimization by Extremum Seeking Control*. John Wiley & Sons, Inc., New York, NY, USA.

Atta, K. and Guay., M. (2017). Fast proportional integral phasor extremum seeking control for a class of nonlinear system. *IFAC-PapersOnLine*, 50(1):5724 – 5730. 20th IFAC World Congress.

Atta, K., Guay, M., and Lucchese, R. (2019). A geometric phasor extremum seeking control approach with measured constraints. In *Proceedings of 58th IEEE Conference on Decision and Control*, pages 1494–1500.

Banaszuk, A., Ariyur, K., Krstić, M., and Jacobson, C. (2004). An adaptive algorithm for control of combustion instability. *Automatica*, 40(11):1965 – 1972.

Bartolini, G., Pisano, A., Punta, E., and Usai, E. (2003). A survey of applications of second-order sliding mode control to mechanical systems. *International Journal of Control*, 76(9-10):875–892.

Bastin, G., Nešić, D., Tan, Y., and Mareels, I. (2009). On extremum seeking in bioprocesses with multivalued cost functions. *Biotechnology Progress*, 25(3):683–689.

Bazanella, A. S., Campestrini, L., and Eckhard, D. (2012). *Data-driven Controller Design: The H_2 Approach*. Springer.

Beerens, R., Bisoffi, A., Zaccarian, L., Heemels, W., Nijmeijer, H., and van de Wouw, N. (2019). Reset integral control for improved settling of PID-based motion systems with friction. *Automatica*, 107:483 – 492.

Beker, O., Hollot, C. V., Chait, Y., and Han, H. (2004). Fundamental properties of reset control systems. *Automatica*, 40(6):905915.

Benosman, M. (2016). Multi-parametric extremum seeking-based iterative feedback gains tuning for nonlinear control. *International Journal of Robust and Nonlinear Control*, 26(18):4035–4055.

Bisoffi, A., Da Lio, M., Teel, A. R., and Zaccarian, L. (2018). Global asymptotic stability of a PID control system with coulomb friction. *IEEE Transactions on Automatic Control*, 63(8):2654–2661.

Bolder, J. and Oomen, T. (2015). Rational basis functions in iterative learning controlwith experimental verification on a motion system. *IEEE Transactions on Control Systems Technology*, 23(2):722–729.

Bolder, J., Witvoet, G., de Baar, M., van de Wouw, N., Haring, M., Westerhof, E., Doelman, N., and Steinbuch, M. (2012). Robust sawtooth period control based on adaptive online optimization. *Nuclear Fusion*, 52(7):074006.

Boyd, S. and Vandenberghe, L. (2004). *Convex Optimization*. Cambridge University Press, USA.

Bristow, D. A., Tharayil, M., and Alleyne, A. G. (2006). A survey of iterative learning control. *IEEE Control Systems Magazine*, 26(3):96–114.

Butler, H. (2011). Position control in lithographic equipment : an enabler for current-day chip manufacturing. *Control Systems, IEEE*, 31(5):28–47.

Bykov, Y., Schaffer, M., Dodonova, S., Albert, S., Plitzko, J., Baumeister, W., Engel, B., and Briggs, J. (2017). The structure of the copi coat determined within the cell. *eLife*, 6:e32493.

Campi, M., Lecchini, A., and Savaresi, S. (2002). Virtual reference feedback tuning: a direct method for the design of feedback controllers. *Automatica*, 38(8):1337 – 1346.

Cao, Z., Dürr, H.-B., Ebenbauer, C., Allgöwer, F., and Gao, F. (2017). Iterative learning and extremum seeking for repetitive time-varying mappings. *IEEE Trans. Autom. Control*, 62(7):3339–3353.

Carnevale, D., Astolfi, A., Centioli, C., Podda, S., Vitale, V., and Zaccarian, L. (2009). A new extremum seeking technique and its application to maximize rf heating on ftu. *Fusion Engineering and Design*, 84(2):554–558. Proc. 25th Symposium on Fusion Technology.

Castanos, F. and Kunusch, C. (2015). Ditherless extremum seeking for hydrogen minimization in pem fuel cells. *IEEE Transactions on Industrial Electronics*, 62(8):5218–5226.

Centioli, C., Iannone, F., Mazza, G., Panella, M., Podda, S., Tuccillo, A., Vitale, V., Pangione, L., and Zaccarian, L. (2005). Extremum seeking applied to the plasma control system of the frascati tokamak upgrade. In *Proc IEEE Conf Decis Control*, pages 8227–8232.

Clegg, J. C. (1958). A nonlinear integrator for servomechanisms. *Transactions of the American Institute of Electrical Engineers, Part II: Applications and Industry*, 77(1):41–42.

Creaby, J., Li, Y., and Seem, J. (2009). Maximizing wind turbine energy capture using multivariable extremum seeking control. *Wind Engineering*, 33(4):361–387.

Deenen, D. A., Heertjes, M. F., Heemels, W. P. M. H., and Nijmeijer, H. (2017). Hybrid integrator design for enhanced tracking in motion control. In *2017 American Control Conference (ACC)*, pages 2863–2868.

DeHaan, D. and Guay, M. (2005). Extremum-seeking control of state-constrained nonlinear systems. *Automatica*, 41(9):1567 – 1574.

Dewasme, L., Srinivasan, B., Perrier, M., and Wouwer, A. V. (2011). Extremum-seeking algorithm design for fed-batch cultures of microorganisms with overflow metabolism. *Journal of Process Control*, 21(7):1092 – 1104.

Dinçmen, E., Güvenç, B. A., and Acarman, T. (2014). Extremum-seeking control of abs braking in road vehicles with lateral force improvement. *IEEE Transactions on Control Systems Technology*, 22(1):230–237.

Drakunov, S., Özgüner, U., Dix, P., and Ashrafi, B. (1995). Abs control using optimum search via sliding modes. *IEEE Transactions on Control Systems Technology*, 3(1):79–85.

Dürr, H. and Ebenbauer, C. (2011). A smooth vector field for saddle point problems. In *2011 50th IEEE Conference on Decision and Control and European Control Conference*, pages 4654–4660.

Dürr, H.-B., Krstić, M., Scheinker, A., and Ebenbauer, C. (2017). Extremum seeking for dynamic maps using Lie brackets and singular perturbations. *Automatica*, 83:91 – 99.

Dürr, H.-B., Stanković, M., Ebenbauer, C., and Johansson, K. (2013). Lie bracket approximation of extremum seeking systems. *Automatica*, 49:1538 – 1552.

Egelman, E. (2016). The current revolution in cryo-em. *Biophysical Journal*, 110(5):1008 – 1012.

Fiacco, A. V. and McCormick, G. P. (1968). *Nonlinear Programming: Sequential Unconstrained Minimization Techniques*. John Wiley & Sons, New York, NY, USA. Reprinted by SIAM Publications in 1990.

Filippov, A. (1988). *Differential Equations with Discontinuous Righthand Sides: Control Systems*. Mathematics and its Applications. Kluwer, USA.

Foster, W. C., Gieseking, D. L., and Waymeyer, W. K. (1966). A Nonlinear Filter for Independent Gain and Phase (With Applications). *Journal of Basic Engineering*, 88(2):457–462.

Frait, J. and Eckman, D. (1962). Optimizing Control of Single Input Extremum Systems. *Journal of Basic Engineering*, 84(1):85–90.

Franklin, G., Powell, D., and Emami-Naeini, A. (2001). *Feedback Control of Dynamic Systems*. Prentice Hall PTR, USA, 4th edition.

Freidovich, L., Robertsson, A., Shiriaev, A., and Johansson, R. (2010). Lugre-model-based friction compensation. *IEEE Transactions on Control Systems Technology*, 18(1):194–200.

Freudenberg, J., Middleton, R., and Stefanpoulou, A. (2000). A survey of inherent design limitations. In *Proc. Am. Control. Conf.*, volume 5, pages 2987–3001.

Frihauf, P., Krstić, M., and Başar, T. (2013). Finite-horizon lq control for unknown discrete-time linear systems via extremum seeking. *European Journal of Control*, 19(5):399 – 407. The Path of Control.

Fu, L. and Özgüner, U. (2011). Extremum seeking with sliding mode gradient estimation and asymptotic regulation for a class of nonlinear systems. *Automatica*, 47(12):2595 – 2603.

Gelbert, G., Moeck, J., Paschereit, C., and King, R. (2012). Advanced algorithms for gradient estimation in one- and two-parameter extremum seeking controllers. *J. Process Control*, 22(4):700–709.

Ghaffari, A., Krstić, M., and Seshagiri, S. (2014). Power optimization and control in wind energy conversion systems using extremum seeking. *IEEE Transactions on Control Systems Technology*, 22(5):1684–1695.

Grushkovskaya, V., Dürr, H.-B., Ebenbauer, C., and Zuyev, A. (2017). Extremum seeking for time-varying functions using Lie bracket approximations. *IFAC-PapersOnLine*, 50(1):5522–5528. 20th IFAC World Congress.

Guay, M. and Dochain, D. (2015). A time-varying extremum-seeking control approach. *Automatica*, 51:356–363.

Guay, M., Dochain, D., and Perrier, M. (2004). Adaptive extremum seeking control of continuous stirred tank bioreactors with unknown growth kinetics. *Automatica*, 40(5):881–888.

Guay, M., Dochain, D., Perrier, M., and Hudon, N. (2007). Flatness-based extremum-seeking control over periodic orbits. *IEEE Trans. Autom. control*, 52(10):2005–2012.

Guay, M., Moshksar, E., and Dochain, D. (2015). A constrained extremum-seeking control approach. *International Journal of Robust and Nonlinear Control*, 25(16):3132–3153.

Hara, S., Yamamoto, Y., Omata, T., and Nakano, M. (1988). Repetitive control system: a new type servo system for periodic exogenous signals. *IEEE Transactions on Automatic Control*, 33(7):659–668.

Haring, M. (2016). *Extremum-seeking control: convergence improvements and asymptotic stability*. PhD thesis, Dept. of Engineering Cybernetics, Norwegian University of Science and Technology, Trondheim.

Haring, M. and Johansen, T. (2018). On the accuracy of gradient estimation in extremum-seeking control using small perturbations. *Automatica*, 95:23 – 32.

Haring, M., van de Wouw, N., and Nešić, D. (2013). Extremum-seeking control for nonlinear systems with periodic steady-state outputs. *Automatica*, 49(6):1883–1891.

Hazeleger, L., Beerens, R., and van de Wouw, N. (2019). A sampled-data extremum-seeking approach for accurate setpoint control of motion systems with friction. *IFAC-PapersOnLine*, 52(16):801 – 806. 11th IFAC Symposium on Nonlinear Control Systems NOLCOS 2019.

Hazeleger, L., Haring, M., and van de Wouw, N. (2018). Extremum-seeking control for steady-state performance optimization of nonlinear plants with time-varying steady-state outputs. In *Proc. Am. Control Conf.*, pages 2990–2995.

Heertjes, M. and Nijmeijer, H. (2012). Self-tuning of a switching controller for scanning motion systems. *Mechatronics*, 22(3):310–319.

Heertjes, M., Perdiguero, N. I., and Deenen, D. (2018). Robust control and data-driven tuning of a hybrid integrator-gain system with applications to wafer scanners. *International Journal of Adaptive Control and Signal Processing*, 33(2):371–387.

Heertjes, M., Tepe, T., and Nijmeijer, H. (2011). Multi-variable iterative tuning of a variable gain controller with application to a scanning stage system. In *Proceedings of the 2011 American Control Conference*, pages 816–820.

Heertjes, M., van den Eijnden, S., Sharif, B., Heemels, M., and Nijmeijer, H. (2019). Hybrid integrator-gain system for active vibration isolation with improved transient response. *IFAC-PapersOnLine*, 52(15):454 – 459. 8th IFAC Symposium on Mechatronic Systems (MECHATRONICS) 2019.

Heertjes, M. F., Schuurbiers, X., and Nijmeijer, H. (2009). Performance-improved design of N-PID controlled motion systems with applications to wafer stages. *IEEE Trans. Ind. Electron.*, 56(5):1347–1355.

Heertjes, M. F., Van der Velden, B., and Oomen, T. (2016). Constrained iterative feedback tuning for robust control of a wafer stage system. *IEEE Transactions on Control Systems Technology*, 24(1):56–66.

Hensen, R., van de Molengraft, M., and Steinbuch, M. (2003). Friction induced hunting limit cycles: A comparison between the lugre and switch friction model. *Automatica*, 39(12):2131 – 2137.

Hespanha, J. and Morse, A. (2002). Switching between stabilizing controllers. *Automatica*, 38(11):1905 – 1917.

Hjalmarsson, H., Gevers, M., Gunnarsson, S., and Lequin, O. (1998). Iterative feedback tuning: theory and applications. *IEEE Control Systems*, 18(4):26–41.

Hjalmarsson, H., Gunnarsson, S., and Gevers, M. (1994). A convergent iterative restricted complexity control design scheme. In *Proceedings of 1994 33rd IEEE Conference on Decision and Control*, volume 2, pages 1735–1740.

Höffner, K., Hudon, N., and Guay, M. (2007). On-line feedback control for optimal periodic control problems. *Can. J. Chem. Eng.*, 85(4):479–489.

Hunnekens, B., Heertjes, M., van de Wouw, N., and Nijmeijer, H. (2014). Performance optimization of piecewise affine variable-gain controllers for linear motion systems. *Mechatronics*, 24(6):648 – 660.

Hunnekens, B. G. B., Di Dino, A., van de Wouw, N., van Dijk, N., , and Nijmeijer, H. (2015). Extremum-seeking control for the adaptive design of variable gain controllers. *IEEE Trans. Control Syst. Technol.*, 23(3):1041–1051.

Hunnekens, B. G. B., Haring, M. A. M., v. d. Wouw, N., and Nijmeijer, H. (2012). Steady-state performance optimization for variable-gain motion control using extremum seeking. In *2012 IEEE 51st IEEE Conference on Decision and Control (CDC)*, pages 3796–3801.

Hunnekens, B. G. B., Haring, M. A. M., van de Wouw, N., and Nijmeijer, H. (2014). A dither-free extremum-seeking control approach using 1st-order least-squares fits for gradient estimation. In *53rd IEEE Conference on Decision and Control*, pages 2679–2684.

Iannelli, L., Johansson, K., and J U. (2006). Averaging of nonsmooth systems using dither. *Automatica*, 42(4):669 – 676.

Jiang, Z.-P. and Wang, Y. (2002). A converse lyapunov theorem for discrete-time systems with disturbances. *Systems & Control Letters*, 45(1):49 – 58.

Johnson, K. E. and Fritsch, G. (2012). Assessment of extremum seeking control for wind farm energy production. *Wind Engineering*, 36(6):701–715.

Jones, D., Perttunen, C., and Stuckman, B. (1993). Lipschitzian optimization without the lipschitz constant. *Journal of Optimization Theory and Applications*, 79(1):157–181.

Karimi, A., Mišković, L., and Bonvin, D. (2004). Iterative correlation-based controller tuning. *International Journal of Adaptive Control and Signal Processing*, 18(8):645–664.

Kellett, C. (2014). A compendium of comparison function results. *Math. Control Signals Syst.*, 26:339–374.

Kellett, C. (2015). Classical converse theorems in lyapunov's second method. *Discrete & Continuous Dynamical Systems - B*, 20(8):2333–2360.

Kellett, C. and Teel, A. (2004). Weak converse lyapunov theorems and control-lyapunov functions. *SIAM Journal on Control and Optimization*, 42(6):1934–1959.

Khalil, H. (2002). *Nonlinear Systems*. Prentice Hall, New Jersey.

Khong, S., Nešić, D., and Krstić, M. (2016). Iterative learning control based on extremum seeking. *Automatica*, 66:238 – 245.

Khong, S., Nešić, D., Manzie, C., and Tan, Y. (2013a). Multidimensional global extremum seeking via the direct optimisation algorithm. *Automatica*, 49(7):1970 – 1978.

Khong, S., Nešić, D., Tan, Y., and Manzie, C. (2013b). Unified frameworks for sampled-data extremum seeking control: Global optimisation and multi-unit systems. *Automatica*, 49(9):2720–2733.

Khong, S. Z., Nei, D., Tan, Y., and Manzie, C. (2013). Trajectory-based proofs for sampled-data extremum seeking control. In *2013 American Control Conference*, pages 2751–2756.

Killingsworth, N. J., Aceves, S. M., Flowers, D. L., Espinosa-Loza, F., and Krstić, M. (2009). Hcci engine combustion-timing control: Optimizing gains and fuel consumption via extremum seeking. *IEEE Trans. Control Syst. Technol*, 17(6):1350–1361.

Killingsworth, N. J. and Krstic, M. (2006). PID tuning using extremum seeking: online, model-free performance optimization. *IEEE Control Systems Magazine*, 26(1):70–79.

Kim, K., Kasnakoğlu, C., Serrani, A., and Samimy, M. (2009). Extremum-seeking control of subsonic cavity flow. *Aiaa Journal -AIAA J*, 47:195–205.

Krstić, M. (2000). Performance improvement and limitations in extremum seeking control. *Systems & Control Letters*, 39(5):313 – 326.

Krstić, M. and Wang, H.-H. (2000). Stability of extremum seeking feedback for general nonlinear dynamic systems. *Automatica*, 36(4):595–601.

Kvaternik, K. and Pavel, L. (2011). Interconnection conditions for the stability of nonlinear sampled-data extremum seeking schemes. In *In Proceedings of the 50th IEEE Conference on Decision and Control*, pages 4448–4454.

Labar, C., Garone, E., Kinnaert, M., and Ebenbauer, C. (2019). Constrained extremum seeking: a modified-barrier function approach. *IFAC-PapersOnLine*, 52(16):694 – 699. 11th IFAC Symposium on Nonlinear Control Systems NOLCOS 2019.

Lamnabhi-Lagarrigue, F., Annaswamy, A., Engell, S., Isaksson, A., Khargonekar, P., Murray, R., Nijmeijer, H., Samad, T., Tilbury, D., and den Hof, P. V. (2017). Systems & control for the future of humanity, research agenda: Current and future roles, impact and grand challenges. *Annual Reviews in Control*, 43:1 – 64.

Lanctot, M., Olofsson, K., Capella, M., Humphreys, D., Eidietis, N., Hanson, J., Paz-Soldan, C., Strait, E., and Walker, M. (2016). Error field optimization in DIII-d using extremum seeking control. *Nuclear Fusion*, 56(7):076003.

Lequin, O., Gevers, M., Mossberg, M., Bosmans, E., and Triest, L. (2003). Iterative feedback tuning of PID parameters: comparison with classical tuning rules. *Control Engineering Practice*, 11(9):1023 – 1033. Special Section on Algorithms and Applications of Iterative Feedback Tuning.

Li, P., Li, Y., and Seem, J. E. (2010). Efficient Operation of Air-Side Economizer Using Extremum Seeking Control. *Journal of Dynamic Systems, Measurement, and Control*, 132(3).

Liao, C.-K., Manzie, C., Chapman, A., and Alpcan, T. (2019). Constrained extremum seeking of a mimo dynamic system. *Automatica*, 108:108496.

Liu, T., Hill, D., and Jiang, Z.-P. (2011). Lyapunov formulation of ISS cyclic-small-gain in continuous-time dynamical networks. *Automatica*, 47(9):2088–2093.

Longman, R. W. (2000). Iterative learning control and repetitive control for engineering practice. *International Journal of Control*, 73(10):930–954.

Makkar, C., Hu, G., Sawyer, W. G., and Dixon, W. E. (2007). Lyapunov-based tracking control in the presence of uncertain nonlinear parameterizable friction. *IEEE Transactions on Automatic Control*, 52(10):1988–1994.

Masiulis, S., Desai, R., Uchanski, T., Serna Martin, I., Laverty, D., Karia, D., Malinauskas, T., Zivanov, J., Pardon, E., Kotecha, A., Steyaert, J., Miller, K., and Aricescu, A. (2019). Gabaa receptor signalling mechanisms revealed by structural pharmacology. *Nature*, 565(7740):454–459.

Mills, G. and Krstić, M. (2014). Constrained extremum seeking in 1 dimension. In *53rd IEEE Conference on Decision and Control*, pages 2654–2659.

Moase, W. and Manzie, C. (2012). Fast extremum-seeking for wienerhammerstein plants. *Automatica*, 48(10):2433 – 2443.

Moase, W. H. and Manzie, C. (2012). Semi-global stability analysis of observer-based extremum-seeking for hammerstein plants. *IEEE Transactions on Automatic Control*, 57(7):1685–1695.

Mohammadi, A., Manzie, C., and Nešić, D. (2014). Online optimization of spark advance in alternative fueled engines using extremum seeking control. *Control Engineering Practice*, 29:201 – 211.

Moore, K. L., Johnson, M., and Grimble, M. J. (1993). *Iterative Learning Control for Deterministic Systems*. Springer-Verlag, Berlin, Heidelberg.

Moura, S. and Chang, Y. (2013). Lyapunov-based switched extremum seeking for photovoltaic power maximization. *Control Engineering Practice*, 21(7):971 – 980.

Mu, B., Li, Y., Salsbury, T. I., and House, J. M. (2016). Optimization and sequencing of chilled-water plant based on extremum seeking control. In *2016 American Control Conference (ACC)*, pages 2373–2378.

Nešić, D. (2009). Extremum seeking control: Convergence analysis. *European Journal of Control*, 15(3):331 – 347.

Nešić, D., Nguyen, T., Tan, Y., and Manzie, C. (2013). A non-gradient approach to global extremum seeking: An adaptation of the shubert algorithm. *Automatica*, 49(3):809 – 815.

Nešić, D., Tan, Y., Moase, W., and Manzie, C. (2010). A unifying approach to extremum seeking: Adaptive schemes based on estimation of derivatives. In *Proc IEEE Conf Decis Control*, pages 4625–4630.

Nešić, D., Teel, A., and Kokotović, P. (1999). Sufficient conditions for stabilization of sampled-data nonlinear systems via discrete-time approximations. *Systems & Control Letters*, 38(4):259 – 270.

Norrlöf, M. and Gunnarsson, S. (2002). Time and frequency domain convergence properties in iterative learning control. *International Journal of Control*, 75(14):1114–1126.

Pavlov, A., Hunnekens, B. G. B., van de Wouw, N., and Nijmeijer, H. (2013). Steady-state performance optimization for nonlinear control systems of Lur´e type. *Automatica*, 49(7):2087–2097.

Pavlov, A. and van de Wouw, N. (2016). Convergent systems: Nonlinear simplicity. In *Nonlinear Systems, Techniques for Dynamical Analysis and Control*, volume 470 of *Lecture Notes in Control and Information Sciences*, pages 51–77. Springer.

Pavlov, A., van de Wouw, N., and Nijmeijer, H. (2006). *Uniform output regulation of nonlinear systems: a convergence dynamics approach*. Birkhäuser, Boston.

Popović, D., Janković, M., Magner, S., and Teel, A. (2006). Extremum seeking methods for optimization of variable cam timing engine operation. *IEEE Trans. Control Syst. Technol.*, 14(3):398–407.

Putra, D., Nijmeijer, H., and van de Wouw, N. (2007). Analysis of undercompensation and overcompensation of friction in 1dof mechanical systems. *Automatica*, 43(8):1387 – 1394.

Ramos, M., Manzie, C., and Shekhar, R. (2017). Online optimisation of fuel consumption subject to nox constraints. *IFAC-PapersOnLine*, 50(1):8901 – 8906. 20th IFAC World Congress.

Ren, B., Frihauf, P., Rafac, R., and Krstić, M. (2012). Laser pulse shaping via extremum seeking. *Control Engineering Practice*, 20(7):674 – 683.

Rušiti, D., Evangelisti, G., Oliveira, T., Gerdts, M., and Krstić, M. (2019). Stochastic extremum seeking for dynamic maps with delays. *IEEE Control Syst. Lett.*, 3(1):61–66.

Sahneh, F., Hu, G., and Xie, L. (2012). Extremum seeking control for systems with time-varying extremum. In *Proc. 31st Chinese Control Conf.*, pages 225–231.

Scheinker, A. (2017). Application of extremum seeking for time-varying systems to resonance control of rf cavities. *IEEE Trans. Autom. control*, 25(4):1521–1528.

Scheinker, A., Huang, X., and Wu, J. (2018). Minimization of betatron oscillations of electron beam injected into a time-varying lattice via extremum seeking. *IEEE Trans. Autom. control*, 26(1):336–343.

Scheinker, A. and Krstić, M. (2013). Minimum-seeking for clfs: Universal semiglobally stabilizing feedback under unknown control directions. *IEEE Trans. Autom. control*, 58(5):1107–1122.

Scheinker, A. and Krstić, M. (2014). Extremum seeking with bounded update rates. *Systems & Control Letters*, 63:25 – 31.

Scheinker, A. and Scheinker, D. (2016). Bounded extremum seeking with discontinuous dithers. *Automatica*, 69:250–257.

Seron, M., Braslavsky, J., and Goodwin, G. (1997). *Fundamental limitations in filtering and control*. Springer-Verlag, London.

Shubert, B. (1972). A sequential method seeking the global maximum of a function. *SIAM Journal on Numerical Analysis*, 9(3):379–388.

Srinivasan, B., Biegler, L., and Bonvin, D. (2008). Tracking the necessary conditions of optimality with changing set of active constraints using a barrier-penalty function. *Computers & Chemical Engineering*, 32(3):572 – 579.

Stanković, M. and Stipanović, D. (2010). Extremum seeking under stochastic noise and applications to mobile sensors. *Automatica*, 46(8):1243 – 1251.

Steinbuch, M. and van de Molengraft, R. (2000). Iterative learning control of industrial motion systems. *IFAC Proceedings Volumes*, 33(26):899 – 904. IFAC Conference on Mechatronic Systems, Darmstadt, Germany, 18-20 September 2000.

Su, Y., Sun, D., and Duan, B. (2005). Design of an enhanced nonlinear PID controller. *Mechatronics*, 15(8):1005 – 1024.

Tan, Y., Li, Y., and Mareels, I. M. Y. (2013). Extremum seeking for constrained inputs. *IEEE Transactions on Automatic Control*, 58(9):2405–2410.

Tan, Y., Moase, W., Manzie, C., Nešić, D., and Mareels, I. (2010). Extremum seeking from 1922 to 2010. In *Proc. 29th Chinese Control Conf.*, pages 14–26.

Tan, Y., Nešić, D., and Mareels, I. (2006). On non-local stability properties of extremum seeking control. *Automatica*, 42(6):889–903.

Tan, Y., Nešić, D., and Mareels, I. (2008). On the choice of dither in extremum seeking systems: A case study. *Automatica*, 44(5):1446 – 1450.

Teel, A. (2000). Lyapunov methods in nonsmooth optimization, part i: Quasi-newton algorithms for lipschitz, regular functions. In *In Proceedings of the 39th Conference on Decision and Control*, volume 1, pages 112–117.

Teel, A. (2000). Lyapunov methods in nonsmooth optimization. part ii: Persistently exciting finite differences. In *Proceedings of the 39th IEEE Conference on Decision and Control*, volume 1, pages 118–123.

Teel, A. and Popović, D. (2001). Solving smooth and nonsmooth multivariable extremum seeking problems by the methods of nonlinear programming. In *Proc. Am. Control Conf.*, volume 3, pages 2394–2399.

Teel, A.R. and Praly, L. (2000). A smooth lyapunov function from a class-$\mathcal{KL}$ estimate involving two positive semidefinite functions. *ESAIM: COCV*, 5:313–367.

van de Wijdeven, J. and Bosgra, O. (2010). Using basis functions in iterative learning control: analysis and design theory. *International Journal of Control*, 83(4):661–675.

van de Wouw, N. and Leine, R. I. (2012). Robust impulsive control of motion systems with uncertain friction. *International Journal of Robust and Nonlinear Control*, 22(4):369–397.

van de Wouw, N., Pastink, H., Heertjes, M., Pavlov, A., and Nijmeijer, H. (2008). Performance of convergence-based variable-gain control of optical storage drives. *Automatica*, 44(1):15 – 27.

van der Meulen, S., de Jager, B., Veldpaus, F., and Steinbuch, M. (2014). Combining extremum seeking control and tracking control for high-performance cvt operation. *Control Engineering Practice*, 29:86 – 102.

van der Meulen, S., de Jager, B., Veldpaus, F., van der Noll, E., van der Sluis, F., and Steinbuch, M. (2012). Improving continuously variable transmission efficiency with extremum seeking control. *IEEE Transactions on Control Systems Technology*, 20(5):1376–1383.

van der Meulen, S., Tousain, R., and Bosgra, O. (2008). Fixed Structure Feedforward Controller Design Exploiting Iterative Trials: Application to a Wafer Stage and a Desktop Printer. *Journal of Dynamic Systems, Measurement, and Control*, 130(5). 051006.

van der Weijst, R., van Keulen, T., and Willems, F. (2019). Constrained multivariable extremum-seeking for online fuel-efficiency optimization of diesel engines. *Control Engineering Practice*, 87:133 – 144.

van Loon, S., Gruntjens, K., Heertjes, M., van de Wouw, N., and Heemels, W. (2017). Frequency-domain tools for stability analysis of reset control systems. *Automatica*, 82:101 – 108.

van Loon, S., Hunnekens, B., Heemels, W., van de Wouw, N., and Nijmeijer, H. (2016). Split-path nonlinear integral control for transient performance improvement. *Automatica*, 66:262–270.

Wagner, C. and Harned, N. (2010). Euv lithography: Lithography gets extreme. *Nat Photon*, 4(1):24–26.

Wang, H.-H. and Krstić, M. (2000). Extremum seeking for limit cycle minimization. *IEEE Trans. Autom. control*, 45(12):2432–2436.

Wang, H.-H., Krstić, M., and Bastin, G. (1999). Optimizing bioreactors by extremum seeking. *Int J Adapt Control Signal Process*, 13(8):651–669.

Wang, Y., Gao, F., and Doyle, F. (2009). Survey on iterative learning control, repetitive control, and run-to-run control. *Journal of Process Control*, 19(10):1589 – 1600.

Xiao, Y., Li, Y., and Rotea, M. A. (2019). Cart3 field tests for wind turbine region-2 operation with extremum seeking controllers. *IEEE Transactions on Control Systems Technology*, 27(4):1744–1752.

Zhang, C. and Ordónez, R. (2007). Numerical optimization-based extremum seeking control with application to abs design. *IEEE Trans. Autom. control*, 52(3):454–467.

Zhang, C. and Ordónez, R. (2009). Robust and adaptive design of numerical optimization-based extremum seeking control. *Automatica*, 45(3):634 – 646.

Zheng, J., Guo, G., and Wang, Y. (2005). Nonlinear PID control of linear plants for improved disturbance rejection. *IFAC Proceedings Volumes*, 38(1):281 – 286. 16th IFAC World Congress.

Summary

Extremum-Seeking Control for Data-Based Performance Optimization of High-Tech Systems

Automatic control of dynamic processes is a key enabling methodology in a substantial variety of technological innovations in many branches of our society, and has proven indispensable in realizing the social welfare and economic prosperity that we benefit today. This becomes particularly evident from the broad range of high-tech industrial applications in which control plays a pivotal role, ranging from photolithography systems, electron microscope systems, pick-and-place machinery, to industrial printing and copying systems, robotics to medical imaging systems. Mechatronic system designs for high-tech applications in these areas of technology often rely on high-cost mechatronic solutions to achieve highly predictable and understandable system dynamics on the basis of accurate system models. These models have enabled skillful control engineers in the high-tech industry to use conventional and well-understood control solutions to meet stringent performance requirements in terms of machine accuracy, operating speed, stability, and reliability.

However, major economic, social and technological trends push performance, cost, and reliability requirements for current and future high-tech systems to unparalleled levels, and will progressively challenge purely model-based approaches to automatic control and optimization. In particular, the increasing complexity in terms of uncertainty, non-stationary nature of system dynamic properties and disturbances, and mode-of-use dependent performance specifications, constitute real challenges in achieving *optimal* performance in current and future high-tech systems using model-based approaches. To account for changing, uncertain, or unknown dynamics and disturbance characteristics, and enable the satisfaction of accuracy and robustness demands, a lot can be gained by combining or supporting model-based control engineering in future complex high-tech systems with *data-based*, *automated* and *adaptive* performance optimization techniques.

In this dissertation, data-based automated performance optimization of high-tech systems is addressed by a technique known as *extremum-seeking control*.

Extremum-seeking control is a data-driven and model-free method for optimizing system performance in real-time, by continuously or iteratively adapting system parameters. Due to its model-free nature, the method is especially valuable in cases where the dynamical behavior of the system at hand can not be represented by an accurate or comprehensible model, or cases where the disturbances are unknown, changing, or mode-of-use dependent.

However, in order to benefit from the full potential of extremum-seeking control to achieve optimal performance in the context of high-tech systems, the state-of-the-art faces three major challenges. In the first place, extremum-seeking control methods are tailored primarily towards the steady-state performance optimization of systems that admit equilibria solutions, or periodic system responses with a known period time. Performance of high-tech systems, however, is generally related to *generically time-varying steady-state behavior*, and is heavily dependent on the (time-varying) disturbances and operating condition at hand. In the second place, extremum-seeking control methods are generally focussed on finding tunable system parameters that optimize steady-state system performance. However, many high-tech systems also have to deal with constraints on operating conditions, originating from *constraints on unknown but measurable variables*. These constraints may conflict with the otherwise performance optimal operational condition of these high-tech systems. In the third place, extremum-seeking control is aimed at finding constant input parameters that optimize the steady-state behavior of dynamical systems, while *transient behavior* in many high-tech systems that perform repetitive tasks may impair the achievable performance.

The main contributions of this dissertation are directly related to the above mentioned challenges. The first contribution is the development of a novel *extremum-seeking control approach for optimization of generically time-varying steady-state behavior of nonlinear dynamical systems.* In particular, an extension of the class of extremum-seeking problems from those involving equilibria solutions or periodic time-varying steady-state responses, to those involving systems exhibiting generically time-varying steady-state responses is provided. The convergent systems property is exploited, and is essential in this generic, time-varying context. To facilitate the use of extremum seeking in this more generic, time-varying context, a user-defined, generic filter structure, the so-called dynamic cost function, is introduced. In addition, a novel extension of an observer-based extremum-seeking control strategy is provided. This extended approach exploits model knowledge about the user-defined dynamic cost function to facilitate enhanced convergence speed of the resulting extremum-seeking control scheme. The effectiveness of both the nominal extremum-seeking control design and the extended approach are evidenced experimentally by application to an industrial motion stage set-up of a high-end lithography system.

The second contribution is the development of a *sampled-data extremum-seeking control framework for constrained optimization of nonlinear dynamical*

systems. In particular, an extension of the classical sampled-data extremum-seeking framework is provided that encompasses 1) a class of dynamical systems in which both the to-be-optimized objective function and the constraint functions are available through measurement only, and 2) a class of smooth and non-smooth optimization algorithms to facilitate extremum-seeking in the presence of unknown but measurable constraints, inspired by the use of barrier function methods. The working principle of the proposed framework is illustrated by means of a representative industrial case study of constrained optimization of extreme ultraviolet light generation in a laser produced plasma source within a state-of-the-art lithography system.

The third contribution is the development of an *iterative learning control strategy based on extremum-seeking control for high-accuracy repetitive setpoint control of frictional motion systems.* First, a novel proportional-integral-derivative-based controller with a time-varying integrator gain design is proposed that facilitates improved time-domain behavior in terms of overshoot and setpoint accuracy for repetitive motion in frictional motion systems. Second, the optimal time-varying integrator gain design is obtained through an automatic iterative controller tuning procedure based on a sampled-data extremum-seeking algorithm, ensuring optimal setpoint positioning accuracy despite unknown friction characteristics and unknown disturbances. Third, the effectiveness of the proposed approach is evidenced experimentally by application to an industrial nano-positioning motion stage set-up of a high-end electron microscope.

This dissertation presents newly developed extremum-seeking control methods that enable data-based performance optimization for a richer class of optimization problems. The developments are inspired by a large variety of industrially relevant optimization problems, and are experimentally demonstrated to illustrate the value it may provide in supporting control engineers to get the most out of their high-tech systems.

List of publications

Peer-reviewed journal articles

- Hazeleger, L., Nešić, D., and van de Wouw, N. (2019). Sampled-data extremum-seeking framework for constrained optimization of nonlinear dynamical systems, *In preparation for submission to Automatica*.
- Hazeleger, L., van de Wijdeven, J., Haring, M., and van de Wouw, N. (2019). Extremum seeking with enhanced convergence speed for optimization of time-varying steady-state behavior of industrial motion stages, *Submitted to Transactions on Control Systems Technology*.
- Hazeleger, L., Beerens, R., and van de Wouw, N. (2019). Proportional-integral-derivative based learning control for high-accuracy repetitive positioning of frictional motion systems, *Submitted to Transactions on Control Systems Technology*
- Hazeleger, L., Haring, M., and van de Wouw, N. (2018). Extremum-seeking control for optimization of time-varying steady-state responses of nonlinear systems", *Accepted for publication in Automatica*.

Peer-reviewed articles in conference proceedings

- Hazeleger, L. and Beerens, R., and van de Wouw, N. (2020). PID-based learning control for frictional motion systems, two-page abstract, *Accepted for the 10th European Nonlinear Dynamics Conference (ENOC 2020)*, Lyon, France.
- Hazeleger, L. and Nešić, D., and van de Wouw, N. (2019). Sampled-data extremum-seeking control for optimization of constrained dynamical systems using barrier function methods, *2019 IEEE* 58*th Conference on Decision and Control (CDC)*, Nice, France, pp 213–219.
- Hazeleger, L., Beerens, R., and van de Wouw, N. (2019). A sampled-data extremum-seeking approach for accurate setpoint control of motion systems with friction, *11th IFAC Symposium on Nonlinear Control Systems*

NOLCOS 2019, Vienna, Austria / IFAC-PapersOnLine, Vol. 52, no. 16, pp. 801–806.

- Hazeleger, L., Haring, M. and van de Wouw, N. (2018). Extremum-seeking control for steady-state performance optimization of nonlinear plants with time-varying steady-state outputs, *American Control Conference (ACC)*, Milwaukee, WI, USA, pp. 2990–2995.

- Hazeleger, L., Heertjes, M.F., and Nijmeijer, H. (2016). Second-order reset elements for stage control design, *American Control Conference (ACC)*, Boston, MA, USA, pp. 2643–2648.

About the author

Leroy Hazeleger was born on August 24, 1990 in Nieuwegein, the Netherlands. In 2008, he completed his pre-university education at the Oosterlicht College in Nieuwegein. Subsequently, he received his Bachelor's degree in Mechanical Engineering at the Eindhoven University of Technology, The Netherlands, in 2012, and his Master's degree (with great appreciation) in Systems and Control within the Department of Mechanical Engineering at the Eindhoven University of Technology, The Netherlands, in 2015. As part of this curriculum, he performed an internship at the Royal Melbourne Institute of Technology, Australia. His Master's thesis was entitled "Second-order reset elements for improved stage control design", and was conducted in collaboration with ASML the Netherlands under the supervision of Henk Nijmeijer and Marcel Heertjes (ASML).

In January 2016, Leroy started his Ph.D. research within the Dynamics and Control Group at the Eindhoven University of Technology, The Netherlands, under supervision of Nathan van de Wouw and Henk Nijmeijer. The research is part of the research programme "Hybrid solutions for cost-aware high-performance motion control", (partly) financed by the Netherlands Organisation for Scientific Research (NWO), and executed in close collaboration with various industrial partners. During the period September-December 2018, Leroy was visiting Dragan Nešić at the Department of Electrical and Electronic Engineering at the University of Melbourne, Australia.

The results of his Ph.D. research are documented in this dissertation, and are focussed on the development of extremum-seeking control methods for data-driven performance optimization of high-tech systems.

Dankwoord

Allereerst wil ik je feliciteren met het bereiken van deze pagina in mijn proefschrift. Waarschijnlijk heb jij dit punt in mijn proefschrift een stuk sneller bereikt dan ik. Desalniettemin, de afgelopen vier+ jaren zijn voor mij voorbij gevlogen, waarschijnlijk vele malen sneller dan dat vier jaar tijd klinkt voor jou. Ik kan niet anders concluderen dan dat dit het gevolg is van de vele hoogtepunten en uitersten gedurende dit avontuur, die dit promotietraject voor mij een heel bijzondere periode hebben gemaakt. Deze pagina's geven mij de beste gelegenheid om de belangrijkste bijdragen aan dit avontuur te kunnen benadrukken; de betrokkenheid, de hulp, de wijze raad, het geduld, en de steun van de geweldige mensen om mij heen.

Graag wil ik als eerste mijn promotoren bedanken. Nathan, ik wil je ontzettend bedanken voor de extreem prettige samenwerking die we de afgelopen vier jaar hebben gehad. Je positieve instelling, je betrokkenheid, en de vrijheid en het vertrouwen dat je me hebt geschonken gedurende mijn onderzoek heb ik altijd erg op prijs gesteld. Ook vond ik het bijzonder fijn dat ik altijd bij je terecht kon voor een gezellige babbel of wat opbeurende en bemoedigende woorden wanneer deze nodig waren. Je altijd scherpe blik en constructieve feedback op mijn werk en de vele discussies die we hebben gevoerd hebben mij zeer geholpen dit werk succesvol af te ronden, en mij doen groeien als onderzoeker. Henk, jij hebt mij al tijdens het afstudeerproject van mijn Masteropleiding weten te interesseren voor een promotietraject. Ik ben je dan ook erg dankbaar dat ik na mijn afstuderen binnen D&C heb mogen werken aan het CHAMeleon project, en dat je mij het vertrouwen en de ruimte hebt gegeven om dit onderzoek (samen met Nathan) een eigen invulling te geven. Ondanks dat jij als promotor iets verder van mijn inhoudelijke onderzoek hebt afgestaan, heeft het me altijd verbaasd dat je met je feedback precies de spijker op zijn kop wist te slaan. Maurice, weliswaar ben je niet één van mijn promotoren, maar wel één van de key-members van het CHAMeleon team, en wil ik je dan ook ontzettend bedanken voor je betrokkenheid en de interesse die je altijd hebt getoond in mijn onderzoek en in mij als persoon. Om even in de CHAMeleon-sfeer te blijven, wil ik graag NWO bedanken, en de leden van de gebruikerscommissie voor hun expertise, toegankelijkheid, en de vruchtbare vergaderingen en discussies gedurende dit project. Met name ben ik Thermo Fisher en ASML dankbaar

voor het beschikbaar stellen van hun experimentele setups. In het bijzonder bedank ik Jeroen van de Wijdeven voor de samenwerking, de interessante discussies die wij hebben gevoerd, en de altijd scherpe feedback op mijn werk gedurende de afgelopen vier jaar. Ook wil ik Mark Haring bedanken. Mark, je (wiskundige) input en bijdrage is van grote waarde geweest voor mijn proefschrift.

I would like to thank Dragan Nešić, Alexey Pavlov, Jan-Willem van Wingerden, and Bram de Jager for their time and effort reading and assessing my dissertation, and participating in my defense committee. In particular, I would like to express my gratitude towards Dragan; thanks a lot for the great and fruitful collaboration the past two+ years, for hosting me at the University of Melbourne, and for your hospitality. Rosanne and I very much enjoyed our time in Melbourne and we hope to visit again.

Ik wil al mijn D&C en CST collega's in de kelders van Gemini bedanken voor de gezelligheid bij de koffie/bier-corner, de uitstapjes, Benelux meetings, LAN-parties, en conferentie-trips de afgelopen vier jaar. Geertje, bedankt voor de ondersteuning vanuit het D&C secretariaat, de fijne gesprekken, en het organiseren van leuke team-uitjes. Mijn (oud-)kantoorgenoten van Gemini -1.115 Daniel, Roeland, Jiquan, en tevens CHAMeleonproject-genoten Ruud en Annemiek wil ik hartelijk danken voor de gezellige tijd binnen en buiten het kantoor, het kunnen delen van de ups & downs, en het improven van mijn dart-skills. In het bijzonder dank ik jou Ruud; het was erg tof om samen met jou het CHAMeleon project te runnen en naar een mooi einde te brengen, en om uiteindelijk onze individuele onderzoeksprojecten te verbinden middels twee gezamenlijke publicaties.

Een speciale shout-out doe ik graag naar mijn Kroepoekclan-bro's en tevens CST collega's Alex, Daniel, en Robin. Het is oprecht een verademing geweest om drie van mijn beste buddies als collega's te hebben gehad. Ik geniet nog altijd van het fervent ontspannen en het bijgaande filosoferen over de serieuze, maar ook de onzinnige dingen van het leven, het techneuten, het lekkere klagen over alles en niets om even te kunnen ontluchten, de sportieve endeavours die we ondernemen, en de niet zo (kuch*) competitieve boardgame avonden. Let's keep this going, thanks boys! Tevens wil ik al mijn familie, vrienden, en oud-huisgenoten bedanken, in het bijzonder Cameron, Jeroen en Peter, voor hun ongoing support en interesse in mij(n onderzoek), en de soms broodnodige afleidingen met de mooie dingen van het leven.

Ik ben mijn families Hazeleger en Franken ontzettend dankbaar voor hun steun, luisterend oor, de diepzinnige gesprekken en wijze raad, niet alleen met betrekking tot dit promotietraject, maar vooral met alles daar buiten. Papa, Mama, Suwie en Ton, bedankt dat jullie altijd klaar voor mij staan.

Ten slotte gaat mijn aller grootste dank uit naar Rosanne. Roos, waar dit avontuur voor mij eindigt, is het onze pas acht+ jaar onderweg. Ik ben je enorm dankbaar voor je oneindige steun en geduld, het ontzettend fijne gezelschap, en het luisterend oor dat je me altijd hebt geboden gedurende mijn studie,

promotietraject, en alles eromheen. Gedurende de momenten waarop ik dat het hardst nodig had, heb je me letterlijk en figuurlijk op twee(!) benen gehouden, en is jou bijdrage aan dit proefschrift niet samen te vatten in één alinea. Ik ben ontzettend blij dat wij samen al vele mooie momenten en dromen hebben kunnen delen, en ik kan niet wachten samen nog vele mooie dingen in het leven te trotseren.

Leroy Hazeleger
Eindhoven, Juli 2020